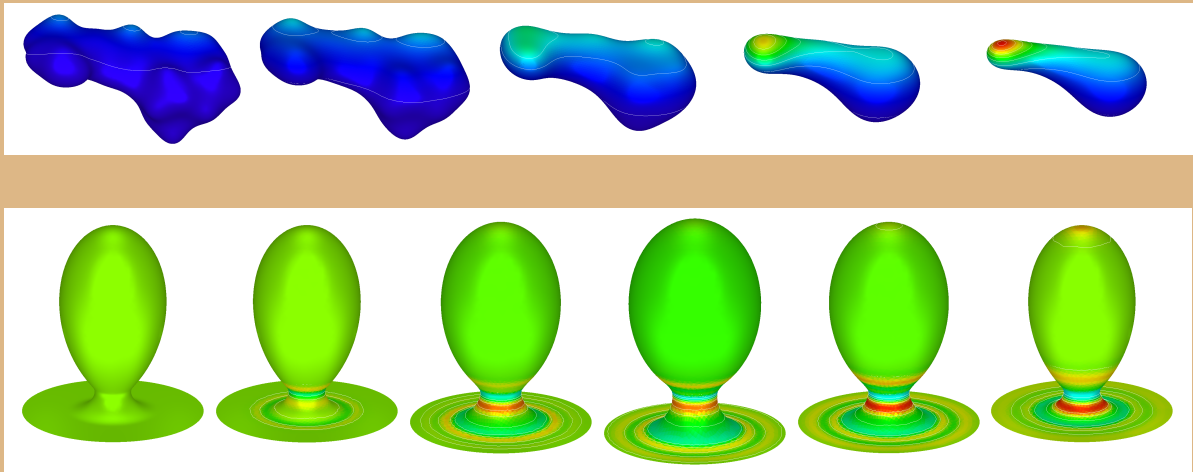


# Mathematics: Numerical analysis and scientific computing

## Finite Volume Methods for Advection Diffusion on Moving Interfaces and Application on Surfactant Driven Thin Film Flow



DISSERTATION

zur Erlangung des Doktorgrades (Dr. rer. nat.)  
der Mathematisch-Naturwissenschaftlichen Fakultät  
der Rheinischen Friedrich-Wilhelms-Universität Bonn

vorgelegt von Simplice Firmin Nemadjieu  
aus Bafang (Kamerun)

Bonn, May 2012

Angefertigt mit Genehmigung der Mathematisch-Naturwissenschaftlichen Fakultät der Rheinischen  
Friedrich-Wilhelms-Universität Bonn  
am Institut für Numerische Simulation.

1. Gutachter: Prof. Dr. Martin Rumpf
2. Gutachter: Prof. Robert Eymard
3. Gutachter: Prof. Dr. Werner Ballmann
4. Gutachter: Prof. Dr. Helmut Schmitz

Tag der Promotion: 12. July 2012  
Erscheinungsjahr: 2012

# Contents

<b>Acknowledgment</b>	<b>iii</b>
<b>Nomenclature</b>	<b>v</b>
<b>General introduction</b>	<b>vii</b>
<b>I Finite volume method on evolving surfaces</b>	<b>1</b>
<b>1 A convergent finite volume scheme for diffusion on evolving surfaces</b>	<b>3</b>
1.1 Introduction . . . . .	3
1.2 Mathematical model . . . . .	4
1.3 Derivation of the finite volume scheme . . . . .	4
1.4 A priori estimates . . . . .	8
1.5 Convergence . . . . .	11
1.5.1 Geometric approximation estimates . . . . .	12
1.5.2 Consistency estimates . . . . .	14
1.5.3 Proof of Theorem 1.5.1 . . . . .	17
1.6 Coupled reaction diffusion and advection model . . . . .	19
1.7 Numerical results . . . . .	21
<b>2 A stable and convergent O-method for general moving hypersurfaces</b>	<b>27</b>
2.1 Introduction . . . . .	27
2.2 Problem setting . . . . .	28
2.3 Surface approximation . . . . .	29
2.4 Derivation of the finite volume scheme . . . . .	31
2.4.1 General setting . . . . .	31
2.4.2 The discrete gradient operator . . . . .	33
2.4.3 Finite Volumes discretization . . . . .	38
2.4.4 Maximum principle . . . . .	42
2.4.5 Implementation . . . . .	43
2.5 A priori estimates . . . . .	44
2.6 Convergence . . . . .	47
2.6.1 Geometric approximation estimates . . . . .	48
2.6.2 Consistency estimates. . . . .	51
2.6.3 Proof of Theorem 2.6.1 . . . . .	54
2.7 Coupled reaction diffusion and advection model . . . . .	57
2.8 Numerical results . . . . .	60
<b>II Modeling and simulation of surfactant driven thin-film flow on moving surfaces</b>	<b>67</b>
<b>3 Modeling of surfactant driven thin-film flow on moving surfaces</b>	<b>69</b>

3.1	Introduction . . . . .	69
3.2	Problem setting . . . . .	71
3.3	Geometry setting . . . . .	73
3.3.1	Coordinate system . . . . .	73
3.3.2	Nondimensionalization/scaling and basic tensor calculus . . . . .	74
3.4	Derivation of surfactant and thin-film equation . . . . .	84
3.4.1	Velocity and its derivatives . . . . .	84
3.4.2	Scaled surfactant equation . . . . .	86
3.4.3	Model reduction for the thin-film equation using lubrication approximation . . . . .	86
<b>4</b>	<b>Simulation of surfactant driven thin-film flow on moving surfaces</b>	<b>93</b>
4.1	Introduction . . . . .	93
4.2	Problem Setting . . . . .	94
4.3	Derivation of the scheme . . . . .	96
4.3.1	Reformulation of the problem . . . . .	96
4.3.2	Geometric setting . . . . .	98
4.3.3	Discrete gradient operators . . . . .	99
4.3.4	Finite volume discretization . . . . .	103
4.4	Numerical results . . . . .	113
	<b>Conclusion and perspectives</b>	<b>121</b>
	<b>Bibliography</b>	<b>123</b>



# Acknowledgment

I am extremely thankful to Prof. Dr. Martin Rumpf for the supervision of this thesis and for the opportunities he has given me throughout to visit and participate actively in outstanding conferences where my mind got opened with regards to several aspects of the finite volume method as well as many other mathematical topics. I would also like to thank him for the opportunity he gave me to visit Prof. Robert Eymard who methodically introduced me to the new trends in the finite volume method. This deeply reoriented my development; may Prof. Eymard find here the expression of my profound gratitude. I am particularly indebted to Martin Lenz, for his patient hearing, the fruitful mathematical discussions, the proofreading of parts of this thesis, his assistance in hardware setup and his involvement in the programming of the visualization tools GRAPE mainly used in this thesis; the same goes to Orestis Vantzou for fruitful mathematical discussions, the proofreading of parts of this thesis and the introduction to Mathematica. I would like to thank Ole Schween and Benedikt Geihe for their assistance in the hardware setting. Many thanks to Ms Sodoge Stork for her assistance in administrative issues, Martina Teusner, Abigail Wachter, Evaristus Fuh Chuo, Stefan Steinerberger and Prof. Dr. Hans-Peter Helfrich for their proofreading. I am very grateful to all the colleagues of the group of Prof. Dr. Martin Rumpf for the nice scientific collaborative environment.

I am deeply grateful to my family, particularly my late father Tchamani Bernard and my mother Sigou Rosalie who despite the particularly difficult times of African developing countries in the Nineties have never spared any effort to provide me with a good education. May they find here a particular sign of love. I would like to thank my friends Leopold Wandji, David Jialeu, Patrice Kouemou, Patrice Nongni, Richard Kamda, Severin Koumene, Jean Bernard Noujep, Aline Mboussi and Franck Olivier Tchatchoua who have always given me a hand at needed time. My thanks go also to my friends Catalin Ionescu, Irene Paniccia, João Carreira, Habiba Kalantarova, Major Pougom, Hugues Kamalieu, Armel Pougom and Eric Yamdjeu for their constant encouragement. Finally I would like to thank my companion in life Evelyne Chouandjeu who has sacrificed a lot for the accomplishment of this work.

May all these persons find here the expression of my profound gratitude.

Of course, all these has been possible only with the blessing of God.

I am therefore infinitely grateful to the Almighty.



# Nomenclature

$t$	time
$\Gamma(t)$	Family of oriented surfaces
$\nu$	Normal to the surface $\Gamma(t)$
$\Gamma^k := \Gamma(t_k)$	Surface at time $t_k$
$\mathcal{N}(t)$	Neighborhood of the surface $\Gamma(t)$
$\mathcal{N}_k := \mathcal{N}(t_k)$	Neighborhood of the surface $\Gamma^k$
$\nu^k$	Normal to the surface $\Gamma^k$
$v_\Gamma$	Velocity of material point
$s_1, s_2$	Local parametric variables of the surface $\Gamma(t)$
$X(t, s_1, s_2)$	Local parameterization of the surface $\Gamma(t)$
$\overline{FS}(t)$	Free surface
$r(t, s_1, s_2)$	Local parameterization of the free surface $\overline{FS}(t)$
$\nu_{FS}$	Normal to the free surface $\overline{FS}(t)$
$v_{FS,pt}$	Velocity of a material point on the free surface
$\bar{H}$	Non scaled thin-film height
$H$	Scaled thin-film height
$\mathcal{H}$	Vertical length scale
$\mathcal{L}$	Horizontal length scale
$\epsilon := \frac{\mathcal{H}}{\mathcal{L}} \ll 1$	
$\bar{K}$	Non scaled curvature tensor of the surface $\Gamma(t)$
$K$	Scaled curvature tensor of the surface $\Gamma(t)$
$\mathcal{K} := \text{tr}(K)$	Trace of $K$ (Mean curvature of the surface $\Gamma(t)$ )
$\mathcal{K}_2 := \text{tr}(K^2)$	Trace of $K^2$
$\mathcal{K}_3 := \text{tr}(K^3)$	Trace of $K^3$
$R_{\bar{H}} := (\text{Id} - \bar{H}\bar{K})^{-1}$	
$R_H := (\text{Id} - \epsilon HK)^{-1}$	
$\bar{\nabla}_\Gamma$	Non scaled surface gradient
$\nabla_\Gamma$	Scaled surface gradient
$\frac{\partial^\Gamma}{\partial t} = \frac{\partial}{\partial t} + v_\Gamma \cdot \nabla$	Material derivative
$\mathcal{P}_{FS,\nu} := (\text{Id} - \nu \otimes (\nu - \epsilon R_H \nabla_\Gamma H))$	Projection operator onto the free surface tangent plane in the direction of the surface normal $\nu$
$\mathcal{P}_e$	Peclet number
$\bar{\nabla}_{FS}$	Non scaled free surface gradient
$\nabla_{FS}$	Scaled free surface gradient
$\Delta_\Gamma$	Scaled surface divergence (Laplace-Beltrami operator)
$\bar{\mathcal{K}}_{FS}$	Non scaled free surface mean curvature
$\mathcal{K}_{FS}$	Scaled free surface mean curvature
$\Pi_{eq}$	Equilibrium concentration of surfactant
$\bar{\Pi}_\infty$	Surfactant concentration in the maximum packing limit
$x = \frac{\Pi_{eq}}{\bar{\Pi}_\infty}$	Surfactant coverage
$R$	Universal gas constant
$T_a$	Absolute temperature in Kelvin
$\Pi$	Surfactant concentration on the free-surface

## Nomenclature

---

$\bar{\gamma}_0$	Surface tension of the clean surface ( $\Pi = 0$ )
$v_{FS}$	Dimensionless velocity of the fluid particle on $\overline{FS}(t)$
$v_{RFS}$	Relative velocity of the fluid particle at the free surface
$v_\Gamma$	Velocity of a substrate material point
$v_{\Gamma,\nu} := v_{\Gamma,\nu} \cdot \nu$	
$v_{\Gamma,tan} := v_\Gamma - \nu v_{\Gamma,\nu}$	
$\gamma$	Surface tension
$g$	Unit gravity vector
$g_\nu := g \cdot \nu$	
$g_{tan} := g - (g \cdot \nu)\nu$	
$A$	Dimensionless Hamaker constant
$\mathcal{B}_0$	Bond number
$C'$	Inverse capillary number
$\phi := AH^{-3}$	Disjoining pressure
$\eta = H - \frac{1}{2}\epsilon H^2 \mathcal{K} + \frac{1}{6}\epsilon^2 H^3 (\mathcal{K}^2 - \mathcal{K}_2)$	Fluid density above the substrate $\Gamma(t)$

# General introduction

In the present thesis, we are devoted to the design and analysis of finite volume schemes for time-dependent partial differential equations (PDEs) on evolving surfaces as well as the modeling and simulation of surfactant driven thin film flow on moving curved surfaces; thus our work is divided into two main parts. The first part “Finite volume method on evolving surfaces” discusses two finite volume schemes for the simulation of time-dependent convection-diffusion and reaction problem while the second part “Modeling and simulation of surfactant driven thin-film flow on moving surfaces” deals with a reduced model for a coupled free boundary problem from fluid dynamics and its simulation via the schemes defined in the first part.

The finite volume method has become one of the most popular simulation tools for PDEs during the last two decades. The method has been extensively studied mathematically and has been applied to complicated problems and to challenging situations such as simulation on strong anisotropic and nonconformal meshes. We refer to the symposium reports Finite Volumes for Complex Applications I-VI for the advances in the field. The main attractions of the method reside in its local conservation properties, its ability to be applied on general meshes, the good adaptation to convection dominated problems and the fact that it is relatively easy to implement. Unfortunately, the application of finite volume method for direct simulation of PDEs on curved surfaces is less understood and is a recent field of investigation. So far, only few research works have been devoted to this issue. Let us point out for example [19] where the authors discuss a finite volume formulation for diffusion problems on spherical domains. Here the authors formulate a finite volume scheme on logically rectangular grids based on a local parameterization of the sphere. This work is later extended in [18] to convection-diffusion-reaction problems on surfaces having curved or spherical domains. We would also like to mention [33, 76, 34] where the authors successively study the finite volume method for diffusion problem on the sphere, then on general surfaces and later the fourth order partial differential equation on general surfaces. In these works, the curved surface is approximated by Voronoi meshes which are based on a particularly good triangulation of the surfaces; the vertices of the triangulation being bounded to the surface. Similar to these works, existing paper that come to our knowledge discussing finite volume on surfaces rely on particular polygonization of the substrate (surface) and for those treating diffusion problems, they concentrate on isotropic diffusion. In the first part of the present work, we discuss two finite volume methods for the simulation of PDEs on curved surfaces among which one is devoted to the simulation on general polygonal approximation of surfaces. The first method (Chapter I) has been already published in SIAM Journal of Numerical Analysis [86]. It extends a finite volume method by Eymard, Gallouët, and Herbin in [45] on evolving curved surfaces. We consider the parabolic problem

$$\dot{u} + u\nabla_{\Gamma} \cdot v - \nabla_{\Gamma} \cdot (\mathcal{D}\nabla_{\Gamma}u) = g \text{ on } \Gamma(t), \quad (0.1)$$

a sequence of triangular surfaces approximating the time-dependent curved surface  $\Gamma(t)$  at different time steps with nodes living on the respective smooth surfaces, and derive a finite volumes scheme based on the two points flux approximation discussed in [45]. By  $\dot{u} = \frac{d}{dt}u(t, x(t))$  we denote the (advective) material derivative of the scalar density  $u$ ,  $\nabla_{\Gamma} \cdot v$  the surface divergence of the vector field  $v$ ,  $\nabla_{\Gamma}u$  the surface gradient of  $u$ ,  $g$  a source term, and  $\mathcal{D}$  a symmetric and elliptic diffusion tensor on the tangent bundle of  $\Gamma(t)$ . We assume a Lagrangian representation of the surface where the approximated surface at a time step  $t_{k+1}$  is obtained by evolving the node of the approximated surface at the previous time step  $t_k$  with the surface velocity, and study the Eulerian evolution of  $u$  on the evolving triangular representation of  $\Gamma(t)$ . The triangular surfaces are assumed to be so

close to the respective curved surfaces that the orthogonal projection of meshes on the respective continuous surfaces define an evolving curved mesh. Then our finite volume scheme is derived by approximating the integral of (0.1) on the path of each evolving curved cell using the Leibniz integral formula for the parabolic part and the divergence theorem on curved surfaces for the space integration of the diffusive part. An implicit discrete time integration is considered for both diffusive and source terms. The derived scheme is implicit, stable and convergent. We also extend the scheme to the convection-diffusion and reaction problem

$$\dot{u} + u\nabla_{\Gamma} \cdot v - \nabla_{\Gamma} \cdot (\mathcal{D}\nabla_{\Gamma}u) + \nabla_{\Gamma} \cdot (wu) = g(u) \quad \text{on } \Gamma = \Gamma(t), \quad (0.2)$$

where  $w$  is an additional tangential velocity on the surface, which transports the density  $u$  along the moving interface  $\Gamma(t)$  and the reaction term  $g$  now depends on  $u$ . We discretize the additional advection term using the first order upwinding procedure similar to the one used on flat surfaces. The advantage here is that we work on the surface without any attempt to use a particular parameterization of the surface, nor computing any geometric feature of the surface; thus the method is suitable for any curved surface. The limits of the method resides on the choice of triangles center points where the unknowns are located. In fact, these points have to satisfy a particular perpendicularity condition introduced on each cell by the tensor  $\mathcal{D}^{-1}$  which can be satisfied for strong anisotropic tensors only if care has been taken during the construction of the mesh. Also, in real world applications, many meshes are generated either from scanning devices or from meshing tools and are not necessarily triangular. Furthermore such processes are error prone and the obtained meshes are rarely satisfactory; thus they most often go through a remeshing machinery for optimization which increases the error on the vertices coordinates. In the context of moving surfaces, we will also notice that for surfaces described implicitly through PDEs as for interface flows, meshes automatically contain error from their numerical computation. Thus, a more rigorous analysis of schemes designed for direct simulation of PDEs on surfaces should take into account such uncertainty. These lacks are taken into account in Chapter II where we derive a new finite volume scheme for general polygonal surfaces based on a proper reconstruction of the gradient of  $u$  around vertices of the mesh. Here we subdivide our finite volume cells into subcells attached to vertices and assume a linear reconstruction of our function  $u$  on subcells; thus constant gradient reconstruction on subcells. The gradient reconstruction on subcells incorporates already the flux continuity through edges, and the integration mentioned above gives the finite volume scheme. We introduce for (0.2) a second order upwinding based on our gradient reconstruction. In fact after we have constructed the gradient on the subcells, we define using the minmod procedure, a new piecewise constant gradient of minimum norm that approximates the gradient of the  $u$  on cells. The values on edges are then chosen using the Taylor formula and the upwinding procedure. The obtained finite volume is suitable for discretization on any evolving curved surface. No surface parameterization is needed, nor any geometric quantity.

In the second part, we first model in Chapter III the coupled surfactant driven thin film flow on an evolving surface using lubrication approximation. A thin film flowing on an evolving curved surface is considered, on top of which a layer of surfactant diffuses. Such a system is present in the mammalian lungs. The thin film is represented by the lining while the surfactant is represented by lipid monolayers. The surfactant plays an important role in the respiratory system. During the expiration phase for example, it lowers the surface tension to prevent the surface to collapse and also facilitate the inspiration. A lack of surfactant would require a lot of energy to reopen the alveoli and allow the ventilation. Let us mention too that often, the lung of prematurely born infants cannot produce enough surfactant to regulate the respiratory system; this leads to the so called respiratory distress syndrome (RDS) often cured by surfactant replacement therapy (SRT) which consists of installing the surfactant in the trachea of the patient where the substance is transported in the large airways. We refer to [15, 63, 66, 78] for more reading in the topic of lung surfactant. Thin films occur also in engineering (aircraft de-icing films), in geology (lava) amongst other. In order to describe the evolution of such a fluid, we rewrite the momentum incompressible Navier-Stokes equation in a curvilinear coordinate system attached to the substrate using some basic tensor cal-

---

culus. This operation leads to the expression of the velocity component of the fluid particle tangent to the substrate as an ordinary differential equation of its height, that we later solve using power series at the lubrication approximation order ( $\mathcal{O}(\epsilon^2)$ ); the quantity  $\epsilon$  represents the ratio between the substrate tangential length scale and the height scale and is assumed to be very small. The final equation which expresses the height's evolution of the film is obtained by rewriting the conservation of mass in the curvilinear coordinate system using the derived equation of the velocity component parallel to the substrate. We chose a surfactant diffusion equation model adopted by Stone in [113] to describe the evolution of the surfactant on the free surface interface. Previous work in this domain include the work of Roy, Roberts and Simpson in [107], which models the thin film on static curved surface using center manifold theory and computer algebra. Howell in [67], models thin film on evolving curved surfaces. In fact, he is only able to derived equations specific to particular phases of the evolution corresponding to the status of the surface. The most recent work in the domain is probably the work of Uwe Fermum, who in his PhD thesis [48] derived an equation describing the evolution of the film density on the evolving curved surface using a weak formulation. Our model here coincides with the model in [107] on fixed surfaces and is more precise than the model in [67] when applicable. Finally in Chapter IV we extend our finite volume method described in Chapter II for the simulation of the fourth order system of degenerated equations obtained here. In particular we combine the operator splitting procedure adopted in [62], the convection splitting procedure in [57] with our finite volume methodology to derive a conservative and less dissipative scheme for the simulation of a fourth order problem. The surfactant equation is transformed to a convection diffusion equation on a ghost free surface displacing only in the normal direction, and an appropriate projection of the scheme in Chapter II on the free surface ensures it discretization. To the best of our knowledge, there is no work treating this simulation in the literature. We end the thesis with a concluding remark. Let us mention that in order to keep the chapters self-contained, we will be repeating some important notions.





Part I

# Finite volume method on evolving surfaces



# 1 A convergent finite volume scheme for diffusion on evolving surfaces

## 1.1 Introduction

In many applications in material science, biology and geometric modeling, evolution problems do not reside on a flat Euclidean domain but on a curved hypersurface. Frequently, this surface is itself evolving in time driven by some velocity field. In general, the induced transport is not normal to the surface but incorporates a tangential motion of the geometry and thus a corresponding tangential advection process on the evolving surface. In [37] Dziuk and Elliot proposed a finite element scheme for the numerical simulation of diffusion processes on such evolving surfaces. In this chapter, we pick up the finite volume methodology introduced by Eymard, Gallouët, and Herbin in [45] on fixed Euclidean domains and discuss a generalization in case of transport and diffusion processes on curved and evolving surfaces. The general motivation for a finite volume formulation is the potential of a further extension to coupled diffusion and dominating nonlinear advection models. Here, we restrict to linear transport.

Applications of the considered model are the diffusion of densities on biological membranes or reaction diffusion equations for texture generation on surfaces [120]. Frequently, partial differential equations on the surface are coupled to the evolution of the geometry itself. Examples are the spreading of thin liquid films or coatings on surfaces [107], transport and diffusion of a surfactant on interfaces in multiphase flow [73], surfactant driven thin film flow [60] on the enclosed surface of lung alveoli coupled with the expansion or contraction of the alveoli, and diffusion induced grain boundary motion [17]. In this chapter, we assume the evolution of the surface to be given a priori and study the finite volume discretization of diffusion on the resulting family of evolving surfaces as a model problem. The evolving surfaces are discretized by simplicial meshes, where grid nodes are assumed to be transported along motion trajectories of the underlying flow field. The approach applies to evolving polygonal curves and triangulated surfaces. In the presentation we focus on the case of moving two-dimensional surfaces. Finite volume methods on curved geometries have been discussed recently in [19, 33], but to the best of our knowledge they have so far not been analyzed on evolving surfaces.

An alternative approach would be to consider a level set representation via an evolving level set function. In this case, projections of the derivatives onto the embedded tangent space provide a mechanism for computing geometric differential operators [10] on fixed level set surfaces. Finite elements in this context are discussed in [16], a narrow band approach with a very thin fitted mesh is presented in [30], and in [56] an improved approximation of tangential differential operators is presented. Furthermore, in [38] a finite element level set method is introduced for the solution of parabolic PDEs on a family of evolving implicit surfaces.

Our finite volume method is closely related to the finite element approach by Dziuk and Elliott [37]. They consider a moving triangulation, where the nodes are propagating with the actual motion velocity, which effectively leads to space time finite element basis functions similar to the Eulerian-Lagrangian localized adjoint method (ELLAM) approach [65]. We consider as well a family of triangulated surfaces with nodes located on motion trajectories where the triangles are treated as finite volume cells. The resulting scheme immediately incorporates mass conservation. An overview on computational approaches which use moving meshes to solve PDEs is given in [89]. Here, the moving mesh reflects the Eulerian coordinates underlying the evolution problem but on a fixed

computational domain.

The chapter is organized as follows. In Section 1.2, the mathematical model is discussed, and in Section 1.3 we derive the finite volume scheme on simplicial grids. Discrete a priori estimates consistently formulated in terms of the evolving geometry are established in Section 1.4. In Section 1.5 we state and prove the main convergence result. Finally, Section 1.6 discusses an operator splitting scheme for the coupling of diffusive and advective transport so far not encoded in the surface motion itself, and in Section 1.7 numerical results are presented.

## 1.2 Mathematical model

We consider a family of compact, smooth, and oriented hypersurfaces  $\Gamma(t) \subset \mathbb{R}^n$  ( $n = 2, 3$ ) for  $t \in [0, t_{max}]$  generated by an evolution  $\Phi : [0, t_{max}] \times \Gamma^0 \rightarrow \mathbb{R}^n$  defined on a reference surface  $\Gamma^0$  with  $\Phi(t, \Gamma^0) = \Gamma(t)$ . Let us assume that  $\Gamma^0$  is  $C^3$  smooth and that  $\Phi \in C^1([0, t_{max}], C^3(\Gamma_0))$ . For simplicity we assume the reference surface  $\Gamma^0$  to coincide with the initial surface  $\Gamma(0)$  (cf. Figure 1.5).

We denote by  $v = \partial_t \Phi$  the velocity of material points and assume the decomposition  $v = v_n \nu + v_{tan}$  into a scalar normal velocity  $v_n$  in direction of the surface normal  $\nu$  and a tangential velocity  $v_{tan}$ . The evolution of a conservative material quantity  $u$  with  $u(t, \cdot) : \Gamma(t) \rightarrow \mathbb{R}$ , which is propagated with the surface and simultaneously undergoes a linear diffusion on the surface, is governed by the parabolic equation

$$\dot{u} + u \nabla_{\Gamma} \cdot v - \nabla_{\Gamma} \cdot (\mathcal{D} \nabla_{\Gamma} u) = g \quad \text{on } \Gamma = \Gamma(t), \quad (1.1)$$

where  $\dot{u} = \frac{d}{dt} u(t, x(t))$  is the (advective) material derivative of  $u$ ,  $\nabla_{\Gamma} \cdot v$  the surface divergence of the vector field  $v$ ,  $\nabla_{\Gamma} u$  the surface gradient of the scalar field  $u$ ,  $g$  a source term with  $g(t, \cdot) : \Gamma(t) \rightarrow \mathbb{R}$ , and  $\mathcal{D}$  is a diffusion tensor on the tangent bundle. Here we assume a symmetric, uniformly coercive  $C^2$  diffusion tensor field on whole  $\mathbb{R}^n$  to be given, whose restriction on the tangent plane is then effectively incorporated in the model. With a slight misuse of notation, we denote this global tensor field also by  $\mathcal{D}$ . Furthermore, we impose an initial condition  $u(0, \cdot) = u_0$  at time 0. Let us assume that the mappings  $(t, x) \rightarrow u(t, \Phi(t, x))$ ,  $v(t, \Phi(t, x))$ , and  $g(t, \Phi(t, x))$  are  $C^1([0, t_{max}], C^3(\Gamma_0))$ ,  $C^0([0, t_{max}], C^3(\Gamma_0))$ , and  $C^1([0, t_{max}], C^1(\Gamma_0))$  regular, respectively. For the ease of presentation we restrict here to the case of a closed surface without boundary. Our results can easily be generalized to surfaces with boundary, on which we either impose a Dirichlet or Neumann boundary condition. For a discussion of existence, uniqueness, and regularity of solutions we refer to [37] and the references therein.

## 1.3 Derivation of the finite volume scheme

For the ease of presentation, we restrict ourselves to the case of two-dimensional surfaces in  $\mathbb{R}^3$ . A generalization of the numerical analysis presented here is straightforward. We consider a sequence of regular surface triangulations interpolating  $\Gamma(t_k)$  for  $t_k = k\tau$  and  $k_{max}\tau = t_{max}$  (cf. Dziuk and Elliott [37] for the same setup with respect to a finite element discretization). Here,  $h$  indicates the maximal diameter of a triangle on the whole sequence of triangulations,  $\tau$  is the time step size, and  $k$  is the index of a time step. All triangulations share the same grid topology, and given the set of vertices  $x_j^0$  on the initial triangular surface  $\Gamma_h^0$ , the vertices of  $\Gamma_h^k$  lie on motion trajectories. Thus, they are evaluated based on the flux function  $\Phi$ , i.e.,  $x_j(t_k) = \Phi(t_k, x_j^0)$  (cf. Figure 1.1). Single closed triangles or edges of the topological grid  $\Gamma_h$  are denoted by  $S$  and  $\sigma$ , respectively. Upper indices denote the explicit geometric realization at the corresponding time step.

Thus, a closed triangle of the triangulated surface geometry  $\Gamma_h^k$  is denoted by  $S^k$ . We assume that the triangulations  $\Gamma_h^k$  are regular; i.e., there exist constants  $c, C > 0$  such that  $ch^2 \leq m_S^k \leq Ch^2$  for all  $S$  and all  $k$ , where  $m_S^k$  denotes the area of  $S^k$ . As in the Euclidean case discussed in [45],

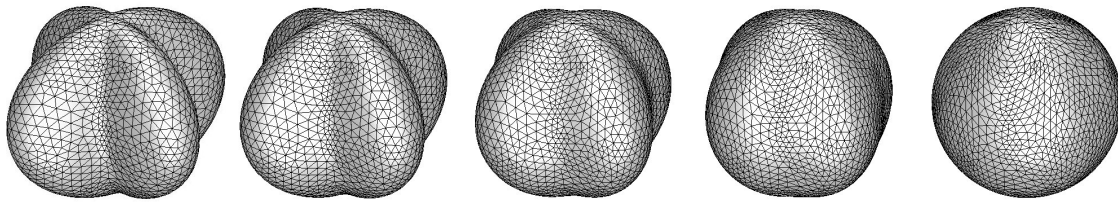


Figure 1.1: Sequence of triangulations  $\Gamma_h^k$  interpolating a fourfold symmetric object in its evolution.

we also assume that for all time steps  $t_k$ , where  $k = 0, \dots, k_{max}$ , and all simplices  $S^k \subset \Gamma_h^k$  there exists a point  $X_S^k \in S^k$  and for each edge  $\sigma^k \subset \partial S^k$  a point  $X_\sigma^k \in \sigma^k$  such that the vector  $\overrightarrow{X_S^k X_\sigma^k}$  is perpendicular to  $\sigma^k$  with respect to the scalar product induced by the inverse of the diffusion tensor on the triangle  $S^k$  at the point  $X_\sigma^k$ , i.e.,

$$(\mathcal{D}(X_\sigma^k))^{-1}(X_S^k - X_\sigma^k) \cdot V = 0, \quad (1.2)$$

where  $V$  is a vector parallel to the edge  $\sigma^k$ . Furthermore, we assume that these points can be chosen such that for two adjacent simplices  $S^k$  and  $L^k$  the corresponding points on the common edge  $\sigma^k = S^k \cap L^k$  coincide (cf. Figure 1.2). The point  $X_S^{k+1}$  at the following time step need not be the consistently transported point  $X_S^k$  under the flow  $\Phi$ . It will turn out that for the error analysis the later stated condition (1.16) is sufficient. This allows us to choose the points  $X_S^k$  in a way that fulfills these requirements without changing the grid topology between time steps, as described in the paragraph after equation (1.16). For a later comparison of discrete quantities on the triangulation  $\Gamma_h^k$

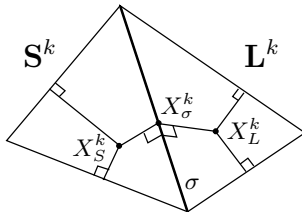


Figure 1.2: A sketch of the local configuration of points  $X_S^k$ ,  $X_L^k$ , and  $X_\sigma^k$  on two adjacent simplices  $S^k$  and  $L^k$ , which in general do not lie in the same plane.

and continuous quantities on  $\Gamma(t_k)$  we define a lifting operator from  $\Gamma_h^k$  onto  $\Gamma(t_k)$  via the orthogonal projection  $\mathcal{P}^k$  onto  $\Gamma(t_k)$  in direction of the surface normal  $\nu$  of  $\Gamma(t_k)$ . For sufficiently small  $h$  this projection is uniquely defined and smooth; we also assume it to be bijective. By  $S^{l,k} := \mathcal{P}^k S^k$  we define the projection of a triangle  $S^k$  on  $\Gamma(t_k)$  and by  $S^{l,k}(t) := \Phi(t, \Phi^{-1}(t_k, S^{l,k}))$  the temporal evolution of  $S^{l,k}$ , which we will take into account for  $t \in [t_k, t_{k+1}]$ . Furthermore, we can estimate the relative change of area of triangles by  $m_S^{k+1} = m_S^k(1 + O(\tau))$  for all simplices  $S^k$  and all  $k$  because of the smoothness of the flux function  $\Phi$ .

Based on these notational preliminaries, we can now derive a suitable finite volume discretization. Thus, let us integrate (1.1) on  $\{(t, x) \mid t \in [t_k, t_{k+1}], x \in S^{l,k}(t)\}$ :

$$\int_{t_k}^{t_{k+1}} \int_{S^{l,k}(t)} g \, da \, dt \approx \tau m_S^{k+1} G_S^{k+1}, \quad (1.3)$$

where  $G_S^{k+1} = g(t_{k+1}, \mathcal{P}^{k+1} X_S^{k+1})$ . Using the Leibniz formula  $\frac{d}{dt} \int_{S^{l,k}(t)} u \, da = \int_{S^{l,k}(t)} \dot{u} + u \nabla_{\Gamma} \cdot \nu \, da$

(cf. [37]), we obtain for the material derivative

$$\begin{aligned} \int_{t_k}^{t_{k+1}} \int_{S^{l,k}(t)} \dot{u} + u \nabla_{\Gamma} \cdot v \, da \, dt &= \int_{S^{l,k}(t_{k+1})} u \, da - \int_{S^{l,k}(t_k)} u \, da \\ &\approx m_S^{k+1} u(t_{k+1}, \mathcal{P}^{k+1} X_S^{k+1}) - m_S^k u(t_k, \mathcal{P}^k X_S^k). \end{aligned} \quad (1.4)$$

Next, integrating the elliptic term again over the temporal evolution of a lifted triangular patch and applying Gauss's theorem we derive the following approximation:

$$\begin{aligned} \int_{t_k}^{t_{k+1}} \int_{S^{l,k}(t)} \nabla_{\Gamma} \cdot (\mathcal{D} \nabla_{\Gamma} u) \, da \, dt &= \int_{t_k}^{t_{k+1}} \int_{\partial S^{l,k}(t)} \mathcal{D} \nabla_{\Gamma} u \cdot n_{\partial S^{l,k}(t)} \, dl \, dt \\ &\approx \tau \sum_{\sigma \subset \partial S} m_{\sigma}^{k+1} \lambda_{S|\sigma}^{k+1} \frac{u(t_{k+1}, \mathcal{P}^{k+1} X_{\sigma}^{k+1}) - u(t_k, \mathcal{P}^{k+1} X_S^{k+1})}{d_{S|\sigma}^{k+1}}, \end{aligned} \quad (1.5)$$

where  $n_{\partial S^{l,k}(t)}$  is the unit outer conormal on  $\partial S^{l,k}(t)$  tangential to  $\Gamma(t)$ ,  $\sigma^{k+1}$  an edge of  $S^{k+1}$ ,  $m_{\sigma}^{k+1}$  the length of  $\sigma^{k+1}$ ,  $d_{S|\sigma}^{k+1} := \|X_S^{k+1} - X_{\sigma}^{k+1}\|$ , and  $\lambda_{S|\sigma}^{k+1} := \|\mathcal{D}_{S|\sigma}^{k+1} n_{S|\sigma}^{k+1}\|$ . The discrete diffusion tensor is defined by  $\mathcal{D}_{S|\sigma}^{k+1} := (P_S^{k+1})^T \mathcal{D}(X_{\sigma}^{k+1}) P_S^{k+1}$ , where  $P_S^{k+1}$  is the orthogonal projection onto the plane given by  $S^{k+1}$  and  $n_{S|\sigma}^{k+1}$  is the unit outer conormal to  $S^{k+1}$  on the edge  $\sigma$ . Indeed, the orthogonality assumption (1.2) implies that  $(X_{\sigma}^{k+1} - X_S^{k+1})$  is parallel to  $\mathcal{D}_{S|\sigma}^{k+1} n_{S|\sigma}^{k+1}$ . Hence,  $\nabla_{\Gamma} u \cdot n_{\partial S^{l,k}(t)}$  can consistently be approximated by the difference quotient  $\lambda_{S|\sigma}^{k+1} \frac{u(t_{k+1}, \mathcal{P}^{k+1} X_{\sigma}^{k+1}) - u(t_k, \mathcal{P}^{k+1} X_S^{k+1})}{d_{S|\sigma}^{k+1}}$ .

Alternatively, one could introduce a diffusion tensor  $\mathcal{D}_S^{k+1} := (P_S^{k+1})^T \mathcal{D}(X_S^{k+1}) P_S^{k+1}$  on triangles and modify (1.2) and the definition of  $\lambda_{S|\sigma}^{k+1}$  accordingly. We will comment on this alternative approach in the context of the convergence analysis in Section 1.5.2.

Now we introduce discrete degrees of freedom  $U_S^k$  and  $U_{\sigma}^k$  for  $u(\mathcal{P}^k X_S^k)$  and  $u(\mathcal{P}^k X_{\sigma}^k)$ , respectively. The values  $U_S^k$  are the actual degrees of freedom; they will be compiled into a function  $U^k$  that is constant on each cell  $S^k$  and is an element of the discrete solution space  $\mathcal{V}_h^k$  which is defined in (1.8) below. The  $U_{\sigma}^k$  are only auxiliary degrees of freedom; cf. (1.6). Then the discrete counterpart of the continuous flux balance

$$\int_{S^{l,k}(t) \cap L^{l,k}(t)} (\mathcal{D} \nabla_{\Gamma} u)|_{S^{l,k}(t)} \cdot n_{\partial S^{l,k}(t)} \, da = - \int_{S^{l,k}(t) \cap L^{l,k}(t)} (\mathcal{D} \nabla_{\Gamma} u)|_{L^{l,k}(t)} \cdot n_{\partial L^{l,k}(t)} \, da$$

on  $S^{l,k}(t) \cap L^{l,k}(t)$  for two adjacent simplices  $S^k$  and  $L^k$  is given by

$$m_{\sigma}^{k+1} \frac{U_{\sigma}^{k+1} - U_S^{k+1}}{d_{S|\sigma}^{k+1}} \lambda_{S|\sigma}^{k+1} = -m_{\sigma}^{k+1} \frac{U_{\sigma}^{k+1} - U_L^{k+1}}{d_{L|\sigma}^{k+1}} \lambda_{L|\sigma}^{k+1}$$

for the edge  $\sigma^k = S^k \cap L^k$ . Let us emphasize that this flux balance holds independently of the tilt of  $S^k$  and  $L^k$  at  $\sigma^k$ . Hence, we can cancel out the degrees of freedom

$$U_{\sigma}^{k+1} = \frac{U_S^{k+1} d_{L|\sigma}^k \lambda_{S|\sigma}^k + U_L^{k+1} d_{S|\sigma}^k \lambda_{L|\sigma}^k}{d_{L|\sigma}^k \lambda_{S|\sigma}^k + d_{S|\sigma}^k \lambda_{L|\sigma}^k} \quad (1.6)$$

on edges and based on the approximations for the parabolic term in (1.4) and the elliptic term in (1.5), we finally obtain the finite volume scheme

$$m_S^{k+1} U_S^{k+1} - m_S^k U_S^k - \tau \sum_{\sigma \subset \partial S} m_{\sigma}^{k+1} \mathcal{M}_{\sigma}^{k+1} \frac{U_L^{k+1} - U_S^{k+1}}{d_{S|L}^{k+1}} = \tau m_S^{k+1} G_S^{k+1}, \quad (1.7)$$

$$\text{where } \mathcal{M}_{\sigma}^k := \frac{\lambda_{S|\sigma}^k \lambda_{L|\sigma}^k d_{S|L}^k}{d_{L|\sigma}^k \lambda_{S|\sigma}^k + d_{S|\sigma}^k \lambda_{L|\sigma}^k}, \quad d_{S|L}^k := d_{S|\sigma}^k + d_{L|\sigma}^k.$$

This requires the solution of a linear system of equations for the cellwise solution values  $U_S^{k+1}$  for  $k = 0, \dots, k_{max} - 1$  and for given initial data  $U_S^0$  at time  $t_0 = 0$ .

REMARK. Different from the finite volume method on Euclidean domains in [45], all coefficients depend on the geometric evolution and thus in particular change in time. A comparison of the discrete and continuous solution requires a mapping from the sequence of triangulations  $\{\Gamma_h^k\}$  onto the continuous family of surfaces  $\{\Gamma(t)\}_{t \in [0, t_{max}]}$ .

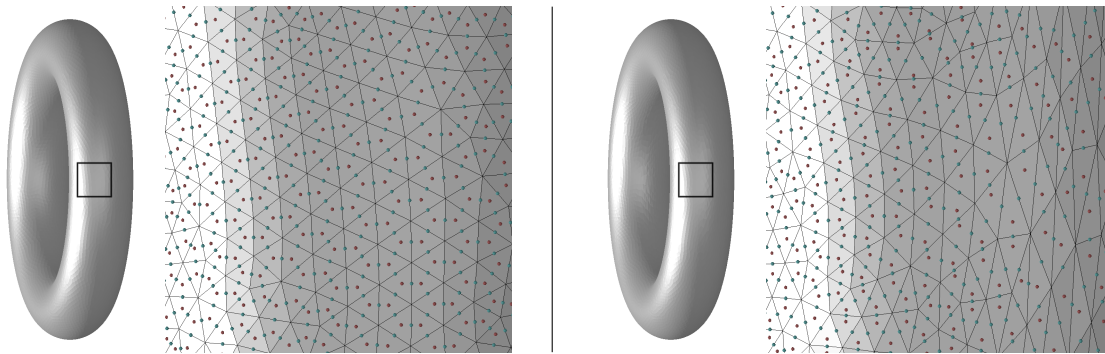


Figure 1.3: On the left an isotropic mesh for a torus is shown together with a zoom in with indicated points  $X_S^k$  on the triangles and  $X_\sigma^k$  on edges. On the right an anisotropic mesh corresponding to an anisotropic diffusion tensor  $\mathcal{D} = \text{diag}(\frac{1}{25}, 1, 1)$  is rendered together with the corresponding zoom. One observes in the blow up of the anisotropic mesh geometry a transition from the strongly anisotropic regime close to the center plane of the torus on the right and the more isotropic mesh on the left.

Figure 1.3 shows two different triangulations of a (rotating) torus (cf. Figure 1.7, 1.8, and 1.9 below for corresponding numerical results). In the first case the underlying diffusion is isotropic; hence an isotropic mesh is used for the simulation of the evolution problem. In the second case an anisotropic diffusion tensor  $\mathcal{D} = \text{diag}(\frac{1}{25}, 1, 1)$  is taken into account. To enable the definition of consistent triangle nodes  $X_S^k$  and edge nodes  $X_\sigma^k$ , an anisotropic mesh has been generated. Even though  $\mathcal{D}$  is constant on  $\mathbb{R}^{3,3}$ , the induced tangential diffusivity varies on the surface. This variation is properly reflected by the generated mesh. We refer to Section 1.7 for some remarks on the mesh generation.

Let us associate with the components  $U_S^k$  on the simplices  $S^k$  of the triangulation  $\Gamma_h^k$  a piecewise constant function  $U^k$  with  $U^k|_{S^k} = U_S^k$ , and let

$$\mathcal{V}_h^k := \left\{ U^k : \Gamma_h^k \rightarrow \mathbb{R} \mid U^k|_{S^k} = \text{const} \quad \forall S^k \subset \Gamma_h^k \right\} \quad (1.8)$$

be the space of these functions on  $\Gamma_h^k$ . Analogously, we denote by  $G^k$  the corresponding piecewise constant function with  $G^k|_{S^k} = G_S^k$ . On the function space  $\mathcal{V}_h^k$ , we can define a discrete energy seminorm based on a weighted sum of squared difference quotients.

**Definition 1.3.1 (Discrete energy seminorm)** For  $U^k \in \mathcal{V}_h^k$  we define

$$\|U^k\|_{1, \Gamma_h^k} := \left( \sum_{\sigma=S \cap L} m_\sigma^k \mathcal{M}_\sigma^k \frac{(U_L^k - U_S^k)^2}{d_{S|L}^k} \right)^{\frac{1}{2}}. \quad (1.9)$$

Before we prove suitable a priori estimates, let us verify the existence and uniqueness of the discrete solution.

**Proposition 1.3.2** *The discrete problem (1.7) has a unique solution.*

**Proof** The system (1.7) has a unique solution  $U^{k+1}$  if the kernel of the corresponding linear operator is trivial. To prove this, we assume  $U^k \equiv 0$  and  $G^{k+1} \equiv 0$  in (1.7); then multiply each equation by the corresponding  $U_S^{k+1}$  for the triangle  $S^{k+1} \subset \Gamma_h^{k+1}$ . Summing up over all simplices and taking into account the symmetry of the second term in (1.7) with respect to the two simplices  $S^k$  and  $L^k$  intersecting at the edge  $\sigma^{k+1} = S^{k+1} \cap L^{k+1}$  we obtain

$$\|U^{k+1}\|_{\mathbb{L}^2(\Gamma_h^{k+1})}^2 + \tau \|U^{k+1}\|_{1,\Gamma_h^{k+1}}^2 = 0,$$

from which  $U^{k+1} = 0$  follows immediately. □

Indeed, Proposition 1.3.2 is a direct consequence of Theorem 1.4.1 to be proved in the next section.

## 1.4 A priori estimates

In what follows we will prove discrete counterparts of continuous a priori estimates. They are related to the discrete energy estimates given in [45] in the case of finite volume methods on fixed Euclidean domains.

**Theorem 1.4.1 (Discrete  $\mathbb{L}^\infty(\mathbb{L}^2)$ ,  $\mathbb{L}^2(\mathbb{H}^1)$  energy estimate)** *Let  $\{U^k\}_{k=1,\dots,k_{max}}$  be the discrete solution of (1.7) for given discrete initial data  $U^0 \in \mathcal{V}_h^0$ . Then there exists a constant  $C$  depending solely on  $t_{max}$  such that*

$$\max_{k=1,\dots,k_{max}} \|U^k\|_{\mathbb{L}^2(\Gamma_h^k)}^2 + \sum_{k=1}^{k_{max}} \tau \|U^k\|_{1,\Gamma_h^k}^2 \leq C \left( \|U^0\|_{\mathbb{L}^2(\Gamma_h^0)}^2 + \tau \sum_{k=1}^{k_{max}} \|G^k\|_{\mathbb{L}^2}^2 \right). \quad (1.10)$$

**Proof** As in the proof of Proposition 1.3.2, we multiply (1.7) by  $U_S^{k+1}$  for every cell  $S^k \in \Gamma_h^k$  and sum over all  $S^k \in \Gamma_h^k$  to obtain (again using the symmetry of the second term in (1.7))

$$\begin{aligned} & \sum_S \left( m_S^{k+1} (U_S^{k+1})^2 - m_S^k U_S^k U_S^{k+1} \right) + \tau \sum_{\sigma=S \cap L} m_\sigma^{k+1} \mathcal{M}_\sigma^{k+1} \frac{(U_L^{k+1} - U_S^{k+1})^2}{d_{S|L}^{k+1}} \\ &= \tau \sum_S m_S^{k+1} G_S^{k+1} U_S^{k+1}, \end{aligned} \quad (1.11)$$

which leads to

$$\begin{aligned} & \|U^{k+1}\|_{\mathbb{L}^2(\Gamma_h^{k+1})}^2 + \tau \|U^{k+1}\|_{1,\Gamma_h^{k+1}}^2 \\ & \leq \|U^k\|_{\mathbb{L}^2(\Gamma_h^k)} \max_S \left( \frac{m_S^k}{m_S^{k+1}} \right)^{\frac{1}{2}} \|U^{k+1}\|_{\mathbb{L}^2(\Gamma_h^{k+1})} + \tau \|G^{k+1}\|_{\mathbb{L}^2(\Gamma_h^{k+1})} \|U^{k+1}\|_{\mathbb{L}^2(\Gamma_h^{k+1})}. \end{aligned}$$



Then, by Young's inequality and the estimate  $\max_k \max_S \left| \frac{m_S^k}{m_S^{k+1}} - 1 \right| \leq C\tau$ , one obtains

$$\begin{aligned} & \frac{1}{2} \|U^{k+1}\|_{\mathbb{L}^2(\Gamma_h^{k+1})}^2 + \tau \|U^{k+1}\|_{1, \Gamma_h^{k+1}}^2 \\ & \leq \frac{1}{2} \|U^k\|_{\mathbb{L}^2(\Gamma_h^k)}^2 + \frac{C}{2} \tau \|U^{k+1}\|_{\mathbb{L}^2(\Gamma_h^{k+1})}^2 + \frac{1}{2} \tau \|G^{k+1}\|_{\mathbb{L}^2(\Gamma_h^{k+1})}^2. \end{aligned} \quad (1.12)$$

Using the notation  $a_k = \|U^k\|_{\mathbb{L}^2(\Gamma_h^k)}^2$  and  $b_k = \|G^k\|_{\mathbb{L}^2(\Gamma_h^k)}^2$ , one can deduce from  $a_k \leq a_{k-1} + C\tau a_k + \tau b_k$  that

$$a_k \leq (1 - C\tau)^{-1} (a_{k-1} + \tau b_k) \leq \dots \leq (1 - C\tau)^{-k} (a_0 + \tau \sum_{j=1}^k b_j).$$

Since

$$(1 - C\tau)^{-k} = \left( \left( 1 - \frac{Ct_k}{k} \right)^{-\frac{k}{Ct_k}} \right)^{Ct_k}$$

is bounded from above by  $2e^{Ct_k}$  for sufficiently small  $\tau$ , we immediately get the desired bound for  $\|U^k\|_{\mathbb{L}^2(\Gamma_h^k)}^2$ :

$$\|U^k\|_{\mathbb{L}^2(\Gamma_h^k)}^2 \leq 2e^{Ct_k} \left( \|U^0\|_{\mathbb{L}^2(\Gamma_h^0)}^2 + \tau \sum_{j=1}^k \|G^j\|_{\mathbb{L}^2}^2 \right).$$

We sum (1.12) over  $k = 0, \dots, k_{max} - 1$  and compensate the terms  $\|U^k\|_{\mathbb{L}^2(\Gamma_h^k)}^2$  on the right hand side for  $k = 1, \dots, k_{max} - 1$  with those on the left, and using the already established estimate for the  $\mathbb{L}^2$  norm gives the bound for  $\sum_{k=1}^{k_{max}} \tau \|U^k\|_{1, \Gamma_h^k}^2$ .

□

**Theorem 1.4.2 (Discrete  $\mathbb{H}^1(L^2)$ ,  $\mathbb{L}^\infty(H^1)$  energy estimate)** *Let  $\{U^k\}_{k=1, \dots, k_{max}}$  be the discrete solution of (1.11) with given initial data  $U^0$ . Then there exist a constant  $C$  such that*

$$\begin{aligned} & \sum_{k=1}^{k_{max}} \tau \|\partial_t^\tau U^k\|_{\mathbb{L}^2(\Gamma_h^k)}^2 + \max_{k=1, \dots, k_{max}} \|U^k\|_{1, \Gamma_h^k}^2 \\ & \leq C \left( \|U^0\|_{\mathbb{L}^2(\Gamma_h^0)}^2 + \|U^0\|_{1, \Gamma_h^0}^2 + \tau \sum_{k=1}^{k_{max}} \|G^k\|_{\mathbb{L}^2(\Gamma_h^k)}^2 \right), \end{aligned} \quad (1.13)$$

where  $\partial_t^\tau U^k := \frac{U^k - U^{k-1}}{\tau}$  is defined as a difference quotient in time.

**Proof** We multiply (1.7) by  $\partial_t^\tau U^{k+1}$  for every triangle  $S^k \in \Gamma_h^k$  and sum over all simplices to obtain

$$\begin{aligned} & \tau \sum_S m_S^{k+1} \left( \frac{U_S^{k+1} - U_S^k}{\tau} \right)^2 \\ & + \sum_{\sigma=S \cap L} m_\sigma^{k+1} \mathcal{M}_\sigma^{k+1} \left( d_{S|L}^{k+1} \left( \frac{U_L^{k+1} - U_S^{k+1}}{d_{S|L}^{k+1}} \right)^2 - \left( \frac{U_S^{k+1} - U_L^{k+1}}{d_{S|L}^{k+1}} \right) (U_S^k - U_L^k) \right) \\ & = \sum_S (m_S^k - m_S^{k+1}) U_S^k \left( \frac{U_S^{k+1} - U_S^k}{\tau} \right) + \tau \sum_S m_S^{k+1} G_S^{k+1} \left( \frac{U_S^{k+1} - U_S^k}{\tau} \right). \end{aligned}$$

Using the notation

$$a_{S|L}^k := \sqrt{d_{S|L}^k m_\sigma^k \mathcal{M}_\sigma^k} \left( \frac{U_S^k - U_L^k}{d_{S|L}^k} \right), \quad b_S^{k+1} := \sqrt{m_S^{k+1}} \left( \frac{U_S^{k+1} - U_S^k}{\tau} \right),$$

$$c_{S|L}^k := \sqrt{\frac{d_{S|L}^k m_\sigma^{k+1} \mathcal{M}_\sigma^{k+1}}{d_{S|L}^{k+1} m_\sigma^k \mathcal{M}_\sigma^k}},$$

this can be written as

$$\begin{aligned} \tau \sum_S (b_S^{k+1})^2 + \sum_{\sigma=S \cap L} \left( (a_{S|L}^{k+1})^2 - a_{S|L}^{k+1} c_{S|L}^k a_{S|L}^k \right) \\ = \sum_S \left( \frac{m_S^k}{m_S^{k+1}} - 1 \right) \frac{\sqrt{m_S^{k+1}}}{\sqrt{m_S^k}} \sqrt{m_S^k} U_S^k b_S^{k+1} + \tau \sum_S \sqrt{m_S^{k+1}} G_S^{k+1} b_S^{k+1}. \end{aligned}$$

Noting that

$$\left( a_{S|L}^{k+1} \right)^2 - a_{S|L}^{k+1} c_{S|L}^k a_{S|L}^k \geq \frac{1}{2} \left( \left( a_{S|L}^{k+1} \right)^2 - \left( a_{S|L}^k \right)^2 \right) + (1 - c_{S|L}^k) \left( \frac{\left( a_{S|L}^{k+1} \right)^2}{2} + \frac{\left( a_{S|L}^k \right)^2}{2} \right)$$

and

$$\sum_{\sigma=S \cap L} \left( a_{S|L}^k \right)^2 = \|U^k\|_{1, \Gamma_h^k}^2, \quad \sum_S (b_S^k)^2 = \|\partial_t^\tau U^{k+1}\|_{\mathbb{L}^2(\Gamma_h^{k+1})}^2,$$

we apply Cauchy's inequality and Young's inequality, and we finally obtain

$$\begin{aligned} \tau \|\partial_t^\tau U^{k+1}\|_{\mathbb{L}^2(\Gamma_h^{k+1})}^2 + \frac{1}{2} \|U^{k+1}\|_{1, \Gamma_h^{k+1}}^2 - \frac{1}{2} \|U^k\|_{1, \Gamma_h^k}^2 \\ \leq C\tau \left( \|U^{k+1}\|_{1, \Gamma_h^{k+1}}^2 + \|U^k\|_{1, \Gamma_h^k}^2 \right. \\ \left. + \left( \|U^k\|_{\mathbb{L}^2(\Gamma_h^k)} + \|G^{k+1}\|_{\mathbb{L}^2(\Gamma_h^{k+1})} \right) \|\partial_t^\tau U^{k+1}\|_{\mathbb{L}^2(\Gamma_h^{k+1})} \right). \quad (1.14) \end{aligned}$$

Here, we have taken into account that  $|1 - c_{S|L}^k| \leq C\tau$  and  $|1 - \frac{m_S^k}{m_S^{k+1}}| \frac{\sqrt{m_S^{k+1}}}{\sqrt{m_S^k}} \leq C\tau$ . Next, as in Theorem 1.4.1 we apply Young's inequality, sum over all time steps and obtain

$$\begin{aligned} \sum_{k=1}^{k_{max}} \left( \frac{\tau}{2} \|\partial_t^\tau U^k\|_{\mathbb{L}^2(\Gamma_h^k)}^2 + \frac{1}{2} \|U^k\|_{1, \Gamma_h^k}^2 - \frac{1}{2} \|U^0\|_{1, \Gamma_h^0}^2 \right) \\ \leq \frac{C}{2} \tau \sum_{k=1}^{k_{max}} \left( \|U^k\|_{1, \Gamma_h^k}^2 + \|U^{k-1}\|_{1, \Gamma_h^{k-1}}^2 + \|U^{k-1}\|_{\mathbb{L}^2(\Gamma_h^{k-1})}^2 + \|G^k\|_{\mathbb{L}^2(\Gamma_h^k)}^2 \right). \quad (1.15) \end{aligned}$$

Finally, an application of Theorem 1.4.1 leads us to the desired estimate.

□

## 1.5 Convergence

In this section we will prove an error estimate for the finite volume solution  $U^k \in \mathcal{V}_h^k$ . At first, we have to state how to compare a discrete solution defined on the sequence of triangulations  $\Gamma_h^k$  and the continuous solution defined on the evolving family of smooth surfaces  $\Gamma(t)$ . Here, we will take into account the lifting operator from the discrete surfaces  $\Gamma_h^k$  onto the continuous surfaces  $\Gamma(t_k)$  already introduced in Section 1.3. As for the error analysis of a finite element approach in [37], we use a pull back from the continuous surface onto a corresponding triangulation to compare the continuous solution  $u(t_k)$  at time  $t_k$  with the discrete solution  $U^k = \sum_S U_S^k \chi_{S^k}$ , where  $\chi_{S^k}$  indicates the characteristic function of the triangle  $S^k$ . In explicit, we consider the pull back of the continuous solution  $u$  at time  $t_k$  under this lift  $u^{-l}(t_k, X_S^k) := u(t_k, \mathcal{P}^k(X_S^k))$  and investigate the error  $u^{-l}(t_k, X_S^k) - U_S^k$  at the cell nodes  $X_S^k$  as the value of a piecewise constant error function on the associated cells  $S^k$ .

Obviously, the consistency of the scheme depends on the behavior of the mesh during the evolution and a proper, in particular, time coherent choice of the nodes  $X_S^k$ . Let us assume that

$$|\Upsilon^{k,k+1}(X_S^k) - X_S^{k+1}| \leq Ch\tau, \quad (1.16)$$

where  $\Upsilon^{k,k+1}(X_S^k)$  denotes the point on  $S^{k+1}$  with the same barycentric coordinates on  $S^{k+1}$  as the node  $X_S^k$  on  $S^k$ . (cf. (1.19) below). This condition is obviously true for  $X_S^k$  being the orthocenter of  $S^k$ , which is admissible for  $\mathcal{D} = \text{Id}$  on acute meshes. In case of an anisotropic diffusivity or nonacute meshes, one chooses nodes  $X_S^k$  close to the barycenters in the least square sense, given the orthogonality relation (1.2). Algorithmically, a mesh optimization strategy enables a corresponding choice of nodes (cf. Section 1.7).

Finally, the following convergence theorem holds.

**Theorem 1.5.1 (Error estimate)** *Suppose that the assumptions listed in Section 1.2 and 1.3 and in (1.16) hold, and define the piecewise constant error functional on  $\Gamma_h^k$  for  $k = 1, \dots, k_{max}$*

$$E^k := \sum_S (u^{-l}(t_k, X_S^k) - U_S^k) \chi_{S^k}$$

*measuring the defect between the pull back  $u^{-l}(t_k, \cdot)$  of the continuous solution  $u(t_k, \cdot)$  of (1.1) at time  $t_k$  and the finite volume solution  $U^k$  of (1.7). Thus, the error function  $E^k$  is actually an element of the same space  $\mathcal{V}_h^k$  of piecewise constant functions on  $\Gamma_h^k$  as the discrete solutions  $U^k$ ; cf. (1.8). Furthermore, let us assume that  $\|E^0\|_{\mathbb{L}^2(\Gamma_h^k)} \leq Ch$ . Then the error estimate*

$$\max_{k=1, \dots, k_{max}} \|E^k\|_{\mathbb{L}^2(\Gamma_h^k)}^2 + \tau \sum_{k=1}^{k_{max}} \|E^k\|_{1, \Gamma_h^k}^2 \leq C(h + \tau)^2 \quad (1.17)$$

*holds for a constant  $C$  depending on the regularity assumptions and the time  $t_{max}$ .*

This error estimate is a generalization of the estimate given in [45], where the same type of first order convergence with respect to the time step size and the grid size are established for a finite volume scheme on a fixed planar domain. As usual in the context of finite volume schemes, the convergence proof is based on consistency estimates for the difference terms in the discrete scheme (1.7). In the context of evolving surfaces considered here, these consistency errors significantly rely on geometric approximation estimates. Thus, Section 1.5.1 we first investigate a set of relevant geometric estimates. Afterwards, in Section 1.5.2 these estimates will be used to establish suitable consistency results. Finally, the actual convergence result is established in Section 1.5.3.

### 1.5.1 Geometric approximation estimates

In this paragraph, we first extend the definition of the projection  $\mathcal{P}^k$  to a time continuous operator  $\mathcal{P}(t, \cdot)$  which, for each  $t \in [0, t_{max}]$ , projects points orthogonally onto  $\Gamma(t)$  (cf. Figure 1.5.1). This operator is well defined in a neighborhood of  $\Gamma(t)$ .

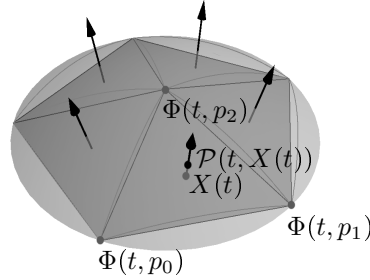


Figure 1.4: In a sketch we depict here a fan of evolving triangles, the transported vertices  $\Phi(t, p_0)$ ,  $\Phi(t, p_1)$ , and  $\Phi(t, p_2)$  of one specific moving triangle  $S^k(t)$ , and the projection  $\mathcal{P}(t, X(t))$  of a point  $X(t)$  in  $S^k(t)$  onto  $\Gamma(t)$ .

We denote by  $p_0, p_1, p_2$  the vertices of a triangle  $S^k$ , and we consider  $\xi_0(x), \xi_1(x), \xi_2(x)$  the barycentric coordinates of a point  $x$  on  $S^k$ ; i.e.,  $x = \xi_0(x)p_0 + \xi_1(x)p_1 + \xi_2(x)p_2$  and  $\xi_0(x) + \xi_1(x) + \xi_2(x) = 1$ . Furthermore, let us now introduce the time continuous lift

$$\Psi^k(t, \cdot) : S^k \longrightarrow S^{l,k}(t), \quad x \longmapsto \Psi^k(t, x) = \Phi(t, \Phi^{-1}(t_k, \mathcal{P}^k(x))) \quad (1.18)$$

and the discrete surface evolution

$$\Upsilon^k(t, \cdot) : S^k \longrightarrow S^k(t), \quad x \longmapsto \sum_{i=0}^2 \xi_i(x) \Psi^k(t, p_i), \quad (1.19)$$

which will be used to go back and forth between evolving domains  $\Gamma(t)$  and the evolving discrete surface  $\Gamma_h(t)$ , where  $S^k(t)$  is the triangle generated via the motion of the vertices  $p$  of  $S^k$  along the trajectories  $\Phi(\cdot, p)$  and  $\Gamma_h(t)$  the time continuous triangular surface consisting of these simplices.

Let us remark that  $\Upsilon^{k,k+1}(X_S^k)$  in condition (1.16) equals  $\Upsilon^k(t_{k+1}, X_S^k)$ . Figure 1.5.1 depicts a

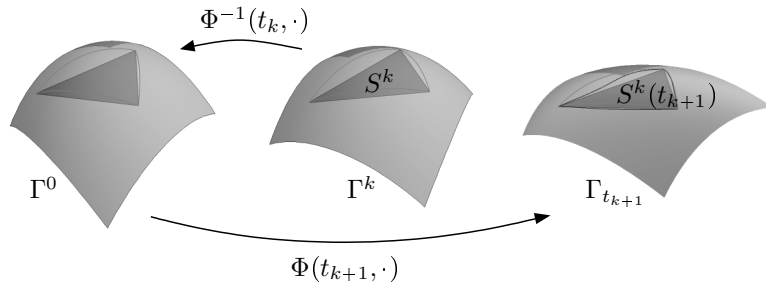


Figure 1.5: A single triangle and the nearby surface patch are shown in the initial configuration and at two consecutive time steps.

sketch of the involved geometric configuration. It is also important to notice here that the smoothness of these functions depends only on the regularity of  $\Phi(\cdot, \cdot)$ .

We now introduce an estimate for the distance between the continuous surface and the triangulation and for the ratio between cell areas and their lifted counterparts.

**Lemma 1.5.2** *Let  $d(t, x)$  be the signed distance from a point  $x$  to the surface  $\Gamma(t)$ , taking to be positive in the direction of the surface normal  $\nu$ , and let  $m_S^{l,k}$  denote the measure of the lifted triangle  $S^{l,k}$ ,  $m_\sigma^{l,k}$  the measure of the lifted edge  $\sigma^{l,k}$ . Then the estimates*

$$\sup_{0 \leq t \leq t_{max}} \|d(t, \cdot)\|_{L^\infty(\Gamma_h(t))} \leq Ch^2, \sup_{k,S} \left| 1 - \frac{m_S^{l,k}}{m_S^k} \right| \leq Ch^2, \sup_{k,\sigma} \left| 1 - \frac{m_\sigma^{l,k}}{m_\sigma^k} \right| \leq Ch^2$$

hold for a constant  $C$  depending only on the regularity assumptions.

**Proof** Notice that the function  $d(t, \cdot)$  is zero at vertices of the triangulation. Thus the piecewise affine Lagrangian interpolation of  $d(t, \cdot)$  vanishes, and the first estimate immediately follows from standard interpolation estimates. Using the smoothness of  $d$  and the fact that, because of the regularity of the mesh, the normal direction on each triangle differs from the normals to the respective curved triangle only to the order  $h$ , we deduce from  $\nabla_{\Gamma(t)} d(t, \cdot) = 0$  on  $\Gamma(t)$  that  $\|\nabla_{S^k(t)} d(t, \cdot)\|_{L^\infty(\Gamma_h(t))} \leq Ch$ , where  $\nabla_{S^k(t)} d(t, \cdot)$  is the component of  $\nabla d(t, \cdot)$  tangential to  $S^k(t)$ . For the second estimate, we fix a triangle  $S^k$  and assume without any restriction that  $S^k \subset \{(\xi, 0) \mid \xi \in \mathbb{R}^2\}$ . Furthermore, we extend the projection  $\mathcal{P}^k$  onto a neighborhood of  $S^k$  in the following way:

$$\mathcal{P}_{ext}^k(\xi, \zeta) = (\xi, 0) + (\zeta - d(t_k, (\xi, 0))) \nabla d^T(t_k, (\xi, 0)).$$

Obviously,  $\mathcal{P}_{ext}^k = \mathcal{P}^k$  on  $S^k$ . From  $|d(t_k, (\xi, 0))| \leq Ch^2$  and  $|\nabla_{S^k} d(t_k, (\xi, 0))| \leq Ch$ , we deduce that

$$|\det(D\mathcal{P}_{ext}^k(\xi, 0))| - 1 \leq Ch^2,$$

where  $D\mathcal{P}_{ext}^k$  denotes the Jacobian of  $\mathcal{P}_{ext}^k$ . Hence, taking into account that the third column of the Jacobian  $\partial_\zeta \mathcal{P}_{ext}^k(\xi, 0) = \nabla d^T(t_k, (\xi, 0))$  has length 1 and is normal to  $\Gamma(t_k)$  at  $\mathcal{P}^k(\xi, 0)$ , we observe that  $|\det(D\mathcal{P}_{ext}^k(\xi, 0))|$  controls the transformation of area under the projection  $\mathcal{P}^k$  from  $S^k$  to  $S^{l,k}$ , which proves the claim.

The third estimate follows along the same line as the second estimate based on a straightforward adaptation of the argument.

□

Next, we control the area defect between a transported lifted versus a lifted transported triangle.

**Lemma 1.5.3** *For each triangle  $S^k$  on  $\Gamma_h^k$  and all  $x$  in  $S^k$  the estimate*

$$|\mathcal{P}(t, \Upsilon^k(t, x)) - \Psi^k(t, x)| \leq C\tau h^2$$

holds for a constant  $C$  depending only the regularity assumptions. Furthermore, for the symmetric difference between  $S^{l,k}(t_{k+1})$  and  $S^{l,k+1}$  with  $A\Delta B := (A \setminus B) \cup (B \setminus A)$  one obtains

$$\mathcal{H}^{n-1}(S^{l,k}(t_{k+1})\Delta S^{l,k+1}) \leq C\tau h m_S^{k+1},$$

where  $\mathcal{H}^{n-1}$  is the  $(n-1)$ -dimensional Hausdorff measure of the considered continuous surface difference.

**Proof** At first, we notice that the function  $\Psi^k(t, \cdot)$  defined in (1.18) parametrizes the lifted and then transported triangle  $S^{l,k}(t)$  over  $S^k$  and  $\mathcal{P}(t, \Upsilon^k(t, \cdot))$  with  $\Upsilon^k(t, \cdot)$  defined in (1.19) parametrizes the transported and then lifted triangle  $\mathcal{P}(t, S^k(t))$  over  $S^k$ . These two functions share the same Lagrangian interpolation  $\Upsilon^k(t, \cdot)$  for any  $t$ , which implies the estimate

$$|\mathcal{P}(t, \Upsilon^k(t, x)) - \Psi^k(t, x)| \leq \beta(t)h^2$$

for every  $x \in S^k$ . Here,  $\beta(t)$  is a non negative and smooth function in time. From  $S^{l,k}(t_k) = S^{l,k}$  one deduces that  $\beta(\cdot)$  can be chosen such that  $\beta(t) \leq C|t - t_k|$  holds. Furthermore,  $C\tau h^2$  is also a bound for the maximum norm of the displacement function  $\mathcal{P}(t, \Upsilon^k(t, \cdot)) - \Psi^k(t, \cdot)$  on edges  $\sigma^k$ . Thus, taking into account that  $h m_\sigma^k \leq C m_S^k$ , we obtain as a direct consequence the second claim.  $\square$

Based on this estimate, we immediately obtain the following corollary.

**Corollary 1.5.4** *For any triangle  $S^k$  on  $\Gamma_h^k$  and any Lipschitz continuous function  $\omega(t, \cdot)$  defined on  $\Gamma(t)$  one obtains*

$$\left| \int_{S^{l,k}(t_{k+1})} \omega(t_{k+1}, x) da - \int_{S^{l,k+1}} \omega(t_{k+1}, x) da \right| \leq C\tau h m_S^{k+1}$$

for a constant  $C$  depending only on the regularity assumptions.

## 1.5.2 Consistency estimates

Next, with these geometric preliminaries at hand, we are able to derive a priori bounds for various consistency errors in conjunction with the finite volume approximation (1.7) of the continuous evolution (1.1).

**Lemma 1.5.5** *Let  $S^k$  be a triangle in  $\Gamma_h^k$  and  $t \in [t_k, t_{k+1}]$ . Then for*

$$\begin{aligned} \mathcal{R}_1(S^{l,k}(t)) &:= \int_{S^{l,k}(t)} \nabla_{\Gamma(t)} \cdot (\mathcal{D}\nabla_{\Gamma(t)} u(t, \cdot)) da \\ &\quad - \int_{S^{l,k}(t_{k+1})} \nabla_{\Gamma(t_{k+1})} \cdot (\mathcal{D}\nabla_{\Gamma(t_{k+1})} u(t_{k+1}, \cdot)) da \end{aligned}$$

we obtain the estimate  $|\mathcal{R}_1(S^{l,k}(t))| \leq C\tau(1 + Ch^2)m_S^{k+1}$ .

**Proof** We recall that  $\nabla_{\Gamma(t)} u(t, x) = \nabla u^{ext}(t, x) - (\nabla u^{ext}(t, x) \cdot \nu(t, x)) \nu(t, x)$ , where  $u^{ext}(t, \cdot)$  is a constant extension of  $u(t, \cdot)$  in the normal direction  $\nu(t, \cdot)$  of  $\Gamma(t)$ . Any continuous and differentiable vector field  $v(t, \cdot)$  on  $\Gamma(t)$  can be extended in the same way for each component. Then we obtain for the surface divergence of  $v(t, \cdot)$  at a point  $x$  on  $\Gamma(t)$  the representation  $\nabla_{\Gamma(t)} \cdot v(t, x) = \text{tr}((\text{Id} - \nu(t, x) \otimes \nu(t, x)) \nabla v^{ext}(t, x))$ . Thus, we deduce from our regularity assumptions in Section 1.2 that the function  $(t, x) \mapsto \nabla_{\Gamma(t)} \cdot (\mathcal{D}\nabla_{\Gamma(t)} u(t, x))$  is Lipschitz in the time and space variable. This observation allows us to estimate  $|\mathcal{R}_1(S^{l,k}(t))|$  by  $C\tau m_S^{l,k+1}$ . Finally, taking into account Lemma 1.5.2 we obtain the postulated estimate.  $\square$

**Lemma 1.5.6** For the edge  $\sigma^k$  between two adjacent triangles  $S^k$  and  $L^k$  the term

$$\mathcal{R}_2(S^{l,k}|L^{l,k}) := \int_{\sigma^{l,k}} (\mathcal{D}\nabla_{\Gamma(t_k)} u(t_k, \cdot)) \cdot \mu_{\partial S^{l,k}} dl - \frac{m_\sigma^k \mathcal{M}_\sigma^k}{d_{S|L}^k} (u^{-l}(t_k, X_L^k) - u^{-l}(t_k, X_S^k)),$$

with  $\sigma^{l,k} = S^{l,k} \cap L^{l,k}$ , obeys the estimated  $|\mathcal{R}_2(S^{l,k}|L^{l,k})| \leq C m_\sigma^k h$ .

**Proof** At first, we split the error term  $\mathcal{R}_2(S^{l,k}|L^{l,k})$  into corresponding consistency errors on the two adjacent triangles  $S^k$  and  $L^k$ , taking into account the flux condition at the edge  $\sigma^{l,k}$ , the definition of  $\mathcal{M}_\sigma^k = \frac{\lambda_{S|\sigma}^k \lambda_{L|\sigma}^k d_{S|L}^k}{d_{L|\sigma}^k \lambda_{S|\sigma}^k + d_{S|\sigma}^k \lambda_{L|\sigma}^k}$ , and the identity  $d_{S|L}^k = d_{S|\sigma}^k + d_{L|\sigma}^k$ . In fact, we obtain

$$\mathcal{R}_2(S^{l,k}|L^{l,k}) = \frac{m_\sigma^k \mathcal{M}_\sigma^k}{d_{S|L}^k} \left( \frac{d_{S|\sigma}^k}{m_\sigma^k \lambda_{S|\sigma}^k} \mathcal{R}_2(S^{l,k}|\sigma^{l,k}) - \frac{d_{L|\sigma}^k}{m_\sigma^k \lambda_{L|\sigma}^k} \mathcal{R}_2(L^{l,k}|\sigma^{l,k}) \right),$$

where

$$\mathcal{R}_2(S^{l,k}|\sigma^{l,k}) := \int_{\sigma^{l,k}} (\mathcal{D}\nabla_{\Gamma(t_k)} u(t_k, \cdot)) \cdot \mu_{\partial S^{l,k}} dl - m_\sigma^k \frac{u^{-l}(t_k, X_\sigma^k) - u^{-l}(t_k, X_S^k)}{d_{S|\sigma}^k} \lambda_{S|\sigma}^k. \quad (1.20)$$

Next, we estimate these error terms separately and obtain

$$\begin{aligned} \mathcal{R}_2(S^{l,k}|\sigma^{l,k}) &= \\ &\int_{\sigma^{l,k}} ((\mathcal{D}\nabla_{\Gamma(t_k)} u(t_k, \cdot)) \cdot \mu_{\partial S^{l,k}} - [(\mathcal{D}\nabla_{\Gamma(t_k)} u) \cdot \mu_{\partial S^{l,k}}](\mathcal{P}(t_k, X_\sigma^k))) dl \\ &+ ([(\mathcal{D}\nabla_{\Gamma(t_k)} u) \cdot \mu_{\partial S^{l,k}}](\mathcal{P}(t_k, X_\sigma^k)) - [(\mathcal{D}\nabla_{\Gamma(t_k)} u^{-l}) \cdot \mu_{\partial S^{l,k}}](t_k, X_\sigma^k)) m_\sigma^{l,k} \\ &+ [(\mathcal{D}\nabla_{\Gamma(t_k)} u^{-l}) \cdot \mu_{\partial S^{l,k}}](t_k, X_\sigma^k) (m_\sigma^{l,k} - m_\sigma^k) \\ &+ ([(\mathcal{D}\nabla_{\Gamma(t_k)} u^{-l}) \cdot \mu_{\partial S^{l,k}}](t_k, X_\sigma^k) - [(\mathcal{D}\nabla_{\Gamma(t_k)} u^{-l}) \cdot \mu_{S|\sigma}^k](t_k, X_\sigma^k)) m_\sigma^k \\ &+ ([(\mathcal{D}\nabla_{\Gamma(t_k)} u^{-l}) \cdot \mu_{S|\sigma}^k](t_k, X_\sigma^k) - [(\mathcal{D}\nabla_{S^k} u^{-l}) \cdot \mu_{S|\sigma}^k](t_k, X_\sigma^k)) m_\sigma^k \\ &+ \left( \nabla_{S^k} u^{-l}(t_k, X_\sigma^k) \cdot (\mathcal{D}_{S|\sigma}^k \mu_{S|\sigma}^k) - \frac{u^{-l}(t_k, X_\sigma^k) - u^{-l}(t_k, X_S^k)}{d_{S|\sigma}^k} \|\mathcal{D}_{S|\sigma}^k \mu_{S|\sigma}^k\| \right) m_\sigma^k. \end{aligned}$$

Taking into account our regularity assumption from Section 1.2, Lemma 1.5.2, and the fact that  $\mathcal{D}_{S|\sigma}^k \mu_{S|\sigma}^k$  is imposed to be parallel to  $\overline{X_S^k X_\sigma^k}$  by (1.2) – indeed, even  $(\mathcal{D}_{S|\sigma}^k \mu_{S|\sigma}^k / \|\mathcal{D}_{S|\sigma}^k \mu_{S|\sigma}^k\|) = ((X_\sigma^k - X_S^k)/d_{S|\sigma}^k)$  – we finally observe that each term can be estimated from above by  $C m_\sigma^k h$  for a constant  $C$ , which depends only on the regularity assumptions. This proves the claim.  $\square$

The proof can be easily adapted to the case where the discrete diffusion tensor is defined on triangles as mentioned in section 1.3.

**Lemma 1.5.7** For a cell  $S^k$  and the residual error term

$$\begin{aligned} \mathcal{R}_3(S^{l,k}|S^{l,k+1}) &= \int_{S^{l,k}(t_{k+1})} u da - \int_{S^{l,k}(t_k)} u da \\ &\quad - (m_S^{k+1} u^{-l}(t_{k+1}, X_S^{k+1}) - m_S^k u^{-l}(t_k, X_S^k)) \end{aligned}$$

one obtains the estimate  $|\mathcal{R}_3(S^{l,k}|S^{l,k+1})| \leq C \tau h m_S^{k+1}$ .

**Proof** At first, let us recall that  $\Psi^k(t, \cdot)$ ,  $\Upsilon^k(t, \cdot)$ , and  $\mathcal{P}(t_{k+1}, \Upsilon^k(t_{k+1}, \cdot))$  parametrize  $S^{l,k}(t)$ ,  $S^k(t)$ , and  $S^{l,k+1}$  over the triangle  $S^k$ . Via standard quadrature error estimates and due to the regularity assumptions on  $\Phi$  and  $u$  given in Section 1.2, we obtain for the smooth quadrature error function

$$Q(t) := \int_{S^{l,k}(t)} u(t, x) \, da - u(t, \mathcal{P}(t, \Upsilon^k(t, X_S^k))) \mathcal{H}^{n-1}(S^{l,k}(t))$$

the estimate  $|Q(t) - Q(t_k)| \leq \tilde{\beta}(t) h \mathcal{H}^{n-1}(S^{l,k}(t))$ , where  $\tilde{\beta}$  is a smooth, non negative function in time. From  $Q(t_k) - Q(t_k) = 0$  we deduce that  $\tilde{\beta}(t) \leq C |t - t_k|$  (cf. also the proof of Lemma 1.5.3). Based on an analogous argument we obtain for the continuity modulus of  $\tilde{Q}(t) := \int_{\mathcal{P}(t, S^k(t))} da - \int_{S^k(t)} da$  that

$$\tilde{Q}(t_{k+1}) - \tilde{Q}(t_k) \leq C\tau h^2 m_S^k.$$

Making use of our notation we observe that the left hand side equals  $(m_S^{l,k+1} - m_S^{k+1}) - (m_S^{l,k} - m_S^k)$ . We now split the residual into

$$\begin{aligned} \mathcal{R}_3(S^{l,k}|S^{l,k+1}) &= Q(t_{k+1}) - Q(t_k) \\ &\quad + u(t_{k+1}, \mathcal{P}(t_{k+1}, \Upsilon^k(t_{k+1}, X_S^k))) \left( \mathcal{H}^{n-1}(S^{l,k}(t_{k+1})) - m_S^{l,k+1} \right) \\ &\quad + \left( u(t_{k+1}, \mathcal{P}(t_{k+1}, \Upsilon^k(t_{k+1}, X_S^k))) - u^{-l}(t_{k+1}, X_S^{k+1}) \right) m_S^{l,k+1} \\ &\quad + u^{-l}(t_{k+1}, X_S^{k+1}) \left[ \left( m_S^{l,k+1} - m_S^{k+1} \right) - \left( m_S^{l,k} - m_S^k \right) \right] \\ &\quad + \left( u^{-l}(t_{k+1}, X_S^{k+1}) - u^{-l}(t_{k+1}, \Upsilon^k(t_{k+1}, X_S^k)) \right) \left( m_S^{l,k} - m_S^k \right) \\ &\quad + \left( u^{-l}(t_{k+1}, \Upsilon^k(t_{k+1}, X_S^k)) - u^{-l}(t_k, X_S^k) \right) \left( m_S^{l,k} - m_S^k \right). \end{aligned}$$

Finally, applying the above estimates, (1.16), Lemmas 1.5.2 and 1.5.3, we get

$$\begin{aligned} |\mathcal{R}_3(S^{l,k}|S^{l,k+1})| &\leq C(\tau h^2 m_S^{k+1} + \tau h m_S^k + \tau h m_S^{k+1} + \tau h^2 m_S^{k+1} + \tau h^3 m_S^k + \tau h^2 m_S^k) \\ &\leq C\tau h m_S^{k+1}. \end{aligned}$$

□

**Lemma 1.5.8** For a cell  $S^k$  and the residual error term

$$\mathcal{R}_4(S^{l,k}|S^{l,k+1}) = \int_{t_k}^{t_{k+1}} \int_{S^{l,k}(t)} g \, da \, dt - \tau m_S^{k+1} g^{-l}(t_{k+1}, X_S^{k+1})$$

one achieves the estimate  $|\mathcal{R}_4(S^{l,k}|S^{l,k+1})| \leq C\tau(\tau + h)m_S^{k+1}$ .

**Proof** We expand the residual by



$$\begin{aligned}
\mathcal{R}_4(S^{l,k}|S^{l,k+1}) &= \int_{t_k}^{t_{k+1}} \left( \int_{S^{l,k}(t)} g(t, x) \, da - \int_{S^{l,k}(t_{k+1})} g(t_{k+1}, x) \, da \right) dt \\
&+ \tau \left( \int_{S^{l,k}(t_{k+1})} g(t_{k+1}, x) \, da - \int_{S^{l,k+1}} g(t_{k+1}, x) \, da \right) \\
&+ \tau \left( \int_{S^{l,k+1}} g(t_{k+1}, x) \, da - g^{-l}(t_{k+1}, X_S^{k+1}) m_S^{l,k+1} \right) \\
&+ \tau \left( m_S^{l,k+1} - m_S^{k+1} \right) g^{-l}(t_{k+1}, X_S^{k+1}).
\end{aligned}$$

Now we use a standard quadrature estimate, Lemmas 1.5.2 and 1.5.3, and Corollary 1.5.4, which yields

$$\begin{aligned}
|\mathcal{R}_4(S^{l,k}|S^{l,k+1})| &\leq C(\tau^2 \mathcal{H}^{n-1}(S^{l,k}(t_{k+1})) + \tau^2 h m_S^{k+1} + \tau h m_S^{k+1} + \tau h^2 m_S^{k+1}) \\
&\leq C\tau(\tau + h)m_S^{k+1}.
\end{aligned}$$

□

### 1.5.3 Proof of Theorem 1.5.1

As in Section 1.2 (cf. (1.3), (1.4), and (1.5)), let us consider the following trianglewise flux formulation of the continuous problem (1.1):

$$\int_{S^{l,k}(t_{k+1})} u \, da - \int_{S^{l,k}(t_k)} u \, da - \int_{t_k}^{t_{k+1}} \int_{\partial S^{l,k}(t)} \mathcal{D}\nabla_{\Gamma} u \cdot n_{\partial S^{l,k}(t)} \, dl \, dt = \int_{t_k}^{t_{k+1}} \int_{S^{l,k}(t)} g \, da \, dt.$$

From this equation we subtract the discrete counterpart (1.7)

$$m_S^{k+1} U_S^{k+1} - m_S^k U_S^k - \tau \sum_{\sigma \subset \partial S} m_{\sigma}^{k+1} \mathcal{M}_{\sigma}^{k+1} \frac{U_L^{k+1} - U_S^{k+1}}{d_{S|L}^{k+1}} = \tau m_S^{k+1} G_S^{k+1}$$

and multiply this with  $E_S^{k+1} = u^{-l}(t_{k+1}, X_S^{k+1}) - U_S^{k+1}$ . Hence, we obtain

$$\begin{aligned}
&\mathcal{R}_3(S^{l,k}|S^{l,k+1}) E_S^{k+1} + m_S^{k+1} (E_S^{k+1})^2 - m_S^k E_S^{k+1} E_S^k \\
&- \left( \int_{t_k}^{t_{k+1}} \mathcal{R}_1(S^{l,k}(t)) \, dt \right) E_S^{k+1} - \tau \sum_{\sigma \subset \partial S} \mathcal{R}_2(S^{l,k+1}|L^{l,k+1}) E_S^{k+1} \\
&- \tau \sum_{\sigma \subset \partial S} \frac{m_{\sigma}^{k+1} \mathcal{M}_{\sigma}^{k+1}}{d_{S|L}^{k+1}} (E_L^{k+1} - E_S^{k+1}) E_S^{k+1} = \mathcal{R}_4(S^{l,k}|S^{l,k+1}) E_S^{k+1}.
\end{aligned}$$

Now we sum over all simplices and obtain

$$\begin{aligned}
&\sum_S m_S^{k+1} (E_S^{k+1})^2 + \tau \sum_{\sigma=S \cap L} \frac{m_{\sigma}^{k+1} \mathcal{M}_{\sigma}^{k+1}}{d_{S|L}^{k+1}} (E_L^{k+1} - E_S^{k+1})^2 = \sum_S m_S^k E_S^{k+1} E_S^k \\
&- \sum_S \left( \mathcal{R}_3(S^{l,k}|S^{l,k+1}) - \int_{t_k}^{t_{k+1}} \mathcal{R}_1(S^{l,k}(t)) \, dt - \mathcal{R}_4(S^{l,k}|S^{l,k+1}) \right) E_S^{k+1} \\
&+ \tau \sum_S \sum_{\sigma \subset \partial S} \mathcal{R}_2(S^{l,k+1}|L^{l,k+1}) E_S^{k+1}.
\end{aligned}$$

Observing that  $\mathcal{R}_2(S^{l,k+1}|L^{l,k+1}) = -\mathcal{R}_2(L^{l,k+1}|S^{l,k+1})$  the last term on the right hand side can be rewritten and estimated as follows:

$$\begin{aligned} & \sum_{\sigma=S \cap L} \mathcal{R}_2(S^{l,k+1}|L^{l,k+1}) \sqrt{\frac{d_{S|L}^{k+1}}{m_\sigma^{k+1} \mathcal{M}_\sigma^{k+1}}} \frac{\sqrt{m_\sigma^{k+1} \mathcal{M}_\sigma^{k+1}} (E_L^{k+1} - E_S^{k+1})}{\sqrt{d_{S|L}^{k+1}}} \\ & \leq \left( \sum_{\sigma=S \cap L} \mathcal{R}_2(S^{l,k+1}|L^{l,k+1})^2 \frac{d_{S|L}^{k+1}}{m_\sigma^{k+1} \mathcal{M}_\sigma^{k+1}} \right)^{\frac{1}{2}} \|E^{k+1}\|_{1, \Gamma_h^{k+1}} \\ & \leq C \left( \sum_S m_S^{k+1} h^2 \right)^{\frac{1}{2}} \|E^{k+1}\|_{1, \Gamma_h^{k+1}} \leq C h \mathcal{H}^{n-1}(\Gamma_h^{k+1})^{\frac{1}{2}} \|E^{k+1}\|_{1, \Gamma_h^{k+1}}. \end{aligned}$$

Here, we have used Lemma 1.5.6 and the estimate  $m_\sigma^{k+1} h \leq C m_S^{k+1}$  for  $\sigma \subset \partial S$ . Now we take into account the consistency results from Corollary 1.5.4, Lemmas 1.5.5, 1.5.7 and 1.5.8, apply Young's inequality and Cauchy's inequality and achieve the estimate

$$\begin{aligned} & \|E^{k+1}\|_{\mathbb{L}^2(\Gamma_h^{k+1})}^2 + \tau \|E^{k+1}\|_{1, \Gamma_h^{k+1}}^2 \\ & \leq \frac{1}{2} \|E^{k+1}\|_{\mathbb{L}^2(\Gamma_h^{k+1})}^2 + \frac{1}{2} \|E^k\|_{\mathbb{L}^2(\Gamma_h^k)}^2 + \frac{1}{2} \max_k \max_S \left| 1 - \frac{m_S^k}{m_S^{k+1}} \right| \|E^k\|_{\mathbb{L}^2(\Gamma_h^k)}^2 \\ & \quad + C(\tau h + \tau^2(1 + C h^2) + \tau(\tau + h)) \mathcal{H}^{n-1}(\Gamma_h^{k+1})^{\frac{1}{2}} \|E^{k+1}\|_{\mathbb{L}^2(\Gamma_h^{k+1})} \\ & \quad + C \tau h \mathcal{H}^{n-1}(\Gamma_h^{k+1})^{\frac{1}{2}} \|E^{k+1}\|_{1, \Gamma_h^{k+1}}. \end{aligned}$$

Based on our assumption that the triangulation is advected in time, we can estimate  $\left| 1 - \frac{m_S^k}{m_S^{k+1}} \right| \leq C \tau$ . Again applying Young's inequality to the last two terms on the right hand side we get

$$\begin{aligned} & C(\tau h + \tau^2(1 + C h^2) + \tau(\tau + h)) \mathcal{H}^{n-1}(\Gamma_h^{k+1})^{\frac{1}{2}} \frac{1}{2} \|E^{k+1}\|_{\mathbb{L}^2(\Gamma_h^{k+1})} \\ & \leq C \tau \|E^{k+1}\|_{\mathbb{L}^2(\Gamma_h^{k+1})}^2 + C \tau (\tau + h)^2 \mathcal{H}^{n-1}(\Gamma_h^{k+1}), \\ & C \tau h \mathcal{H}^{n-1}(\Gamma_h^{k+1})^{\frac{1}{2}} \|E^{k+1}\|_{1, \Gamma_h^{k+1}} \leq \frac{\tau}{2} \|E^{k+1}\|_{1, \Gamma_h^{k+1}}^2 + \frac{\tau C^2 h^2}{2} \mathcal{H}^{n-1}(\Gamma_h^{k+1}). \end{aligned}$$

Hence, taking into account that  $\mathcal{H}^{n-1}(\Gamma_h^{k+1})$  is uniformly bounded we obtain the estimate

$$(1 - C\tau) \|E^{k+1}\|_{\mathbb{L}^2(\Gamma_h^{k+1})}^2 + \frac{\tau}{2} \|E^{k+1}\|_{1, \Gamma_h^{k+1}}^2 \leq (1 + C\tau) \|E^k\|_{\mathbb{L}^2(\Gamma_h^k)}^2 + C\tau(\tau + h)^2. \quad (1.21)$$

At first, we skip the second term on the left hand side, use the inequality  $\frac{(1+C\tau)}{(1-C\tau)} \leq (1+c\tau)$  for sufficiently small time step  $\tau$  and a constant  $c > 0$ , and obtain via iteration (cf. also the proof of Theorem 1.4.1)

$$\begin{aligned} \|E^{k+1}\|_{\mathbb{L}^2(\Gamma_h^{k+1})}^2 & \leq (1 + c\tau) \|E^k\|_{\mathbb{L}^2(\Gamma_h^k)}^2 + C\tau(\tau + h)^2 \\ & \leq \dots \leq (1 + c\tau)^{k+1} \|E^0\|_{\mathbb{L}^2(\Gamma_h^0)}^2 + \sum_{i=1}^k \tau(1 + c\tau)^{i-1} (\tau + h)^2 \\ & \leq e^{c t_k} \left( \|E^0\|_{\mathbb{L}^2(\Gamma_h^0)}^2 + t_k (\tau + h)^2 \right). \end{aligned}$$

This implies the first claim of the theorem:

$$\max_{k=1, \dots, k_{max}} \|E^k\|_{L^2(\Gamma_h^k)}^2 \leq C(\tau + h)^2.$$

Finally, taking into account this estimate and summing over  $k = 0, \dots, k_{max} - 1$  in (1.21) we obtain also the claimed estimate for the discrete  $H^1$ -norm of the error:

$$\sum_{k=1, \dots, k_{max}} \tau \|E^k\|_{1, \Gamma_h^k}^2 \leq C(\tau + h)^2.$$

□

## 1.6 Coupled reaction diffusion and advection model

In what follows, we will generalize our finite volume approach by considering a source term  $g$  which depends on the solution and an additional tangential advection term  $\nabla_\Gamma \cdot (wu)$ . Here,  $w$  is an additional tangential transport velocity on the surface, which transports the density  $u$  along the moving interface  $\Gamma$  instead of just passively advecting it with the interface. We assume the mapping  $(t, x) \rightarrow w(t, \Phi(t, x))$  to be in  $C^1([0, t_{max}], C^1(\Gamma_0))$ . Furthermore, we suppose  $g$  to be Lipschitz continuous. An extension to a reaction term which also explicitly depends on time and position is straightforward. Hence, we investigate the evolution problem

$$\dot{u} + u \nabla_\Gamma \cdot v - \nabla_\Gamma \cdot (\mathcal{D} \nabla_\Gamma u) + \nabla_\Gamma \cdot (wu) = g(u) \quad \text{on } \Gamma = \Gamma(t). \quad (1.22)$$

In what follows, let us consider an appropriate discretization for both terms. For the reaction term, we consider the time-explicit approximation

$$\int_{t_k}^{t_{k+1}} \int_{S^{l,k}(t)} g(u(t, x)) \, da \, dt \approx \tau m_S^k g(u(t_k, \mathcal{P}^k X_S^k)) \quad (1.23)$$

and then replace  $u(t_k, \mathcal{P}^k(X_S^k))$  by  $U_S^k$  in the actual numerical scheme. Furthermore, we take into account an upwind discretization of the additional transport term to ensure robustness also in a regime where the transport induced by  $w$  dominates the diffusion. Here, we confine to a classical first order upwind discretization. Thus, on each edge  $\sigma^k = S^k \cap L^k$  of a triangle  $S^k$  facing to the adjacent triangle  $L^k$  we define an averaged outward pointing conormal  $n_{S|L}^k = |n_{\partial S} - n_{\partial L}|^{-1}(n_{\partial S} - n_{\partial L})$ . In particular  $n_{S|L}^k = -n_{L|S}^k$  holds. If  $n_{S|L}^k \cdot w^{-l}(t_k, X_\sigma^k) \geq 0$ , the upwind direction is pointing inward and we define  $u^+(t_k, X_\sigma^k) := u^{-l}(t_k, X_S^k)$ , otherwise  $u^+(t_k, X_\sigma^k) := u^{-l}(t_k, X_L^k)$ . Once the upwind direction is identified, we take into account the classical approach by Engquist and Osher [43] and obtain the approximation

$$\int_{t_k}^{t_{k+1}} \int_{S^{l,k}(t)} \nabla_\Gamma \cdot (wu) \, da \, dt \approx \tau \sum_{\sigma \subset \partial S} m_\sigma^k (n_{\sigma,S}^k \cdot w^{-l}(t_k, X_\sigma^k)) \cdot u^+(t_k, X_\sigma^k). \quad (1.24)$$

Finally, we again replace  $u^{-l}(t_k, X_S^k)$  by the discrete nodal values  $U_S^k$  and denote these by  $U_\sigma^{k,+}$ . For the sake of completeness let us resume the following resulting scheme:

$$\begin{aligned} m_S^{k+1} U_S^{k+1} - m_S^k U_S^k &= \tau \sum_{\sigma \subset \partial S} m_\sigma^{k+1} \mathcal{M}_\sigma^{k+1} \frac{U_L^{k+1} - U_S^{k+1}}{d_{S|L}^{k+1}} \\ &\quad + \tau m_S^k g(U_S^k) - \tau \sum_{\sigma \subset \partial S} m_\sigma^k \left( n_{S|L}^k \cdot w^{-l}(t_k, X_\sigma^k) \right) U_\sigma^{k,+}. \end{aligned} \quad (1.25)$$

Obviously, due to the fully explicit discretization of the additional terms, Proposition 1.3.2 still applies and guarantees the existence and uniqueness of a discrete solution. Furthermore, the convergence result can be adapted, and the error estimate postulated in Theorem 1.5.1 holds. To see this, let us first consider the nonlinear source term  $g(u)$  and estimate

$$\begin{aligned}
 & \int_{t_k}^{t_{k+1}} \int_{S^{l,k}(t)} g(u(t, x)) \, da \, dt - \tau m_S^k g(U_S^k) \\
 \leq & \int_{t_k}^{t_{k+1}} \left( \int_{S^{l,k}(t)} g(u(t, x)) \, da - \int_{S^{l,k}} g(u(t_k, x)) \, da \right) dt \\
 & + \tau \left( \int_{S^{l,k}} g(u(t_k, x)) \, da - m_S^{l,k} g(u^{-l}(t_k, X_S^k)) \right) dt + \tau (m_S^{l,k} - m_S^k) g(u^{-l}(t_k, X_S^k)) \\
 & + \tau m_S^k (g(u^{-l}(t_k, X_S^k)) - g(U_S^k)) \\
 \leq & C (\tau^2 \mathcal{H}^{n-1}(S^{l,k}) + \tau h m_S^k + \tau h^2 m_S^k + C_{Lip}(g) \tau m_S^k E_S^k),
 \end{aligned}$$

where  $C_{Lip}(g)$  denotes the Lipschitz constant of  $g$ . In the proof of Theorem 1.5.1 we already have treated terms identical to the first three on the right hand side. For the last term, we obtain after multiplication with the nodal error  $E_S^{k+1}$  and a summation over all cells  $S$ ,

$$\begin{aligned}
 C_{Lip}(g) \tau \sum_S m_S^k E_S^k E_S^{k+1} & \leq C_{Lip}(g) \tau \max_S \left( \frac{m_S^k}{m_S^{k+1}} \right)^{\frac{1}{2}} \|E^k\|_{\mathbb{L}^2(\Gamma_h(t_k))} \|E^{k+1}\|_{\mathbb{L}^2(\Gamma_h(t_k))} \\
 & \leq C \tau \left( \|E^k\|_{\mathbb{L}^2(\Gamma_h(t_k))}^2 + \|E^{k+1}\|_{\mathbb{L}^2(\Gamma_h(t_{k+1}))}^2 \right).
 \end{aligned}$$

Taking into account these additional error terms, the estimate (1.21) remains unaltered. Next, we investigate the error due to the additional advection term and rewrite

$$\begin{aligned}
 & \int_{t_k}^{t_{k+1}} \int_{S^{l,k}(t)} \nabla_\Gamma \cdot (wu) \, da \, dt - \tau \sum_{\sigma \subset \partial S} m_\sigma^k (n_{\sigma,S}^k \cdot w^{-l}(t_k, X_\sigma^k)) U_\sigma^{k,+} \\
 = & \int_{t_k}^{t_{k+1}} \int_{S^{l,k}(t)} \nabla_\Gamma \cdot (wu) \, da \, dt - \tau \int_{S^{l,k}} \nabla_\Gamma \cdot (wu) \, da \\
 & + \sum_{\substack{\sigma \subset \partial S \\ \sigma = S \cap L}} (\tau \mathcal{R}_5(S^{l,k}|L^{l,k}) + \tau \mathcal{F}(S^{l,k}|L^{l,k}) E_\sigma^{k,+}),
 \end{aligned}$$

where  $\mathcal{R}_5(S^{l,k}|L^{l,k}) = \int_{\sigma^{l,k}} n_{\partial S^{l,k}} \cdot w u \, dl - m_\sigma^k w^{-l}(t_k, X_\sigma^k) \cdot \mu_{S|L}^k u^+(t_k, X_\sigma^k)$  is an edge residual,  $\mathcal{F}(S^{l,k}|L^{l,k}) = m_\sigma^k w^l(t_k, X_\sigma^k) \cdot \mu_{S|L}^k$  is a flux term on the edge  $\sigma^{l,k} = S^{l,k} \cap L^{l,k}$ , and  $E_\sigma^{k,+} = u^+(t_k, X_\sigma^k) - U_\sigma^{k,+}$  is a piecewise constant upwind error function on the discrete surface  $\Gamma_h^k$ . The first term in the above error representation can again be estimated by  $C \tau^2 \mathcal{H}^{n-1}(S^{l,k})$ . From  $|u^+(t_k, X_\sigma^k) - u^{-l}(t_k, X_\sigma^k)| \leq Ch$ , we deduce by similar arguments as in the proof of Lemma 1.5.6 that  $|\mathcal{R}_5(S^{l,k}|L^{l,k})| \leq Ch m_\sigma^k$ . Furthermore, the antisymmetry relations  $\mathcal{R}_5(S^{l,k}|L^{l,k}) = -\mathcal{R}_5(L^{l,k}|S^{l,k})$  and  $\mathcal{F}(S^{l,k}|L^{l,k}) = -\mathcal{F}(L^{l,k}|S^{l,k})$  hold (cf. the same relation for  $\mathcal{R}_2(S^{l,k}|L^{l,k})$ ). After multiplication with the nodal error  $E_S^{k+1}$  and summation over all cells  $S$  we obtain

$$\begin{aligned}
 & \tau \sum_S \sum_{\substack{\sigma \subset \partial S \\ \sigma = S \cap L}} (\mathcal{R}_5(S^{l,k}|L^{l,k}) + \tau \mathcal{F}(S^{l,k}|L^{l,k}) E_\sigma^{k,+}) E_S^{k+1} \\
 \leq & \tau \sum_{\sigma = S \cap L} (\mathcal{R}_5(S^{l,k}|L^{l,k}) (E_S^{k+1} - E_L^{k+1}) + \mathcal{F}(S^{l,k}|L^{l,k}) E_\sigma^{k,+} (E_S^{k+1} - E_L^{k+1}))
 \end{aligned}$$

$$\begin{aligned}
&\leq \tau \left( \sum_{\sigma=S \cap L} (\mathcal{R}_5(S^{l,k}|L^{l,k}) + \mathcal{F}(S^{l,k}|L^{l,k}) E_\sigma^{k,+})^2 \frac{d_{S|L}^{k+1}}{m_\sigma^{k+1} \mathcal{M}_\sigma^{k+1}} \right)^{\frac{1}{2}} \|E^{k+1}\|_{1,\Gamma_h^{k+1}} \\
&\leq C \tau \left( h \mathcal{H}^{n-1}(\Gamma_h^k)^{\frac{1}{2}} + \left( \sum_{\sigma=S \cap L} m_\sigma^k (E_\sigma^{k,+})^2 \right)^{\frac{1}{2}} \right) \|E^{k+1}\|_{1,\Gamma_h^{k+1}} \\
&\leq \frac{\tau}{4} \|E^{k+1}\|_{1,\Gamma_h^{k+1}}^2 + C \tau h^2 + C \tau \|E^k\|_{\mathbb{L}^2(\Gamma_h^k)}^2.
\end{aligned}$$

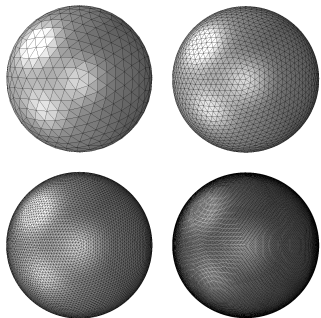
Here, we have applied the straightforward estimate  $\|E^{k,+}\|_{\mathbb{L}^2(\Gamma_h^k)} \leq C \|E^k\|_{\mathbb{L}^2(\Gamma_h^k)}$  and Young's inequality. Again, taking into account these error terms due to the added advection in the original error estimate (1.21), solely the constant in front of the term  $\|E^{k+1}\|_{1,\Gamma_h^{k+1}}^2$  on the left hand side of (1.21) is slightly reduced.

Thus, both the explicit discretization of a nonlinear reaction term and the upwind discretization of the additional tangential advection still allow us to establish the error estimate postulated in Theorem 1.5.1.

## 1.7 Numerical results

To numerically simulate the evolution problem (1.1), we first have to setup a family of triangular meshes, which are consistent with the assumption made above. We generate these meshes based on an implicit description of the underlying initial surface and apply an adaptive polygonization method proposed by de Araújo and Jorge in [29, 28]. This method polygonizes implicit surfaces along an evolving front with triangles whose sizes are adapted to the local radius of curvature. Afterward, using a technique similar to the one developed by Persson in [99] we modify triangles to ensure the orthogonality condition (1.2). We refer also to [36] for a computational approach to anisotropic centroidal Voronoi meshes. Already in Figures 1.1 and 1.3 we have depicted a corresponding family of meshes.

As a first example, we consider a family of expanding and collapsing spheres with radius  $r(t) = 1 + \sin^2(\pi t)$ , and a function  $u(t, \theta, \lambda) = \frac{1}{r^2(t)} \exp\left(-6 \int_0^t \frac{1}{r^2(\tau)} d\tau\right) \cdot \sin(2\theta) \cos(\lambda)$ , where  $\theta$  is the inclination and  $\lambda$  is the azimuth. The function  $u$  solves (1.1) on this family of spheres for  $\mathcal{D} = \text{Id}$  and  $g = 0$ . We compute the numerical solution on successively refined surface triangulations on the time interval  $[0, 1]$ . Table 1.1 presents the different grids and the errors in the discrete  $\mathbb{L}^\infty(\mathbb{L}^2)$  norm and discrete energy seminorm (1.9), respectively. Indeed, the observed error decay is consistent with the convergence result in Theorem 1.5.1.



$h(0)$	$\max_{t \in [0,1]} h(t)$	norm of the error	
		$\mathbb{L}^\infty(\mathbb{L}^2)$	$\mathbb{L}^\infty(\mathbb{H}^1)$
0.2129	0.4257	$32.941 \cdot 10^{-4}$	$22.999 \cdot 10^{-3}$
0.1069	0.2138	$8.036 \cdot 10^{-4}$	$8.348 \cdot 10^{-3}$
0.0535	0.1070	$1.764 \cdot 10^{-4}$	$2.950 \cdot 10^{-3}$
0.0268	0.0536	$0.423 \cdot 10^{-4}$	$1.047 \cdot 10^{-3}$

Table 1.1: On the left, the different triangulations used for the convergence test are depicted. The table on the right displays the numerical error on these grids in two different norms when compared to the explicit solution. The time discretization was chosen as  $\tau = 1/32000 \ll h^2$  in all four computations.

Next, we consider on the same geometry the advection vector  $\omega(t, x) = (0, 0, 30) - (\nu(t, x) \cdot (0, 0, 30))\nu(t, x)$  with  $\nu(t, x)$  being the normal to the surface  $\Gamma(t)$ , and the source term

$g(t, \theta, \lambda) = 2c(t) (-\sin(2\theta) \cos(\lambda) (\omega(t, x) \cdot \nu(t, x)) + \cos(2\theta) \cos(\lambda) (\omega \cdot e_\theta) - \cos(\theta) \sin(\lambda) (\omega \cdot e_\lambda))$ , where  $e_\theta = (\cos(\theta) \cos(\lambda), \cos(\theta) \sin(\lambda), -\sin(\theta))$ ,  $e_\lambda = (-\sin(\lambda), \cos(\lambda), 0)$ , and

$c(t) = \frac{1}{r^3(t)} \exp\left(-6 \int_0^t \frac{1}{r^2(\tau)} d\tau\right)$ . The function  $u(t, \theta, \lambda) = \frac{1}{r^2(t)} \exp\left(-6 \int_0^t \frac{1}{r^2(\tau)} d\tau\right) \cdot \sin(2\theta) \cos(\lambda)$  now solves (1.22). In fact  $\omega$  has been chosen to be at the limit of the CFL condition on the finest grid, characterizing the strength of the advection. Table 1.2 presents the errors in the discrete  $\mathbb{L}^\infty(\mathbb{L}^2)$  norm and discrete energy seminorm (1.9), using the same triangulations as above. The observed error decay is again consistent with the convergence result in Theorem 1.5.1. In fact, even though the solution – and thus its interpolation properties – are identical to the previous example, we see a reduced order of convergence due to the transport part of the equation. In general, we could improve the order of convergence by using a higher order slope limiting and replacing condition (1.16) by

$$|\Upsilon^{k,k+1}(X_S^k) - X_S^{k+1}| \leq Ch^2\tau.$$

$h(0)$	$\max_{t \in [0,1]} h(t)$	norm of the error	
		$\mathbb{L}^\infty(\mathbb{L}^2)$	$\mathbb{L}^\infty(\mathbb{H}^1)$
0.2129	0.4257	$25.53 \cdot 10^{-2}$	$11.615 \cdot 10^{-1}$
0.1069	0.2138	$14.26 \cdot 10^{-2}$	$7.089 \cdot 10^{-1}$
0.0535	0.1070	$7.61 \cdot 10^{-2}$	$3.985 \cdot 10^{-1}$
0.0268	0.0536	$3.95 \cdot 10^{-2}$	$2.125 \cdot 10^{-1}$

Table 1.2: The table displays the numerical error when compared to the explicit solution in the advection dominated setting on the same grids as in Table 1.1. The time discretization was chosen as  $\tau = 1/32000 \ll h^2$  in all four computations.

Figure 1.6 shows the finite volume solution for the heat equation without source term. In the first row the sphere expands with constant velocity in normal direction and initial data have local support, while in the second row the sphere expands into an ellipsoid and initial data are constant. Furthermore, we have computed isotropic and anisotropic diffusion on a rotating torus with zero initial data and time constant or time periodic source term, respectively. Figures 1.7 and 1.8 demonstrate the different joint effects of transport and isotropic diffusion, similar to Figures 2 and 3 in [38]. In Figure 1.9 we consider the same problem as in Figure 1.8 except that this time the underlying diffusion tensor is anisotropic; i.e., we have chosen the tensor

$$\mathcal{D} = \begin{pmatrix} \frac{1}{25} & 0 & 0 \\ 0 & 1 & 0 \\ 0 & 0 & 1 \end{pmatrix}$$

in  $\mathbb{R}^{3,3}$  whose restriction on the tangent bundle is considered as the diffusion in (1.1). The underlying grids have already been rendered in Figure 1.3. Finally, we combine the diffusion process on evolving surfaces with an additional (gravity-type) advection term. As evolving geometry, we have selected one with an initial fourfold symmetry undergoing a transition to the sphere (cf. Figure 1.1 for a corresponding triangular mesh, which is further refined for the actual computation). The advection direction is the projection of a downward pointing gravity vector along the symmetry line on the tangent plane. Figure 1.10 shows the results on the evolving geometry, whereas Figure 1.11 allows

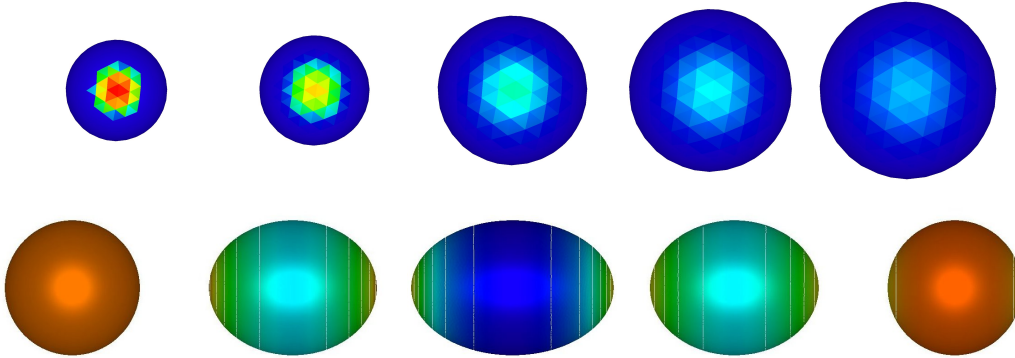


Figure 1.6: In the top row the heat equation ( $\mathcal{D} = \text{Id}$ ) is solved on an expanding sphere for initial data with local support on a relatively coarse evolving grid consisting of 956 triangles. The density is color coded from blue to red at different time steps. In the bottom row, an anisotropic expansion and later reverse contraction of a sphere with constant initial data computed on an evolving surface are depicted. Here a significantly finer discretization consisting of 18462 triangles is taken into account. Again we plot the density at different time steps. One clearly observes an inhomogeneous density with maxima on the less stretched poles during the expansion phase followed by an advective concentration of density close to the symmetry plane during the contraction phase.

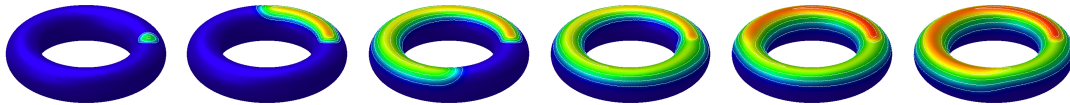


Figure 1.7: The solution of the isotropic heat equation is computed on a torus with smaller radius 1 and larger radius 4. The torus is triangulated with 21852 triangles and 10926 points, and it rotates around its center twice during the evolution process. As initial data, we consider  $u_0 = 0$  and take into account a source term  $g$  with local support inside a geodesic ball of radius 0.5. The source term is considered to be time independent. The surface velocity implies a transport which together with the source term and the isotropic diffusion lead to the observed trace-type solution pattern.

a comparison of the same evolution law on a fixed surface. One clearly notices the impact of the surface evolution on the diffusion and advection process caused by the temporal variation of the angle of attack of the gravity force.

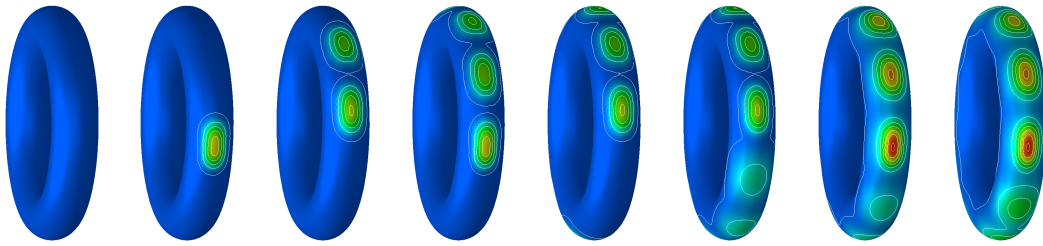


Figure 1.8: A similar computation as in Figure 1.7 has been performed, but with a pulsating source  $g$  with 10 pulses during a complete rotation of the torus. The source is located at a slightly different position, and in order to pronounce the effect of the dynamics, the color scale is logarithmic.

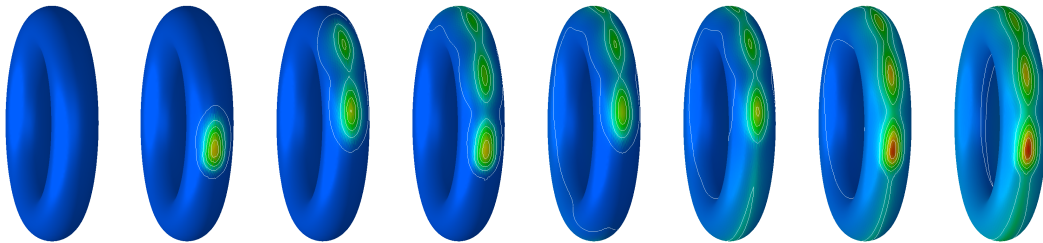


Figure 1.9: As in Figure 1.8, diffusion on a rotating torus with a pulsating source is investigated. This time the diffusion is anisotropic with a smaller diffusion coefficient in the direction perpendicular to the torus' center plane. Again the color scale is logarithmic. The different diffusion lengths in the different directions can be clearly observed in the shape and distance of the isolines at later times and further away from the source.

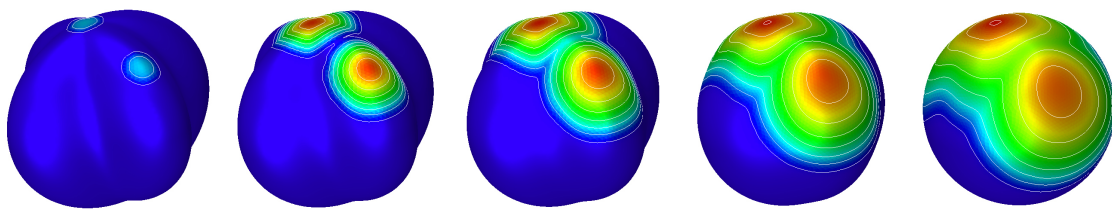


Figure 1.10: The evolution of a density governed by a diffusion and advection process on an evolving geometry with a localized source term is shown at different time steps. The underlying grid consists of 21960 triangles and 10982 vertices.



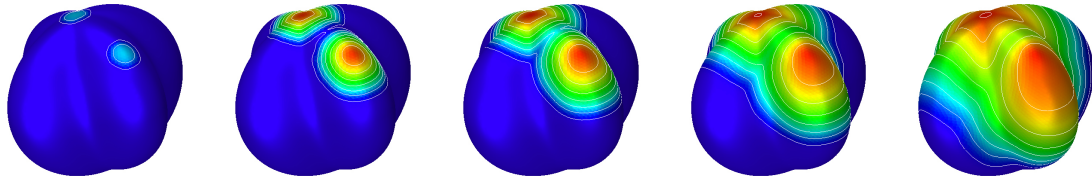


Figure 1.11: As in Figure 1.10, the evolution of a density under diffusion and advection by gravity is investigated. This time the underlying geometry is fixed.



# 2 A stable and convergent O-method for general moving hypersurfaces

## 2.1 Introduction

In Chapter I, we have defined a consistent and convergent finite volume scheme for the simulation of diffusion and advection processes on moving surfaces. Although the proposed scheme is stable and convergent, it is subject to strong constraints on the mesh, namely the orthogonality condition which is related to the diffusion tensor. This makes the mesh used in the algorithm problem-dependent and it becomes difficult to couple interdependent phenomena involving many spatially varying anisotropic diffusion tensors on the same mesh. Also, even on fixed surfaces, it would be difficult using this algorithm to simulate problems with time and space dependent diffusion tensors when variations on eigenvectors of diffusion tensors become important as time evolves. In this case one is obliged to remesh the substrate often as needed. This might introduce some inaccuracy in the result depending on the remeshing method and the approximation method used to reallocate values on cells. In the last two decades, researchers have invested a lot of effort in developing finite volume schemes for anisotropic diffusion problems on unstructured meshes which tackle the best these issues. Unfortunately, focus has been put on planar 2-dimensional and on 3-dimensional problems. We refer to the benchmark parts of [47] and [49], Proceedings of Finite Volumes for Complex Applications V and VI, for the state of art on research in this domain. Nevertheless, the methods developed in the context of finite volumes rely on a suitable approximation of fluxes across edges of control volumes. One constructs fluxes either using only the two unknowns across interfaces or a set of unknowns around edges. The first strategy is referred to as the two-point flux approximation method while the second is known as the multi-point flux approximation method. The method defined in Chapter I is an example of the two-point flux approximation method on curved surfaces and one will find in [45] a more extended description and analysis of the method applied on various problems on flat surfaces. As already said above, it is unfortunately very restrictive in terms of meshes and problems on which it can be applied. The multi-point flux approximation is the up-to-date strategy in the finite volume simulation and is much more flexible. It can be divided into two main groups:

- The Discrete Duality Finite Volumes: In this class of methods, one interplays simultaneously between two meshes; the primal mesh and the dual mesh. The computation is done here on the two nested meshes and the degrees of freedom include the center points of the primal mesh as well as its vertices which are in fact the center points of the dual mesh. We refer to [32, 64, 77, 94] for more insight in the methodology.
- The Mixed or Hybrid Finite Volumes: Here, the degrees of freedom are maintained at the cell centers and one explicitly constructs the gradient operators using different strategies: O-Method [1, 85, 87], L-Method [1], scheme using stabilization and hybrid interfaces [46], finite element strategy [2], least square reconstruction [96] among others.

Since most of these schemes use properties valid only in Cartesian geometry, they cannot be directly transferred to curved surfaces. Also, the fact that a general curved geometry can only be approximated requires a special treatment of schemes on curved surfaces since one should combine the accuracy of the geometric approximation and the accuracy of the scheme. Nevertheless, the methodology in [2] has been analyzed on curved surfaces in [34, 76]. We should also mention the finite volume approach on logically rectangular grids studied in [19] for diffusion and advection in circular and spherical domains. As in these few papers, the few works devoted to finite volumes

on curved surfaces encountered in the literature rely either on a good triangulation of the domain or on a special partitioning of the curved geometry; this restricts their domain of application. In this chapter, we present a finite volume type O-method for general polygonal meshes on curved and moving surfaces. Our method is close to the ones developed by Le Potier in [85] and K. Lipnikov, M. Shashkov and I. Yotov in [87]. Similar to these authors, we first partition each cell of the given discrete domain into subcells attached to cells vertices; this implies a partition of each edge into two subedges and a virtually refined domain where the subcells are effectively the new cells and are grouped around vertices. Next around each vertex, we construct an approximate constant gradient of our solution on surrounding subcells using surrounding cell center unknowns and the continuity of fluxes on subedges. We also take into account worse situations that can occur when the diffusion coefficients become almost degenerate, by using a suitable minimization process which controls the norm of the chosen solution gradients around vertices. These gradients are latter included properly in the flux formulation of the diffusion operator to obtain its discretization. Finally, we use the approximate gradients issued from the identity operator on surfaces to construct a slope limited gradient of the solution function on each control volume. These last gradients approximation are used to develop a second order upwind scheme for the advection part of our model equation. Since the stencil of our slope limited gradients remains unchanged during the process, we experimentally have a second order space convergence of the whole scheme. We should mention that our method is identical to the methods developed in [85, 87] for diffusion on flat surfaces and to the method discussed in [76] for diffusion on curved surfaces when applied with the same parameters, but the scope of meshes that we can handle in that case is wider. Nevertheless, we would like to emphasize that we primarily deal with moving curved surfaces. This includes surfaces whose evolution is implicitly defined through partial differential equations and surfaces whose evolution is explicitly given among others. Let us also mention that this method can be reduced to the method discussed in Chapter I for appropriate meshes designed for this purpose. In the following, we explicitly introduce the model problem discussed in this chapter, next we present the method and give a possible implementation algorithm. Furthermore, we prove some stability results and the convergence of the scheme and finally we present some numerical results to validate the theory. For the purpose of self containment, we will reproduce some proofs from Chapter I.

## 2.2 Problem setting

We consider a family of compact hypersurfaces  $\Gamma(t) \subset \mathbb{R}^n$  ( $n = 2, 3, \dots$ ) for  $t \in [0, t_{max}]$  generated by a time-dependent function  $\Phi : [0, t_{max}] \times \Gamma^0 \rightarrow \mathbb{R}^n$  defined on a reference frame  $\Gamma^0$  with  $\Phi(t, \Gamma^0) = \Gamma(t)$ . We assume that  $\Phi(t, \cdot)$  is the restriction of a function that we abusively call  $\Phi(t, \cdot) : \mathcal{N}_0 = \mathcal{N}(0) \rightarrow \mathcal{N}(t)$ , where  $\mathcal{N}_0$  and  $\mathcal{N}(t)$  are respectively neighborhoods of  $\Gamma^0$  and  $\Gamma(t)$  in  $\mathbb{R}^n$ . We also take  $\Gamma^0$  to be  $C^3$  smooth and  $\Phi \in C^1([0, t_{max}], C^3(\mathcal{N}_0))$ . For simplicity, we assume the reference surface  $\Gamma^0$  to coincide with the initial surface  $\Gamma(0)$ . We denote by  $v = \partial_t \Phi$  the velocity of material points and assume the decomposition  $v = v_n \nu + v_{tan}$  into a scalar normal velocity  $v_n$  in the direction of the surface normal  $\nu$  and a tangential velocity  $v_{tan}$ . The evolution of a conservative material quantity  $u$  with  $u(t, \cdot) : \Gamma(t) \rightarrow \mathbb{R}$ , which is propagated with the surface and at the same time, undergoes a linear diffusion on the surface, is governed by the parabolic equation

$$\dot{u} + u \nabla_\Gamma \cdot v - \nabla_\Gamma \cdot (\mathcal{D} \nabla_\Gamma u) = g \text{ on } \Gamma(t), \quad (2.1)$$

where  $\dot{u} = \frac{d}{dt} u(t, x(t))$  is the (advective) material derivative of  $u$ ,  $\nabla_\Gamma \cdot v$  the surface divergence of the vector field  $v$ ,  $\nabla_\Gamma u$  the surface gradient of the scalar field  $u$ ,  $g$  a source term with  $g(t, \cdot) : \Gamma(t) \rightarrow \mathbb{R}$  and  $\mathcal{D}$  the diffusion tensor on the tangent bundle. Here we assume a symmetric, uniformly coercive  $C^2$  diffusion tensor field on whole  $\mathbb{R}^n$  to be given, whose restriction on the tangent plane is then effectively incorporated in the model. With slight misuse of notation, we denote this global tensor also by  $\mathcal{D}$ . Furthermore, we impose an initial condition  $u(0, \cdot) = u_0$  at time  $t = 0$ . Since we have already introduced the subject in Chapter I in a relative simple setup, we will treat in this chapter a more

general case of surfaces with boundary. Surfaces without boundary fall into this setup since they are merely surfaces with empty boundary. Then in case of surfaces with nonempty boundary, we impose a Dirichlet boundary condition. We will nevertheless mention how more general boundary conditions can be included in the algorithm. We assume that the mappings  $(t, x) \rightarrow u(t, \Phi(t, x))$ ,  $v(t, \Phi(t, x))$  and  $g(t, \Phi(t, x))$  are  $C^1([0, t_{max}], C^3(\Gamma^0))$ ,  $C^0([0, t_{max}], (C^3(\Gamma^0))^3)$ , and  $C^1([0, t_{max}], C^1(\Gamma^0))$ , respectively. For the discussion on existence, uniqueness and regularity, we refer to [37] and references therein.

## 2.3 Surface approximation

We introduce in this part a more general notion of surface approximation.

**Definition 2.3.1** (*Cell, cell center and vertices*) Let  $(p_1, p_2, \dots, p_{n_S})$  and  $X_S$  be  $(n_S + 1)$  distinct points in  $\mathbb{R}^3$ . We call cell  $S$  the closed fan of triangles  $S_{\{i,j\}} = [X_S, p_i, p_j]$  ( $j = (i \bmod n_S) + 1$ ) where  $X_S$  is the shared vertex. The point  $X_S$  is called cell center or center point and the points  $p_i$  the vertices of the cell and are not necessarily coplanar. Figure 2.1 shows an example of a cell.

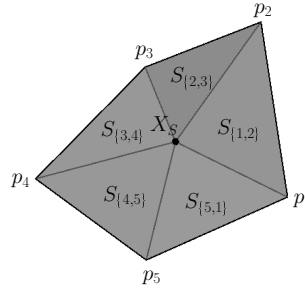


Figure 2.1: Cell  $S$  made of subtriangles  $S_{\{i,i+1\}}$ .

In the following, we adopt the notation  $j = i + 1$  for the cyclic addition ( $j = (i \bmod n_S) + 1$ ) if there is no confusion.

**Definition 2.3.2** (*Admissible cell*)

Let  $S$  be a cell,  $X_S$  its center point and  $p_i$  ( $i = 1, \dots, n_S$ ) its  $n_S$  vertices. For a given vertex  $p_i$  we denote by  $\nu_{S_{\{i,i+1\}}} = \overrightarrow{X_S p_i} \wedge \overrightarrow{X_S p_{i+1}} / \|\overrightarrow{X_S p_i} \wedge \overrightarrow{X_S p_{i+1}}\|$  the oriented normal of the triangle  $[X_S, p_i, p_{i+1}]$  if the triangle has a nonzero measure and we define a pseudo-normal to the cell by  $\nu_S = (\sum_i \overrightarrow{X_S p_i} \wedge \overrightarrow{X_S p_{i+1}}) / \|\sum_i \overrightarrow{X_S p_i} \wedge \overrightarrow{X_S p_{i+1}}\|$ . We will then call the cell admissible if for any  $i, m$  and  $r \in \{1, 2, \dots, n_S\}$ ,  $\|\overrightarrow{X_S p_i}\| \leq \max_{m,r} \|\overrightarrow{p_m p_r}\|$  and  $\nu_{S_{\{i,i+1\}}} \cdot \nu_S > 0$  for well defined normals.

**Remark 2.3.3** The vector  $\nu_S$  depends only on the vertices and not on  $X_S$ . In fact  $\forall r \in \{1, 2, \dots, n_S\}$   $\nu_S := (\sum_i \overrightarrow{X_S p_i} \wedge \overrightarrow{X_S p_{i+1}}) / (\|\sum_i \overrightarrow{X_S p_i} \wedge \overrightarrow{X_S p_{i+1}}\|) = (\sum_i \overrightarrow{p_r p_i} \wedge \overrightarrow{p_r p_{i+1}}) / (\|\sum_i \overrightarrow{p_r p_i} \wedge \overrightarrow{p_r p_{i+1}}\|)$ .

**Definition 2.3.4** (*admissible polygonal surface*)

We define an admissible polygonal surface as a union of admissible cells which form a partition of a  $C^0$  surface  $\Gamma_h$ . Also, the normals  $\nu_{S_i}$  and  $\nu_{S_j}$  of two different cells  $S_i, S_j \subset \Gamma_h$  with  $S_i \cap S_j \neq \emptyset$ , must satisfy  $\nu_{S_i} \cdot \nu_{S_j} > 0$ . We refer to Figure 2.2 for an example of admissible mesh (polygonal surface). The index  $h$  in  $\Gamma_h$  represents the maximum distance between two points in a given cell  $S \subset \Gamma_h$ .

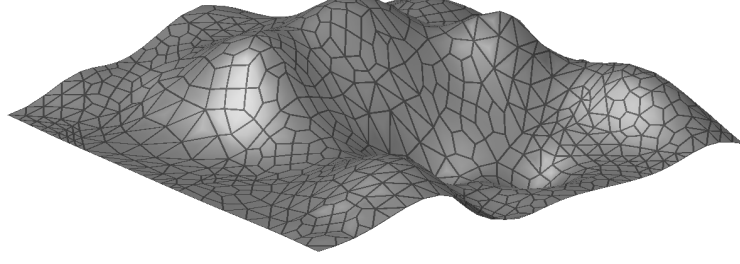


Figure 2.2: Admissible polygonal surface

In the sequel, we assume for surfaces with nonempty boundary a piecewise  $C^2$  boundary. In that case, we assume  $\Gamma^0$  to be part of a larger surface  $\Omega_0 \subset \mathcal{N}_0$  with the same properties as  $\Gamma^0$ , and which is transformed by the map  $\Phi(\cdot, \cdot)$  to  $\Omega(t, \cdot)$  as time evolves. We also denote by  $\mathcal{C}$  a generic constant.

**Definition 2.3.5** ( *$(m, h)$ -polygonal approximation of a surface*)

We will say that the polygonal surface  $\Gamma_h^0$  is an  $(m, h)$ -approximation ( $m \geq 2$ ) of the surface  $\Gamma^0$  if and only if  $\Gamma_h^0$  is admissible and there exists a neighborhood  $\mathcal{N}_{\delta,0} := \{x \mid d(x, \Omega_0) = \inf_{p \in \Omega_0} \|\overline{px}\| \leq \delta\}$  ( $\delta \leq Ch^2$ ) of  $\Omega_0 \supset \Gamma^0$  which satisfies the following conditions:

- i)  $\Gamma_h^0 \subset \mathcal{N}_{\delta,0}$ .
- ii) The perpendicular lines to  $\Omega_0$  at two different points do not intersect within  $\mathcal{N}_{\delta,0}$ .
- iii) The orthogonal projection  $\mathcal{P}\Gamma_h^0$  of  $\Gamma_h^0$  onto  $\Omega_0$  is a bijection between  $\Gamma_h^0$  and its image.
- iv) The orthogonal projection of any cell of  $\Gamma_h^0$  onto  $\Omega_0$  intersects  $\Gamma^0$ .
- v) There exists  $\Gamma_{rest}^0 \subset \Gamma^0$  and  $\Gamma_{ext}^0 \supset \Gamma^0$  satisfying  $\Gamma_{rest}^0 \subset \mathcal{P}\Gamma_h^0 \subset \Gamma_{ext}^0 \subset \Omega_0$  (cf. Figure 2.3) and  $m(\Gamma_{ext}^0 \setminus \Gamma_{rest}^0) \leq Ch^2$  where  $m(\cdot)$  represents the  $(n-1)$ -dimensional Hausdorff measure.
- vi) Let us denote by  $\mathcal{P}_{\partial\Gamma^0} : x \mapsto y = \operatorname{argmin} d(x, \partial\Gamma^0)$  the map that projects points orthogonally on the boundary  $\partial\Gamma^0$  of  $\Gamma^0$ . This map should be well defined in a neighborhood of  $\partial\Gamma^0$  containing  $(\Gamma_{ext}^0 \setminus \Gamma_{rest}^0)$ , and its restriction on  $\mathcal{P}(\partial\Gamma_h^0)$  should be bijective. Furthermore, we assume that the reverse image of a vertex of  $\Gamma^0$  onto  $\mathcal{P}(\partial\Gamma_h^0)$  is the projection of a vertex of  $\Gamma_h^0$  onto  $\Gamma_{ext}^0$  (cf. Figure 2.3).
- vii) For two different vertices  $p_i$  and  $p_j$  of the same cell  $S$ , we have  $Ch \leq \|\overline{p_i p_j}\| \leq h$ .
- viii) For any cell  $S$ , there exists a point  $p_S \in S$  and a vector  $\vec{b}_S$  such that the trace on  $S$  of the cylinder with principal axis  $(p_S, \vec{b}_S)$  and the radius  $Ch$  do not intersect the boundary of  $S$ .
- ix) The distance between a vertex and its projection on  $\Gamma_{ext}^0$  is less than  $Ch^m$ .

**Remark 2.3.6** In the above definition,

- v) expresses the convergence of  $\mathcal{P}\Gamma_h^0$  toward  $\Gamma^0$  as  $h$  tends to 0.
- i), iii) and v) ensure the convergence of the discrete surface  $\Gamma_h^0$  toward  $\Gamma^0$  as  $h$  tends to 0.
- ii) will allow for an extension of functions defined on the reference surface  $\Gamma^0$  onto a narrow band around  $\Gamma^0$  which includes  $\Gamma_h^0$ .

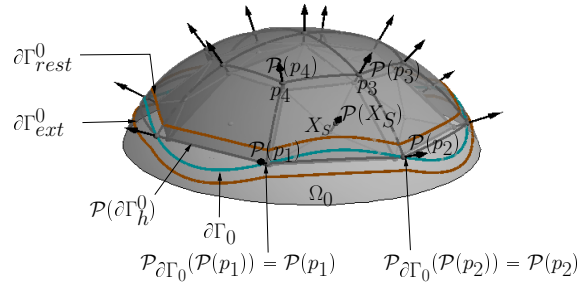


Figure 2.3: Representation of  $\Gamma^0 \subset \Omega_0$ ,  $\Gamma_h^0$ ,  $\mathcal{P}(\Gamma_h^0)$ ,  $\Gamma_{rest}^0$  and  $\Gamma_{ext}^0$  delimited respectively by  $\partial\Gamma^0$  (green line),  $\partial\Gamma_h^0$  (hidden behind the surface),  $\partial\mathcal{P}(\Gamma_h^0)$  (gray line),  $\partial\Gamma_{rest}^0$  (inner brown line) and  $\partial\Gamma_{ext}^0$  (outer brown line).

- *vii) ensures the nondegeneracy of sides while viii) ensures the nondegeneracy of cells. For usual triangular meshes, viii) is expressed as  $C_1 h^2 \leq m_S \leq C_2 h^2 \forall S \subset \Gamma_h^0$  where  $C_1, C_2$  are some fixed constants and  $m_S$  is the  $(n-1)$ -dimensional measure of  $S$ .*
- *iv) ensures that there is no unnecessary cell.*
- *ix) allows us to see that the best paraboloid that can be fitted to a closed set of points will be an  $m$ -order approximation of the original surface. In fact, if some intrinsic properties have to be computed, we will need a good approximation of vertices. This is for example the case in the fourth example considered in this chapter where we have to discretize an additional advection term which involves the curvature tensor. To evaluate the curvature tensor at center points, the best method in the literature to do such a computation at a desired order on a parametric surface is the least square fitting. Of course the consistency of the fitting is at most the consistency of points used which should be  $m \geq 3$  in this case. Furthermore, this general setting is much closer to the real world application than considering vertices bound to the original surface. Most often, the movement of surfaces are described by another partial differential equation; the mean curvature flow considered in the fourth example of this chapter is an illustration. Another example is the two phase flow problem presented in Chapter IV; the Surfactant spreads on top of a thin film which at the same time evolves on a moving surface. In this last case, there is no way to tackle the exact position of free surface points; hence the importance of introducing some inaccuracy on points used to approximate the surface.*

## 2.4 Derivation of the finite volume scheme

### 2.4.1 General setting

We consider a family of admissible polygonal surfaces  $\{\Gamma_h^k\}_{k=0, \dots, k_{max}}$ , with  $\Gamma_h^k$  approximating  $\Gamma(t_k) \subset \Omega^k \subset \mathcal{N}(t_k)$  for  $t_k = k\tau$  and  $k_{max}\tau = t_{max}$ . Here  $\Omega^k := \Omega(t_k) = \Phi(t_k, \Omega_0)$  is a sequence of two dimensional surfaces as defined above in Section 2.3 and, as in Chapter I,  $h$  denotes the maximum diameter of a cell on the whole family of polygonizations,  $\tau$  the time step size and  $k$  the index of a time step. Successive polygonizations share the same grid topology and given the set of vertices  $p_j^k$  on the polygonal surface  $\Gamma_h^k$ , the vertices of  $\Gamma_h^{k+1}$  lie on motion trajectories; thus they are evaluated based on the flux function  $\Phi$ , i.e.,  $p_j^{k+1} = \Phi\left(t_{k+1}, \Phi^{-1}\left(p_j^k, t_k\right)\right)$ . Upper indices denote the time steps and foot indices “ $j$ ” are vertex indices. Let us for the moment merely assume the center points being chosen at each time step such that the discrete surfaces remain uniformly admissible

(2,  $h$ )–polygonizations of the original surfaces; i.e., the constants in Definition 2.3.5 remain the same for all time steps. In Section 2.5, we will give more detail precisions on their choice. Next, at each time step  $t_k$ , we consider a virtual subdivision of each cell  $S^k$  into  $n_S$  subcells (virtual cells)  $S_{p_i}^k$  ( $i = 1, \dots, n_S$ ) which share the common vertex  $X_S^k$  as depicted on Figure 2.4. We recall that  $n_S$

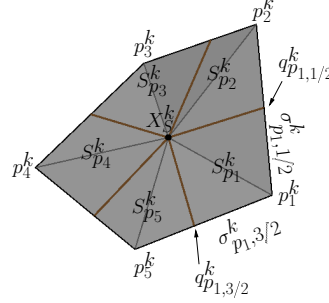


Figure 2.4: Subdivision of cell  $S^k$  into polygonal subcells  $S_{p_i}^k$  and subedges  $\sigma_{p_i, l-1/2}^k := [q_{p_i, l-1/2}^k, p_i^k]$ ,  $\sigma_{p_i, 3/2}^k := [q_{p_i, 3/2}^k, p_i^k]$  induced by  $S_{p_i}^k$  around  $p_i^k$ .

denotes the number of vertices of the cell  $S^k$ . This subdivision, as we can notice again on Figure 2.4, induces a partition of each edge  $\sigma = [p_i^k, p_{i+1}^k] \subset \partial S^k$  into two subedges  $\sigma_{p_i, l-1/2}^k := [q_{p_i, l-1/2}^k, p_i^k]$  and  $\sigma_{p_{i+1}, m+1/2}^k := [q_{p_{i+1}, m+1/2}^k, p_{i+1}^k]$ ;  $q_{p_i, l-1/2}^k = q_{p_{i+1}, m+1/2}^k := S_{p_i}^k \cap S_{p_{i+1}}^k \cap [p_i, p_{i+1}]$ ,  $l$  and  $m$  are subindices used to reference the cell  $S^k$  around the vertices  $p_i^k$  and  $p_{i+1}^k$  respectively. We will come back on how these indices are built in Section 2.4.2. We furthermore assume that two virtual cells  $S_{p_i}^k$  and  $L_{p_i}^k$  of two different cells  $S^k$  and  $L^k$ , which have the vertex  $p_i^k$  in common, share either a common subedge or the only vertex  $p_i^k$  as depicted on Figure 2.5. For later comparison

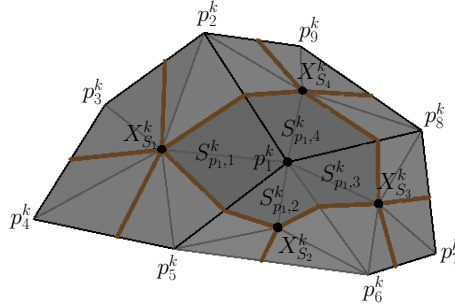


Figure 2.5: Cells and subcells around a vertex.

of discrete quantities on polygonal surfaces  $\Gamma_h^k$  and continuous surfaces  $\Gamma^k = \Gamma(t_k)$ , we first extend functions defined on  $\Gamma^k$  or  $\Gamma_h^k$  in their neighborhood  $\mathcal{N}(t_k)$ . The resulting functions still bear their original names and will be understood from the context. A function  $u(t_k, \cdot)$  defined on  $\Gamma^k$  is then extended by requiring  $\nabla u(t_k, \cdot) \cdot \nabla d(\cdot, \Gamma^k) \equiv 0$ ;  $d(\cdot, \Gamma^k)$  being a signed distance function from  $\Gamma^k$ . This means in other words that, given a point  $x \in \mathcal{N}(t_k)$ , the extended function  $u(t_k, \cdot)$  is constant along the shortest line segment from  $x$  to the surface  $\Gamma^k$ . The restriction of this new function on  $\Gamma_h^k$  will be denoted  $u^{-l}(t_k, \cdot)$  or shortly  $u^{-l, k}$ . On the other hand, the extension of a function  $u_h(t_k, \cdot)$  defined on  $\Gamma_h^k$  is done in two steps. We first extend as constant along the normal  $\nu$  to  $\mathcal{P}^k(\Gamma_h^k)$ ;  $\mathcal{P}^k(\cdot)$  being the orthogonal projection operator onto  $\Omega^k$ . The resulting function, still called  $u_h(t_k, \cdot)$ , is finally extended by requiring  $\nabla u_h(t_k, \cdot) \cdot \nabla d(\cdot, \mathcal{P}^k(\Gamma_h^k)) \equiv 0$ . The restriction of the final

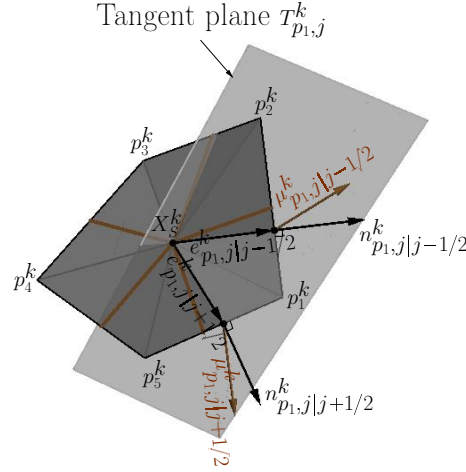


extended function on  $\Gamma^k$  will be termed  $u_h^l(t_k, \cdot)$  or simply  $u^{l,k}$  and the operation which transforms  $u_h(t_k, \cdot)$  to  $u_h^l(t_k, \cdot)$  will be called “lift” operator. These extension operations are by definition well defined in a neighborhood of  $\Gamma(t_k)$  in which  $\Gamma_h^k$  lies, thus the lift operator is well defined. We will also refer to the orthogonal projection as a lift operator; and therefore lift operators will be understood from the context. We denote by  $S^{l,k} := \mathcal{P}^k S^k$  the orthogonal projection of  $S^k$  onto  $\Omega^k$ , by  $S^{l,k}(t) = \Phi(t, \Phi^{-1}(t_k, S^{l,k}))$  the temporal evolution of  $S^{l,k}$  and by  $m_S^k$  the area of  $S^k$ . We should mention here that the symbol “ $l$ ” written as upper index is meant for the “lift” operator; therefore  $x^{l,k}$  will literally mean lift of  $x^k$  onto the surface  $\Omega^k$ . Along the same line, we will call  $S_{p_i}^{l,k} := \mathcal{P}^k S_{p_i}^k$  the orthogonal projection of  $S_{p_i}^k$  onto  $\Omega^k$ . So defined, the subcells  $S_{p_i}^{l,k}$  form a curved mesh on  $S^{l,k}$ . The key of our approach will be to define on these subcells a reasonable approximation of the surface gradient operators  $\nabla_{\Gamma} u$ , and deduce a suitable approximation of  $\nabla_{\Gamma} \cdot (\mathcal{D}_{\Gamma} \nabla_{\Gamma} u)$  in the cells  $S^k$ . Our algorithm can be identified as a hybrid algorithm between mixed finite volume and the usual finite volume procedure. The mixed finite volume defines fluxes or even  $v = \mathcal{D}_{\Gamma} \nabla_{\Gamma} u$  as unknowns which have to be found together with the solution  $u$ . This often leads to a system of equations that has to be stabilized via some restriction on meshes and some appropriate techniques. In our case we define an approximate gradient  $\nabla_h^k u$  of  $\nabla_{\Gamma} u(t_k, \cdot)$  as a piecewise constant gradient  $\left\{ \nabla_{p_i, \mathcal{J}(p_i, S)}^k u \right\}_{p_i, S}$  on subcells  $\{S_{p_i}^k\}_{p_i, S}$ ;  $\mathcal{J}(p_i, S)$  being the local index of subcell  $S_{p_i}^k$  around  $p_i$ . The construction of  $\nabla_h^k u$  is done locally around vertices  $p_i$  via a proper use of the flux continuity condition on subedges as will be explained below. This procedure leads to a local system of equations which in some worse case scenario (very bad mesh and highly anisotropic tensor) is underdetermined. In that case, a suitable minimization procedure is used to stabilize the system which is thereafter partially solved and introduced into the global system of equations that represents (2.1) to obtain a cell center scheme. The procedure of restricting oneself around vertices to construct subfluxes in the finite volume procedure has already been used in [1, 85, 87] for finite volumes on flat surfaces. Restricting to that case, the method developed in [85] is a particular case of the present one. In fact, it loses consistency for polygonal meshes having very deformed quadrangles or nonconvex starshaped cells (flat version of admissible cells which are not convex), while the present method produces good results in those cases. Let us now introduce the construction of the piecewise gradient operator.

## 2.4.2 The discrete gradient operator

Let us first consider a vertex  $p_i$ . We locally reorder the cells  $S_j^k$ , the subcells  $S_{p_i, j}^k$  and the subedges  $\sigma_{p_i, j-1/2}^k$  counterclockwise around the normal at  $p_i$ . The subedges are reordered in a way that  $\sigma_{p_i, j-1/2}^k$  and  $\sigma_{p_i, j+1/2}^k$  are subedges of the cell  $S_j^k$  and the subcell  $S_{p_i, j}^k$ . We also locally rename by  $X_{p_i, j}^k$  the center point of  $S_j^k$ . We refer to Figure 2.4 and Figure 2.5 for the illustration of this setup. Next, we define on each subedge  $\sigma_{p_i, j-1/2}^k$  the virtual point  $X_{p_i, j-1/2}^k$  and on each subcell  $S_{p_i, j}^k$ , we define the covariant vectors  $e_{p_i, j|j-1/2}^k := X_{p_i, j-1/2}^k - X_{p_i, j}^k$  and  $e_{p_i, j|j+1/2}^k := X_{p_i, j+1/2}^k - X_{p_i, j}^k$  which are used to define the local approximate tangent plane  $T_{p_i, j}^k := \text{Span} \left\{ e_{p_i, j|j-1/2}^k, e_{p_i, j|j+1/2}^k \right\}$  to points of the subcell  $S_{p_i, j}^k$ . We also define on  $T_{p_i, j}^k$  the contravariant (dual) basis  $(\mu_{p_i, j|j-1/2}^k, \mu_{p_i, j|j+1/2}^k)$  such that  $e_{p_i, j|j-1/2}^k \cdot \mu_{p_i, j|j-1/2}^k = 1$ ,  $e_{p_i, j|j-1/2}^k \cdot \mu_{p_i, j|j+1/2}^k = 0$ ,  $e_{p_i, j|j+1/2}^k \cdot \mu_{p_i, j|j-1/2}^k = 0$ , and  $e_{p_i, j|j+1/2}^k \cdot \mu_{p_i, j|j+1/2}^k = 1$ . Figure 2.6 illustrates this setup. Using this dual system of vectors, we define for a continuous and derivable scalar function  $u(t_k, \cdot)$  on  $\Gamma^k$ , constant gradients  $\nabla_{p_i, j}^k u$  which approximate  $\nabla u(t_k, \cdot)|_{S_{p_i, j}^{l,k}}$ , restrictions of  $\nabla u(t_k, \cdot)$  on  $S_{p_i, j}^{l,k} \cap \Gamma^k$ .

$$\nabla_{p_i, j}^k u := \left( U_{p_i, j-1/2}^k - U_{p_i, j}^k \right) \mu_{p_i, j|j-1/2}^k + \left( U_{p_i, j+1/2}^k - U_{p_i, j}^k \right) \mu_{p_i, j|j+1/2}^k \quad (2.2)$$


 Figure 2.6: Approximate tangent plane  $T_{p_{i,j}}^k$  to  $S_{p_{i,j}}^{l,k}$ .

where  $U_{p_{i,j-1/2}}^k$ ,  $U_{p_{i,j+1/2}}^k$ ,  $U_{p_{i,j}}^k$ , are appropriate approximations of  $u(t_k, \mathcal{P}^k(X_{p_{i,j-1/2}}^k))$ ,  $u(t_k, \mathcal{P}^k(X_{p_{i,j+1/2}}^k))$  and  $u(t_k, \mathcal{P}^k(X_{p_{i,j}}^k))$  respectively. In this notation, if a point  $X^k$  is on the boundary of  $\Gamma_h^k$ ,  $u(t_k, \mathcal{P}^k(X^k))$  will be taken to be the value of  $u$  at the closest point of  $\Gamma^k$  to  $\mathcal{P}^k(X^k)$ . The definition of our piecewise constant gradient will be completed if we give the explicit expression of the virtual unknowns  $U_{p_{i,j-1/2}}^k$ . For this purpose, let us introduce without proof the following proposition.

**Proposition 2.4.1** *Let  $\Omega$  be an open and bounded set in  $\Gamma(t)$ , made up of two disjoint open sets  $\Omega_1$  and  $\Omega_2$  which share a curved segment  $\sigma^l := \partial\Omega_1 \cap \partial\Omega_2$  as border. Let  $v$  be a tangential vector function which is  $C^1$  on  $\Omega_1$  and  $\Omega_2$ .  $v$  has a weak tangential divergence in  $\mathbb{L}^2(\Omega)$  if and only if its normal component through  $\sigma^l$  is continuous.*

The prerequisites in this proposition can also be weakened by assuming  $v$  being  $\mathbb{H}^1$  on  $\Omega_1$  and  $\Omega_2$ . In that case, the continuity in the conclusion becomes a continuity almost everywhere.

Also, for a line segment  $\sigma^k \subset \Gamma_h^k$  we define

$$\sigma^{l,k} := \{y = x - d(x, \Gamma(t)) \nabla d^T(x, \Gamma(t_k)), x \in \sigma^k\}.$$

It is worth mentioning here that  $\sigma^{l,k}$  can be different from  $\mathcal{P}^k(\sigma^k)$  in some cases. For example, considering the line segment  $\sigma^k := [p_1, p_2]$  on Figure 2.3,  $\sigma^{l,k}$  is the blue curve joining  $\mathcal{P}(p_1)$  and  $\mathcal{P}(p_2)$ . Let us now consider a subcell  $S_{p_{i,j}}^{l,k}$  of a cell  $S_j^{l,k}$ . We approximate the diffusion tensor  $\mathcal{D}$  in (2.1) on  $S_{p_{i,j}}^{l,k}$  by

$$\mathcal{D}_{p_{i,j}}^k := (\text{Id} - \nu_{p_{i,j}}^k \otimes \nu_{p_{i,j}}^k) \left( \frac{1}{m(S_j^{l,k})} \int_{S_j^{l,k}} \mathcal{D} dS_j^{l,k} \right) (\text{Id} - \nu_{p_{i,j}}^k \otimes \nu_{p_{i,j}}^k),$$

where  $\nu_{p_{i,j}}^k := (e_{p_{i,j}|j+1/2}^k \wedge e_{p_{i,j}|j-1/2}^k) / \|e_{p_{i,j}|j+1/2}^k \wedge e_{p_{i,j}|j-1/2}^k\|$  is the normal to  $T_{p_{i,j}}^k$  that we take as the approximation of the oriented normal  $\nu$  to  $S_{p_{i,j}}^{l,k}$ . We also approximate the unit outer conormals to  $\sigma_{p_{i,j-1/2}}^{l,k} := (\sigma_{p_{i,j-1/2}}^k)^l$  and  $\sigma_{p_{i,j+1/2}}^{l,k} := (\sigma_{p_{i,j+1/2}}^k)^l$  by  $n_{p_{i,j}|j-1/2}^k$  and  $n_{p_{i,j}|j+1/2}^k$ , respectively. These are vectors of  $T_{p_{i,j}}^k$  which are respectively normal to  $\sigma_{p_{i,j-1/2}}^k$  and  $\sigma_{p_{i,j+1/2}}^k$  (cf. Figure 2.6) and which point outward from the projection in the direction of  $\nu$  of  $S_{p_{i,j}}^{l,k}$  onto  $T_{p_{i,j}}^k$ .

Finally, we approximate  $m_{p_i,j-1/2}^{l,k}$ , the measure of  $\sigma_{p_i,j-1/2}^{l,k}$ , by  $m_{p_i,j-1/2}^k$ , the measure of  $\sigma_{p_i,j-1/2}^k$ . Since  $\mathcal{D}\nabla_{\Gamma}u$  has a weak divergence in  $\mathbb{L}^2(\Gamma)$ , we apply a discrete version of Proposition 2.4.1 on subcells surrounding vertices  $p_i^k$ ; Namely,

$$m_{p_i,j-1/2}^k \mathcal{D}_{p_i,j-1}^k \nabla_{p_i,j-1}^k u \cdot n_{p_i,j-1|j-1/2}^k + m_{p_i,j-1/2}^k \mathcal{D}_{p_i,j}^k \nabla_{p_i,j}^k u \cdot n_{p_i,j|j-1/2}^k = 0 \quad (2.3)$$

for the subedge  $\sigma_{p_i,j-1/2}^k$ . Rewriting the system of equations given by (2.3) around  $p_i^k$  in the matrix form gives

$$M_{p_i}^k \tilde{U}_{p_i,\sigma}^k = N_{p_i}^k \tilde{U}_{p_i}^k, \quad (2.4)$$

where  $\tilde{U}_{p_i,\sigma}^k := (U_{p_i,1/2}^k, U_{p_i,3/2}^k, \dots)^\top$ ,  $\tilde{U}_{p_i}^k := (U_{p_i,1}^k, U_{p_i,2}^k, \dots)^\top$ , and the entries of  $M_{p_i}^k$  and  $N_{p_i}^k$  are  $(M_{p_i}^k)_{j,j-1} = m_{p_i,j-1/2}^k \lambda_{p_i,j-3/2|j-1|j-1/2}^k$ ,  $(M_{p_i}^k)_{j,j} = m_{p_i,j-1/2}^k (\lambda_{p_i,j-1|j-1/2}^k + \lambda_{p_i,j|j-1/2}^k)$ ,  $(M_{p_i}^k)_{j,j+1} = m_{p_i,j-1/2}^k \lambda_{p_i,j+1/2|j|j-1/2}^k$ ,  $(N_{p_i}^k)_{j,j-1} = m_{p_i,j-1/2}^k (\lambda_{p_i,j-1|j-1/2}^k + \lambda_{p_i,j-3/2|j-1|j-1/2}^k)$ ,  $(N_{p_i}^k)_{j,j} = m_{p_i,j-1/2}^k (\lambda_{p_i,j|j-1/2}^k + \lambda_{p_i,j+1/2|j|j-1/2}^k)$ , and 0 elsewhere; with  $\lambda_{p_i,j|j-1/2}^k = n_{p_i,j|j-1/2}^k \cdot \mathcal{D}_{p_i,j}^k \mu_{p_i,j|j-1/2}^k$ ,  $\lambda_{p_i,j+1/2|j|j-1/2}^k = n_{p_i,j|j-1/2}^k \cdot \mathcal{D}_{p_i,j}^k \mu_{p_i,j|j+1/2}^k$ ,  $\lambda_{p_i,j-1/2|j|j+1/2}^k = n_{p_i,j|j+1/2}^k \cdot \mathcal{D}_{p_i,j}^k \mu_{p_i,j|j-1/2}^k$ ,  $\lambda_{p_i,j|j+1/2}^k = n_{p_i,j|j+1/2}^k \cdot \mathcal{D}_{p_i,j}^k \mu_{p_i,j|j+1/2}^k$ . If  $p_i^k$  is a boundary point, making use of the Dirichlet boundary condition, we rewrite (2.4) using the same notation  $M_{p_i}^k \tilde{U}_{p_i,\sigma}^k = N_{p_i}^k \tilde{U}_{p_i}^k$  with  $\tilde{U}_{p_i,\sigma}^k := (U_{p_i,3/2}^k, \dots, U_{p_i,n_{p_i}-1/2}^k)^\top$ ,  $\tilde{U}_{p_i}^k := (U_{p_i,1/2}^k, U_{p_i,1}^k, \dots, U_{p_i,n_{p_i}}^k, U_{p_i,n_{p_i}+1/2}^k)^\top$ .  $n_{p_i}$  denotes the number of cells around  $p_i^k$  and  $U_{p_i,1/2}^k := u(t_k, \mathcal{P}^k(X_{p_i,1/2}^k))$ ,  $U_{p_i,n_{p_i}+1/2}^k := u(t_k, \mathcal{P}^k(X_{p_i,n_{p_i}+1/2}^k))$  at the boundary. The matrix  $M_{p_i}^k$  is then a square matrix whose dimension is the number of subedges around  $p_i^k$  on which we have unknowns while the matrix  $N_{p_i}^k$  is a square matrix for interior vertices (vertices which do not belong to the boundary) and a rectangular matrix for boundary vertices. We should mention here that for consistency reasons, the subedge points  $X_{p_i,j-1/2}^k$  should be chosen in such a way that the angle  $\theta_{p_i,j}^k := \angle(X_{p_i,j-1/2}^k X_j^k X_{p_i,j+1/2}^k)$  between  $e_{p_i,j|j+1/2}^k$  and  $e_{p_i,j|j-1/2}^k$  is always greater than a threshold angle  $\theta$  during the entire process. This condition also leads to the invertibility of  $M_{p_i}^k$  when the diffusion tensors  $\mathcal{D}_{p_i,j}^k$  involved in the system are uniformly elliptic on corresponding tangent plane, with the elliptic constant far from 0, and the incident angles at  $p_i^k$  acute and far from 0 and  $\pi$  ( $0 \ll \angle(X_{p_i,j+1/2}^k p_i^k X_{p_i,j-1/2}^k) \ll \pi$ ). In that case, equation (2.4) will be transformed to

$$\tilde{U}_{p_i,\sigma}^k = (M_{p_i}^k)^{-1} N_{p_i}^k \tilde{U}_{p_i}^k. \quad (2.5)$$

If there exist a subcell  $S_{p_i,j}^{l,k}$  in which  $\mathcal{D}_{p_i,j}^k$  is almost one dimensional, for example

$$\mathcal{D}_{p_i,j}^k := (\text{Id} - \nu_{p_i,j}^k \otimes \nu_{p_i,j}^k) \begin{pmatrix} 1 & 0 & 0 \\ 0 & \alpha & 0 \\ 0 & 0 & \alpha \end{pmatrix} (\text{Id} - \nu_{p_i,j}^k \otimes \nu_{p_i,j}^k), \quad \alpha = 1/10000, \quad M_{p_i}^k \text{ can become noninvertible}$$

if the mesh is not aligned with the anisotropy and the virtual points  $X_{p_i,j-1/2}^k$  as well as the center points  $X_j^k$  chosen consequently. Simulation of strong anisotropic flow on such a general moving mesh will often encounter this problem if we did not take care from the beginning by trying to produce an adequate mesh near to what has been described in Chapter I for the triangular case. By doing so, we limit a lot the possibilities of the actual scheme. Then if  $M_{p_i}^k$  is singular, we will first make sure that the choice of the virtual points on subedges guarantees that the range of  $N_{p_i}^k$  is a subset of the range of  $M_{p_i}^k$ ; i.e  $\text{Im}(N_{p_i}^k) \subset \text{Im}(M_{p_i}^k)$ . Thereafter, we choose  $\tilde{U}_{p_i,\sigma}^k$  as the solution of (2.4) whose the induced discrete gradient around  $p_i^k$  has the minimum  $\mathbb{H}_0^1$ -norm. The problem of finding

$\tilde{U}_{p_i,\sigma}^k$  is then stated numerically as follows:

$$\left\{ \begin{array}{l} \text{Find } \tilde{U}_{p_i,\sigma}^k \text{ in } \mathcal{B}_{p_i}^k := \left\{ \tilde{V}_{p_i,\sigma}^k := (V_{p_i,1/2}^k, V_{p_i,3/2}^k, \dots)^\top \mid M_{p_i}^k \tilde{V}_{p_i,\sigma}^k = N_{p_i}^k \tilde{U}_{p_i}^k \right\} \text{ such that} \\ \tilde{U}_{p_i,\sigma}^k = \operatorname{argmin}_{\tilde{V}_{p_i,\sigma}^k \in \mathcal{B}_{p_i}^k} \sum_j m_{p_i,j}^k \left\| \left[ V_{p_i,j-1/2}^k - U_{p_i,j}^k \right] \mu_{p_i,j|j-1/2}^k + \left[ V_{p_i,j+1/2}^k - U_{p_i,j}^k \right] \mu_{p_i,j|j+1/2}^k \right\|^2, \end{array} \right. \quad (2.6)$$

where  $m_{p_i,j}^k := m(S_{p_i,j}^k)$  approximates  $m(S_{p_i,j}^{l,k})$ . One easily verifies that this problem is equivalent to the following least square problem

$$\left\{ \begin{array}{l} \text{Find } \tilde{U}_{p_i,\sigma}^k \text{ in } \mathcal{B}_{p_i}^k := \left\{ \tilde{V}_{p_i,\sigma}^k := (V_{p_i,1/2}^k, V_{p_i,3/2}^k, \dots)^\top \mid M_{p_i}^k \tilde{V}_{p_i,\sigma}^k = N_{p_i}^k \tilde{U}_{p_i}^k \right\} \text{ such that} \\ \tilde{U}_{p_i,\sigma}^k = \operatorname{argmin}_{\tilde{V}_{p_i,\sigma}^k \in \mathcal{B}_{p_i}^k} \left\| \sqrt{\mathbf{B}_{p_i}^k} \tilde{V}_{p_i,\sigma}^k - \left( \sqrt{\mathbf{B}_{p_i}^k} \right)^{-1} \mathbf{C}_{p_i}^k \tilde{U}_{p_i}^k \right\|^2, \end{array} \right.$$

where  $\sqrt{\mathbf{B}_{p_i}^k}$  is the square root of the symmetric positive definite matrix  $\mathbf{B}_{p_i}^k$  (i.e.  $\sqrt{\mathbf{B}_{p_i}^k} \sqrt{\mathbf{B}_{p_i}^k} = \mathbf{B}_{p_i}^k$ ) defined by

$$\begin{aligned} (\mathbf{B}_{p_i}^k)_{j,j} &= m_{p_i,j-1}^k \|\mu_{p_i,j-1|j-1/2}^k\|^2 + m_{p_i,j}^k \|\mu_{p_i,j|j-1/2}^k\|^2, \\ (\mathbf{B}_{p_i}^k)_{j,j+1} &= (\mathbf{B}_{p_i}^k)_{j+1,j} = m_{p_i,j}^k \mu_{p_i,j|j-1/2}^k \cdot \mu_{p_i,j|j+1/2}^k; \end{aligned}$$

and  $\mathbf{C}_{p_i}^k$  the matrix defined by

$$\begin{aligned} (\mathbf{C}_{p_i}^k)_{j,j} &= m_{p_i,j}^k \left( \|\mu_{p_i,j|j-1/2}^k\|^2 + \mu_{j|j-1/2}^k \cdot \mu_{p_i,j|j+1/2}^k \right), \\ (\mathbf{C}_{p_i}^k)_{j+1,j} &= m_{p_i,j}^k \left( \|\mu_{p_i,j|j+1/2}^k\|^2 + \mu_{j|j-1/2}^k \cdot \mu_{p_i,j|j+1/2}^k \right). \end{aligned}$$

Our aim here is not to solve this least square problem at this stage but to build a relation between the solution  $\tilde{U}_{p_i,\sigma}^k$  and the cell center values  $\tilde{U}_{p_i}^k$ . Lars Eldén discussed the solution of this class of problems extensively in [41] and it turns out that this problem has a unique solution if the intersection of the null space of  $\sqrt{\mathbf{B}_{p_i}^k}$  and the null space of  $M_{p_i}^k$  is the null vector. This is the case

here since  $\sqrt{\mathbf{B}_{p_i}^k}$  is invertible. The use of the new variable  $\tilde{W}_{p_i,\sigma}^k := \sqrt{\mathbf{B}_{p_i}^k} \tilde{V}_{p_i,\sigma}^k - \left( \sqrt{\mathbf{B}_{p_i}^k} \right)^{-1} \mathbf{C}_{p_i}^k \tilde{U}_{p_i}^k$  reduces the problem to

$$\left\{ \begin{array}{l} \text{Find } \tilde{W}_{p_i,\sigma}^k \text{ in } \tilde{\mathcal{B}}_{p_i}^k := \left\{ \tilde{V}_{p_i,\sigma}^k := (V_{p_i,1/2}^k, V_{p_i,3/2}^k, \dots)^\top \mid \right. \\ \left. M_{p_i}^k \left( \sqrt{\mathbf{B}_{p_i}^k} \right)^{-1} \tilde{V}_{p_i,\sigma}^k = \left( N_{p_i}^k - M_{p_i}^k \left( \mathbf{B}_{p_i}^k \right)^{-1} \mathbf{C}_{p_i}^k \right) \tilde{U}_{p_i}^k \right\} \text{ such that } \tilde{W}_{p_i,\sigma}^k = \operatorname{argmin}_{\tilde{V}_{p_i,\sigma}^k \in \tilde{\mathcal{B}}_{p_i}^k} \left\| \tilde{V}_{p_i,\sigma}^k \right\|^2. \end{array} \right.$$

From the solution of this last problem, one easily deduces the solution to the original problem

$$\tilde{U}_{p_i,\sigma}^k = \mathbf{Coef}_{p_i}^k \tilde{U}_{p_i}^k, \quad (2.7)$$

$$\text{where } \mathbf{Coef}_{p_i}^k = \left( \sqrt{\mathbf{B}_{p_i}^k} \right)^{-1} \left( M_{p_i}^k \left( \sqrt{\mathbf{B}_{p_i}^k} \right)^{-1} \right)^\dagger \left( N_{p_i}^k - M_{p_i}^k \left( \mathbf{B}_{p_i}^k \right)^{-1} \mathbf{C}_{p_i}^k \right) + \left( \mathbf{B}_{p_i}^k \right)^{-1} \mathbf{C}_{p_i}^k \quad (2.8)$$

$\left( M_{p_i}^k \left( \sqrt{\mathbf{B}_{p_i}^k} \right)^{-1} \right)^\dagger$  is the Moore-Penrose inverse of  $M_{p_i}^k \left( \sqrt{\mathbf{B}_{p_i}^k} \right)^{-1}$ . We recall that the Moore-Penrose inverse of a matrix  $\mathbf{A}$  is the unique matrix  $\mathbf{A}^\dagger$  that satisfies

$$\begin{aligned} \mathbf{A} \mathbf{A}^\dagger \mathbf{A} &= \mathbf{A}, & \mathbf{A}^\dagger \mathbf{A} \mathbf{A}^\dagger &= \mathbf{A}^\dagger, \\ \operatorname{tr} (\mathbf{A} \mathbf{A}^\dagger) &= \operatorname{tr} (\mathbf{A}) \operatorname{tr} (\mathbf{A}^\dagger), & \operatorname{tr} (\mathbf{A}^\dagger \mathbf{A}) &= (\operatorname{tr} \mathbf{A}^\dagger) \operatorname{tr} (\mathbf{A}); \end{aligned}$$

$\text{tr}(\cdot)$  being the trace operator. The Moore-Penrose inverse coincides with the usual inverse of an invertible matrix; thus (2.5) is recovered in (2.7) and we can consider the least square problem as being the problem to be solve to find the virtual unknowns. We refer to [20, 24, 27, 40, 41, 79, 102, 116] for details on the general topic of generalized inverse of matrices. Let us remark that the sum of line element of the matrix  $\mathbf{Coef}_{p_i}^k$  is 1, i.e  $\mathbf{Coef}_{p_i}^k \mathbf{1}_{p_i} = \mathbf{1}_{p_i,\sigma}$  where  $\mathbf{1}_{p_i} := (1, 1, \dots)^\top$ ,  $\mathbf{1}_{p_i,\sigma} := (1, 1, \dots)^\top$  are respectively vector of ones with the same length as  $\tilde{U}_{p_i}^k$  and  $\tilde{U}_{p_i,\sigma}^k$ . In fact,  $\mathbf{1}_{p_i,\sigma}$  is the unique solution of the above least square problem for  $\tilde{U}_{p_i}^k = \mathbf{1}_{p_i}$ . Therefore  $U_{p_i,j-1/2}^k$  can be seen as a barycenter of the values  $U_{p_i}^k$ . Such an idea to introduce the barycenter of values at cell centers to approximate values on edges in the finite volume context was already used by Eymard, Gallouët and Herbin in [46]. Unfortunately, due to the random choice of the barycentric coefficients, their resulting fluxes were poorly approximated, did not respect the flux continuity in the usual sense of finite volume methods and therefore needed extra treatment to guarantee good accuracy of the simulation result. This is a reason of our special treatment of virtual unknowns. Also, by minimizing the gradient, we try to avoid extra extrema on edges which would cause oscillations while keeping the consistency of the approximations. This enforces the monotonicity whenever possible. On the other hand, (2.2), (2.7) and (2.8) define a special quadrature rule to construct the gradient of a function on subcells around a vertex  $p_i^k$  knowing the surrounding cell center values. In one dimension, this is exactly the usual finite volume procedure. One can easily extend the procedure to three dimensions.

**Remark 2.4.2**

a) Let us point out some trivial setup on triangular meshes.

- i) First we assume the center points at the isobarycenter of triangles and subcells constructed such that the edges are divided exactly in the middle. We assume the virtual subedge points  $X_{p_i,j-1/2}^k$  being placed such that  $\|\overrightarrow{p_i^k X_{p_i,j-1/2}^k}\| = (2/3)m_{p_i,j-1/2}^k$  (cf. Figure 2.7); then (2.7) reduces to (2.5).

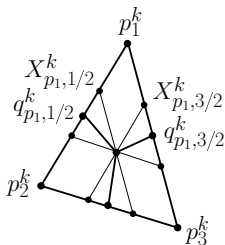


Figure 2.7: Subdivision of triangle cell using isobarycenter and the middle of edges.

- ii) Secondly, we assume the setup defined in Chapter I; namely, the center points  $X_S^k$  and the subcells are constructed such that the boundary points  $q_{p_i,j-1/2}^k$  on  $\sigma_{p_i,j-1/2}^k$  with  $\|\overrightarrow{p_i^k q_{p_i,j-1/2}^k}\| = m_{p_i,j-1/2}^k$  satisfy the orthogonality conditions  $(\mathcal{D}_{p_i,j-1}^k)^{-1} (\overrightarrow{X_{p_i,j-1}^k q_{p_i,j-1/2}^k}) \cdot \overrightarrow{p_i^k q_{p_i,j-1/2}^k} = 0$  and  $(\mathcal{D}_{p_i,j}^k)^{-1} (\overrightarrow{X_{p_i,j}^k q_{p_i,j-1/2}^k}) \cdot \overrightarrow{p_i^k q_{p_i,j-1/2}^k} = 0$  (cf. Figure 2.8). If we choose  $X_{p_i,j-1/2}^k = q_{p_i,j-1/2}^k$ , (2.7) reduces to (2.5). Here, (2.3) links the virtual unknown  $U_{p_i,j-1/2}^k$  only to the cells unknowns  $U_{p_i,j-1}^k$  and  $U_{p_i,j}^k$  across the subedge  $\sigma_{p_i,j-1/2}^k$ ; thus the local matrices  $M_{p_i}^k$  are diagonal.
- iii) We could also define  $\mathcal{D}_{p_i,j}^k$  as being constant around vertices  $p_i^k$ ; for instance

$$\mathcal{D}_{p_i,j}^k = \mathcal{D}_{p_i}^k := \left( 1 / \sum_j m_{p_i,j}^k \right) \sum_j \int_{S_j^{l,k}} \mathcal{D} dS_{p_i,j}^{l,k}.$$

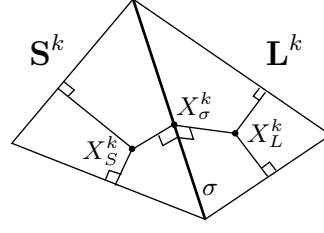


Figure 2.8: A sketch of the local configuration of center points and subedge points satisfying the orthogonality condition. The two neighboring cells are not always coplanar.

*i.e.*, The summation is done on subcells around  $p_i^k$ . Let us restrict ourselves to triangular meshes on flat surfaces. We consider the dual mesh obtained by first joining the center points of triangles sharing a common edge, secondly join the middle of triangle edges  $\sigma^k$  that belong to the mesh boundary ( $\sigma^k \subset \partial\Gamma_h^k$ ) to the center of the corresponding triangles. This setup is depicted on Figure 2.9. We adopt the vertices of the previous mesh as the center points of this new mesh. Each interior vertex of the dual mesh is surrounded by exactly three subcells and

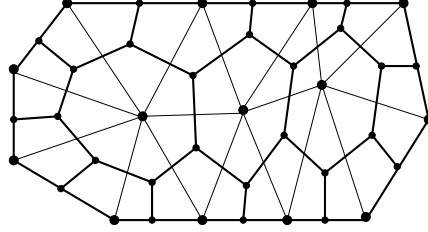


Figure 2.9: A sketch of a triangular mesh (delimited by thin line) and its dual (delimited by thick line).

(2.7) reduces to (2.5) since there is only one way to build a gradient from three noncolinear points.

- b) If we had to treat the case of Neumann boundary condition or mixed boundary condition (Dirichlet-Neumann), then for any subedge  $\sigma_{p_i,j}^k \subset \Gamma_h^k$ , only one type of boundary condition should be defined on  $\sigma_{p_i,j}^{l,k}$ . We obtain (2.4) by adding extra equations to (2.3) which correspond to the realization of the Neumann boundary condition at corresponding subedge virtual points.

Based on these preliminaries, we can now introduce the finite volume discretization.

### 2.4.3 Finite Volumes discretization

Let us integrate (2.1) on  $\{(t, x) | t \in [t_k, t_{k+1}], x \in S^{l,k}(t) \cap \Gamma(t)\}$ , where  $S^{l,k}(t) := \Phi(t, \Phi^{-1}(t_k, S^{l,k}))$ .

$$\int_{t_k}^{t_{k+1}} \int_{S^{l,k}(t) \cap \Gamma(t)} g \, da \, dt \approx \tau m_S^{k+1} G_S^{k+1}, \quad (2.9)$$

where  $G_S^{k+1} := g(t, \mathcal{P}^{k+1} X_S^{k+1})$ . As in Chapter I, the use of the Leibniz formula leads to the following approximation of the material derivative

$$\begin{aligned} \int_{t_k}^{t_{k+1}} \int_{S^{l,k}(t) \cap \Gamma(t)} (\dot{u} + u \nabla_{\Gamma} v) \, da \, dt &= \int_{S^{l,k}(t_{k+1}) \cap \Gamma(t_{k+1})} u \, da - \int_{S^{l,k}(t_k) \cap \Gamma(t_k)} u \, da \\ &\approx m_S^{k+1} U_S^{k+1} - m_S^k U_S^k, \end{aligned} \quad (2.10)$$

where we recall that the discrete quantities  $U_S^k$  and  $U_S^{k+1}$  approximate  $u(t_k, \mathcal{P}^k X_S^k)$  and  $u(t_{k+1}, \mathcal{P}^{k+1} X_S^{k+1})$ , respectively. Integrating the elliptic term again over the temporal evolution of a lifted cell and applying the Gauss' theorem, leads to the following approximation

$$\begin{aligned} & \int_{t_k}^{t_{k+1}} \int_{S^{l,k}(t) \cap \Gamma(t)} \nabla_{\Gamma} \cdot (\mathcal{D} \nabla_{\Gamma} u) \, da \, dt = \int_{t_k}^{t_{k+1}} \int_{\partial(S^{l,k}(t) \cap \Gamma(t))} (\mathcal{D} \nabla_{\Gamma} u) \cdot n_{\partial(S^{l,k}(t) \cap \Gamma(t))} \, dl \, dt \\ & \approx \tau \sum_{p_i \in \partial S^k} \left( m_{p_i, \mathcal{J}(p_i, S)}^{k+1} \mathcal{D}_{p_i, \mathcal{J}(p_i, S)}^k \nabla_{p_i, \mathcal{J}(p_i, S)}^{k+1} u \cdot n_{p_i, \mathcal{J}(p_i, S) | \mathcal{J}(p_i, S) - 1/2}^{k+1} \right. \\ & \left. + m_{p_i, \mathcal{J}(p_i, S) + 1/2}^{k+1} \mathcal{D}_{p_i, \mathcal{J}(p_i, S)}^k \nabla_{p_i, \mathcal{J}(p_i, S)}^{k+1} u \cdot n_{p_i, \mathcal{J}(p_i, S) | \mathcal{J}(p_i, S) + 1/2}^{k+1} \right). \end{aligned} \quad (2.11)$$

where  $n_{\partial(S^{l,k}(t) \cap \Gamma(t))}$  is the unit outer conormal to the curved boundary  $\partial(S^{l,k}(t) \cap \Gamma(t))$  of  $(S^{l,k}(t) \cap \Gamma(t))$ . We recall that  $\mathcal{J}(p_i, S^k)$  denotes the local number of the cell  $S^k$  around  $p_i^k$ . Combining (2.2), (2.9), (2.10) and (2.11) gives the finite volume scheme

$$\begin{aligned} & m_S^{k+1} U_S^{k+1} - m_S^k U_S^k \\ & - \tau \sum_{p_i \in \partial S^k} \left[ m_{p_i, \mathcal{J}(p_i, S) - 1/2}^{k+1} \left( U_{p_i, \mathcal{J}(p_i, S) - 1/2}^{k+1} - U_{p_i, \mathcal{J}(p_i, S)}^{k+1} \right) \lambda_{p_i, \mathcal{J}(p_i, S) | \mathcal{J}(p_i, S) - 1/2}^{k+1} \right. \\ & + m_{p_i, \mathcal{J}(p_i, S) - 1/2}^{k+1} \left( U_{p_i, \mathcal{J}(p_i, S) + 1/2}^{k+1} - U_{p_i, \mathcal{J}(p_i, S)}^{k+1} \right) \lambda_{p_i, \mathcal{J}(p_i, S) + 1/2 | \mathcal{J}(p_i, S) | \mathcal{J}(p_i, S) - 1/2}^{k+1} \\ & + m_{p_i, \mathcal{J}(p_i, S) + 1/2}^{k+1} \left( U_{p_i, \mathcal{J}(p_i, S) - 1/2}^{k+1} - U_{p_i, \mathcal{J}(p_i, S)}^{k+1} \right) \lambda_{p_i, \mathcal{J}(p_i, S) - 1/2 | \mathcal{J}(p_i, S) | \mathcal{J}(p_i, S) + 1/2}^{k+1} \\ & \left. + m_{p_i, \mathcal{J}(p_i, S) + 1/2}^{k+1} \left( U_{p_i, \mathcal{J}(p_i, S) + 1/2}^{k+1} - U_{p_i, \mathcal{J}(p_i, S)}^{k+1} \right) \lambda_{p_i, \mathcal{J}(p_i, S) | \mathcal{J}(p_i, S) + 1/2}^{k+1} \right] \\ & = \tau m_S^{k+1} G_S^{k+1}. \end{aligned} \quad (2.12)$$

where the subedge virtual unknowns  $U_{p_i, \mathcal{J}(p_i, S) - 1/2}^{k+1}$  and  $U_{p_i, \mathcal{J}(p_i, S) + 1/2}^{k+1}$  are given by equation (2.7) in terms of cells unknowns  $U_{p_i, \mathcal{J}(p_i, S)}^{k+1}$ . The system of equations (2.12) is completely determined by the initial data  $U_S^0 := u(t_0, \mathcal{P}^0(X_S^0))$ . Let us now associate to cells unknowns and subedges virtual unknowns the piecewise constant functions  $U^k$  defined on  $\Gamma_h^k$  with  $U^k|_S = U_S^k$ , and  $U_{\partial\Gamma}^k$  defined on  $\partial\Gamma_h^k$  with  $U_{\partial\Gamma}^k|_{\sigma_{p_i, 1/2}^k} = U_{p_i, 1/2}^k$ ,  $U_{\partial\Gamma}^k|_{\sigma_{p_i, n_{p_i} + 1/2}^k} = U_{p_i, n_{p_i} + 1/2}^k$  for any boundary vertex  $p_i$  and its surrounding boundary subedges  $\sigma_{p_i, 1/2}^k$  and  $\sigma_{p_i, n_{p_i} + 1/2}^k$ . We denote by

$$\mathcal{V}_h^k := \{ U^k : \Gamma_h^k \rightarrow \mathbb{R} \mid \forall S^k \subset \Gamma_h^k, U^k|_{S^k} = \text{const} \} \quad (2.13)$$

$$\mathcal{V}_{\partial\Gamma}^k := \left\{ U_{\partial\Gamma}^k : \partial\Gamma_h^k \rightarrow \mathbb{R} \mid \forall p_i^k \in \partial\Gamma_h^k, U_{\partial\Gamma}^k|_{\sigma_{p_i, 1/2}^k} = \text{const}, U_{\partial\Gamma}^k|_{\sigma_{p_i, n_{p_i} + 1/2}^k} = \text{const} \right\} \quad (2.14)$$

the sets of such functions. (2.2) can be considered as a quadrature rule that builds an approximate gradient of a continuous function on  $\Gamma^k$  out of its projection (representant) in  $\mathcal{V}_h^k \cup \mathcal{V}_{\partial\Gamma}^k$ . We wish to build a seminorm on  $\mathcal{V}_h^k$ . For this sake, we first denote by

$$\begin{aligned} \Omega_S^k & := \frac{1}{m_S^k} \sum_{p_i \in \partial S^k} \left( m_{p_i, \mathcal{J}(p_i, S) - 1/2}^k \mathcal{D}_{p_i, \mathcal{J}(p_i, S)}^k \nabla_{p_i, \mathcal{J}(p_i, S)}^k u \cdot n_{p_i, \mathcal{J}(p_i, S) | \mathcal{J}(p_i, S) - 1/2}^k \right. \\ & \left. + m_{p_i, \mathcal{J}(p_i, S) + 1/2}^k \mathcal{D}_{p_i, \mathcal{J}(p_i, S)}^k \nabla_{p_i, \mathcal{J}(p_i, S)}^k u \cdot n_{p_i, \mathcal{J}(p_i, S) | \mathcal{J}(p_i, S) + 1/2}^k \right) \end{aligned} \quad (2.15)$$

the approximation of  $\int_{S^{l,k}(t_k) \cap \Gamma(t_k)} \nabla_{\Gamma} \cdot (\mathcal{D} \nabla_{\Gamma} u) \, da$ . We thereafter multiply each equation of (2.15) by the corresponding cell center value  $-U_S^k$ , and each equation of (2.3) by the corresponding subedge virtual unknown  $U_{p_i, j-1/2}^k$ . Finally, we sum the resulting equations over all cells and subedges and

obtain

$$\begin{aligned}
 - \sum_{S^k} m_S^k U_S^k \mathbf{D}_S^k &= \sum_{S^k} \sum_{p_i^k \in S^k} \left[ (U_{p_i, \mathcal{J}(p_i, S^k)+1/2}^k - U_S^k), (U_{p_i, \mathcal{J}(p_i, S^k)-1/2}^k - U_S^k) \right] \\
 &\quad Q_{p_i, \mathcal{J}(p_i, S^k), \text{sym}}^k \left[ (U_{p_i, \mathcal{J}(p_i, S^k)+1/2}^k - U_S^k), (U_{p_i, \mathcal{J}(p_i, S^k)-1/2}^k - U_S^k) \right]^\top \quad (2.16) \\
 &\quad - \sum_{p_i^k \in \partial \Gamma_h^k} \left( m_{p_i, 1/2}^k U_{p_i, 1/2}^k \mathcal{D}_{p_i, 1}^k \nabla_{p_i, 1}^k u \cdot n_{p_i, 1|1/2}^k \right. \\
 &\quad \left. + m_{p_i, n_{p_i}+1/2}^k U_{p_i, n_{p_i}+1/2}^k \mathcal{D}_{p_i, n_{p_i}}^k \nabla_{p_i, n_{p_i}}^k u \cdot n_{p_i, n_{p_i}|n_{p_i}+1/2}^k \right),
 \end{aligned}$$

where  $Q_{p_i, \mathcal{J}(p_i, S^k), \text{sym}}^k = (Q_{p_i, \mathcal{J}(p_i, S^k)}^k + (Q_{p_i, \mathcal{J}(p_i, S^k)}^k)^\top) / 2$  with

$$\begin{aligned}
 (Q_{p_i, \mathcal{J}(p_i, S^k)}^k)_{11} &:= m_{p_i, \mathcal{J}(p_i, S^k)-1/2}^k \lambda_{p_i, \mathcal{J}(p_i, S^k)|\mathcal{J}(p_i, S^k)-1/2}^k, \\
 (Q_{p_i, \mathcal{J}(p_i, S^k)}^k)_{12} &:= m_{p_i, \mathcal{J}(p_i, S^k)-1/2}^k \lambda_{p_i, \mathcal{J}(p_i, S^k)+1/2|\mathcal{J}(p_i, S^k)|\mathcal{J}(p_i, S^k)-1/2}^k, \\
 (Q_{p_i, \mathcal{J}(p_i, S^k)}^k)_{21} &:= m_{p_i, \mathcal{J}(p_i, S^k)+1/2}^k \lambda_{p_i, \mathcal{J}(p_i, S^k)-1/2|\mathcal{J}(p_i, S^k)|\mathcal{J}(p_i, S^k)+1/2}^k, \\
 (Q_{p_i, \mathcal{J}(p_i, S^k)}^k)_{22} &:= m_{p_i, \mathcal{J}(p_i, S^k)+1/2}^k \lambda_{p_i, \mathcal{J}(p_i, S^k)|\mathcal{J}(p_i, S^k)+1/2}^k.
 \end{aligned}$$

We rewrite (2.16) in a matrix form using (2.7) as follows

$$\begin{aligned}
 - \sum_{S^k} m_S^k U_S^k \mathbf{D}_S^k &= \sum_{p_i \in \Gamma_h^k} (\tilde{U}_{p_i}^k)^\top A_{p_i}^k \tilde{U}_{p_i}^k - \sum_{p_i^k \in \partial \Gamma_h^k} \left( m_{p_i, 1/2}^k U_{p_i, 1/2}^k \mathcal{D}_{p_i, 1}^k \nabla_{p_i, 1}^k u \cdot n_{p_i, 1|1/2}^k \right. \\
 &\quad \left. + m_{p_i, n_{p_i}+1/2}^k U_{p_i, n_{p_i}+1/2}^k \mathcal{D}_{p_i, n_{p_i}}^k \nabla_{p_i, n_{p_i}}^k u \cdot n_{p_i, n_{p_i}|n_{p_i}+1/2}^k \right), \quad (2.17)
 \end{aligned}$$

where  $A_{p_i}^k$  is defined by:

$A_{p_i}^k := A_{p_i, c}^k - A_{p_i, \sigma}^k \mathbf{Coef}_{p_i}^k$  with  $A_{p_i, c}^k$  being a diagonal matrix and  $A_{p_i, \sigma}^k$  a sparse matrix whose nonzero elements are given by

$$\begin{aligned}
 (A_{p_i, c}^k)_{j, j} &:= m_{p_i, j-1/2}^k (\lambda_{p_i, j|j-1/2}^k + \lambda_{p_i, j+1/2|j-1/2}^k) \\
 &\quad + m_{p_i, j+1/2}^k (\lambda_{p_i, j|j+1/2}^k + \lambda_{p_i, j-1/2|j+1/2}^k), \\
 (A_{p_i, \sigma}^k)_{j, j} &:= m_{p_i, j-1/2}^k \lambda_{p_i, j|j-1/2}^k + m_{p_i, j+1/2}^k \lambda_{p_i, j-1/2|j+1/2}^k, \\
 (A_{p_i, \sigma}^k)_{j, j+1} &:= m_{p_i, j-1/2}^k \lambda_{p_i, j+1/2|j-1/2}^k + m_{p_i, j+1/2}^k \lambda_{p_i, j|j+1/2}^k,
 \end{aligned}$$

for interior points. For boundary points,

$A_{p_i}^k := A_{p_i, c}^k - A_{p_i, \sigma}^k \mathbf{Coef}_{p_i}^k$  with  $A_{p_i, c}^k$  being a sparse square matrix and  $A_{p_i, \sigma}^k$  a sparse rectangular matrix whose nonzero elements are given by

$$\begin{aligned}
 (A_{p_i, c}^k)_{1, 1} &:= m_{p_i, 1/2}^k \lambda_{p_i, 1|1/2}^k, \\
 (A_{p_i, c}^k)_{1, 2} &:= -m_{p_i, 1/2}^k (\lambda_{p_i, 1|1/2}^k + \lambda_{p_i, 3/2|1|1/2}^k), \\
 (A_{p_i, c}^k)_{2, 1} &:= -(m_{p_i, 1/2}^k \lambda_{p_i, 1|1/2}^k + m_{p_i, 3/2}^k \lambda_{p_i, 1/2|1|3/2}^k), \\
 (A_{p_i, c}^k)_{j, j} &:= m_{p_i, j-1/2}^k (\lambda_{p_i, j|j-1/2}^k + \lambda_{p_i, j+1/2|j-1/2}^k) \\
 &\quad + m_{p_i, j+1/2}^k (\lambda_{p_i, j|j+1/2}^k + \lambda_{p_i, j-1/2|j+1/2}^k), \quad \forall j = 2, 3, \dots, n_{p_i} + 1, \\
 (A_{p_i, c}^k)_{n_{p_i}+1, n_{p_i}+2} &:= -(m_{p_i, n_{p_i}-1/2}^k \lambda_{p_i, n_{p_i}+1/2|n_{p_i}|n_{p_i}-1/2}^k + m_{p_i, n_{p_i}+1/2}^k \lambda_{p_i, n_{p_i}|n_{p_i}+1/2}^k), \\
 (A_{p_i, c}^k)_{n_{p_i}+2, n_{p_i}+1} &:= -m_{p_i, n_{p_i}+1/2}^k (\lambda_{p_i, n_{p_i}-1/2|n_{p_i}|n_{p_i}+1/2}^k + \lambda_{p_i, n_{p_i}|n_{p_i}+1/2}^k), \\
 (A_{p_i, c}^k)_{n_{p_i}+2, n_{p_i}+2} &:= m_{p_i, n_{p_i}+1/2}^k \lambda_{p_i, n_{p_i}|n_{p_i}+1/2}^k,
 \end{aligned}$$



$$\begin{aligned}
 (A_{p_i, \sigma}^k)_{1,1} &:= -m_{p_i, 1/2}^k \lambda_{p_i, 3/2|1|1/2}^k, \\
 (A_{p_i, \sigma}^k)_{2,1} &:= m_{p_i, 1/2}^k \lambda_{p_i, 3/2|1|1/2}^k + m_{p_i, 3/2}^k \lambda_{p_i, 1|3/2}^k, \\
 (A_{p_i, \sigma}^k)_{j+2, j} &:= m_{p_i, j-1/2}^k \lambda_{p_i, j|j-1/2}^k + m_{p_i, j+1/2}^k \lambda_{p_i, j-1/2|j|j+1/2}^k, \\
 (A_{p_i, \sigma}^k)_{j+2, j+1} &:= m_{p_i, j-1/2}^k \lambda_{p_i, j+1/2|j|j-1/2}^k + m_{p_i, j+1/2}^k \lambda_{p_i, j|j+1/2}^k, \quad \forall j = 1, 2, \dots, n_{p_i} - 2, \\
 (A_{p_i, \sigma}^k)_{n_{p_i}+1, n_{p_i}-1} &:= m_{p_i, n_{p_i}-1/2}^k \lambda_{p_i, n_{p_i}|n_{p_i}-1/2}^k + m_{p_i, n_{p_i}+1/2}^k \lambda_{p_i, n_{p_i}-1/2|n_{p_i}|n_{p_i}+1/2}^k, \\
 (A_{p_i, \sigma}^k)_{n_{p_i}+2, n_{p_i}-1} &:= -m_{p_i, n_{p_i}+1/2}^k \lambda_{p_i, n_{p_i}-1/2|n_{p_i}|n_{p_i}+1/2}^k.
 \end{aligned}$$

Since  $\mathbf{Coef}_{p_i}^k$  is not defined for  $n_{p_i} = 1$ ,  $A_{p_i}^k := A_{p_i, c}^k$  in that case.

The submatrices  $A_{p_i}^k$  satisfy  $A_{p_i}^k \mathbf{1}_{p_i} = \mathbf{0}_{p_i}$ , where  $\mathbf{1}_{p_i} := (1, 1, \dots)^\top$  and  $\mathbf{0}_{p_i} := (0, 0, \dots)^\top$ . This is due to the minimization procedure introduced in the interpolation of the virtual values on subedges. The procedure forces the system to pick the solution of minimum gradient norm. Let us also remark that if the submatrices  $A_{p_i}^k + (\mathbf{1}_{p_i} \otimes \mathbf{1}_{p_i})/n_{p_i}$  are positive semi-definite for all vertices,  $\sum_{p_i \in \Gamma_h^k} \left( \tilde{U}_{p_i}^k \right)^\top A_{p_i}^k \tilde{U}_{p_i}^k$  defines a seminorm on  $\mathcal{V}_h^k \cup \mathcal{V}_{\partial\Gamma}^k$ . Also, if the submatrices  $A_{p_i}^k + (\mathbf{1}_{p_i} \otimes \mathbf{1}_{p_i})/n_{p_i}$  are strictly positive definite for all vertices,  $\sum_{p_i \in \Gamma_h^k} \left( \tilde{U}_{p_i}^k \right)^\top A_{p_i}^k \tilde{U}_{p_i}^k$  will define a norm on  $\mathcal{V}_h^k \cup \{0_{\mathcal{V}_{\partial\Gamma}^k}\}$ , where  $0_{\mathcal{V}_{\partial\Gamma}^k} = (0, 0, \dots, 0)$  is the zero element of  $\mathcal{V}_{\partial\Gamma}^k$ . Since the submatrices  $A_{p_i}^k$  basically depend on the choice of the subedges virtual points and the discrete cell tensor  $\mathcal{D}_{p_i, j}^k$  around  $p_i^k$ , we can assume the virtual points being chosen such that the submatrices  $A_{p_i}^k + (\mathbf{1}_{p_i} \otimes \mathbf{1}_{p_i})/n_{p_i}$  are strictly positive definite as the diffusion tensors are supposed to be strictly positive definite. Although this assumption is reasonable, it is not useful to require its realization for all the vertices. In case a highly anisotropic tensor is involved in the computation and the mesh very distorted too, the condition might not be satisfied. We will then weaken the assumption by introducing a slight modification of the algorithm. Let us assume the center points being chosen in advance.

**Definition 2.4.3** (Regular vertex and uniformly regular vertex)

We will say that a vertex  $p_i^k$  is regular if the following is satisfied:

- i) It is possible to choose the virtual subcells  $S_{p_i, j}^k$  and the subedge virtual points  $X_{p_i, j-1/2}^k$  around  $p_i^k$  such that  $A_{p_i}^k + (\mathbf{1}_{p_i} \otimes \mathbf{1}_{p_i})/n_{p_i}$  is strictly elliptic,
- ii) If  $p_i^k$  is an interior vertex, then it is surrounded by at least three cells.

Any vertex which does not fulfill these requirements will be called nonregular.

A vertex will be called uniformly regular if it is regular for any time step  $k$ .

**Definition 2.4.4** (Regular polygonisation and uniformly regular polygonisation)

We will say that an admissible polygonal surface  $\Gamma_h^k$  is regular if any of its nonregular vertex is surrounded by regular vertices.

$\Gamma_h^k$  will be called uniformly regular if it is regular and any of its regular vertex is uniformly regular.

In the sequel we assume our polygonal surfaces to be uniformly regular. We now introduce a slight modification of the scheme. For any nonregular vertex  $p_i$ , we assume that the surrounding subcells have zero measure; which means that the subedges  $\sigma_{p_i, j-1/2}^k$  around  $p_i^k$  have zero measure. Thus there is no equation written around that vertex. We will also assume the submatrices

$A_{p_i}^k + (\mathbf{1}_{p_i} \otimes \mathbf{1}_{p_i})/n_{p_i}$  to be uniformly strictly elliptic for all regular points (i.e.  $\exists \alpha > 0 \mid \forall p_i^k, \forall U_{p_i}^k, (U_{p_i}^k)^\top (A_{p_i}^k + (\mathbf{1}_{p_i} \otimes \mathbf{1}_{p_i})/n_{p_i}) U_{p_i}^k \geq \alpha \|U_{p_i}^k\|^2$ ). The resulting scheme remains the same, except that the summation over vertices will be done over regular vertices. From now on, any summation over

vertices will simply mean summation over regular vertices unless specified otherwise. A straightforward example of meshes needing this setup can be found on Figure 2.5, when we consider the dual mesh to our primary mesh. Let us mention here that the dual mesh of a primal mesh is the mesh whose cells are the union of virtual subcells around vertices and center points the vertices of the primal mesh. Here the points  $q_{p_i, j-1/2}^k$  on edges which limit the virtual subcells of the primal mesh (*cf.* Figure 2.4) are nonregular vertices of the dual mesh and therefore will be subject to this treatment. We then define a discrete energy seminorm on  $\mathcal{V}_h^k \cup \mathcal{V}_{\partial\Gamma}^k$ .

**Definition 2.4.5** (*Discrete  $\mathbb{H}_0^1$  seminorm*) For  $U^k \in \mathcal{V}^k$  and  $U_{\partial\Gamma}^k \in \mathcal{V}_{\partial\Gamma}^k$ , we define

$$\|U^k\|_{1, \Gamma_h^k}^2 = \sum_{p_i} \left( \tilde{U}_{p_i}^k \right)^\top A_{p_i}^k \tilde{U}_{p_i}^k \quad (2.18)$$

We also define the discrete  $\mathbb{L}^2$  norm as follows

**Definition 2.4.6** (*Discrete  $\mathbb{L}^2$  norm*) For  $U^k \in \mathcal{V}^k$  we define

$$\|U^k\|_{\mathbb{L}^2(\Gamma_h^k)}^2 = \sum_S m_S^k (U_S^k)^2 \quad (2.19)$$

**Proposition 2.4.7** (*Existence and uniqueness*) The discrete problem (2.12) has a unique solution.

**Proof** The system (2.12) has a unique solution  $U^k \in \mathcal{V}^k$  if the kernel of the corresponding linear operator is trivial. To prove this, we consider the homogeneous system obtained by assuming  $U^k \equiv 0$ ,  $G^k \equiv 0$  and the homogeneous Dirichlet boundary condition  $U_{\partial\Gamma}^{k+1} \equiv 0$ . Next, we multiply each equation of (2.12) by the corresponding cell center unknown  $U_S^{k+1}$  and sum over all cells. Taking into account (2.17), we obtain

$$\|U^{k+1}\|_{\mathbb{L}^2(\Gamma_h^k)}^2 + \tau \|U^{k+1}\|_{1, \Gamma_h^k}^2 = 0,$$

from which  $U^{k+1} \equiv 0$  follows. □

#### 2.4.4 Maximum principle

Let us consider around each uniformly regular vertex  $p_i^k$ , the matrix  $\mathbf{W}_{p_i}^k$  whose entries are defined by

$$\begin{aligned} (\mathbf{W}_{p_i}^k)_{j,j} &:= m_{p_i, j-1/2}^k \lambda_{j|j-1/2}^k + m_{p_i, j+1/2}^k \lambda_{j-1/2|j+1/2}^k, \\ (\mathbf{W}_{p_i}^k)_{j,j+1} &:= m_{p_i, j-1/2}^k \lambda_{j+1/2|j-1/2}^k + m_{p_i, j+1/2}^k \lambda_{j|j+1/2}^k, \end{aligned}$$

and 0 elsewhere. We also consider the column vector  $\mathbf{e}_{p_i, j}$  of length the number of columns of  $\mathbf{Coef}_{p_i}^k$  with components  $(\mathbf{e}_{p_i, j})_j := 1$  and 0 elsewhere (i.e.  $\mathbf{e}_{p_i, j} := (0, \dots, 0, 1, 0, \dots, 0)^\top$ ) and the augmented matrix of coefficients  $\mathbf{ACoef}_{p_i}^k$  defined by  $\mathbf{ACoef}_{p_i}^k := \mathbf{Coef}_{p_i}^k$  if  $p_i^k$  is an interior uniformly regular point. For boundary points,  $\mathbf{ACoef}_{p_i}^k := \left[ (\mathbf{e}_{p_i, 1})^\top; \mathbf{Coef}_{p_i}^k; (\mathbf{e}_{p_i, n_{p_i}+1})^\top \right]$ , concatenation of the vector  $(\mathbf{e}_{p_i, 1})^\top$ , the matrix  $\mathbf{Coef}_{p_i}^k$ , and the vector  $(\mathbf{e}_{p_i, n_{p_i}+1})^\top$ .

**Proposition 2.4.8** If  $\forall S, U_S^0 \geq 0$  and at any time step  $t_k$ ,  $(U_{\partial\Gamma}^k)_i \geq 0 \forall i$ ,  $G_S^k \geq 0 \forall S$ , and the matrices  $\mathbf{W}_{p_i}^k \mathbf{ACoef}_{p_i}^k$  are positive  $\left( (\mathbf{W}_{p_i}^k \mathbf{ACoef}_{p_i}^k)_{i,j} \geq 0 \forall i, j \right)$ , then  $U_S^k \geq 0 \forall k, \forall S$ .

**Proof** Let us first assume the uniformly regular vertices  $p_i$  of a given cell  $S$  being numbered by  $s(p_i)$ . We define for the cell  $S$  the column vectors  $\mathbf{e}_{S,j}$  of length the number of subcells on  $S$ , with components  $(\mathbf{e}_{S,j})_j := 1$  and 0 elsewhere (i.e.  $\mathbf{e}_{S,j} := (0, \dots, 0, 1, 0, \dots, 0)^\top$ ). The system (2.12) can be rewritten as

$$\begin{aligned} & m_S^{k+1} U_S^{k+1} - m_S^k U_S^k - \tau \sum_{p_i \in \partial S^k} (\mathbf{e}_{S,s(p_i)})^\top \left( \mathbf{W}_{p_i}^{k+1} \mathbf{A} \mathbf{Coef}_{p_i}^{k+1} \right) (U_{p_i}^{k+1} - U_S^{k+1} \mathbf{1}_{p_i}) \\ &= \tau m_S^{k+1} G_S^{k+1}. \end{aligned} \quad (2.20)$$

Let us assume that  $U_S^k \geq 0 \forall S^k$ , the minimum of  $U^{k+1}$  ( $\min_S U_S^{k+1}$ ) is reached in a cell  $S_0^{k+1}$ , and that  $U_{S_0}^{k+1} := \min_S U_S^{k+1} < 0$ ; then (2.20) cannot be satisfied for the cell  $S_0^{k+1}$  since all components of the vector  $(U_{p_i}^{k+1} - U_S^{k+1} \mathbf{1}_{p_i})$  are nonnegative. Hence, we conclude that  $U_{S_0}^{k+1} \geq 0$ .

□

This proposition will be of great importance in the next paragraph, especially when one of our aim will be to satisfy the maximum principle.

### 2.4.5 Implementation

Let us first consider the setups defined for triangular meshes in Remark 2.4.2 a) part *i*) and *ii*). For these setups, the submatrices  $Q_{p_i,j}^k$  defined for equation (2.16) are symmetric and strictly positive definite; thus the vertices  $p_i^k$  are uniformly regular. Hence the scheme works for any triangular mesh as long as cells do not degenerate. Restricting to the flat case and using the setup in Remark 2.4.2 a) part *i*), the present scheme coincides exactly with the scheme proposed by K. Lipnikov, M. Shashkov and I. Yotov in [87] and as already said, is identical to the one presented by Le Potier in [85]. We should also mention that for the setup presented in Remark 2.4.2 a) part *ii*), we obtain exactly the scheme presented in Chapter I; moreover, the hypotheses of Proposition 2.4.8 are satisfied and the resulting matrix is a  $M$ -matrix. This last property is not evident for all meshes. We can nevertheless enforce it whenever possible. This will be one of our goals when trying to build on a given mesh, a setup on which the present scheme can be applied. Next, we consider a dual mesh of a triangular mesh. As defined above, this is constructed from the primal mesh and its virtual subcells by grouping the virtual subcells around each vertex  $p_i^k$  to form the cells of the dual mesh. We refer again to Figure 2.9 for an example of a triangular dual mesh in a flat case. We should nevertheless mention that in the curved case, virtual subcells around the vertices are not coplanar. For these meshes, virtual subcells of primal meshes are also considered as virtual subcells of dual meshes. As already mentioned in Remark 2.4.2 a) part *iii*), each new vertex  $X_S^k$ , center of the triangle  $S^k$ , is surrounded by exactly three virtual subcells and therefore the construction of the gradient does not need any regularization. Also, the points  $X_S^k$  are uniformly regular points; consequently, any mesh which is the dual of a triangular mesh is suitable for the scheme. If we restrict ourselves to fixed surfaces, this last setup gives exactly the scheme presented by Lili Ju and Qiang Du in [76] when the diffusion tensor is taken to be constant on triangles. As already reported there, if the triangles edge points  $q_{p_i,j-1/2}^k$  that limit the subcells are taken to be the middle of triangles edges and the diffusion tensor taken to be constant on triangles, the resulting matrix is a symmetric  $M$ -matrix. In some cases it can be advantageous to use the dual mesh since one can reduce the number of variables.

Except in the trivial case of triangular meshes where one has some trivial choices of discrete points, we do need a good algorithm which always delivers the discrete points in such a way that the surface remains a uniformly regular polygonisation and the angle condition in Section 2.4.2 satisfied for appropriate virtual points  $X_{p_i,j-1/2}^k$  around vertices. Also, for some problems, especially in the field of chemistry, one needs to have additionally the maximum principle satisfied by the scheme. We give in the sequel an algorithm to construct the discrete points such that the maximum principle is

satisfied if possible. To begin with, we chose the center points in such a way that the surface of our cell is minimal. This is done by minimizing for each cell  $S^k$  the energy functional

$$E_S^k := \sum_{i=1:n_S} \|(X - p_i^k) \wedge (p_{i+1}^k - p_i^k)\|^2$$

over  $X$ . This energy is in fact the sum of the square measure of the triangles  $[X, p_i^k, p_{i+1}^k]$ ;  $p_i^k$  and  $p_{i+1}^k$  being two consecutive vertices of  $S^k$ . The resulting  $X_S^k := \operatorname{argmin}_{X \in \mathbb{R}^3} E_S^k$  guarantees the status of admissible cell to  $S^k$  and when the vertices are coplanar,  $X_S^k$  is the isobarycenter for triangular cells, rectangular cells and regular polygonal cells. Next, we define the edge points  $X_\sigma^k$  that limit the subcells on cell's boundary  $\sigma$  as the mid point of  $\sigma$ ; but if an interior vertex  $p_i^k$  is surrounded by less than three cells, then all the points  $X_\sigma^k$  around the given vertex are set to  $p_i^k$ . We refer to Figure 2.10 for more illustration. We shall now fix the subedge virtual points. From Proposition 2.4.8,

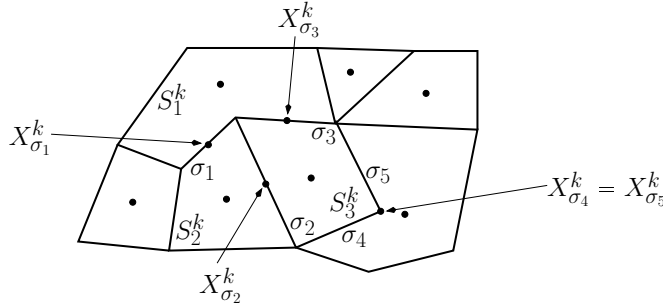


Figure 2.10: Representation of edge points  $X_{\sigma_j}^k$  and center points in cells.

the scheme will satisfy the maximum principle if the submatrices  $W_{p_i}^{k+1} \mathbf{ACoef}_{p_i}^{k+1}$  defined around uniformly regular points are positive. To enforce this, we find the virtual points by minimizing the energy

$$E_3^k := \operatorname{tr} \left[ \left( W_{p_i}^{k+1} \mathbf{ACoef}_{p_i}^{k+1} - \alpha \mathbf{1}_{p_i, S} \otimes \mathbf{1}_{p_i} \right) \left( W_{p_i}^{k+1} \mathbf{ACoef}_{p_i}^{k+1} - \alpha \mathbf{1}_{p_i, S} \otimes \mathbf{1}_{p_i} \right)^\top \right]$$

under the constraints that  $A_{p_i}^k + (\mathbf{1}_{p_i} \otimes \mathbf{1}_{p_i})/n_{p_i}$  is strictly elliptic and the angles

$\theta_{p_i, j}^k := \angle(X_{p_i, j-1/2}^k, X_j^k, X_{p_i, j+1/2}^k)$  between the covariant vectors  $e_{p_i, j|j+1/2}^k$  and  $e_{p_i, j|j-1/2}^k$  are greater than a threshold angle  $\theta$  as requested in Section 2.4.2. Here,  $\alpha$  is a positive constant and  $\mathbf{1}_{p_i, S} = (1, 1, \dots)^\top$  is a vector of ones with length  $n_{p_i}$ . This process tries to pull the coefficients of the submatrices  $W_{p_i}^{k+1} \mathbf{ACoef}_{p_i}^{k+1}$  near  $\alpha$  as possible. Finally, if the symmetric property of the global matrix is important, one can impose it here by setting the symmetry of the submatrices  $Q_{p_i, j}^k$  as a constraint in this last minimization problem.

## 2.5 A priori estimates

We will now give the discrete counterparts of continuous a-priori estimates. They obviously depend on the behavior of the mesh during the evolution and a proper, in particular time coherent choice of center points  $X_S^k$ , subedge points  $X_{p_i, j-1/2}^k$  and edge points  $X_\sigma^k$ . Let us assume that the center points  $X_S^k$  describe a time continuous  $C^1$  curve  $\gamma(t, X_S^0)$  (i.e.  $X_S^k(t) := \gamma(t, \gamma^{-1}(t_k, X_S^k))$ ) during the time evolution. The algorithm described in Section 2.4.5 provides such a curve. We refer to [103, 112] for reading about the regularity of the solution of parametric minimization problems. One can also imagine  $X_S^k$  being transported by  $\Phi$  (i.e.  $X_S^k(t) := \Phi(t, \Phi^{-1}(t_k, X_S^k))$ ); of course, with the resulting

$X_S^k(t)$  satisfying the necessary condition for the scheme to be applied. Let us identify a point  $x$  on the triangle  $[X_S^k, p_i^k, p_{i+1}^k] \subset S^k$  by its barycentric coordinates  $\beta_S^k(x), \beta_{S,i}^k(x), \beta_{S,i+1}^k(x)$  with respect to  $X_S^k, p_i^k$ , and  $p_{i+1}^k$  respectively (i.e.  $x = \beta_S^k(x)X_S^k + \beta_{S,i}^k(x)p_i^k + \beta_{S,i+1}^k(x)p_{i+1}^k$ ). We construct the following map that transforms the cells during the time evolution:

$$\Upsilon^k(t, \cdot) : S^k \longrightarrow \mathbb{R}^3, \quad x \longmapsto x(t) := \beta_S^k(x)X_S^k(t) + \beta_{S,i}^k(x)p_i^k(t) + \beta_{S,i+1}^k(x)p_{i+1}^k(t), \quad (2.21)$$

where  $p_i^k(t) := \Phi(t, \Phi^{-1}(t_k, p_i^k))$ . We also assume

$$\|\Upsilon^k(t_{k+1}, X_{j+1/2}^{k,i}) - X_{j+1/2}^{k+1,i}\| \leq Ch\tau \quad (2.22)$$

$$|m_{p_i, j+1/2}^{k+1} - m_{p_i, j+1/2}^k| \leq Ch\tau. \quad (2.23)$$

These conditions are obviously satisfied for the setups described in Section 2.4.5. Thanks to the conditions above, one easily establishes that  $\max_k \max_S \left| \frac{m_S^k}{m_S^{k+1}} - 1 \right| \leq C\tau$ , and the 2-norm

$$\left\| (A_{p_i, sym}^{k+1})^{1/2} (A_{p_i, sym}^k)^\dagger (A_{p_i, sym}^{k+1})^{1/2} - \left( (A_{p_i, sym}^{k+1})^{1/2} \right)^\dagger (A_{p_i, sym}^{k+1})^{1/2} \right\|_2 \leq C\tau.$$

**Theorem 2.5.1** (*Discrete  $\mathbb{L}^\infty(\mathbb{L}^2), \mathbb{L}^2(\mathbb{H}^1)$  energy estimate*). *Let  $\{U^k\}_{k=1, \dots, k_{max}}$  be the discrete solution of (2.12) for a given discrete initial data  $U^0 \in \mathcal{V}_h^0$  and the homogenous boundary condition  $\{U_{\partial\Gamma}^k\}_{k=1, \dots, k_{max}} \equiv 0$ , then there exists a constant  $C$  depending solely on  $t_{max}$  such that*

$$\max_{k=1, \dots, k_{max}} \|U^k\|_{\mathbb{L}^2(\Gamma_h^k)}^2 + \sum_{k=1}^{k_{max}} \tau \|U^k\|_{1, \Gamma_h^k}^2 \leq C \left( \|U^0\|_{\mathbb{L}^2(\Gamma_h^0)}^2 + \tau \sum_{k=1}^{k_{max}} \|G^k\|_{\mathbb{L}^2(\Gamma_h^k)}^2 \right). \quad (2.24)$$

**Proof** As in the proof of Proposition 2.4.7, we multiply each equation of (2.12) by the corresponding cell center value unknown  $U_S^{k+1}$  and sum up the resulting equations. Thanks to (2.17), we obtain

$$\sum_S \left( m_S^{k+1} (U_S^{k+1})^2 - m_S^k U_S^k U_S^{k+1} \right) + \tau \|U^{k+1}\|_{1, \Gamma_h^k}^2 = \sum_S m_S^{k+1} G_S^{k+1} U_S^{k+1}, \quad (2.25)$$

and using Young's inequality and the estimate  $\max_k \max_S \left| \frac{m_S^k}{m_S^{k+1}} - 1 \right| \leq C\tau$ , one obtains

$$\begin{aligned} & \frac{1}{2} \|U^{k+1}\|_{\mathbb{L}^2(\Gamma_h^k)}^2 + \tau \|U^{k+1}\|_{1, \Gamma_h^k}^2 \\ & \leq \frac{1}{2} \|U^k\|_{\mathbb{L}^2(\Gamma_h^k)}^2 + \frac{C}{2} \tau \|U^{k+1}\|_{\mathbb{L}^2(\Gamma_h^{k+1})}^2 + \frac{1}{2} \tau \|G^{k+1}\|_{\mathbb{L}^2(\Gamma_h^{k+1})}^2. \end{aligned} \quad (2.26)$$

The rest follows exactly as in the proof of Theorem 4.1 in Chapter I.  $\square$

**Theorem 2.5.2** (*Discrete  $\mathbb{H}^1(\mathbb{L}^2), \mathbb{L}^\infty(\mathbb{H}^1)$  energy estimate*). *Let us assume the submatrices  $A_{p_i}^k$  around regular vertices to be symmetric. We also consider  $\{U^k\}_{k=1, \dots, k_{max}}$ , the discrete solution of (2.12) for given discrete initial data  $U^0 \in \mathcal{V}_h^0$  and the homogenous boundary condition  $\{U_{\partial\Gamma}^k\}_{k=1, \dots, k_{max}} \equiv 0$ , then there exists a constant  $C$  depending solely on  $t_{max}$  such that*

$$\begin{aligned} & \sum_{k=1}^{k_{max}} \tau \|\partial_t^\tau U^k\|_{\mathbb{L}^2(\Gamma_h^k)}^2 + \max_{k=1, \dots, k_{max}} \|U^k\|_{1, \Gamma_h^k}^2 \\ & \leq C \left( \|U^0\|_{\mathbb{L}^2(\Gamma_h^0)}^2 + \|U^0\|_{1, \Gamma_h^0}^2 + \tau \sum_{k=1}^{k_{max}} \|G^k\|_{\mathbb{L}^2(\Gamma_h^k)}^2 \right), \end{aligned} \quad (2.27)$$

where  $\partial_t^\tau U^k = \frac{U^k - U^{k-1}}{\tau}$  is defined as a difference quotient in time.

**Proof** We multiply each equation of (2.12) by the corresponding cell center difference quotient value  $\partial_t^T U_S^{k+1} \equiv \partial_t^T U^{k+1}|_S$ , each equation of (2.3) by the corresponding subedge difference quotient value  $\frac{U_{p_i, j+1/2}^{k+1} - (U_{p_i, j+1/2}^k)'}{\tau}$ , where the values  $(U_{p_i, j+1/2}^k)'$ , components of the vector  $(\tilde{U}_{p_i, \sigma}^k)'$ , are interpolation of the components of  $\tilde{U}_{p_i}^k$  on subedges  $\sigma_{p_i, j+1/2}^{k+1}$  around  $p_i^{k+1}$  through formula (2.7) (i.e.  $(\tilde{U}_{p_i, \sigma}^k)' = \mathbf{Coef}_{p_i}^{k+1} \tilde{U}_{p_i}^k$ ). Next, we sum the resulting equations over all cells and subedges to obtain

$$\begin{aligned} & \tau \sum_{S^{k+1}} m_S^{k+1} \left( \frac{U_S^{k+1} - U_S^k}{\tau} \right)^2 + \sum_{p_i^k} (\tilde{U}_{p_i}^{k+1})^\top A_{p_i}^{k+1} \tilde{U}^{k+1} - (\tilde{U}_{p_i}^{k+1})^\top A_{p_i}^{k+1} \tilde{U}^k \\ &= \sum_S (m_S^k - m_S^{k+1}) U_S^k \frac{U_S^{k+1} - U_S^k}{\tau} + \tau \sum_S m_S^{k+1} G_S^{k+1} \frac{U_S^{k+1} - U_S^k}{\tau}. \end{aligned} \quad (2.28)$$

Since the matrices  $A_{p_i}^k$  ( $k = 0, 1, 2, \dots$ ) are symmetric and have the same kernel,

$$A_{p_i}^{k+1} = A_{p_i}^{k+1} \left( (A_{p_i}^k)^{1/2} \right)^\dagger (A_{p_i}^k)^{1/2},$$

where  $(A_{p_i}^k)^{1/2}$  is the symmetric matrix satisfying  $A_{p_i}^k = (A_{p_i}^k)^{1/2} (A_{p_i}^k)^{1/2}$ . Now, applying Young's inequality to equation (2.28) gives

$$\begin{aligned} & \tau \sum_{S^{k+1}} m_S^{k+1} \left( \frac{U_S^{k+1} - U_S^k}{\tau} \right)^2 + \|U^{k+1}\|_{1, \Gamma_h^{k+1}}^2 \\ & \leq \frac{1}{2} \|U^k\|_{1, \Gamma_h^k}^2 + \frac{1}{2} \sum_{p_i^k} (\tilde{U}_{p_i}^{k+1})^\top A_{p_i}^{k+1} (A_{p_i}^k)^\dagger A_{p_i}^{k+1} \tilde{U}^{k+1} \\ & \quad + \sum_{p_i^k} \sum_S (m_S^k - m_S^{k+1}) U_S^k \frac{U_S^{k+1} - U_S^k}{\tau} + \tau \sum_S m_S^{k+1} G_S^{k+1} \frac{U_S^{k+1} - U_S^k}{\tau}. \end{aligned}$$

Taking into account that

$$\begin{aligned} & A_{p_i}^{k+1} (A_{p_i}^k)^\dagger A_{p_i}^{k+1} - A_{p_i}^{k+1} \\ &= (A_{p_i}^{k+1})^{1/2} \left[ (A_{p_i}^{k+1})^{1/2} (A_{p_i}^k)^\dagger (A_{p_i}^{k+1})^{1/2} - \left( (A_{p_i}^{k+1})^{1/2} \right)^\dagger (A_{p_i}^{k+1})^{1/2} \right] (A_{p_i}^{k+1})^{1/2}, \end{aligned}$$

the 2-norm  $\left\| (A_{p_i}^{k+1})^{1/2} (A_{p_i}^k)^\dagger (A_{p_i}^{k+1})^{1/2} - \left( (A_{p_i}^{k+1})^{1/2} \right)^\dagger (A_{p_i}^{k+1})^{1/2} \right\|_2 \leq C\tau$ , and

$\left| \frac{m_S^k}{m_S^{k+1}} - 1 \right| \frac{\sqrt{m_S^{k+1}}}{\sqrt{m_S^k}} \leq C\tau$ , we deduce the inequality

$$\tau \frac{1}{2} \|\partial_t^T U^{k+1}\|^2 + \frac{1}{2} \|U^{k+1}\|_{1, \Gamma_h^{k+1}}^2 \leq \frac{1}{2} \|U^k\|_{1, \Gamma_h^k}^2 + \frac{C}{2} \tau \left( \|U^{k+1}\|_{1, \Gamma_h^{k+1}}^2 + \|U^k\|_{\Gamma_h^k}^2 + \|G^{k+1}\|_{\Gamma_h^{k+1}}^2 \right)$$

Finally, summing over all time steps and using Theorem 2.5.1 gives the desired result.  $\square$

## 2.6 Convergence

In this section, we prove an error estimate for the finite volume solution  $U^k \in \mathcal{V}_h^k$ . At first, we have to state how to compare a discrete solution defined on the sequence of polygonizations  $\Gamma_h^k$  and a continuous solution defined on the evolving family of smooth surfaces  $\Gamma(t)$ . Here, we will take into account the lifting operator from the discrete surfaces  $\Gamma_h^k$  onto the continuous surfaces  $\Gamma(t_k)$  already introduced in Section 2.4.1. As for the error analysis in Chapter I, we use the pull back from the continuous surface onto a corresponding polygonization to compare the continuous solution  $u(t_k)$  at time  $t_k$  with the discrete solution  $U^k = \sum_S U_S^k \chi_{S^k}$  where  $\chi_{S^k}$  is the characteristic function of the cell  $S^k$ . To be explicit, we consider the pull back  $u^{-l}(t_k, X_S^k)$  of the continuous solution  $u$  at time  $t_k$  and investigate the error  $u^{-l}(t_k, X_S^k) - U_S^k$  at the cell node  $X_S^k$ . As already mentioned, the consistency of the scheme depends on the proper choice of center points, edge points and the behavior of the mesh during the evolution; therefore we assume (2.22), (2.23) and the following extra condition on  $X_S^k$  and  $X_{p_i, j+1/2}^k$ :

**A3** There exists  $\mathcal{C} > 0$  and  $\theta \in ]0, \pi/2]$  such that for two consecutive vertices  $p_i^k, p_{i+1}^k$  of any cell  $S^k$

1) if  $m([X_S^k, p_i^k, p_{i+1}^k]) \neq 0$ , then there exist three points  $x_{p_i,1}^k, x_{p_i,2}^k, x_{p_i,3}^k$  in the intersection of the convex hull of  $S^k$  and the plane generated by the points  $\{X_S^k, p_i^k, p_{i+1}^k\}$  satisfying  $\|x_{p_i,1}^k x_{p_i,2}^k\| \geq Ch$ ,  $\|x_{p_i,1}^k x_{p_i,3}^k\| \geq Ch$  and  $\theta \leq \angle(x_{p_i,1}^k x_{p_i,2}^k, x_{p_i,1}^k x_{p_i,3}^k) \leq \pi - \theta$ . Here  $\angle(x_{p_i,1}^k x_{p_i,2}^k, x_{p_i,1}^k x_{p_i,3}^k)$  represents the oriented angle between the vectors  $\overrightarrow{x_{p_i,1}^k x_{p_i,2}^k}$  and  $\overrightarrow{x_{p_i,1}^k x_{p_i,3}^k}$ , taken around the axis  $(X_S^k p_i^k \wedge X_S^k p_{i+1}^k)$ .

2) there exists three points  $y_{p_i,1}^k, y_{p_i,2}^k, y_{p_i,3}^k$  in the intersection of the convex hull of  $S^k$  and the plane generated by the points  $(X_S^k, X_{\mathcal{J}(p_i, S)+1/2}^k, X_{\mathcal{J}(p_i, S)-1/2}^k)$  satisfying  $\|y_{p_i,1}^k y_{p_i,2}^k\| \geq Ch$ ,  $\|y_{p_i,1}^k y_{p_i,3}^k\| \geq Ch$ , and  $\theta \leq \angle(y_{p_i,1}^k y_{p_i,2}^k, y_{p_i,1}^k y_{p_i,3}^k) \leq \pi - \theta$ . As above,  $\angle(y_{p_i,1}^k y_{p_i,2}^k, y_{p_i,1}^k y_{p_i,3}^k)$  represents the oriented angle between the vectors  $\overrightarrow{y_{p_i,1}^k y_{p_i,2}^k}$  and  $\overrightarrow{y_{p_i,1}^k y_{p_i,3}^k}$  taken around  $(X_S^k X_{\mathcal{J}(p_i, S)+1/2}^k \wedge X_S^k X_{\mathcal{J}(p_i, S)-1/2}^k)$ .

We recall that  $\mathcal{J}(p_i, S)$  is the local index of the cell  $S^k$  around the vertex  $p_i^k$ . We also assume that  $\theta \leq \angle(X_S^k X_{\mathcal{J}(p_i, S)+1/2}^k, X_S^k X_{\mathcal{J}(p_i, S)-1/2}^k) \leq \pi - \theta$ , and for closed cells  $S^k$  intersecting the boundary  $\partial\Gamma_h^k$  and any edge unknown  $x = X_{\mathcal{J}(p_i, S)+1/2}^k$  or  $x = X_{\mathcal{J}(p_i, S)-1/2}^k$  in  $S^k \cap \partial\Gamma_h^k$ ,  $\|X_S^k - x\| \geq Ch$ .

We shall precise here that the assumption **A3** part 1) aims at having cells whose surfaces approximate correctly (in the sense of Lemma 2.6.2) the surface of their lifted counterparts. If the vertices of  $S^k$  are coplanar, this assumption is true for any star-shaped point  $x = X_S^k \in S^k$  (point whose any line connection to a vertex of  $S^k$  is entirely in  $S^k$ ); but in general, on curved surface meshes, one must pay a careful attention. On the other hand, **A3** part 2) will guaranty the consistency of the approximations of surface normals and gradient operators. We refer to Section 2.4.5, for an example of an algorithm enabling the choice of nodes  $X_S^k$  and the subedge virtual points  $X_{p_i, j+1/2}^k$ .

Finally, the following convergence theorem holds:

**Theorem 2.6.1** (Error estimate). *Suppose that the assumptions listed from Section 2.4 hold and define the piecewise constant error functional on  $\Gamma_h^k$  for  $k = 1, \dots, k_{max}$*

$$E^k := \sum_{S^k} (u^{-l}(t_k, X^k) - U_S^k) \chi_{S^k}$$

*measuring the pull back  $u^{-l}(t_k, \cdot)$  of the continuous solution  $u(t_k, \cdot)$  of (2.1) at time  $t_k$  and the finite volume solution  $U^k \in \mathcal{V}_h^k$  of (2.12). Furthermore, let us assume that  $\|E^0\|_{L^2(\Gamma_h^0)} \leq Ch$ , then the*

error estimate

$$\max_{k=1, \dots, k_{max}} \|E^k\|_{L^2(\Gamma_h^k)}^2 + \tau \sum_{k=1}^{k_{max}} \|E^k\|_{1, \Gamma_h^k}^2 \leq C(h + \tau)^2 \quad (2.29)$$

holds for a constant  $C$  depending on the regularity assumptions and the time  $t_{max}$ .

This error estimate generalizes the error estimate given in Chapter I. As already mentioned there, it depends on the consistency estimates of different terms which rely on geometric estimates; thus the proof of this theorem will follow the same procedure. The main difference here is that cells are not necessarily triangular and vertices are not necessarily bound to the surface, but we will always reformulate the results in order to use the gains of Chapter I. In what follows, we first establish the relevant geometric estimates, then prove the consistency of the scheme and finally establish the convergence result.

### 2.6.1 Geometric approximation estimates

Let us first extend the definition of  $\mathcal{P}^k$  into a time continuous operator  $\mathcal{P}(t, \cdot)$  which for each time  $t \in [0, t_{max}]$ , projects points orthogonally onto  $\Gamma(t)$ . This operator is well defined in a neighborhood of  $\Gamma(t)$ . We also introduce the time continuous lift operator

$$\Psi^k(t, \cdot) : S^k \longrightarrow S^{l,k}(t), \quad x \longmapsto \Psi^k(t, x) := \Phi(t, \Phi^{-1}(t_k, \mathcal{P}^k(x))) \quad (2.30)$$

which helps to follow the transported lifted cell  $S^{l,k}(t) := \Psi^k(t, S^k)$ . We then introduce an estimate for the distance between the continuous surface and the polygonization and for the ratio between cell areas and their lifted counterparts.

**Lemma 2.6.2** *Let  $d(t, x)$  be the signed distance from a point  $x$  to the surface  $\Omega(t)$  taken to be positive in the direction of the surface normal  $\nu$ ,  $\Gamma_h(t)$  an  $(m, h)$  – approximation of  $\Gamma(t) \subset \Omega(t)$ , and let  $m_S^{l,k}$  denote the measure of the lifted cell  $S^{l,k}$ ,  $m_{p_i, j+1/2}^{l,k}$  the measure of the lifted subedge  $\sigma_{p_i, j+1/2}^k$ . The estimates*

$$\sup_{0 \leq t \leq t_{max}} \|d(t, \cdot)\|_{L^\infty(\Gamma_h(t))} \leq Ch^2, \quad \sup_{k, S} \left| 1 - \frac{m_S^{l,k}}{m_S^k} \right| \leq Ch^2, \quad \sup_{i, j, k} \left| 1 - \frac{m_{p_i, j+1/2}^{l,k}}{m_{p_i, j+1/2}^k} \right| \leq Ch^2$$

hold for a constant  $C$  depending only on the regularity assumptions. Let us also consider the planes  $T_{S_{\{i, i+1\}}}^k$  generated by the center point  $X_S^k$ , and the vertices  $p_i^k, p_{i+1}^k$  of  $S^k$ ; and the plane  $T_{p_i, S}^k$  generated by  $X_S^k$  and the virtual points  $X_{p_i, j-1/2}^k$  and  $X_{p_i, j+1/2}^k$  around  $p_i^k$ . There exists a constant  $C$  depending only on the regularity assumptions such that

$$\max_{x \in S_{\{i, i+1\}}^k} \|\nabla_{T_{S_{\{i, i+1\}}}^k} d(t_k, x)\| \leq Ch \quad \text{and} \quad \max_{x \in S_{p_i, S}^k} \|\nabla_{T_{p_i, S}^k} d(t_k, x)\| \leq Ch.$$

We recall that  $S_{\{i, i+1\}}^k$  is the triangle  $[X_S^k, p_i^k, p_{i+1}^k]$  and  $S_{p_i, S}^k$  is the virtual subcell of  $S^k$  containing  $p_i^k$ .

**Proof** First notice that  $d(t, \cdot)$  is a  $C^2$  function. Let us consider a cell  $S^k(t) := \Upsilon(t, S^k)$  with center  $X_S^k(t)$  and vertices  $\Psi^k(t, p_i^k)$ , a point  $x = \beta_S^k(x)X_S^k(t) + \beta_{S_i}^k(x)\Psi^k(t, p_i^k) + \beta_{S_{i+1}}^k(x)\Psi^k(t, p_{i+1}^k)$  where  $\beta_S^k(x)$ ,  $\beta_{S_i}^k(x)$ , and  $\beta_{S_{i+1}}^k(x)$  are barycentric coordinates of  $x$  with respect to  $X_S^k(t)$ ,  $\Psi^k(t, p_i^k)$ , and  $\Psi^k(t, p_{i+1}^k)$  respectively. The Taylor expression of  $d(t, \cdot)$  at each vertex  $y$  of the triangle  $[X_S^k(t), \Psi^k(t, p_i^k), \Psi^k(t, p_{i+1}^k)]$  can be expressed in terms of  $d(t, x)$  as

$$d(t, y) = d(t, x) + (y - x) \cdot \nabla d(t, x) + \mathcal{O}(\|y - x\|^2).$$



Finally, multiplying each of these equations by the corresponding barycentric coefficients and summing up all the equations, one obtains that  $d(t, x) = \mathcal{O}(h^2)$  since the barycentric coefficients are bounded and we have assumed that  $\Gamma_h(t)$  is an  $(m, h)$ -polygonization of  $\Gamma(t)$ . Next, the points  $x_{p_i, j}^k \in T_{S_{\{i, i+1\}}}^k$  and  $y_{p_i, j}^k \in T_{p_i, S}^k$  ( $j \in \{1, 2, 3\}$ ) provided by assumption **A3** satisfy

$\|\nabla_{T_{S_{\{i, i+1\}}}^k} d(t_k, x_{p_i, j}^k)\| \leq Ch$  and  $\|\nabla_{T_{p_i, S}^k} d(t_k, y_{p_i, 1}^k)\| \leq Ch$ . Since these points are in the convex hull of  $S^k$ , one concludes that  $\max_{S_{\{i, i+1\}}^k} \|\nabla_{T_{S_{\{i, i+1\}}}^k} d(t_k, x)\| \leq Ch$  and  $\max_{S_{p_i, j}^k} \|\nabla_{T_{p_i, S}^k} d(t_k, x)\| \leq Ch$ , where we recall that  $S_{\{i, i+1\}}^k$  is the triangle  $[X_S^k, p_i^k, p_{i+1}^k]$ .

For the second estimate, we consider the triangle  $S_{\{i, i+1\}}^k$  and assume without any restriction that  $S_{\{i, i+1\}}^k \subset \{(\xi, 0) | \xi \in \mathbb{R}^2\}$ . As in the proof of Lemma 1.5.2, we define  $\mathcal{P}_{ext}^k$  in a neighborhood of  $S_{\{i, i+1\}}^k$  as follows

$$\mathcal{P}_{ext}^k(\xi, \zeta) = (\xi, 0) + (\zeta - d(t_k, (\xi, 0)))\nabla d^T(t_k, (\xi, 0)).$$

Obviously,  $\mathcal{P}_{ext}^k = \mathcal{P}^k$  on  $S_{\{i, j\}}^k$  and from the results above, we deduce that

$$|\det(D\mathcal{P}_{ext}^k(\xi, 0)) - 1| \leq Ch^2,$$

where  $D\mathcal{P}_{ext}^k$  is the Jacobian of  $\mathcal{P}_{ext}^k$ . We can clearly see that  $|\det(D\mathcal{P}_{ext}^k(\xi, 0))|$  controls the transformation of the area under the projection  $\mathcal{P}^k$  from  $S_{\{i, i+1\}}^k$  to  $S_{\{i, i+1\}}^{l, k} := \mathcal{P}^k(S_{\{i, i+1\}}^k)$ ; since the third column of the Jacobian  $\partial_\zeta \mathcal{P}_{ext}^k(\xi, 0) = \nabla d^T(t_k, (\xi, 0))$  has length 1 and is normal to  $\Gamma(t_k)$  at  $\mathcal{P}^k(\xi, 0)$ . The claim is therefore proven since the subcells  $S_{\{i, i+1\}}^{l, k}$  as well as  $S_{\{i, i+1\}}^k$  form a partition of  $S^{l, k}$  and  $S^k$ , respectively.

The third estimate is obtained via an adaptation of arguments of the second estimate. □

Let us also give the following lemma which states the consistency of the approximation of conormals to curved boundaries.

**Lemma 2.6.3** *Let  $p_i^k$  and  $p_{i+1}^k$  be two consecutive vertices of a cell  $S^k$ ,  $X_S^k$  its center and  $\sigma_{p_i, j-1/2}^k$  the subedge around  $p_i^k$  satisfying  $\sigma_{p_i, j-1/2}^k \subset [p_i^k, p_{i+1}^k]$ . We also consider  $\sigma_{p_i, j-1/2}^{l, k}$  the corresponding curved boundary on  $\Gamma(t_k)$  and  $X_{p_i, j-1/2}^k, X_{p_i, j+1/2}^k$  the subedge points of  $S^k$  around  $p_i^k$ . Finally, we assume  $X_{p_i, j-1/2}^k \in \sigma_{p_i, j-1/2}^k$ , then the conormal to  $\sigma_{p_i, j-1/2}^{l, k}$  outward from  $S^{l, k} \cap \Gamma^k$  is given by*

$$n_{p_i, j|j-1/2}^{l, k}(x) = n_{p_i, j|j-1/2}^k + \epsilon(x)$$

where  $n_{p_i, j|j-1/2}^k := \left( \frac{p_{i+1}^k - p_i^k}{\|p_{i+1}^k - p_i^k\|} \wedge \nu_{p_i, j}^k \right) / \left\| \frac{p_{i+1}^k - p_i^k}{\|p_{i+1}^k - p_i^k\|} \wedge \nu_{p_i, j}^k \right\|$  and  $\epsilon(x)$  is a vector satisfying  $\|\epsilon(x)\| \leq Ch$ .

**Proof** We will distinguish the case where  $\sigma_{p_i, j+1/2}^k$  is a boundary subedge ( $\sigma_{p_i, j+1/2}^k \subset \partial\Gamma_h^k$ ) and the case where  $\sigma_{p_i, j+1/2}^k$  is an interior subedge ( $\sigma_{p_i, j+1/2}^k \in \Gamma_h^k \setminus \partial\Gamma_h^k$ ).

Let us consider the first case where  $\sigma_{p_i, j+1/2}^k \subset \partial\Gamma_h^k$ . We define the following map

$$\begin{aligned} \eta_{S, i|j+1}^k : x := p_i^k + \alpha \frac{p_{i+1}^k - p_i^k}{\|p_{i+1}^k - p_i^k\|} &\longmapsto \eta_{S, i|j+1}^k(x) := x - d(t_k, x)\nabla d^T(t_k, x) \\ &\quad - d(\mathcal{P}^k(x), \Gamma^k)\nabla d^T(\mathcal{P}^k(x), \Gamma^k), \end{aligned}$$

where  $\alpha \in [0, \|p_{i+1}^k - p_i^k\|]$ . Since this map transforms  $\sigma_{p_i, j-1/2}^k$  to  $\sigma_{p_i, j-1/2}^{l, k}$ , a tangent vector to  $\sigma_{p_i, j-1/2}^{l, k}$  is given by

$$\begin{aligned} \varpi_{S, i|i+1}^k(\eta_{S, i|i+1}^k(x)) &= \frac{p_{i+1}^k - p_i^k}{\|p_{i+1}^k - p_i^k\|} - \left( \nabla d^T(t_k, x) \cdot \frac{p_{i+1}^k - p_i^k}{\|p_{i+1}^k - p_i^k\|} \right) \nabla d^T(t_k, x) \\ &\quad - d(t_k, x) \nabla(\nabla d^T(t_k, x)) \frac{p_{i+1}^k - p_i^k}{\|p_{i+1}^k - p_i^k\|} \\ &\quad - \left( \nabla d^T(\mathcal{P}^k(x), \Gamma^k) \cdot \frac{p_{i+1}^k - p_i^k}{\|p_{i+1}^k - p_i^k\|} \right) \nabla d^T(\mathcal{P}^k(x), \Gamma^k) \\ &\quad - d(\mathcal{P}^k(x), \Gamma^k) \nabla(\nabla d^T(\mathcal{P}^k(x), \Gamma^k)) \frac{p_{i+1}^k - p_i^k}{\|p_{i+1}^k - p_i^k\|} \end{aligned}$$

for points  $x$  where  $\eta_{S, i|i+1}^k$  has enough regularity. Since  $\eta_{S, i|i+1}^k$  is regular enough almost everywhere and referring to the assumption (v) and (vi) on the surface approximation in Definition 2.3.5 as well as to Lemma 2.6.2, one concludes that

$$\varpi_{S, i|i+1}^k(\eta_{S, i|i+1}^k(x)) = \frac{p_{i+1}^k - p_i^k}{\|p_{i+1}^k - p_i^k\|} + \epsilon_1(x),$$

where  $\epsilon_1(x)$  is a vector satisfying  $\|\epsilon_1(x)\| \leq Ch$ . Next, one deduces from the last two inequalities of Lemma 2.6.2 that

$$\nu_{p_i, j}^k \cdot \frac{p_{i+1}^k - p_i^k}{\|p_{i+1}^k - p_i^k\|} = \mathcal{O}(h)$$

and the normal  $\nu(\eta_{S, i|i+1}^k(x))$  to the surface  $\Gamma^k$  at  $\eta_{S, i|i+1}^k(x)$  is given by

$$\nu(\eta_{S, i|i+1}^k(x)) = \nu_{p_i, j}^k + \epsilon_2(x),$$

where  $\epsilon_2(x)$  is a vector satisfying  $\|\epsilon_2(x)\| \leq Ch$ . Finally, one deduces that the unit normal to  $\sigma_{p_i, j+1/2}^{l, k}$  outward from  $S^{l, k} \cap \Gamma^k$  is given by

$$\varpi_{S, i|i+1}^k(\eta_{S, i|i+1}^k(x)) \wedge \nu(\eta_{S, i|i+1}^k(x)) = n_{p_i, j|j-1/2}^k + \epsilon(x).$$

where  $\epsilon(x)$  is a vector satisfying  $\|\epsilon(x)\| \leq Ch$ .

For the second case,  $\eta_{S, i|i+1}^k(\cdot)$  is merely  $\mathcal{P}(\cdot)$  and the above proof remains valid. □

Next we control the area defect between the transported lifted versus a lifted transported cell.

**Lemma 2.6.4** *For each cell  $S^k$  on  $\Gamma_h^k$ , and all  $x$  in  $S^k$ , the estimate*

$$\|\mathcal{P}(t, \Upsilon^k(t, x)) - \Psi(t, x)\| \leq C\tau h^2$$

holds for a constant  $C$  depending only on the regularity assumptions. Furthermore, for the symmetric difference between  $S^{l, k}$  and  $S^{l, k+1}$ , one obtains

$$\mathcal{H}^{n-1}(S^{l, k}(t_{k+1}) \Delta S^{l, k+1}) \leq C\tau h m_S^{k+1}$$

where  $\mathcal{H}^{n-1}(\cdot)$  represents the  $(n-1)$ -dimensional Hausdorff measure. We recall that the symmetric difference between two sets  $A$  and  $B$  is defined by  $A \Delta B = (A \setminus B) \cup (B \setminus A)$ .

**Proof** The proof here is identical to the proof of Lemma 1.5.3 in Chapter I, up to minor modifications due to the fact that vertices are not bound to the surface and the cells are nontriangular. In fact, as in that Lemma, we first notice that the function  $\Psi^k(t, \cdot)$  defined in (2.30) parameterizes the lifted and then transported cell  $S^{l,k}(t)$  over  $S^k$ , and  $\mathcal{P}(t, \Upsilon^k(t, \cdot))$  with  $\Upsilon^k(t, \cdot)$  defined in (2.21) parameterizes the transported and then lifted cell  $\mathcal{P}(t, S^k(t))$  over  $S^k$ . Next, one uses the Taylor expansion of respective functions at vertices of triangles  $S_{i,i+1}^k$  considered as neighboring points of a point  $x \in S_{i,i+1}^k$ , and in the same way as in the proof of Lemma 2.6.2, one obtains

$$\|\mathcal{P}(t, \Upsilon^k(t, x)) - \Psi(t, x)\| \leq \beta(t)h^2.$$

Here  $\beta(\cdot)$  is a nonnegative and smooth function in time. As in Lemma 1.5.3 in Chapter I, one deduces from  $S^{l,k}(t_k) = S^{l,k}$  that  $\beta(\cdot)$  can be chosen such that  $\beta(t) \leq C|t - t_k|$  holds. This result shows that the maximum norm of the displacement  $\mathcal{P}(t, \Upsilon^k(t, \cdot)) - \Psi(t, \cdot)$  on the boundary  $\sigma^k$  is  $C\tau h^2$ . The second claim is then obvious.  $\square$

Based on this estimate, we immediately obtain the following corollary already formulated for the triangular mesh in Chapter I (Corollary 5.4):

**Corollary 2.6.5** *For any cell  $S^k$  on  $\Gamma_h^k$  and any Lipschitz continuous function  $\omega(t, \cdot)$  defined on  $\Gamma(t)$  one obtains*

$$\left| \int_{S^{l,k}(t_{k+1}) \cap \Gamma(t_{k+1})} \omega(t_{k+1}, a) da - \int_{S^{l,k+1} \cap \Gamma(t_{k+1})} \omega(t_{k+1}, a) da \right| \leq C\tau h m_S^{k+1}$$

for a constant  $C$  depending only on the regularity assumptions.

## 2.6.2 Consistency estimates.

With these geometric preliminaries at hand, we are now able to derive a-priori bounds for various consistency errors in conjunction with the finite volume approximation (2.12) of the continuous evolution (2.1). Let us first reformulate Lemma 1.5.5 of Chapter I in this context.

**Lemma 2.6.6** *Let  $S^k$  be a cell in  $\Gamma_h^k$  and  $t \in [t_k, t_{k+1}]$ , then for*

$$\begin{aligned} \mathcal{R}_1(S^{l,k}(t) \cap \Gamma(t)) &:= \int_{S^{l,k}(t) \cap \Gamma(t)} \nabla_{\Gamma(t)} \cdot (\mathcal{D}\nabla_{\Gamma(t)} u(t, \cdot)) da \\ &\quad - \int_{S^{l,k+1} \cap \Gamma(t_{k+1})} \nabla_{\Gamma(t_{k+1})} \cdot (\mathcal{D}\nabla_{\Gamma(t_{k+1})} u(t_{k+1}, \cdot)) da \end{aligned}$$

we obtain the estimate  $|\mathcal{R}_1(S^{l,k}(t) \cap \Gamma(t))| \leq C\tau(1 + Ch)m_S^{k+1}$ .

This Lemma is proved along the same line as Lemma 1.5.5 via an adaptation of arguments. Next, we have the following result.

**Lemma 2.6.7** *Let the subedge  $\sigma_{p_i, j+1/2}^{l,k}$  be the intersection between two adjacent subcells  $S_{p_i, j}^{l,k}$  and  $S_{p_i, j+1}^{l,k}$  or, with a slight misuse of notation, the intersection between  $S_{p_i, j}^{l,k}$  and the boundary  $\partial(\mathcal{P}^k(\Gamma_h^k) \cap \Gamma^k)$  of  $\mathcal{P}^k(\Gamma_h^k) \cap \Gamma^k$ ; the term*

$$\begin{aligned} \mathcal{R}_2(S_{p_i, j}^k | S_{p_i, j+1}^k) &:= \int_{\sigma_{p_i, j+1/2}^{l,k}} (\mathcal{D}\nabla_{\Gamma(t_k)} u) \cdot n_{p_i, j+1/2}^{l,k}(t_k, x) dx \\ &\quad - m_{p_i, j+1/2}^k \left( u(t_k, \mathcal{P}^k(X_{p_i, j+1/2}^k)) - u(t_k, \mathcal{P}^k(X_{p_i, j}^k)) \right) \lambda_{p_i, j|j+1/2}^k \\ &\quad - m_{p_i, j+1/2}^k \left( u(t_k, \mathcal{P}^k(X_{p_i, j-1/2}^k)) - u(t_k, \mathcal{P}^k(X_{p_i, j}^k)) \right) \lambda_{p_i, j-1/2|j+1/2}^k, \end{aligned}$$

where  $n_{p_i,j+1/2}^{l,k}(t_k, \cdot)$  is the function describing the outward pointing unit conormal of  $S_{p_i,j}^{l,k}$  on the subedge  $\sigma_{p_i,j|j+1/2}^{l,k}$  and the other terms are defined in Section 2.4.2, obeys the estimate

$$|\mathcal{R}_2(S_{p_i,i}^k | S_{p_i,i+1}^k)| \leq Cm_{i(S)+1/2}^k h.$$

**Proof** As in Lemma 2.6.6, we consider the continuous extension of  $u(t, \cdot)$ , still called  $u(t, \cdot)$ . Next, we write the surface gradient of  $u(t_k, \cdot)$  at a point  $x$  on  $S_{p_i,j}^{l,k} \cap \Gamma^k$  as follows:

$$\nabla_{\Gamma^k} u(x) = \nabla u = \nabla_{T_{p_i,S}^k} u(x) + (\nabla u(x) \cdot \nu_{p_i,S}^k) \nu_{p_i,S}^k.$$

Since  $\nabla_{T_{p_i,S}^k} u(x) = (\nabla_{T_{p_i,S}^k} \cdot e_{p_i,j|j-1/2}^k) \mu_{p_i,j|j-1/2}^k + (\nabla_{T_{p_i,S}^k} \cdot e_{p_i,j|j+1/2}^k) \mu_{p_i,j|j+1/2}^k$  and  $\nu(x) = \nu_{p_i,S}^k + \vartheta_j(t_k, x)h$  with  $\|\vartheta_j(t_k, x)\| \leq C$  on  $S_{p_i,j}^{l,k} \cap \Gamma^k$ , we obtain using the Taylor expansion, Definition 2.3.5 and assumption **A3.2** that

$$\begin{aligned} \nabla_{\Gamma^k} u(x) &= \left( u(t_k, X_{p_i,j-1/2}^k) - u(t_k, X_{p_i,j}^k) \right) \mu_{p_i,j|j-1/2}^k \\ &\quad + \left( u(t_k, X_{p_i,j+1/2}^k) - u(t_k, X_{p_i,j}^k) \right) \mu_{p_i,j|j+1/2}^k - \epsilon(t_k, x), \end{aligned}$$

where  $\epsilon(t_k, x)$  is a three dimensional vector satisfying  $\|\epsilon(t_k, x)\| \leq Ch$ . Thus, using the regularity assumptions on  $\mathcal{D}$ , Lemma 2.6.3 and assumption **A3.2** we obtain

$$\begin{aligned} \int_{\sigma_{p_i,j+1/2}^{l,k}} (\mathcal{D} \nabla_{\Gamma^k} u) \cdot n_{p_i,j|j+1/2}^{l,k} dx &= m_{p_i,j+1/2}^k \left( u(t_k, X_{p_i,j-1/2}^k) - u(t_k, X_{p_i,j}^k) \right) \lambda_{p_i,j-1/2|j+1/2}^k \\ &\quad + m_{p_i,j+1/2}^k \left( u(t_k, X_{p_i,j+1/2}^k) - u(t_k, X_{p_i,j}^k) \right) \lambda_{p_i,j|j+1/2}^k \\ &\quad + \mathcal{O}(m_{p_i,j+1/2}^k h). \end{aligned} \tag{2.31}$$

We now need to prove that the approximation of the subedge values  $u(t_k, X_{p_i,j-1/2}^k)$  are  $\mathcal{O}(h^2)$  consistent. To this end, we apply the continuous version of Proposition 2.4.1 on the above relation which gives

$$M_{p_i}^k \bar{U}_{p_i,\sigma}^k = N_{p_i}^k \bar{U}_{p_i}^k + v_1, \tag{2.32}$$

where  $\bar{U}_{p_i,\sigma}^k := \left( u(t_k, X_{p_i,1/2}^k), u(t_k, X_{p_i,3/2}^k), \dots \right)^\top$ ,  $\bar{U}_{p_i}^k := \left( u(t_k, X_{p_i,1}^k), u(t_k, X_{p_i,2}^k), \dots \right)^\top$  and  $v_1$  is a vector satisfying  $\|v_1\| \leq Ch^2$ . Also, the  $\mathbb{H}^1$ -norm of the continuous solution reads

$$\begin{aligned} \sum_j \int_{S_{p_i,j}^{l,k} \cap \Gamma^k} \|\nabla_{\Gamma^k} u\|^2 dx &= \sum_j \int_{S_{p_i,j}^{l,k} \cap \Gamma^k} \left\| \left( u(t_k, X_{p_i,j-1/2}^k) - u(t_k, X_{p_i,j}^k) \right) \mu_{p_i,j|j-1/2}^k \right. \\ &\quad \left. + \left( u(t_k, X_{p_i,j+1/2}^k) - u(t_k, X_{p_i,j}^k) \right) \mu_{p_i,j|j+1/2}^k + \epsilon(t_k, x) \right\|^2 dx. \end{aligned}$$

The continuous setup of problem (2.6) is formulated as

$$\left\{ \begin{array}{l} \text{Find } \bar{U}_{p_i,\sigma}^k \text{ in } \bar{\mathcal{B}}_{p_i}^k := \left\{ \bar{V}_{p_i,\sigma}^k := (V_{p_i,1/2}^k, V_{p_i,3/2}^k, \dots)^\top \mid M_{p_i}^k \bar{V}_{p_i,\sigma}^k = N_{p_i}^k \bar{U}_{p_i}^k + v_1 \right\} \text{ such that} \\ \bar{U}_{p_i,\sigma}^k = \operatorname{argmin}_{\bar{V}_{p_i,\sigma}^k \in \bar{\mathcal{B}}_{p_i}^k} \sum_j \int_{S_{p_i,j}^{l,k} \cap \Gamma^k} \left\| \left[ V_{p_i,j-1/2}^k - \bar{U}_{p_i,j}^k \right] \mu_{p_i,j|j-1/2}^k \right. \\ \quad \left. + \left[ V_{p_i,j+1/2}^k - \bar{U}_{p_i,j}^k \right] \mu_{p_i,j|j+1/2}^k + \epsilon(t_k, x) \right\|^2 dx; \end{array} \right.$$

which in a simplified setup reads

$$\left\{ \begin{array}{l} \text{Find } \bar{U}_{p_i, \sigma}^k \text{ in } \bar{\mathcal{B}}_{p_i}^k := \left\{ \bar{V}_{p_i, \sigma}^k := (V_{p_i, 1/2}^k, V_{p_i, 3/2}^k, \dots)^\top \mid M_{p_i}^k \bar{V}_{p_i, \sigma}^k = N_{p_i}^k \bar{U}_{p_i}^k + v_1 \right\} \text{ such that} \\ \bar{U}_{p_i, \sigma}^k = \operatorname{argmin}_{\bar{V}_{p_i, \sigma}^k \in \bar{\mathcal{B}}_{p_i}^k} \left\| \sqrt{B_{p_i}^k} \bar{V}_{p_i, \sigma}^k - \left( \sqrt{B_{p_i}^k} \right)^{-1} (\mathbf{C}_{p_i}^k \bar{U}_{p_i}^k + v_2) \right\|^2 \end{array} \right.$$

since the error  $\epsilon(t_k, x)$  is assumed to be known.  $v_2$  is a vector satisfying  $\|v_2\| \leq Ch^2$ . Following the same procedure as in Section 2.4.2, one obtains

$$\bar{U}_{p_i, \sigma}^k = \mathbf{Coef}_{p_i}^k \bar{U}_{p_i}^k + v_3,$$

where  $v_3 = \left( \sqrt{B_{p_i}^k} \right)^{-1} \left( M_{p_i}^k \left( \sqrt{B_{p_i}^k} \right)^{-1} \right)^\dagger \left( v_1 - M_{p_i}^k (B_{p_i}^k)^{-1} v_2 \right) + (B_{p_i}^k)^{-1} v_2$ . It is clear that  $\|v_3\| \leq Ch^2$ . We have just proven that a perturbation on the equation leads to a consistent solution. It is left to prove that the solution is also consistent with the expected data (values of functions at virtual points). In the flat case, this is evident since the reconstruction of affine functions using this method is exact if the tensor  $\mathcal{D}$  is constant on  $\cup_j S_{p_i, j}^{l, k} \cap \Gamma^k$  and  $\mathcal{O}(h^2)$  consistent in general. In the curved case we consider the closest plane to the center points around  $p_i$ . There exists  $h_0$  such that this plane is included in  $\mathcal{N}(t_k)$  for any  $h \leq h_0$ . Next we project on the defined plane, in the direction of the surface normal  $\nu$ , the whole geometrical setup represented around  $p_i$  and adopt the new subcells as discrete subcells. Let us consider the function  $f(x) = u(t_k, X_1^k) + (\nabla_{\Gamma^k} u(t_k, X_1^k)) \cdot (x - X_1^k)$  defined in a neighborhood of  $\cup_j S_{p_i, j}^{l, k} \cap \Gamma^k$  whose restriction on  $\Gamma^k$  is considered for the reconstruction. The above problem posed on the new discrete subcells gives an  $\mathcal{O}(h^2)$  consistent value of  $f$  at projected virtual points; These values are in an  $\mathcal{O}(h^2)$  neighborhood of the values of  $f$  at the corresponding surface points. Also, due to the consistency of the geometric approximation, the newly stated problem can be stated as the above problem with an  $\mathcal{O}(h^2)$  perturbation of the right hand side which means that the solution is evidently the solution of problem (2.6) with an uncertainty of  $\mathcal{O}(h^2)$ . This concludes that the right values of a continuous function is in an  $\mathcal{O}(h^2)$  neighborhood of the value proposed by this reconstruction's method. Now, including this result in equation (2.31) gives the desired estimate. □

Finally, Lemma 1.5.7 and Lemma 1.5.8 of Chapter I are also satisfied in this context and they can be respectively reformulated as follows

**Lemma 2.6.8** *For a cell  $S^k$  and the residual error term*

$$\begin{aligned} \mathcal{R}_3(S^{l, k} | S^{l, k+1}) &= \int_{S^{l, k}(t_{k+1}) \cap \Gamma^{k+1}} u da - \int_{S^{l, k}(t_k) \cap \Gamma^k} u da \\ &\quad - (m_S^{k+1} u^{-l}(t_{k+1}, X_S^{k+1}) - m_S^k u^{-l}(t_k, X_S^k)) \end{aligned}$$

one obtains the estimate  $|\mathcal{R}_3(S^{l, k} | S^{l, k+1})| \leq C\tau h m_S^{k+1}$ .

**Lemma 2.6.9** *For a cell  $S^k$  and the residual error term*

$$\mathcal{R}_4(S^{l, k} | S^{l, k+1}) = \int_{t_k}^{t_{k+1}} \int_{S^{l, k}(t) \cap \Gamma(t)} g(t, a) da dt - \tau m_S^{k+1} g^{-l}(t_{k+1}, X_S^{k+1})$$

one achieves the estimate  $|\mathcal{R}_4(S^{l, k} | S^{l, k+1})| \leq C\tau(\tau + h)m_S^{k+1}$ .

### 2.6.3 Proof of Theorem 2.6.1

As in Section 2.4.3 (cf. (2.9), (2.10) and (2.11)), let us consider the following cellwise flux formulation of the continuous problem (2.1):

$$\int_{S^{l,k}(t_{k+1}) \cap \Gamma^{k+1}} u \, da - \int_{S^{l,k} \cap \Gamma^k} u \, da - \int_{t_k}^{t_{k+1}} \int_{\partial(S^{l,k}(t) \cap \Gamma(t))} \mathcal{D}\nabla_{\Gamma(t)} u \cdot \mu_{\partial S^{l,k}(t)} \, dl \, dt = \int_{t_k}^{t_{k+1}} \int_{S^{l,k}(t) \cap \Gamma(t)} g \, da \, dt.$$

From this equation we subtract the discrete counterpart (2.12)

$$\begin{aligned} & m_S^{k+1} U_S^{k+1} - m_S^k U_S^k \\ & - \tau \sum_{p_i \in \partial S^k} \left[ m_{p_i, \mathcal{J}(p_i, S)}^{k+1} \left( U_{p_i, \mathcal{J}(p_i, S)}^{k+1} - U_{p_i, \mathcal{J}(p_i, S)}^{k+1} \right) \lambda_{p_i, \mathcal{J}(p_i, S)}^{k+1} |_{\mathcal{J}(p_i, S)} - 1/2 \right. \\ & + m_{p_i, \mathcal{J}(p_i, S)}^{k+1} \left( U_{p_i, \mathcal{J}(p_i, S)}^{k+1} - U_{p_i, \mathcal{J}(p_i, S)}^{k+1} \right) \lambda_{p_i, \mathcal{J}(p_i, S)}^{k+1} |_{\mathcal{J}(p_i, S)} + 1/2 |_{\mathcal{J}(p_i, S)} |_{\mathcal{J}(p_i, S)} - 1/2 \\ & + m_{p_i, \mathcal{J}(p_i, S)}^{k+1} \left( U_{p_i, \mathcal{J}(p_i, S)}^{k+1} - U_{p_i, \mathcal{J}(p_i, S)}^{k+1} \right) \lambda_{p_i, \mathcal{J}(p_i, S)}^{k+1} |_{\mathcal{J}(p_i, S)} - 1/2 |_{\mathcal{J}(p_i, S)} |_{\mathcal{J}(p_i, S)} + 1/2 \\ & \left. + m_{p_i, \mathcal{J}(p_i, S)}^{k+1} \left( U_{p_i, \mathcal{J}(p_i, S)}^{k+1} - U_{p_i, \mathcal{J}(p_i, S)}^{k+1} \right) \lambda_{p_i, \mathcal{J}(p_i, S)}^{k+1} |_{\mathcal{J}(p_i, S)} + 1/2 \right] \\ & = \tau m_S^{k+1} G_S^{k+1}. \end{aligned}$$

and multiply this with  $E_S^{k+1} = u^{-l}(t_{k+1}, X_S^{k+1}) - U_S^{k+1}$  to obtain

$$\begin{aligned} & \mathcal{R}_3(S^{l,k} | S^{l,k+1}) E_S^{k+1} - \left( \int_{t_k}^{t_{k+1}} \mathcal{R}_1(S^{l,k}(t) \cap \Gamma(t)) \, dt \right) E_S^{k+1} \\ & - \tau \sum_{p_i^{k+1} \in S^{k+1}} \left[ \mathcal{R}_2(S_{p_i, \mathcal{J}(p_i, S)}^{k+1} | S_{p_i, \mathcal{J}(p_i, S)}^{k+1}) + \mathcal{R}_2(S_{p_i, \mathcal{J}(p_i, S)}^{k+1} | S_{p_i, \mathcal{J}(p_i, S)}^{k+1}) \right] E_{p_i, \mathcal{J}(p_i, S)}^{k+1} \\ & + (m_S^{k+1} (E_S^{k+1})^2 - m_S^k E_S^k E_S^{k+1}) \\ & - \tau \sum_{p_i^{k+1} \in S^{k+1}} \left[ m_{p_i, \mathcal{J}(p_i, S)}^{k+1} \left( E_{p_i, \mathcal{J}(p_i, S)}^{k+1} - E_{p_i, \mathcal{J}(p_i, S)}^{k+1} \right) E_{p_i, \mathcal{J}(p_i, S)}^{k+1} \lambda_{p_i, \mathcal{J}(p_i, S)}^{k+1} |_{\mathcal{J}(p_i, S)} + 1/2 \right. \\ & + m_{p_i, \mathcal{J}(p_i, S)}^{k+1} \left( E_{p_i, \mathcal{J}(p_i, S)}^{k+1} - E_{p_i, \mathcal{J}(p_i, S)}^{k+1} \right) E_{p_i, \mathcal{J}(p_i, S)}^{k+1} \lambda_{p_i, \mathcal{J}(p_i, S)}^{k+1} |_{\mathcal{J}(p_i, S)} - 1/2 |_{\mathcal{J}(p_i, S)} |_{\mathcal{J}(p_i, S)} + 1/2 \\ & + m_{p_i, \mathcal{J}(p_i, S)}^{k+1} \left( E_{p_i, \mathcal{J}(p_i, S)}^{k+1} - E_{p_i, \mathcal{J}(p_i, S)}^{k+1} \right) E_{p_i, \mathcal{J}(p_i, S)}^{k+1} \lambda_{p_i, \mathcal{J}(p_i, S)}^{k+1} |_{\mathcal{J}(p_i, S)} + 1/2 |_{\mathcal{J}(p_i, S)} |_{\mathcal{J}(p_i, S)} - 1/2 \\ & \left. + m_{p_i, \mathcal{J}(p_i, S)}^{k+1} \left( E_{p_i, \mathcal{J}(p_i, S)}^{k+1} - E_{p_i, \mathcal{J}(p_i, S)}^{k+1} \right) E_{p_i, \mathcal{J}(p_i, S)}^{k+1} \lambda_{p_i, \mathcal{J}(p_i, S)}^{k+1} |_{\mathcal{J}(p_i, S)} - 1/2 \right] \\ & = \mathcal{R}_4(S^{l,k} | S^{l,k+1}) E_S^{k+1}, \end{aligned} \tag{2.33}$$

where  $E_{p_i, \mathcal{J}(p_i, S)}^{k+1} := \left( u^{-l}(t_{k+1}, X_j^{k+1}) - U_{j-1/2}^{k+1} \right)$  and  $E_{p_i, \mathcal{J}(p_i, S)}^{k+1}$  is defined analogously. We recall that the summation is always done on regular vertices (cf. Definition 2.4.3). Next, we subtract from the flux continuity equation on subedges between neighboring sub-cell  $S_{p_i, \mathcal{J}(p_i, S)}^{l,k+1}$  and  $S_{p_i, \mathcal{J}(p_i, S)}^{l,k+1}$

$$\begin{aligned} & \int_{\sigma_{p_i, \mathcal{J}(p_i, S)}^{l,k+1}} (\mathcal{D}\nabla_{\Gamma} u) |_{S_{p_i, \mathcal{J}(p_i, S)}^{l,k+1}(t)} \cdot \mu_{\partial S_{p_i, \mathcal{J}(p_i, S)}^{l,k+1}(t)} \, dl \\ & + \int_{\sigma_{p_i, \mathcal{J}(p_i, S)}^{l,k+1}} (\mathcal{D}\nabla_{\Gamma} u) |_{S_{p_i, \mathcal{J}(p_i, S)}^{l,k+1}(t)} \cdot \mu_{\partial S_{p_i, \mathcal{J}(p_i, S)}^{l,k+1}(t)} \, dl = 0, \end{aligned}$$

its discrete counterpart

$$\begin{aligned}
& m_{p_i, \mathcal{J}(p_i, S)+1/2}^{k+1} \left[ \left( U_{p_i, \mathcal{J}(p_i, S)+1/2}^{k+1} - U_{\mathcal{J}(p_i, S)}^{k+1} \right) \lambda_{\mathcal{J}(p_i, S)|\mathcal{J}(p_i, S)+1/2}^{k+1, i} \right. \\
& + \left. \left( U_{p_i, \mathcal{J}(p_i, S)-1/2}^{k+1} - U_{p_i, \mathcal{J}(p_i, S)}^{k+1} \right) \lambda_{p_i, \mathcal{J}(p_i, S)-1/2|\mathcal{J}(p_i, S)|\mathcal{J}(p_i, S)+1/2}^{k+1, i} \right] \\
& + m_{p_i, \mathcal{J}(p_i, S)+1/2}^{k+1} \left[ \left( U_{p_i, \mathcal{J}(p_i, S)+3/2}^{k+1} - U_{\mathcal{J}(p_i, S)+1}^{k+1, i} \right) \lambda_{p_i, \mathcal{J}(p_i, S)+2|\mathcal{J}(p_i, S)+1|\mathcal{J}(p_i, S)}^{k+1, i} \right. \\
& + \left. \left( U_{p_i, \mathcal{J}(p_i, S)+1/2}^{k+1} - U_{\mathcal{J}(p_i, S)+1}^{k+1, i} \right) \lambda_{p_i, \mathcal{J}(p_i, S)+1|\mathcal{J}(p_i, S)}^{k+1} \right] = 0.
\end{aligned}$$

Furthermore, we multiply the result by  $\tau E_{p_i, \mathcal{J}(p_i, S)+1/2}^{k+1}$  and obtain

$$\begin{aligned}
& \tau m_{p_i, \mathcal{J}(p_i, S)+1/2}^{k+1} \left( E_{p_i, \mathcal{J}(p_i, S)+1/2}^{k+1} - E_{p_i, \mathcal{J}(p_i, S)}^{k+1} \right) E_{p_i, \mathcal{J}(p_i, S)+1/2}^{k+1} \lambda_{p_i, \mathcal{J}(p_i, S)|\mathcal{J}(p_i, S)+1/2}^{k+1} \\
& + \tau m_{p_i, \mathcal{J}(p_i, S)+1/2}^{k+1} \left( E_{p_i, \mathcal{J}(p_i, S)-1/2}^{k+1} - E_{p_i, \mathcal{J}(p_i, S)}^{k+1} \right) E_{p_i, \mathcal{J}(p_i, S)+1/2}^{k+1} \lambda_{p_i, \mathcal{J}(p_i, S)-1/2|\mathcal{J}(p_i, S)|\mathcal{J}(p_i, S)+1/2}^{k+1} \\
& + \tau m_{p_i, \mathcal{J}(p_i, S)+1/2}^{k+1} \left( E_{p_i, \mathcal{J}(p_i, S)+1/2}^{k+1} - E_{p_i, \mathcal{J}(p_i, S)+1}^{k+1} \right) E_{p_i, \mathcal{J}(p_i, S)+1/2}^{k+1} \lambda_{p_i, \mathcal{J}(p_i, S)+1|\mathcal{J}(p_i, S)+1/2}^{k+1} \quad (2.34) \\
& + \tau m_{p_i, \mathcal{J}(p_i, S)+1/2}^{k+1} \left( E_{p_i, \mathcal{J}(p_i, S)+3/2}^{k+1} - E_{p_i, \mathcal{J}(p_i, S)+1}^{k+1} \right) E_{p_i, \mathcal{J}(p_i, S)+1/2}^{k+1} \lambda_{p_i, \mathcal{J}(p_i, S)+3/2|\mathcal{J}(p_i, S)+1|\mathcal{J}(p_i, S)+1/2}^{k+1} \\
& + \tau \mathcal{R}_2(S_{\mathcal{J}(p_i, S)}^{k+1} | S_{p_i, \mathcal{J}(p_i, S)+1}^{k+1}) E_{p_i, \mathcal{J}(p_i, S)+1/2}^{k+1} + \tau \mathcal{R}_2(S_{p_i, \mathcal{J}(p_i, S)+1}^{k+1} | S_{p_i, \mathcal{J}(p_i, S)}^{k+1}) E_{p_i, \mathcal{J}(p_i, S)+1/2}^{k+1} = 0.
\end{aligned}$$

Now, summing up (2.33) and (2.34) respectively over all cells and subedges leads to

$$\begin{aligned}
& \|E^{k+1}\|_{\mathbb{L}^2(\Gamma_h^{k+1})}^2 + \tau \|E^{k+1}\|_{1, \Gamma_h^{k+1}}^2 \\
& = \sum_S m_S^k E_S^k E_S^{k+1} + \sum_S \mathcal{R}_4(S^{l, k} | S^{l, k+1}) E_S^{k+1} - \sum_S \mathcal{R}_3(S^{l, k} | S^{l, k+1}) E_S^{k+1} \\
& + \sum_S \left( \int_{t_k}^{t_{k+1}} \mathcal{R}_1(S^{l, k}(t) \cap \Gamma(t)) dt \right) E_S^{k+1} \\
& - \tau \sum_{S^{k+1}} \sum_{p_i^{k+1} \in S^{k+1}} \left[ \mathcal{R}_2(S_{p_i, \mathcal{J}(p_i, S)}^{k+1} | S_{p_i, \mathcal{J}(p_i, S)+1}^{k+1}) \left( E_{p_i, \mathcal{J}(p_i, S)+1/2}^{k+1} - E_{p_i, \mathcal{J}(p_i, S)}^{k+1} \right) \right. \\
& + \left. \mathcal{R}_2(S_{p_i, \mathcal{J}(p_i, S)}^{k+1} | S_{\mathcal{J}(p_i, S)-1}^{k+1}) \left( E_{p_i, \mathcal{J}(p_i, S)-1/2}^{k+1} - E_{p_i, \mathcal{J}(p_i, S)}^{k+1} \right) \right].
\end{aligned}$$

Let us denote by  $E_{p_i}^k := \left( \sum_{S_{p_i, j}^k} E_{p_i, j}^k \right) / n_{p_i}$  the mean value of  $E_{p_i, j}^k$  around  $p_i^k$ . The last term on the right hand side can be written as follows

$$\begin{aligned}
Z & := -\tau \sum_{S^{k+1}} \sum_{p_i^{k+1} \in S^{k+1}} \left[ \mathcal{R}_2(S_{p_i, \mathcal{J}(p_i, S)}^{k+1} | S_{p_i, \mathcal{J}(p_i, S)+1}^{k+1}) \left( E_{p_i, \mathcal{J}(p_i, S)+1/2}^{k+1} - E_{p_i, \mathcal{J}(p_i, S)}^{k+1} \right) \right. \\
& + \left. \mathcal{R}_2(S_{p_i, \mathcal{J}(p_i, S)}^{k+1} | S_{p_i, \mathcal{J}(p_i, S)-1}^{k+1}) \left( E_{p_i, \mathcal{J}(p_i, S)-1/2}^{k+1} - E_{p_i, \mathcal{J}(p_i, S)}^{k+1} \right) \right] \\
& = -\tau \sum_{S^{k+1}} \sum_{p_i^{k+1} \in S^{k+1}} \left[ \mathcal{R}_2(S_{p_i, \mathcal{J}(p_i, S)}^{k+1} | S_{p_i, \mathcal{J}(p_i, S)+1}^{k+1}) \cdot \left( (E_{p_i, \mathcal{J}(p_i, S)+1/2}^{k+1} - E_{p_i}^k) - (E_{p_i, \mathcal{J}(p_i, S)}^{k+1} - E_{p_i}^k) \right) \right. \\
& + \left. \mathcal{R}_2(S_{p_i, \mathcal{J}(p_i, S)}^{k+1} | S_{p_i, \mathcal{J}(p_i, S)-1}^{k+1}) \left( (E_{p_i, \mathcal{J}(p_i, S)-1/2}^{k+1} - E_{p_i}^k) - (E_{p_i, \mathcal{J}(p_i, S)}^{k+1} - E_{p_i}^k) \right) \right] \\
& = -\tau \sum_{p_i^{k+1} \in \Gamma_h^{k+1}} \left( \left( \bar{\mathcal{R}}_{2, p_i}^{k+1} \right)^\top \text{Coef}_{p_i}^k - \left( \bar{\mathcal{R}}_{2, p_i}^{k+1} \right)^\top \right)^\top (\bar{E}_{p_i}^{k+1} - E_{p_i}^{k+1} \mathbf{1}_{p_i}), \quad (2.35)
\end{aligned}$$

where  $\bar{\mathcal{R}}_{2, p_i}^{k+1}$  is the vector with components  $\left( \bar{\mathcal{R}}_{2, p_i}^{k+1} \right)_j := \left( \mathcal{R}_2^{k+1}(S_{p_i, j}^{k+1} | S_{p_i, j-1}^{k+1}) + \mathcal{R}_2^{k+1}(S_{p_i, j-1}^{k+1} | S_{p_i, j}^{k+1}) \right)$ ,  $\bar{\mathcal{R}}_{2, p_i}^{k+1}$  is the vector with components  $\left( \bar{\mathcal{R}}_{2, p_i}^{k+1} \right)_j := \left( \mathcal{R}_2^{k+1}(S_{p_i, j}^{k+1} | S_{p_i, j-1}^{k+1}) + \mathcal{R}_2^{k+1}(S_{p_i, j}^{k+1} | S_{p_i, j+1}^{k+1}) \right)$  and

$\bar{E}_{p_i}^{k+1} := (E_{p_i,1}^{k+1}, E_{p_i,2}^{k+1}, \dots)$ . Of course we have to readjust these vectors around boundary points according to the boundary condition in the similar way as in Section 2.4.4. Next we introduce the local gradient operator in expression 2.35 and derive the following estimate

$$\begin{aligned}
 Z &= -\tau \sum_{p_i^{k+1} \in \Gamma_h^{k+1}} \left( \left( \bar{\mathcal{R}}_{2,p_i}^{k+1} \right)^\top \mathbf{Coef}_{p_i}^k - \left( \bar{\mathcal{R}}_{2,p_i}^{k+1} \right)^\top \right)^\top (\bar{E}_{p_i}^{k+1} - E_{p_i}^{k+1} \mathbf{1}_{p_i}) \\
 &= -\tau \sum_{p_i^{k+1} \in \Gamma_h^{k+1}} \left( \left( \bar{\mathcal{R}}_{2,p_i}^{k+1} \right)^\top \mathbf{Coef}_{p_i}^k - \left( \bar{\mathcal{R}}_{2,p_i}^{k+1} \right)^\top \right)^\top \left( \sqrt{A_{p_i}^{k+1} + (\mathbf{1}_{p_i} \otimes \mathbf{1}_{p_i})/n_{p_i}} \right)^{-1} \\
 &\quad \left( \sqrt{A_{p_i}^{k+1} + (\mathbf{1}_{p_i} \otimes \mathbf{1}_{p_i})/n_{p_i}} \right) (\bar{E}_{p_i}^{k+1} - E_{p_i}^{k+1} \mathbf{1}_{p_i}) \\
 &\leq \tau \left( \sum_{p_i^{k+1} \in \Gamma_h^{k+1}} \left( \left( \bar{\mathcal{R}}_{2,p_i}^{k+1} \right)^\top \mathbf{Coef}_{p_i}^k - \left( \bar{\mathcal{R}}_{2,p_i}^{k+1} \right)^\top \right)^\top (A_{p_i}^{k+1} + (\mathbf{1}_{p_i} \otimes \mathbf{1}_{p_i})/n_{p_i})^{-1} \right. \\
 &\quad \left. \left( \left( \bar{\mathcal{R}}_{2,p_i}^{k+1} \right)^\top \mathbf{Coef}_{p_i}^k - \left( \bar{\mathcal{R}}_{2,p_i}^{k+1} \right)^\top \right) \right)^{-1/2} \left( \sum_{p_i^{k+1} \in \Gamma_h^{k+1}} (\bar{E}_{p_i}^{k+1})^\top A_{p_i}^{k+1} \bar{E}_{p_i}^{k+1} \right)^{-1/2}
 \end{aligned}$$

since  $A_{p_i}^{k+1} \mathbf{1}_{p_i} = 0 \cdot \mathbf{1}_{p_i}$  and  $(\mathbf{1}_{p_i})^\top A_{p_i}^{k+1} = 0 \cdot (\mathbf{1}_{p_i})^\top$ . Finally, using Lemma 2.6.7, the estimate  $h^2 \leq C m_S^{k+1}$ , the fact that the number of cell's vertices is uniformly bounded and the submatrices  $A_{p_i}^{k+1} + (\mathbf{1}_{p_i} \otimes \mathbf{1}_{p_i})/n_{p_i}$  are uniformly elliptic, we obtain

$$Z \leq \tau C \left( \sum_{S^{k+1}} m_S^{k+1} h^2 \right)^{1/2} \|E_S^{k+1}\|_{1,\Gamma_h^{k+1}} \leq \tau C h (\mathcal{H}^{n-1}(\Gamma_h^{k+1}))^{1/2} \|E_S^{k+1}\|_{1,\Gamma_h^{k+1}}.$$

Now, we take into account the consistency results from Lemma 2.6.6, Lemma 2.6.8, Lemma 2.6.9, apply Young's and Cauchy's inequality and achieve the result

$$\begin{aligned}
 &\|E^{k+1}\|_{\mathbb{L}^2(\Gamma_h^{k+1})}^2 + \tau \|E^{k+1}\|_{1,\Gamma_h^{k+1}}^2 \\
 &\leq \frac{1}{2} \|E^{k+1}\|_{\mathbb{L}^2(\Gamma_h^{k+1})}^2 + \frac{1}{2} \|E^k\|_{\mathbb{L}^2(\Gamma_h^k)}^2 + \frac{1}{2} \max_S \max_k \left| 1 - \frac{m_S^k}{m_S^{k+1}} \right| \|E^k\|_{\mathbb{L}^2(\Gamma_h^k)}^2 \\
 &\quad + C (\tau(\tau + h) + \tau h + \tau^2(1 + Ch)) (\mathcal{H}^{n-1}(\Gamma_h^{k+1}))^{1/2} \|E^{k+1}\|_{\mathbb{L}^2(\Gamma_h^{k+1})} \\
 &\quad + C \tau h (\mathcal{H}^{n-1}(\Gamma_h^{k+1}))^{1/2} \|E^{k+1}\|_{1,\Gamma_h^{k+1}}.
 \end{aligned}$$

Based on the fact that the center points  $X_S$  describe a  $C^1$  continuous curve  $X_S(t) := \gamma(t, X_S)$ , one easily proves that  $\left| 1 - \frac{m_S^k}{m_S^{k+1}} \right| \leq C\tau$  as already mentioned in Section 2.5. Again, applying Young's inequality to the last two terms on the right side gives

$$\begin{aligned}
 &C (\tau(\tau + h) + \tau h + \tau^2(1 + Ch)) (\mathcal{H}^{n-1}(\Gamma_h^{k+1}))^{1/2} \|E^{k+1}\|_{\mathbb{L}^2(\Gamma_h^{k+1})} \\
 &\leq \frac{C}{2} \tau(\tau + h)^2 \mathcal{H}^{n-1}(\Gamma_h^{k+1}) + \frac{C}{2} \tau \|E^{k+1}\|_{\mathbb{L}^2(\Gamma_h^{k+1})}^2, \\
 &C \tau h (\mathcal{H}^{n-1}(\Gamma_h^{k+1}))^{1/2} \|E^{k+1}\|_{1,\Gamma_h^{k+1}} \leq \frac{C^2 \tau}{2} h^2 \mathcal{H}^{n-1}(\Gamma_h^{k+1}) + \frac{\tau}{2} \|E^{k+1}\|_{1,\Gamma_h^{k+1}}^2.
 \end{aligned}$$

Now, taking into account that  $\mathcal{H}^{n-1}(\Gamma_h^{k+1})$  is uniformly bounded, we obtain the estimate

$$(1 - C\tau) \|E^{k+1}\|_{\mathbb{L}^2(\Gamma_h^{k+1})}^2 + \frac{\tau}{2} \|E^{k+1}\|_{1,\Gamma_h^{k+1}}^2 \leq (1 + C\tau) \frac{1}{2} \|E^k\|_{\mathbb{L}^2(\Gamma_h^k)}^2 + C\tau(\tau + h)^2 \mathcal{H}^{n-1}(\Gamma_h^{k+1}). \quad (2.36)$$



Next, we first skip the second term on the left hand side, use the inequality  $\frac{1+C\tau}{1-C\tau} \leq (1+c\tau)$  for sufficiently small  $\tau$  and a constant  $c > 0$  and obtain via iteration

$$\begin{aligned} \|E^{k+1}\|_{\mathbb{L}^2(\Gamma_h^{k+1})}^2 &\leq (1+c\tau)\|E^k\|_{\mathbb{L}^2(\Gamma_h^k)}^2 + C\tau(\tau+h)^2 \\ &\quad \dots\dots\dots \\ &\leq (1+c\tau)^{k+1}\|E^0\|_{\mathbb{L}^2(\Gamma_h^0)}^2 + C\sum_{i=1}^k(1+c\tau)^{i-1}\tau(\tau+h)^2 \\ &\leq Ce^{ct_k}(\tau+h)^2 \end{aligned}$$

since  $\|E^0\|_{\mathbb{L}^2(\Gamma_h^0)}^2 \leq Ch$ . This implies the first claim of the theorem

$$\max_{k=1,\dots,k_{max}} \|E^k\|_{\mathbb{L}^2(\Gamma_h^k)}^2 \leq C(\tau+h)^2.$$

Finally, taking into account this estimate and summing over  $k = 1, \dots, k_{max}$  in (2.36), we also obtain the claim for the discrete  $\mathbb{H}_0^1$ -norm of the error

$$\sum_{k=1,\dots,k_{max}} \tau \|E^{k+1}\|_{1,\Gamma_h^{k+1}}^2 \leq C(\tau+h)^2.$$

**Remark 2.6.10** *It is worth mentioning here that the exact solution of Equation 2.7 did not intervene in the actual development; thus Theorem 2.5.1, Theorem 2.5.2 and Theorem 2.6.1 remain valid even when Equation 2.7 is not satisfied. In that case the solution will not be locally conservative in the usual sense of finite volumes anymore. This situation was already reported in [46] where they also use barycentric coefficients to approximate solution values on edges. An advantage of our approach is that we reduce the residual of the mentioned equation in a way to avoid any undesirable oscillation on the solution. Nevertheless, we have not found any experimental evidence where this situation happens but, we have also not deeply studied the local matrices to be able to know whether this worst case scenario is even plausible.*

## 2.7 Coupled reaction diffusion and advection model

In this part, we wish to extend our method to the more general case of reaction diffusion and advection problems. We then consider a source term  $g$  which depends on the solution and an additional tangential advection term  $\nabla_{\Gamma} \cdot (wu)$ . Here,  $w$  is an additional tangential transport velocity on the surface, which transports the density  $u$  along the moving interface  $\Gamma$  instead of just passively advecting it with the interface. We assume the mapping  $(t, x) \rightarrow w(t, \Phi(t, x))$  to be in  $C^1([0, t_{max}], C^1(\Gamma_0))$ . Furthermore, we suppose  $g$  to be Lipschitz continuous. An extension to a reaction term which also explicitly depends on time and position is straightforward. Hence, we investigate the evolution problem

$$\dot{u} + u\nabla_{\Gamma} \cdot v - \nabla_{\Gamma} \cdot (\mathcal{D}\nabla_{\Gamma}u) + \nabla_{\Gamma} \cdot (wu) = g(u) \quad \text{on } \Gamma = \Gamma(t). \quad (2.37)$$

In what follows, let us consider an appropriate discretization for both terms. For the reaction term, we consider the time explicit approximation

$$\int_{t_k}^{t_{k+1}} \int_{S^{l,k}(t) \cap \Gamma(t)} g(u(t, x)) da dt \approx \tau m_S^k g(u(t_k, \mathcal{P}^k X_S^k)) \quad (2.38)$$

and then replace  $u(t_k, \mathcal{P}^k(X_S^k))$  by  $U_S^k$  in the actual numerical scheme. Furthermore, we take into account an upwind discretization of the additional transport term to ensure robustness also in a regime where the transport induced by  $w$  dominates the diffusion. Different from Chapter I, we introduce

here a second order slope limiting upwind discretization derived from the above described method. Thus, since the solution  $u$  of problem 2.37 is  $\mathbb{H}^1$  on  $\Gamma(t)$  and  $\nabla_{\Gamma(t)}u$  has a weak divergence, we use the procedure described in Section 2.4.2 to construct the subgradients  $\nabla_{p_i, \mathcal{J}(p_i, S)}^k u$  of  $u$  around the vertices  $p_i^k$ . In this last procedure, we keep the center points obtained for the discretization of the diffusion operator while the virtual subedge points might vary. Let us now consider a cell  $S^k$ , the pseudo unit normal  $e_{3,S}^k := \left( \sum_{p_i^k \in S^k} (p_i^k - p_1^k) \wedge (p_{i+1}^k - p_1^k) \right) / \left\| \sum_{p_i^k \in S^k} (p_i^k - p_1^k) \wedge (p_{i+1}^k - p_1^k) \right\|$  of  $S^k$ , the vectors  $e_{1,S}^k := ((p_1^k - X_S^k) - ((p_1^k - X_S^k) \cdot e_{3,S}^k) e_{3,S}^k) / \|(p_1^k - X_S^k) - ((p_1^k - X_S^k) \cdot e_{3,S}^k) e_{3,S}^k\|$  and  $e_{2,S}^k := e_{3,S}^k \wedge e_{1,S}^k$ . We define  $\nabla_S^k u := ((\nabla_S^k u) \cdot e_{1,S}^k) e_{1,S}^k + ((\nabla_S^k u) \cdot e_{2,S}^k) e_{2,S}^k + ((\nabla_S^k u) \cdot e_{3,S}^k) e_{3,S}^k$ , the slope limited gradient on  $S^k$  as follows:  $\forall j = 1, 2, 3$

$$\begin{cases} (\nabla_S^k u) \cdot e_{j,S}^k := \text{sign} \left( (\nabla_{p_1, \mathcal{J}(p_1, S)}^k u) \cdot e_{j,S}^k \right) \min_{p_i^k \in S^k} \left| (\nabla_{p_i, \mathcal{J}(p_i, S)}^k u) \cdot e_{j,S}^k \right| \\ \quad \text{if } \text{sign} \left( (\nabla_{p_i, \mathcal{J}(p_i, S)}^k u) \cdot e_{j,S}^k \right) = \text{const } \forall p_i, \\ (\nabla_S^k u) \cdot e_{j,S}^k := 0 \quad \text{else.} \end{cases}$$

This gradient reconstruction is similar to the minmod gradient reconstruction method (cf. [8, 55, 100]). Let us now consider an edge  $\sigma^k$  common boundary of two cells  $S^k$  and  $L^k$  (i.e.  $\sigma^k = S^k \cap L^k$ ). We assume  $\sigma^k$  being delimited by the points  $p_i^k$  and  $p_{i+1}^k$  (i.e.  $\sigma^k = [p_i^k, p_{i+1}^k]$ ); we call  $S_{p_i, j}^k, S_{p_i, j+1}^k$  the respective subcells of  $S^k$  around  $p_i^k$  and  $S_{p_{i+1}, m}^k, S_{p_{i+1}, m-1}^k$  the respective subcells of  $S^k$  and  $L^k$  around  $p_{i+1}^k$ . We refer to Figure 2.11 for the illustration of this setup.

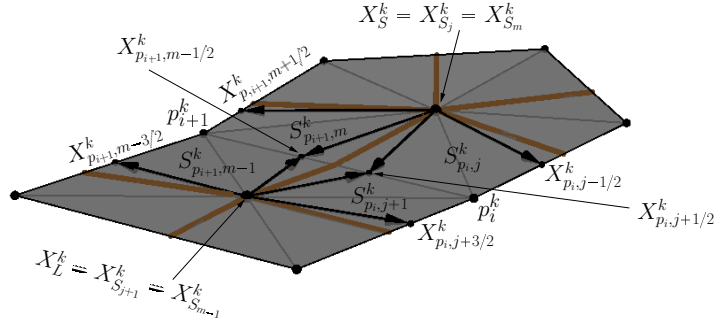


Figure 2.11: Subcells across the edge  $\sigma^k = [p_i^k, p_{i+1}^k]$  and virtual points around  $p_i^k$  and  $p_{i+1}^k$ .

We also denote by  $n_{S|L}^k := n_{S, \sigma}^k = \frac{n_{p_i, j|j+1/2}^k + n_{p_i, m|m-1/2}^k - n_{p_i, j+1|j+1/2}^k - n_{p_i, m-1|m-1/2}^k}{\|n_{p_i, j|j+1/2}^k + n_{p_i, m|m-1/2}^k - n_{p_i, j+1|j+1/2}^k - n_{p_i, m-1|m-1/2}^k\|}$  the average unit

outward pointing conormal vectors of  $S^k$  on  $\sigma^k$  and by  $p_\sigma^k := \frac{p_i^k + p_{i+1}^k}{2}$  the middle of  $\sigma^k$ . Here

$n_{S, \sigma}^k = -n_{L, \sigma}^k$  holds. We will later denote by  $n_{S, \sigma}^{l, k}(a)$  the unit conormal at  $a \in \sigma^{l, k}$  pointing out-

ward from  $S^{l, k}$ . Now if  $n_{S, \sigma}^k \cdot w(t_k, p_\sigma^k) \geq 0$ , the upwind direction is pointing inward and we define  $u^+(t_k, p_\sigma^k) := u^-(t_k, X_S^k) + (\nabla_S^k u) \cdot (p_\sigma^k - X_S^k)$ , otherwise  $u^+(t_k, p_\sigma^k) := u^-(t_k, X_L^k) + (\nabla_L^k u) \cdot (p_\sigma^k - X_L^k)$ .

If  $\sigma^k$  is a boundary segment, the average unit outward pointing conormal of  $S^k$  on  $\sigma^k$  is defined by

$n_{S, \sigma}^k = \frac{n_{p_i, j|j+1/2}^k + n_{p_i, m|m-1/2}^k}{\|n_{p_i, j|j+1/2}^k + n_{p_i, m|m-1/2}^k\| - 1}$ . In this case too, if  $n_{S, \sigma}^k \cdot w(t_k, p_\sigma^k) \geq 0$ , the upwind direction is point-

ing inward and we define  $u^+(t_k, p_\sigma^k) := u^-(t_k, X_S^k) + (\nabla_S^k u) \cdot (p_\sigma^k - X_S^k)$ , but  $u^+(t_k, p_\sigma^k) := u^-(t_k, p_\sigma^k)$  if  $n_{S, \sigma}^k \cdot w(t_k, p_\sigma^k) < 0$ . Once, the upwind direction is identified, we take into account the classical

approach by Engquist and Osher [43] and obtain the approximation:

$$\int_{t_k}^{t_{k+1}} \int_{S^{l, k}(t) \cap \Gamma(t)} \nabla_\Gamma \cdot (wu) \, da \, dt \approx \tau \sum_{\sigma^k \subset \partial S^k} m_\sigma^k (n_{S, \sigma}^k \cdot w^-(t_k, p_\sigma^k)) u^+(t_k, p_\sigma^k). \quad (2.39)$$

Finally, we again replace  $u^{-l}(t_k, X_S^k)$  by the discrete nodal values  $U_S^k$  and denote the edge values  $u^+(t_k, p_\sigma^k)$  by  $U_\sigma^{k,+}$ . For the sake of completeness let us resume the resulting scheme:

$$\begin{aligned}
 & m_S^{k+1} U_S^{k+1} - m_S^k U_S^k \\
 & - \tau \sum_{p_i \in \partial S^k} \left[ m_{p_i, \mathcal{J}(p_i, S)-1/2}^{k+1} \left( U_{p_i, \mathcal{J}(p_i, S)-1/2}^{k+1} - U_{p_i, \mathcal{J}(p_i, S)}^{k+1} \right) \lambda_{p_i, \mathcal{J}(p_i, S)|\mathcal{J}(p_i, S)-1/2}^{k+1} \right. \\
 & + m_{p_i, \mathcal{J}(p_i, S)-1/2}^{k+1} \left( U_{p_i, \mathcal{J}(p_i, S)+1/2}^{k+1} - U_{p_i, \mathcal{J}(p_i, S)}^{k+1} \right) \lambda_{p_i, \mathcal{J}(p_i, S)+1/2|\mathcal{J}(p_i, S)|\mathcal{J}(p_i, S)-1/2}^{k+1} \\
 & + m_{p_i, \mathcal{J}(p_i, S)+1/2}^{k+1} \left( U_{p_i, \mathcal{J}(p_i, S)-1/2}^{k+1} - U_{p_i, \mathcal{J}(p_i, S)}^{k+1} \right) \lambda_{p_i, \mathcal{J}(p_i, S)-1/2|\mathcal{J}(p_i, S)|\mathcal{J}(p_i, S)+1/2}^{k+1} \\
 & \left. + m_{p_i, \mathcal{J}(p_i, S)+1/2}^{k+1} \left( U_{p_i, \mathcal{J}(p_i, S)+1/2}^{k+1} - U_{p_i, \mathcal{J}(p_i, S)}^{k+1} \right) \lambda_{p_i, \mathcal{J}(p_i, S)|\mathcal{J}(p_i, S)+1/2}^{k+1} \right] \\
 & + \tau \sum_{\sigma^k \subset \partial S^k} m_\sigma^k (n_{S, \sigma}^k \cdot w^{-l}(t_k, p_\sigma^k)) U_\sigma^{k,+} \\
 & = \tau m_S^k g(U_S^k). \tag{2.40}
 \end{aligned}$$

Obviously, due to the fully explicit discretization of the additional terms, Proposition 2.4.7 still applies and guarantees existence and uniqueness of a discrete solution. Furthermore, the convergence result can be adapted and the error estimate postulated in Theorem 2.6.1 holds. To see this, let us first consider the nonlinear source term  $g(u)$  and the following estimate already presented in Chapter I for the triangular mesh;

$$\begin{aligned}
 & \int_{t_k}^{t_{k+1}} \int_{S^{l,k}(t) \cap \Gamma(t)} g(u(t, x)) \, da \, dt - \tau m_S^k g(U_S^k) \\
 & = - \int_{t_k}^{t_{k+1}} \int_{S^{l,k}(t) \setminus \Gamma(t)} g(u(t, x)) \, da + \int_{t_k}^{t_{k+1}} \left( \int_{S^{l,k}(t)} g(u(t, x)) \, da - \int_{S^{l,k}} g(u(t_k, x)) \, da \right) dt \\
 & + \tau \left( \int_{S^{l,k}} g(t_k, x) \, da - \int_{S^{l,k}} g(u(t_k, X_S^k)) \, da \right) + \tau (m_S^{l,k} - m_S^k) g(u(t_k, X_S^k)) \\
 & + \tau m_S^k (g^{-l}(u(t_k, X_S^k)) - g(U_S^k)) \\
 & \leq C(\tau h m_S^k + \tau^2 \mathcal{H}^{n-1}(S^{l,k})) + \tau h m_S^k + \tau h^2 m_S^k + C_{Lip}(g) \tau m_S^k E_S^k,
 \end{aligned}$$

where  $C_{Lip}(g)$  denotes the Lipschitz constant of  $g$ . In the proof of Theorem 2.6.1 we already have treated terms identical to the first four on the right hand side. For the last term we obtain after multiplication with the nodal error  $E_S^{k+1}$  and summation over all cells  $S$

$$\begin{aligned}
 C_{Lip}(g) \tau \sum_S m_S^k E_S^k E_S^{k+1} & \leq C_{Lip}(g) \tau \max_S \left( \frac{m_S^k}{m_S^{k+1}} \right)^{\frac{1}{2}} \|E^k\|_{\mathbb{L}^2(\Gamma_h(t_k))} \|E^{k+1}\|_{\mathbb{L}^2(\Gamma_h(t_k))} \\
 & \leq C \tau \left( \|E^k\|_{\mathbb{L}^2(\Gamma_h(t_k))}^2 + \|E^{k+1}\|_{\mathbb{L}^2(\Gamma_h(t_{k+1}))}^2 \right).
 \end{aligned}$$

Taking into account these additional error terms the estimate (2.36) remains unaltered. Next, we investigate the error due to the additional advection term and rewrite

$$\begin{aligned}
 & \int_{t_k}^{t_{k+1}} \int_{S^{l,k}(t) \cap \Gamma(t)} \nabla_\Gamma \cdot (wu) \, da \, dt - \tau \sum_{\sigma^k \subset \partial S^k} m_\sigma^k (\mu_{\sigma, S}^k \cdot w^{-l}(t_k, X_\sigma^k)) U_\sigma^{k,+} \\
 & = \int_{t_k}^{t_{k+1}} \int_{S^{l,k}(t) \cap \Gamma(t)} \nabla_\Gamma \cdot (wu) \, da \, dt - \tau \int_{S^{l,k} \cap \Gamma(t_k)} \nabla_\Gamma \cdot (wu) \, da \\
 & + \sum_{\substack{\sigma^k \subset \partial S^k \\ \sigma^k = S^k \cap L^k}} (\tau \mathcal{R}_5(S^{l,k}|L^{l,k}) + \tau \mathcal{F}(S^{l,k}|L^{l,k}) E_\sigma^{k,+}),
 \end{aligned}$$

where  $\mathcal{R}_5(S^{l,k}|L^{l,k}) = \int_{\sigma^{l,k}} n_{S,\sigma}^{l,k} \cdot w u \, dl - m_\sigma^k w^{-l}(t_k, p_\sigma^k) \cdot n_{S,\sigma}^k u^+(t_k, p_\sigma^k)$  is an edge residual,  $\mathcal{F}(S^{l,k}|L^{l,k}) = m_\sigma^k w^l(t_k, p_\sigma^k) \cdot n_{S,\sigma}^k$  a flux term on the edge  $\sigma^{l,k} = S^{l,k} \cap L^{l,k}$  and  $E_\sigma^{k,+} = u^+(t_k, p_\sigma^k) - U_\sigma^{k,+}$  a piecewise constant upwind error function on the discrete surface  $\Gamma_h^k$ . For the sake of consistency in the notation, we have assumed here as in the following any curved boundary segment  $\sigma^{l,k}$  being the intersection of a curved cell  $S^{l,k} \subset \Gamma^k$  and the curved cell  $L^{l,k} := \sigma^{l,k}$  of measure 0. In this case, the cell's center value as well as any error coming from  $L^{l,k}$  are taken to be 0 and the subedges values are known from the boundary condition. Now the first term in the above error representation can again be estimated by  $C \tau^2 \mathcal{H}^{n-1}(S^{l,k})$ . From  $|u^+(t_k, p_\sigma^k) - u^-(t_k, p_\sigma^k)| \leq C h^2$ , we deduce by similar arguments as in the proof of Lemma 2.6.7 that  $|\mathcal{R}_5(S^{l,k}|L^{l,k})| \leq C h m_\sigma^k$ . Furthermore, the antisymmetry relations  $\mathcal{R}_5(S^{l,k}|L^{l,k}) = -\mathcal{R}_5(L^{l,k}|S^{l,k})$  and  $\mathcal{F}(S^{l,k}|L^{l,k}) = -\mathcal{F}(L^{l,k}|S^{l,k})$  hold. After multiplication with the nodal error  $E_S^{k+1}$  and summation over all cells  $S$  we obtain

$$\begin{aligned}
 Z &= \tau \sum_S \sum_{\substack{\sigma^k \subset \partial S^k \\ \sigma^k = S^k \cap L^k}} (\mathcal{R}_5(S^{l,k}|L^{l,k}) + \tau \mathcal{F}(S^{l,k}|L^{l,k}) E_\sigma^{k,+}) E_S^{k+1} \\
 &= \tau \sum_{\sigma^k = S^k \cap L^k} [\mathcal{R}_5(S^{l,k}|L^{l,k}) + \mathcal{F}(S^{l,k}|L^{l,k}) E_\sigma^{k,+}] (E_S^{k+1} - E_L^{k+1}) \\
 &= \tau \sum_{p_i^k \in \Gamma_h^k} (\bar{\mathcal{R}}_{5,p_i}^k)^\top (\bar{E}_{p_i}^{k+1} - E_{p_i}^{k+1} \mathbf{1}_{p_i}) + (\bar{\mathcal{R}}_{6,p_i}^k)^\top (\bar{E}_{p_i}^{k+1} - E_{p_i}^{k+1} \mathbf{1}_{p_i}),
 \end{aligned}$$

where  $\bar{\mathcal{R}}_{5,p_i}^k$  and  $\bar{\mathcal{R}}_{6,p_i}^k$  are vectors with entries

$(\bar{\mathcal{R}}_{5,p_i}^k)_j := (m_{p_i,j-1/2}^k / \bar{m}_{p_i,j-1/2}^k) (\mathcal{R}_5(S_{p_i,j}^{l,k}|S_{p_i,j-1}^{l,k}) + \mathcal{R}_5(S_{p_i,j}^{l,k}|S_{p_i,j+1}^{l,k}))$  and  $(\bar{\mathcal{R}}_{6,p_i}^k)_j := (m_{p_i,j-1/2}^k / \bar{m}_{p_i,j-1/2}^k) (\bar{\mathcal{F}}(S_{p_i,j}^{l,k}|S_{p_i,j-1}^{l,k}) E_{\sigma_{p_i,j-1/2}^{k,+}} + \bar{\mathcal{F}}(S_{p_i,j}^{l,k}|S_{p_i,j+1}^{l,k}) E_{\sigma_{p_i,j+1/2}^{k,+}})$  respectively;  $\bar{m}_{p_i,j-1/2}^k$  being the length of the entire edge  $\sigma$  containing  $\sigma_{p_i,j-1/2}^k$  and  $E_{\sigma_{p_i,j+1/2}^{k,+}} := E_\sigma^{k,+}$ . Using similar arguments as in the proof of Theorem 2.6.1 and the definition of upwind values on edges, one deduces that

$$\begin{aligned}
 Z &\leq \tau \left[ \sum_{p_i^k \in \Gamma_h^k} (\bar{\mathcal{R}}_{5,p_i}^k)^\top (A_{p_i}^{k+1} + (\mathbf{1}_{p_i} \otimes \mathbf{1}_{p_i}) / n_{p_i})^{-1} \bar{\mathcal{R}}_{5,p_i}^k \right]^{1/2} \left[ \sum_{p_i^k \in \Gamma_h^k} (\bar{E}_{p_i}^{k+1})^\top A_{p_i}^{k+1} \bar{E}_{p_i}^{k+1} \right]^{1/2} \\
 &\quad + \tau \left[ \sum_{p_i^k \in \Gamma_h^k} (\bar{\mathcal{R}}_{6,p_i}^k)^\top (A_{p_i}^{k+1} + (\mathbf{1}_{p_i} \otimes \mathbf{1}_{p_i}) / n_{p_i})^{-1} \bar{\mathcal{R}}_{6,p_i}^k \right]^{1/2} \left[ \sum_{p_i^k \in \Gamma_h^k} (\bar{E}_{p_i}^{k+1})^\top A_{p_i}^{k+1} \bar{E}_{p_i}^{k+1} \right]^{1/2} \\
 &\leq C \tau \left( h \mathcal{H}^{n-1}(\Gamma_h^k)^{\frac{1}{2}} + \left( \sum_{p_i \in \Gamma_h^k} (\bar{\mathcal{R}}_{6,p_i}^k)^\top \bar{\mathcal{R}}_{6,p_i}^k \right)^{\frac{1}{2}} \right) \|E^{k+1}\|_{1,\Gamma_h^{k+1}} \\
 &\leq \frac{\tau}{4} \|E^{k+1}\|_{1,\Gamma_h^{k+1}}^2 + C \tau h^2 + C \tau \|E^k\|_{\mathbb{L}^2(\Gamma_h^k)}^2.
 \end{aligned}$$

Again, taking into account these error terms due to the added advection in the original error estimate (2.36) solely the constant in front of the term  $\|E^{k+1}\|_{1,\Gamma_h^{k+1}}^2$  on the left hand side of (2.36) is slightly reduced. Thus, both the explicit discretization of a nonlinear reaction term and the upwind discretization of the additional tangential advection still allow us to establish the error estimate postulated in Theorem 2.6.1.

## 2.8 Numerical results

In this paragraph, we present several simulation results. To begin with, we consider the time evolving parametric surface  $\Gamma(t)$  described by the evolution of the material point

$M(t, x, y) = (x, y, h(t, x, y))^T$ , where  $(x, y) \in [-0.6, 0.6] \times [-0.5, 0.5]$ ,  $h(t, x, y) = x^2 f_1(t) + y^3 f_2(t)$  with  $f_1(t) = \sin(\pi t/t_{max})^2 \sin(2\pi t/t_{max})$  and  $f_2(t) = \sin(\pi t/t_{max})^2 \cos(2\pi t/t_{max})$ ;  $t_{max}$  being the maximum time. We define on  $\Gamma(t)$  the surface tangential matrix

$$\mathcal{D}_0(t, x, y) := \frac{1 + 4x^2 f_1(t)^2 + 9y^4 f_2(t)^2}{1 + 4f_1(t)^2 + 9f_2(t)^2} [e_1(t, x, y), e_2(t, x, y)] \begin{pmatrix} 5 & 0 \\ 0 & 1 \end{pmatrix} [\mu_1(t, x, y), \mu_2(t, x, y)]^T$$

and the tangential vector  $w(t, x, y) := 10 e_1(t, x, y)$ , where  $e_1(t, x, y) := (1, 0, 2x f_1(t))^T$ ,  $e_2(t, x, y) := (0, 1, 3y^2 f_2(t))^T$  are tangential vectors of  $\Gamma(t)$  and  $\mu_1(t)$ ,  $\mu_2(t)$  their corresponding contravariant counterparts defined through the four equations  $e_1(t, x, y) \cdot \mu_1(t, x, y) = 1$ ,  $e_1(t, x, y) \cdot \mu_2(t, x, y) = 0$ ,  $e_2(t, x, y) \cdot \mu_1(t, x, y) = 0$  and  $e_2(t, x, y) \cdot \mu_2(t, x, y) = 1$ . We approximate on successive refined polygonal meshes (cf. Figure 2.12), the solution  $u := h(t, x, y) + 0.5$  of Problem 2.37 for  $\mathcal{D} := (\mathcal{D}_0 + \mathcal{D}_0^T)/2$ ,  $w$  defined above and  $g$  computed from the data. The Dirichlet boundary condition is considered. On Figure 2.12 we present the successively refined polygonal surfaces used

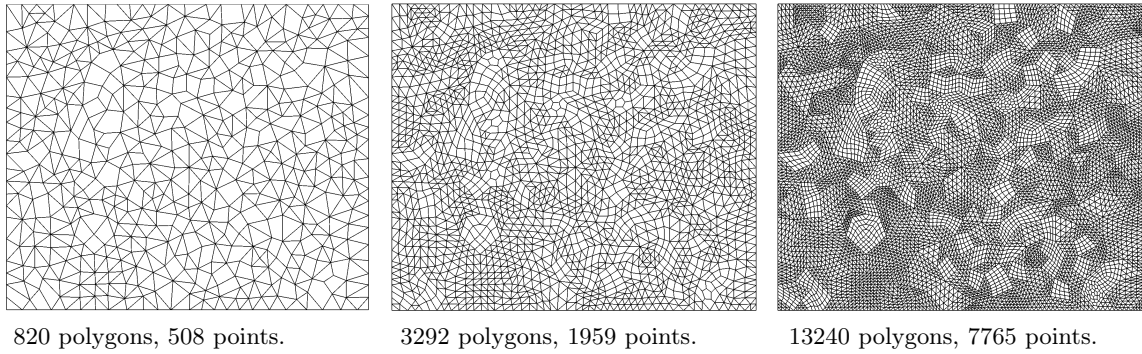


Figure 2.12: Successively refined polygonal mesh used for the convergence test. At each refined step, sizes of cells are divided into 2.

for this simulation test case. At each refined step, edges of the previous step have been divided into two. The computation is done for  $t \in [0, 1]$  and we present in Figure 2.13 a sequence of frames from the simulation result. Here, as in the sequel, color shading range from blue to red representing minimum to maximum values. Finally, in Table 2.1, we display the errors in the discrete  $\mathbb{L}^\infty(\mathbb{L}^2)$  norm and discrete energy seminorm (2.18), respectively. Indeed, the observed error decay is consistent with the convergence result in Theorem 2.6.1.

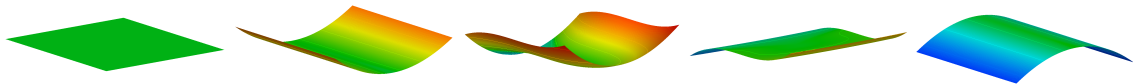


Figure 2.13: Solution of the first simulation at different time steps.

Next, we compute a second example using the same successive initial surfaces and compare the result to the result of the refined surface. We consider the evolution of the surface material point described by  $M(t, x, y) = (x, y, h(t, x, y))^T$ , where  $h(t, x, y) = (f(t)/4.5) \sum_{i=1}^{12} \beta(i) \exp(-\alpha(i))$  with  $f(t) = (\sin(\pi t - \pi/2) + 1)/2$  and  $\alpha(i) := [(x - P(i, 1))^2 / (2V(i, 1)^2)] + [(y - P(i, 2))^2 / (2V(i, 2)^2)]$ . The variables  $P$ ,  $V$  and  $\beta$  are defined by

$$P = \begin{pmatrix} 3 & 22 & 4 & 8 & 12 & 18 & 21 & 0 & 8 & 14 & 10 & 8 \\ 3 & 6 & 16 & 16 & 16 & 12 & 21 & 24 & 24 & 5 & 8 & 2 \end{pmatrix}^T / 24,$$

$$V = \begin{pmatrix} 3 & 2 & 2 & 4 & 4 & 2 & 3 & 2 & 3 & 1.5 & 2 & 2 \\ 3 & 4 & 4 & 2 & 4 & 2 & 3 & 2 & 3 & 1.5 & 1.5 & 2 \end{pmatrix}^T / 24 \text{ and}$$

$\min_{t \in [0,1]} h(t)$	$\max_{t \in [0,1]} h(t)$	norm of the error	
		$\mathbb{L}^\infty(\mathbb{L}^2)$	$\mathbb{L}^\infty(\mathbb{H}^1)$
0.0294	0.1168	$91.617 \cdot 10^{-5}$	$14.8 \cdot 10^{-3}$
0.0119	0.0595	$21.269 \cdot 10^{-5}$	$5.3 \cdot 10^{-3}$
0.0041	0.0302	$5.768 \cdot 10^{-5}$	$2.0 \cdot 10^{-3}$

Table 2.1: The table displays the numerical error on grids presented in Figure 2.12 in two different norms, when compared to the explicit solution. The time discretization was chosen as  $\tau = 1/30000$  in all three computations.

$$\beta = (3.5 \quad 4 \quad 4 \quad 2 \quad 6 \quad 5 \quad 3 \quad 1.75 \quad 4 \quad -2.5 \quad -3 \quad -2)^\top / 6.$$

For  $t = 1$ ,  $f(t) = 1$  and we recover the surface presented on Figure 2.2; therefore the evolution considered here is obtained by continuously scaling the height of the given surface by  $f(t)$  as time evolves. We also consider the advection vector  $w$ , tangential component of  $w_0 = -50(0, 0, 1)^\top$  and the source term  $g(t) = (1 - f(t))(1.5 \exp(-\alpha_1) + \exp(-\alpha_2) + \exp(-\alpha_3))$ , where  $\alpha_1 := \|M(t, x, y) - (3/6, 4/6, 0)^\top\|^2 / (0.035^2)$ ,  $\alpha_2 := \|M(t, x, y) - (18/24, 12/24, 0)^\top\|^2 / (0.035^2)$ , and  $\alpha_3 := \|M(t, x, y) - (1/6, 4/6, 0)^\top\|^2 / (0.035^2)$ . The function  $g(t)$  defines three localized sources (cf. Figure 2.14) whose density reduces as time evolves and vanishes at the end of the process. We depict on Figure 2.14 a sequence frame from the simulation result of problem 2.37 with homogeneous Dirichlet boundary condition in the time interval  $[0, 1]$ ; isolines are also drawn. We can clearly notice the dominance of the diffusion at the beginning of the process and progressively the dominance of the advection.

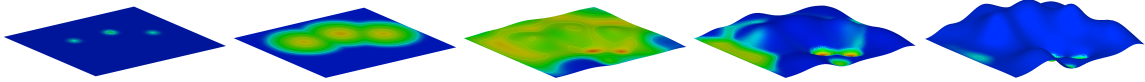


Figure 2.14: The evolution of a density under diffusion and advection by gravity is investigated.

The results have been compared to the solution obtained on the refined mesh in  $\mathbb{L}^\infty(\mathbb{L}^2)$  norm and discrete energy seminorm (2.18), respectively. The result is reported in Table 2.2. Comparing these

$\min_{t \in [0,1]} h(t)$	$\max_{t \in [0,1]} h(t)$	norm of the error	
		$\mathbb{L}^\infty(\mathbb{L}^2)$	$\mathbb{L}^\infty(\mathbb{H}^1)$
0.0294	0.1382	$4.85 \cdot 10^{-4}$	$5.4 \cdot 10^{-3}$
0.0119	0.0722	$1.28 \cdot 10^{-4}$	$1.9 \cdot 10^{-3}$

Table 2.2: The table displays the numerical error of the solution on the first two grids of Figure 2.12 in two different norms, when compared to the solution of the last grid (refined grid). The time discretization was chosen as  $\tau = 1/60000$  in all three computations.

results to the simulation results of Chapter I, we notice the improvement in the spatial convergence which is  $\mathcal{O}(h^2)$  for the  $\mathbb{L}^\infty(\mathbb{L}^2)$  norm. This is due to the use of barycenter of cells as presented in Section 2.4.5 and the slope limiting procedure introduced in Section 2.7.

As third example, we consider the fixed triangulated geometry of an elephant as presented in Figure 2.15 and solve Problem 2.1 in the time interval  $[0, 1]$ , with the diffusion tensor  $\mathcal{D}$  being the tangential component of the tensor  $\mathcal{D}_0 := \begin{pmatrix} 25 & 0 & 0 \\ 0 & 0.1 & 0 \\ 0 & 0 & 0.001 \end{pmatrix}$ ; the  $X$ -direction points to the right and the

$Z$ -direction points up. Five sources are put in the  $(Y, Z)$ -plane around the front legs as can be noticed on the second picture of Figure 2.15 (two at the elephant front side, two at the elephant back side and one at symmetric upper point). We present on Figure 2.15 a sequence of frames from this simulation. One effectively observes a rapid diffusion in the  $X$ -direction and a very slow diffusion in the  $Z$ -direction.

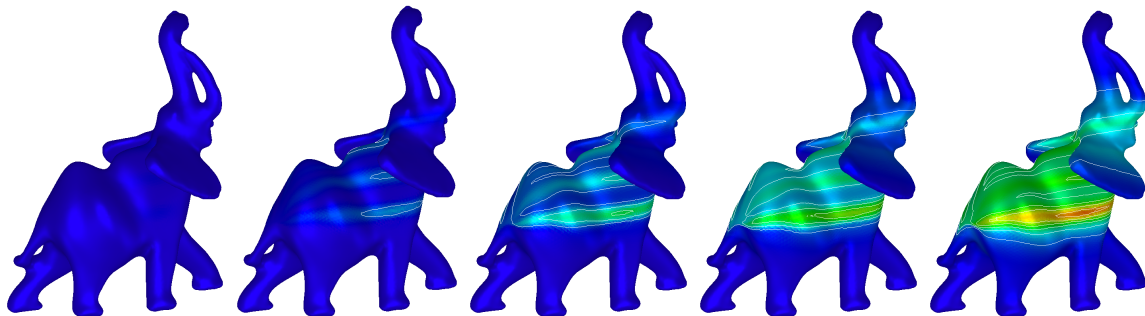


Figure 2.15: Strong anisotropic diffusion of a density on a fixed elephant geometry. The polygonal mesh is made up of 83840 triangles and 41916 points.

Now in our fourth example, we consider a diffusion advection problem which involves the curvature tensor. In fact, we consider the advection vector  $w = 13(\text{Id} - 0.0015(\mathcal{K}\text{Id} + 4K))(0, 0, 1)^\top$ , where  $K$  is the curvature tensor of the considered surface and  $\mathcal{K} := \text{tr}(K)$  (trace of  $K$ ) is the mean curvature. We also consider a source term  $g$  made up of three localized sources as depicted on the first pictures of Figure 2.16 and Figure 2.17. The intensity of the source is a decreasing function in time  $t \in [0, 1]$  which vanishes at the end of the process. First we consider an evolution by mean curvature flow  $\partial M(t, s_1, s_2)/\partial t = (\mathcal{K}/30)\nu(t, s_1, s_2)$ , where  $M(t, s_1, s_2)$  is the material point of the surface,  $\nu(t, s_1, s_2)$  the normal at  $M(t, s_1, s_2)$  and  $s_1, s_2$  some parameters used to locally parameterize the surface. Here, we use an adaptive time step  $\tau^{k+1} = \min(1/(\mathcal{K}_2^k + 10^{-8}), 13l^2)/10.2$ , where  $\mathcal{K}_2^k := \text{tr}((K^k)^2)$  is the trace of the squared curvature tensor ( $K^2$ ) at the time step  $t_k$  and  $l$  the smallest length of the polygons sides. Noticing that  $(\nabla_\Gamma z) = (0, 0, 1)^\top$  ( $z$  being the third spatial coordinate), we evaluate  $\mathcal{K}$  and  $K$  at cell centers using a weighted least square fitting and then use the procedure described in Section 2.4.2 to compute the flux of the advection vector on subedges while the flux on entire edges is obtained by summing the flux on subedges as for the diffusion operator. There is no need to compute conormal vectors anymore and our slope limiting procedure is applied using these fluxes. Since the evaluation of the curvature can only be consistent if one has a  $(3, h)$ -approximation of the surface, we solve the mean curvature flow equation for nodal points using a semi-implicit scheme. Figure 2.16 presents a sequence of frames from this simulation. Due to the advection process which is dominant where the tangential component of  $(0, 0, 1)^\top$  is pronounced, the density would try to concentrate where the  $Z$ -coordinate of the material points presents a local maximum; but due to the smoothening process, the local maxima of the  $Z$ -coordinate tends to disappear and the density moves and concentrates at the point of highest  $Z$ -coordinate.

Next the same simulation is done on the fixed initial surface. We effectively notice the concentration of density at points of local maximum on the  $Z$ -coordinate due to the advection process. Figure 2.17 presents a sequence of the result of this simulation.

Examples of practical use of reaction diffusion equations include texture generation [120, 123] and bi-



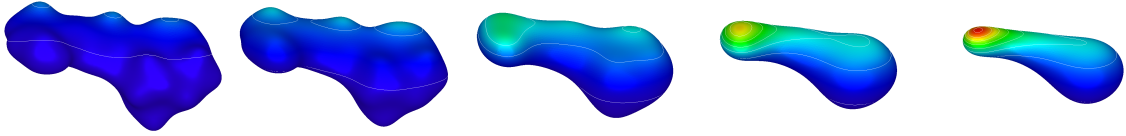


Figure 2.16: Evolution of a density under diffusion and advection on a surface moving by mean curvature. The initial polygonal surface is made up of 26848 triangles and 13426 points.

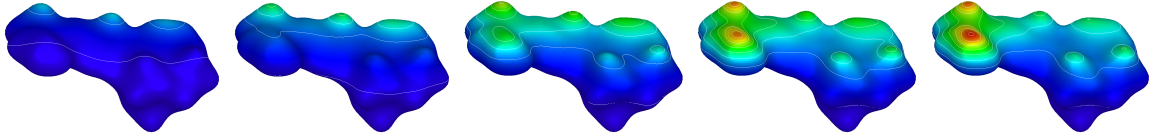


Figure 2.17: Evolution of a density under diffusion and advection on a fixed surface.

ological pattern formation [7, 88, 119]. In these fields, one uses a system of coupled reaction-diffusion equations introduced by A. Turing in 1952 [119] to explain the formation of patterns on animals. He assumed the existence of two kinds of morphogenes diffusing on a surface and interacting with each other and showed that the presence of diffusion could drive a system instability leading to the formation of spatial patterns by the morphogenes distribution. Here we consider the Turing system

$$\begin{aligned}\frac{\partial u}{\partial t} &= c\delta\Delta_{\Gamma}u + \alpha u(1 - r_1v^2) + v(1 - r_2u) \\ \frac{\partial v}{\partial t} &= \delta\Delta_{\Gamma}v + \beta v(1 + \frac{\alpha r_1}{\beta}uv) + u(\gamma + r_2v)\end{aligned}$$

presented by R. A. Barrio et al. in [7] and describing the interaction between two morphogenes  $u$  and  $v$ . The coefficient  $c$  is the ratio of diffusion coefficients,  $\delta$  is a parameter that can be viewed either as a relative strength of the diffusion compared to the interaction terms or the measure of length scale and  $\alpha, \beta, \gamma, r_1, r_2$  are some coefficients. We refer to [7] for how these coefficients are chosen to generate particular patterns. We should nevertheless mention that cubic interaction favors stripes and quadratic interaction produces spot patterns. We simulate this system on the closed triangulated surface using the coefficients provided in [19] for the simulation on a sphere. As in this reference, we chose as initial condition for  $u$  and  $v$  random values between  $-1/2$  and  $1/2$ . Figure 2.18 and Figure 2.19 show some sequence of the simulation result of the solution  $u$  which leads to the striped pattern and the spotted pattern respectively.

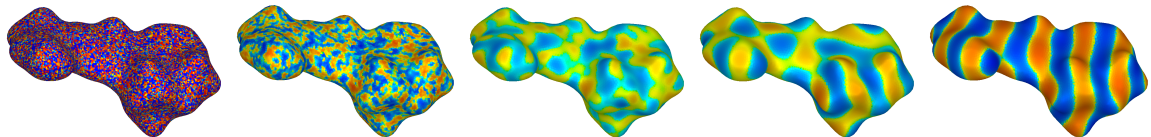


Figure 2.18: Striped pattern formation from the Turing system.

$$\delta = 0.0021, c = 0.516, r_1 = 3.5, r_2 = 0, \alpha = 0.899, \beta = -0.91, \gamma = -\alpha.$$



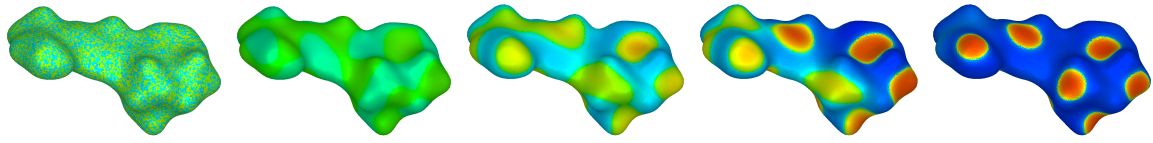


Figure 2.19: Dotted pattern formation from the Turing system.

$$\delta = 0.0045, c = 0.516, r_1 = 0.02, r_1 = 0.2, \alpha = 0.899, \beta = -0.91, \gamma = -\alpha.$$



## Part II

# Modeling and simulation of surfactant driven thin-film flow on moving surfaces



# 3 Modeling of surfactant driven thin-film flow on moving surfaces

## 3.1 Introduction

Thin liquid films are ubiquitous in nature and technology and therefore, understanding their mechanics is very useful in many applications. As reported in [98], they appear in geology as gravity currents underwater or as lava flows [69, 70], in biophysics as membranes, as lining of mammalian lungs [58, 74], as tear films in the eyes ([75, 91, 90, 110, 124] and references therein), etc. They also occur in Langmuir films [50] and in foam dynamics [13, 44, 111, 122, 125]. In engineering, thin-films serve in heat and mass transfer processes to limit fluxes and to protect surfaces [3]. Applications in this area include flow behavior of paints and other surface coatings, chemical and nuclear reactor design. However, the common and probably the simplest thin-film encountered in everyday life is the flow of a droplet down an inclined plane. At this basic level one observes that the velocity component parallel to the plane is much larger than the perpendicular component. Considering an incompressible fluid, this main characteristic leads to the consideration that the ratio  $\epsilon = \mathcal{H}/\mathcal{L}$  between the vertical length scale  $\mathcal{H}$  and the tangential length scale  $\mathcal{L}$  is very small ( $\epsilon \ll 1$ ). This useful remark is usually exploited to reduce the level of complexity of the original free boundary problem modeled by the Navier-Stokes equations. Therefore, one commonly does a model reduction using lubrication approximation (long-wave approximation) due to Orchard [97], or applies center manifold theory [105]. Discussions of this issue can be found in [80, 82, 95, 98]. There, gravity driven thin-film flow on uniformly smooth planar substrates is discussed and the general equation modeling the fluid with a clean interface (without any contaminant such as the surfactant (surface active agent)) is derived. The general nondimensional equation derived by considering a no-slip condition on the substrate-fluid interface, gravity  $g$  and constant surface tension  $\gamma$  reads

$$\frac{\partial H}{\partial t} = -\frac{1}{3}\nabla_{\Gamma} \cdot \left( H^3 \nabla_{\Gamma} (C\gamma\mathcal{K}_{FS}) + \mathcal{B}_0 H^3 g_{tan} + H^3 \epsilon \mathcal{B}_0 g_{\nu} \nabla_{\Gamma} H \right), \quad (3.1)$$

where  $\nabla_{\Gamma}$  represents the surface nabla operator,  $H$  the height of the film and  $\mathcal{K}_{FS} = \Delta_{\Gamma} H$  the free surface mean curvature with  $\Delta_{\Gamma}$  being the Laplace-Beltrami operator.  $\mathcal{B}_0$  is the Bond number,  $C$  is the inverse capillary number,  $g_{tan}$  the tangential component of the unit gravity vector  $g$  and  $g_{\nu} = g \cdot \nu$  with  $\nu$  denoting the unit normal to the substrate. Unfortunately, this equation is not suitable for a partially wetted surface since it shows that a nonintegrable singularity is developed at the contact line junction (Substrate-Fluid-Air line junction). This prevents any fluid particle at the contact line to move. Moreover, for any particle at the contact line, the limit of the velocity along the moving free surface (Fluid-Air interface) is nonzero [11, 68, 42] while we have set the velocity on the substrate to zero (no-slip boundary condition). This makes the velocity field being multi-valued at the contact line and therefore not well defined. This paradox is probably due to the lack of introducing the surface chemistry into the hydrodynamic model; therefore, researchers agree to add additional effects on the microscopic length scale. The slip boundary condition and a precursor layer are then commonly used in the literature [12, 31, 81, 95] to overcome the problem. It is also common to add some disjoining pressure such as van der Waals forces to control dewetting processes. The general equation obtained by considering these effects is

$$\frac{\partial H}{\partial t} = -\nabla_{\Gamma} \cdot \left[ \left( \frac{1}{3} H^3 + H^2 \beta^{-1} \right) \left[ \nabla_{\Gamma} (-\phi + C'\gamma\mathcal{K}_{FS}) + \mathcal{B}_0 g_{tan} + \epsilon \mathcal{B}_0 g_{\nu} \nabla_{\Gamma} H \right] \right], \quad (3.2)$$

where  $\phi$  is the disjoining pressure and  $\beta$  is the slip coefficient. These equations were first generalized to curved surfaces by Schwartz and Weidner in 1994 [109]. They mainly concentrated on the curve case and the effect of curvature on the flow of thin-films driven by surface tension. They proved for example that short wavelength irregularities are quickly levelled by surface tension forces while long term evolution of the flow is primarily determined by the curvature of the substrate. They also extrapolated their results to two dimensional hypersurfaces. Later on, careful analysis of thin-film flow on curved surfaces were undertaken in [72, 93, 98, 107, 115, 121] but the most general and unified model is probably the one developed by Roy, Roberts and Simpson in [107]. We also refer to these references for more precise development in this area. Roy, Roberts and Simpson considered a general curved surface with a bounded curvature, defined a curvilinear coordinate system attached to the substrate and used center manifold theory to derive an equation describing the movement of the free surface (Fluid-Air interface) in terms of surface variables and derivatives. The effects considered in their results are gravity and constant surface tension and the resulting equation using a proper scaling of variables reads

$$\begin{aligned} \frac{\partial \eta}{\partial t} &= -\frac{1}{3} \nabla_{\Gamma} \cdot \left( \eta \mathbb{H}^2 \nabla_{\Gamma} \mathcal{K}_{FS} - \frac{1}{2} \epsilon \mathbb{H}^4 (\mathcal{K} \text{Id} - K) \nabla_{\Gamma} \mathcal{K} \right) \\ &\quad - \frac{1}{3} \mathcal{B}_0 \left[ \mathbb{H}^3 g_{tan} - \epsilon \mathbb{H}^4 \left( \mathcal{K} \text{Id} + \frac{1}{2} K \right) + \epsilon \mathbb{H}^3 g_{\nu} \nabla_{\Gamma} \mathbb{H} \right], \end{aligned} \quad (3.3)$$

where  $\text{Id}$  is the identity matrix,  $K$  the substrate's curvature tensor,  $\mathcal{K} := \text{tr} K$  the mean curvature,  $\eta := \mathbb{H} - \epsilon \mathcal{K} \mathbb{H} + \frac{1}{6} \epsilon^2 (\mathcal{K}^2 - \mathcal{K}_2)$  ( $\mathcal{K}_2 := \text{tr} (K^2)$ ) is the fluid density above the substrate and  $\mathcal{K}_{FS} := \mathcal{K} + \epsilon (\mathcal{K}_2 \mathbb{H} + \Delta_{\Gamma} \mathbb{H})$  is the free surface mean curvature. As we will see in the next chapter, such setting is suitable for numerical simulations on parametric surfaces. The stability of the resulting equation follows from the theory of center manifolds. We refer to [21, 25, 106] for further reading on the application of center manifold theory for the construction of low dimensional systems.

In real world applications, the fluids considered above contain almost always chemicals. The most common is the surfactant. This substance, distributed on top of a thin liquid support, will cause spontaneous and fast spreading when it creates region of lower surface tension than the supporting fluid [92]. In fact it reduces the surface tension which gives rise to Marangoni effect due to the gradient in the surface tension. This main property justifies its presence in the mammalian lung; by reducing the surface tension when the alveoli are compressed during expiration for example, it prevents alveoli to collapse [63, 108]. The surfactant also imparts an effective elasticity to the interface and can be used on fluids to suppress motion characterized by nonzero surface divergence. This last remark has been used for centuries by spear-fishermen, who poured oil on the water to increase their ability to see their prey and by sailors, who would do similarly in an attempt to calm troubled sea. It is then interesting to incorporate the effect of surfactant in the study of thin-film flow. This results in the coupling of two partial differential equations. The basic equation used to model the evolution of nonsoluble surfactant reads

$$\frac{\partial \Pi}{\partial t} + (\nabla_{FS} \cdot (\Pi v_{FS})) = \frac{1}{\mathcal{P}_e} \Delta_{FS} \Pi, \quad (3.4)$$

where  $\nabla_{FS}$  is the free surface nabla operator,  $\Delta_{FS}$  the free surface Laplace-Beltrami operator,  $\Pi$  the surfactant concentration,  $v_{FS}$  the velocity of the free surface particle and  $\mathcal{P}_e$  the Peclet number. This equation is often rewritten in terms of substrate variables using lubrication approximation. For flat surfaces, the equation obtained considering van der Waals forces and no gravity for example is

$$\frac{\partial \mathbb{H}}{\partial t} = -\frac{1}{2} \nabla_{\Gamma} (\mathbb{H}^2 \nabla_{\Gamma} \gamma) - \frac{1}{3} \nabla_{\Gamma} (\mathbb{H}^3 \nabla_{\Gamma} (-\phi + C \gamma \mathcal{K}_{FS})) \quad (3.5)$$

$$\frac{\partial \Pi}{\partial t} = -\nabla_{\Gamma} (\mathbb{H} \Pi \nabla_{\Gamma} \gamma) - \frac{1}{2} \nabla_{\Gamma} (\mathbb{H}^2 \Pi \nabla_{\Gamma} (-\phi + C \gamma \mathcal{K}_{FS})) + \frac{1}{\mathcal{P}_e} \Delta_{\Gamma} \cdot \Pi, \quad (3.6)$$

where  $\mathcal{K}_{FS} := \Delta_r H$  represents as above the free surface mean curvature,  $\phi := AH^{-3}$  is the disjoining pressure of the van der Waals force and  $A$  is the nondimensional Hamaker constant. The relation between  $\Pi$  and  $\gamma$  is given by the Langmuir equation of state and one of its linearized version using a proper scaling is  $\gamma = 1 - \Pi$ . One might also consider a soluble surfactant. We refer to [53, 98] and references therein for further reading on the topic. In the present work, we follow the path of Roy Roberts and Simpson in [107] and Howel in [67] to derive a general thin-film equation driven by surfactant on a moving surface. In fact, considering a general curvilinear coordinate system attached to the substrate and evolving in time, we use basic notions of tensor calculus to derive a general equation. This method provides a very simple way to reason as in the case of flat surfaces. The whole complexity of curved surfaces is hidden in the differential operators used. In fact, a simplification of the momentum equation of the Navier-Stokes equations using lubrication approximation will lead us as in the flat case to a system of ordinary differential equations (ODEs) along the vertical line for the determination of the component of the relative velocity tangent to the substrate. This system of ODEs will be solved at the given order of the lubrication approximation ( $\mathcal{O}(\epsilon^2)$ ) using power series and the result will be incorporated in the conservation of mass equation to obtain an equation describing the free surface profile. The method provides the same results as the one obtained by Roy, Roberts and Simpson in [107] using computer algebra to find the center manifold of the Navier-Stokes equation in this case. We will not apply the lubrication approximation to the surfactant equation since we aim in the next chapter to use a direct discretization of this equation using a variant of the interface tracking method. Howell studied already the evolution of surface-tension driven thin-film flow but used too much simplification and focused essentially on special cases. In fact, he assume the term  $\epsilon\mathcal{K}$  to be of order  $\mathcal{O}(\epsilon)$  and neglected all terms of that order in the lubrication approximation process. He also could only derive equations corresponding to special behavior of the curvature of the substrate during the evolution; Equations corresponding to transition phase between the states he studied are not presented in his work. Ida and Miksis modeled the surfactant driven thin-film in [72] using the surface described by the mid height as the reference surface. This might also be considered as moving surface since the motion of the fluid is transferred to the reference surface. Unfortunately, in this case the motion of the reference does not influence the behavior of the thin-film. The most recent work in the domain is the work of Uwe Fermum, who in his PhD thesis [48] used the weak formulation to model surfactant driven thin-film flow on evolving surfaces. The rest of the chapter is organized as follow: We formulate the problem in Section 3.2. In Section 3.3 we introduce the differential geometry ingredients used and the basic tensor calculus needed. Finally, in Section 3.4, we derive the coupled surfactant and thin-film equations.

## 3.2 Problem setting

We consider a family of compact, smooth and oriented hypersurfaces  $\Gamma(t) \subset \mathbb{R}^n$  ( $n = 2, 3$ ) for  $t \in [0, t_{max}]$  generated by a flux function  $\Phi : [0, t_{max}] \times \Gamma_0 \rightarrow \mathbb{R}^n$  defined on a reference surface  $\Gamma_0 = \Gamma(0)$  with  $\Gamma(t) = \Phi(t, \Gamma_0)$ . We also assume our initial surface  $\Gamma_0$  to be at least  $C^5$  smooth and  $\Phi \in C^1([0, t_{max}], C^5(\Gamma_0))$ . We denote by  $\bar{v}_\Gamma = \partial_t \Phi$  the velocity of material points and assume its decomposition  $\bar{v}_\Gamma = \bar{v}_{\Gamma, \nu} \nu + \bar{v}_{\Gamma, tan}$  into a scalar velocity  $\bar{v}_{\Gamma, \nu}$  in the direction of the surface normal  $\nu$  and a tangential velocity  $\bar{v}_{\Gamma, tan}$ .

Let us consider a thin, viscous and incompressible liquid film bounded from below by the substrate  $\Gamma(t)$  and from above by the air as depicted in Figure 3.1. We assume the presence of an insoluble surfactant with concentration  $\bar{\Pi}$  at the free surface  $\bar{FS}$  (Fluid-Air interface) and the influence of a body force  $\bar{f}$  on the flow of the fluid. The body force  $\bar{f}$  models the sum of external forces such as gravity  $\bar{g}$  and Van der Waals forces among others. Of course the surface undergoes its movement while the fluid dynamics is taking place and the surfactant is spreading at the same time on the free surface. A typical example of such a setup is the modeling of the flow of a surfactant driven thin-film flow on the human lung. During the respiration phases (inspiration and expiration) the lung expands and compresses while the thin-film flows. The spreading of the surfactant on the thin-film helps to

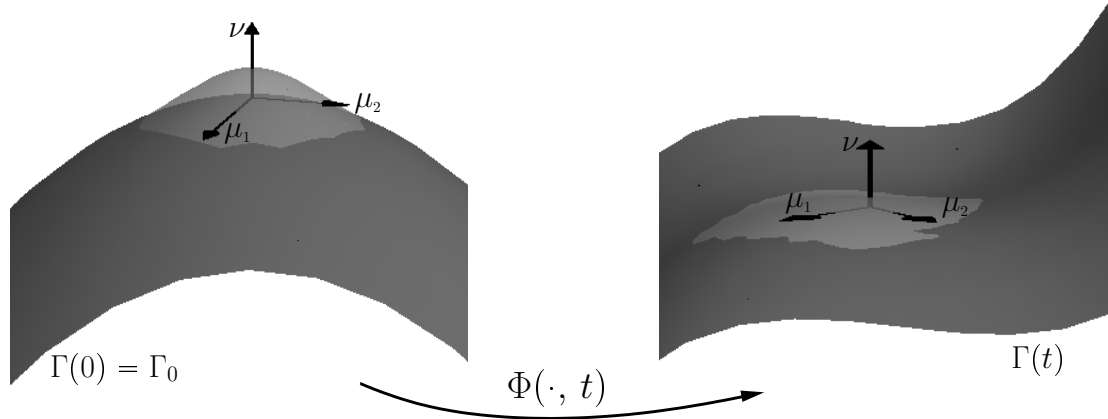


Figure 3.1: Representation of the substrate  $\Gamma$  at the time instants 0 (left) and  $t$  (right).

regularize the process. We refer to [66] for more information on this topic.

We model the evolution of the surfactant concentration by the time-dependant convection-diffusion equation

$$\frac{\partial \bar{\Pi}}{\partial t} + (\bar{\nabla}_{FS} \cdot (\bar{\Pi} \bar{v}_{FS})) = \bar{\nabla}_{FS} \cdot (\bar{D}_{FS} \bar{\nabla}_{FS} \bar{\Pi}) \quad \text{on the free surface } \bar{FS} \quad (3.7)$$

derived by Stone in [113]. Here  $\bar{\nabla}_{FS}$  represents the tangential nabla operator at the free surface and  $\bar{D}_{FS}$  the surface diffusivity tensor (matrix). The diffusivity tensor is often taken as  $\bar{D}_{FS} = \bar{c} \text{Id}$  where  $\bar{c}$  is a constant. This setup assumes an isotropic diffusion of the surfactant on the free surface but in general the diffusivity depends on the fluid viscosity, the fluid constituents and many other external factors. In that case, a full tensor  $\bar{D}_{FS}$  is the suitable way to model anisotropic behavior. Thus,  $\bar{D}_{FS}$  will be considered to be a full three dimensional elliptic tensor whose restriction to the free surface tangent bundle is the tangential operator incorporated in the model. Since the surfactant spreads only on the free surface, we close the system by imposing the Neumann boundary condition

$$(\bar{D}_{FS} \bar{\nabla}_{FS} \bar{\Pi}) \cdot n_{FS}^l = 0 \quad (3.8)$$

at the contact line (Substrate-Fluid-Air).  $n_{FS}^l$  represents the free surface outer unit conormal.

The flow of the thin-film at its turn is governed by the incompressible Navier-Stokes equations

$$\bar{\nabla} \cdot \bar{v}_{\mathcal{F}} = 0 \quad (3.9)$$

$$\mu \bar{\nabla} \cdot (\bar{\nabla} \bar{v}_{\mathcal{F}}) = \rho \frac{d\bar{v}_{\mathcal{F}}}{dt} + \bar{\nabla} \bar{P} - \bar{f}, \quad (3.10)$$

where  $\bar{v}_{\mathcal{F}}$  is the fluid particle velocity,  $\mu$  is the fluid viscosity,  $\rho$  is the fluid density,  $\bar{P}$  is the pressure and  $\bar{f}$  is the sum of body forces applied to a fluid particle as said above. We associate to these equations the following boundary conditions:

- a) On the substrate-fluid interface  $\Gamma(t)$ , we consider the no-penetration boundary condition  $(\bar{v}_{\mathcal{F}} - \bar{v}_{\Gamma}) \cdot \nu = 0$  and the friction slip condition  $\mu [\bar{T}_{\mathcal{F}} \nu]_{tan} = \bar{\beta} (\bar{v}_{\mathcal{F}} - \bar{v}_{\Gamma})$  where the slip tensor  $\bar{\beta}$  is a three dimensional elliptic tensor whose restriction to the substrate tangent bundle is the tangential tensor incorporated in the model [4, 84],  $\bar{T}_{\mathcal{F}} := (\bar{\nabla} \bar{v}_{\mathcal{F}} + (\bar{\nabla} \bar{v}_{\mathcal{F}})^{\top})$  is the stress tensor, and  $[\bar{T}_{\mathcal{F}} \nu]_{tan}$  is the tangential component of  $\bar{T}_{\mathcal{F}} \nu$ .



- b) On the fluid-air interface  $\overline{FS}$  (free surface), we consider the kinematic boundary condition which states that the fluid particles follow the free surface. We also impose that the shear stress on  $\overline{FS}$  is balanced by the free surface tangential gradient of the surface tension  $\bar{\gamma}$ ;  $\mu [\overline{T}_{\mathcal{F}\nu_{FS}}]_{FS,tan} = \overline{\nabla}_{FS}\bar{\gamma}$ . The index “ $FS,tan$ ” refers to the free surface tangent plane.
- c) Finally we consider the Laplace-Young law on  $\overline{FS}$  which states that the jump of the normal stress is proportional to the mean curvature of  $\overline{FS}$ , i.e.,  $[-(\bar{P} - \bar{P}_0)\nu_{FS} + \mu\overline{T}_{\mathcal{F}\nu_{FS}}] \cdot \nu_{FS} = \bar{\gamma}\bar{\mathcal{K}}_{FS}$  where  $\bar{P}_0$  is the ambient pressure (atmospheric pressure in the air phase) and  $\bar{\mathcal{K}}_{FS}$  the curvature of the free surface.

The problem is completely modeled by the knowledge of the equation of state which links the surface tension  $\bar{\gamma}$  and the surfactant concentration  $\bar{\Pi}$ . Many equations of states exist in the literature but the most popular is probably the nonlinear Langmuir equation of states [26, 83, 101, 127]

$$\bar{\gamma} = \bar{\gamma}_0 + RT_a \bar{\Pi}_{\infty} \ln(1 - \bar{\Pi}/\bar{\Pi}_{\infty}) \quad (3.11)$$

that we adopt here.  $\bar{\gamma}_0$  denotes the surface tension of a clean film ( $\bar{\Pi} = 0$ ),  $R$  the universal gas constant,  $T_a$  the absolute (Kelvin) temperature and  $\bar{\Pi}_{\infty}$  the surfactant concentration in the maximum packing limit.  $\bar{\Pi}_{\infty}$  exists because each molecule occupies a finite surface area and therefore limits the maximum possible surface concentration.

As usual, the mathematical study of the properties of a physical process needs first a nondimensionalization and a proper scaling of variables. In addition in the context of fluid mechanics, the choice of reference frames is very important. A good choice simplifies the work and facilitates the analysis of the problem. In our case, we will simultaneously use a laboratory frame and a moving frame attached to the substrate. In what follows, we will define the coordinate system, introduce the scaling procedure and present the essential parts of tensor theory needed for an appropriate description of this problem.

## 3.3 Geometry setting

### 3.3.1 Coordinate system

Let us consider a neighborhood  $\Omega_0 \subset \Gamma_0$  of a point  $P_0 \in \Gamma_0$  and follow the evolution of  $\Omega(\bar{t}) := \Phi(\bar{t}, \Omega_0)$ . We assume  $\Omega_0$  to be parameterized by  $\bar{X}(\bar{s}) = \bar{X}(0, \bar{s})$ ,  $\bar{s} = (\bar{s}_1, \bar{s}_2)$ , and consequently  $\bar{X}(\bar{t}, \bar{s}) := \Phi(\bar{t}, \bar{X}(\bar{s}))$  parameterizes  $\Omega(\bar{t})$ .  $(\Omega_0, \bar{X}(\bar{t}, \cdot))$  can be seen as a chart of an atlas describing the geometric properties of  $\Gamma(\bar{t})$ . We assume the basis  $(\mu_1(\bar{t}, \bar{s}), \mu_2(\bar{t}, \bar{s})) := \left( \frac{\partial \bar{X}(\bar{t}, \bar{s})}{\partial \bar{s}_1}, \frac{\partial \bar{X}(\bar{t}, \bar{s})}{\partial \bar{s}_2} \right)$  of the tangent plane at  $P(\bar{t}) := \Phi(\bar{t}, P_0)$  to be direct and we define  $\nu(\bar{t}, P(\bar{t})) = \nu(\bar{t}, \bar{s}) := \mu_1(\bar{t}, \bar{s}) \wedge \mu_2(\bar{t}, \bar{s}) / \|\mu_1(\bar{t}, \bar{s}) \wedge \mu_2(\bar{t}, \bar{s})\|$  the unit normal of  $\Gamma(\bar{t})$  at  $P(\bar{t})$ . So defined, we assume that during the entire process, lines normal to the substrate do not intersect within the film. This condition is fulfilled if and only if the matrix  $(\text{Id} - \bar{H}(\bar{t}, \bar{s})\bar{K}(\bar{t}, \bar{s}))$  is strictly positive definite;  $\bar{H}(\bar{t}, \bar{s})$  being the distance along  $\nu(\bar{t}, P(\bar{t}))$  from  $P(\bar{t})$  to the free surface and  $\bar{K}(\bar{t}, \bar{s})$  being the Weingarten map at  $P(\bar{t})$ . Then, it is clear that any fluid particle at the point  $M$  on the axis  $[P(\bar{t}), \nu(\bar{t}, P(\bar{t}))]$  can be uniquely represented by  $\bar{r}(\bar{t}, \bar{s}, \bar{y}) = \bar{X}(\bar{t}, \bar{s}) + \bar{y}\nu(\bar{t}, \bar{s})$ , where  $\bar{y} = \|\overline{P(\bar{t})M}\|$ , i.e.,  $0 \leq \bar{y} \leq \bar{H}(\bar{t}, \bar{s})$ . It therefore appears that the appropriate way to describe the dynamic of the above stated problem is to use a curvilinear coordinate system. Before we continue, let us mention here that the functions used in this chapter will be time and space dependent unless specified otherwise; thus we will be omitting variables whenever there is no possible misunderstanding.

**Definition 3.3.1** For  $t = 0$ , let  $\mathcal{N}_0 = \mathcal{N}(0) \subset \mathbb{R}^{n+1}$  be a small open neighborhood of  $\Gamma_0$  in which the lines normal to the substrate do not intersect and assume that this includes the domain  $\mathcal{F}$  occupied

by the fluid. The map

$$\begin{aligned} \mathcal{N}_0 &\longrightarrow \mathbb{R}^{n+1} \\ x &\longmapsto \nu(x) \text{ a unit vector normal to } \Gamma_0 \text{ such that} \\ &\quad \exists a \in \Gamma_0, \nu(x) \text{ is the normal to } \Gamma_0 \text{ at } a, \\ &\quad x = a + (\bar{x}\bar{a} \cdot \nu)\nu \text{ and } [x, a] \subset \mathcal{N}_0 \end{aligned}$$

is well defined. We also define  $\mathcal{N}(\bar{t}) := \{\bar{r}(\bar{t}, \bar{s}, \bar{y}) = \bar{X}(\bar{t}, \bar{s}) + \bar{y}\nu(\bar{t}, \bar{s}) / \bar{X}(0, \bar{s}) + \bar{y}\nu(0, \bar{s}) \in \mathcal{N}_0\}$  and assume that the lines normal to  $\Gamma(\bar{t})$  do not intersect within  $\mathcal{N}(\bar{t})$ . At each point  $M$  with coordinates  $\bar{r}(\bar{t}, \bar{s}, \bar{y}) = \bar{X}(\bar{t}, \bar{s}) + \bar{y}\nu(\bar{t}, \bar{s})$  we define the natural basis as follows

$$\begin{aligned} t_1(\bar{t}, \bar{s}, \bar{y}) &:= \frac{\partial \bar{r}}{\partial \bar{s}_1}(\bar{t}, \bar{s}, \bar{y}) = (\text{Id} - \bar{y}\bar{K}(\bar{t}, \bar{s}))\mu_1(\bar{t}, \bar{s}), \\ t_2(\bar{t}, \bar{s}, \bar{y}) &:= \frac{\partial \bar{r}}{\partial \bar{s}_2}(\bar{t}, \bar{s}, \bar{y}) = (\text{Id} - \bar{y}\bar{K}(\bar{t}, \bar{s}))\mu_2(\bar{t}, \bar{s}), \\ t_3(\bar{t}, \bar{s}, \bar{y}) &:= \frac{\partial \bar{r}}{\partial \bar{y}}(\bar{t}, \bar{s}, \bar{y}) = \nu(\bar{t}, \bar{s}). \end{aligned}$$

We recall that  $\nabla \nu(\bar{t}, \bar{s}) = -K(\bar{t}, \bar{s})$ .

### 3.3.2 Nondimensionalization/scaling and basic tensor calculus

In the context of thin-film flow, the representation of the fluid particle presents two characteristic lengths scales: a reference length  $\mathcal{L}$  measured along the substrate in the direction of the main flow and a reference thickness  $\mathcal{H}$  of the fluid above the substrate  $\Gamma(\bar{t})$ . We also scale the time by  $\mathcal{T}$ . The nondimensional variables are then related to their dimensional counterparts which are written with overbar by:

$\bar{s} = \mathcal{L}s$  where  $s = (s_1, s_2)$  (i.e.  $\bar{s}_1 = \mathcal{L}s_1$ ,  $\bar{s}_2 = \mathcal{L}s_2$ ),  $\bar{y} = \mathcal{H}y$ ,  $\bar{t} = \mathcal{T}t$ ,  $\bar{X}(\bar{t}, \bar{s}) = \mathcal{L}X(t, s)$ ,  $\bar{r}(\bar{t}, \bar{s}, \bar{y}) = \mathcal{L}r(t, s, y)$ . The last relation gives  $r(t, s, y) = X(t, s) + \epsilon y \nu(t, s)$  where  $\epsilon = \mathcal{H}/\mathcal{L}$  is assumed to be very small compared to 1 ( $\epsilon \ll 1$ ) and  $y$  becomes an  $\mathcal{O}(1)$  variable. We should emphasize that, so defined, the dimensional surface coordinates  $\bar{s}_1$  and  $\bar{s}_2$  must have the length's dimension, so that care should be taken when the natural parameterization involves an angle. For example, for a flow on a circular cylinder of radius  $R_a$ , a natural choice is  $\bar{s}_1 = \theta$ , the cylindrical polar coordinate, but the correct dimensional coordinate is the arc-length  $\bar{s}_1 = R_a\theta$ .

These definitions lead to  $\frac{\partial \bar{X}}{\partial \bar{s}_1} = \frac{\partial X}{\partial s_1}$  and  $\frac{\partial \bar{X}}{\partial \bar{s}_2} = \frac{\partial X}{\partial s_2}$ . With a slight misuse of notation, we define  $\mu_1(t, s) := \frac{\partial X}{\partial s_1}$  and  $\mu_2(t, s) := \frac{\partial X}{\partial s_2}$ . According to the context, one will distinguish them from  $\mu_1(\bar{t}, \bar{s}) := \frac{\partial \bar{X}}{\partial \bar{s}_1}$  and  $\mu_2(\bar{t}, \bar{s}) := \frac{\partial \bar{X}}{\partial \bar{s}_2}$ . We can nevertheless notice that  $\mu_1(\bar{t}, \bar{s}) = \mu_1(t, s)$  and  $\mu_2(\bar{t}, \bar{s}) = \mu_2(t, s)$ ; thus  $\nu(\bar{t}, \bar{s}) = \nu(t, s)$ .

Again, with a slight misuse of notation, we define the corresponding curvilinear coordinate system to the nondimensional flow as follow:

$$\begin{aligned} t_1(t, s, y) &:= \frac{\partial r}{\partial s_1}(t, s, y) = (\text{Id} - \epsilon y K(t, s))\mu_1(t, s) \\ t_2(t, s, y) &:= \frac{\partial r}{\partial s_2}(t, s, y) = (\text{Id} - \epsilon y K(t, s))\mu_2(t, s) \\ t_3(t, s, y) &:= \frac{\partial r}{\partial y}(t, s, y) = \epsilon \nu(t, s), \end{aligned}$$

where  $K$  is the nondimensional Weingarten map at  $P(t)$ . From the definition of the shape operator (Weingarten map), it is easy to see that  $\bar{K} = (1/\mathcal{L})K$ . This remark allows us to see that

$$\begin{aligned} t_1(\bar{t}, \bar{s}, \bar{y}) &= t_1(t, s, y) \\ t_2(\bar{t}, \bar{s}, \bar{y}) &= t_2(t, s, y) \end{aligned}$$

With a misuse of notation, we define the dual basis of the basis  $(\mu_1(\bar{t}, \bar{s}), \mu_2(\bar{t}, \bar{s}), \nu(\bar{t}, \bar{s}))$ ,  $(\mu_1(t, s), \mu_2(t, s), \nu(t, s))$ ,  $(t_1(\bar{t}, \bar{s}, \bar{y}), t_2(\bar{t}, \bar{s}, \bar{y}), t_3(\bar{t}, \bar{s}, \bar{y}))$ ,  $(t_1(t, s, y), t_2(t, s, y), t_3(t, s, y))$  respectively by  $(\mu^1(\bar{t}, \bar{s}), \mu^2(\bar{t}, \bar{s}), \nu(\bar{t}, \bar{s}))$ ,  $(\mu^1(t, s), \mu^2(t, s), \nu(t, s))$ ,  $(t^1(\bar{t}, \bar{s}, \bar{y}), t^2(\bar{t}, \bar{s}, \bar{y}), t^3(\bar{t}, \bar{s}, \bar{y}))$ ,  $(t^1(t, s, y), t^2(t, s, y), t^3(t, s, y))$  such that

$$\mu^i(\bar{t}, \bar{s}) \cdot \mu_j(\bar{t}, \bar{s}) = \delta_j^i, \quad \mu^i(t, s) \cdot \mu_j(t, s) = \delta_j^i, \quad (i, j = 1, 2)$$

$$\text{and} \quad t^i(\bar{t}, \bar{s}, \bar{y}) \cdot t_j(\bar{t}, \bar{s}, \bar{y}) = \delta_j^i, \quad t^i(t, s, y) \cdot t_j(t, s, y) = \delta_j^i, \quad (i, j = 1, 2, 3).$$

$\delta_j^i$  is the Kronecker-Delta symbol, i.e.,  $\delta_j^i = 1$  if  $i = j$  and 0 in other cases. It is clear that

$$(\mu^1(\bar{t}, \bar{s}), \mu^2(\bar{t}, \bar{s}), \nu(\bar{t}, \bar{s})) = (\mu^1(t, s), \mu^2(t, s), \nu(t, s)).$$

Let us define

$$R_y(t, s, y) = (\text{Id} - \epsilon y K(t, s))^{-1}, \quad (3.12)$$

$$\begin{aligned} \text{then} \quad (t^1(\bar{t}, \bar{s}, \bar{y}), t^2(\bar{t}, \bar{s}, \bar{y}), t^3(\bar{t}, \bar{s}, \bar{y})) &= (t^1(t, s, y), t^2(t, s, y), (1/\epsilon)\nu(t, s)) \\ &= (R_y(t, s, y)\mu^1(t, s), R_y(t, s, y)\mu^2(t, s), (1/\epsilon)\nu(t, s)). \end{aligned}$$

We refer to Figure 3.2 for the illustration of these vectors.

**Definition 3.3.2** *Let us call  $(e_1, e_2, e_3)$  the canonical basis of  $\mathbb{R}^3$ . For any scalar function  $\eta$ , defined on  $\mathcal{N}(\bar{t})$ , we define its nonscaled gradient by*

$$\bar{\nabla}\eta := \frac{\partial\eta}{\partial x_1}e_1 + \frac{\partial\eta}{\partial x_2}e_2 + \frac{\partial\eta}{\partial x_3}e_3 = \frac{\partial\eta}{\partial \bar{s}_1}t^1 + \frac{\partial\eta}{\partial \bar{s}_2}t^2 + \frac{\partial\eta}{\partial \bar{y}}\nu. \quad (3.13)$$

Let us call  $\Gamma_{\Omega}(\bar{y}, \bar{t})$  the parallel surface to  $\Omega(\bar{t})$  that intersects the axis  $(P(\bar{t}), \nu(\bar{s}_1, \bar{s}_2, \bar{t}))$  at  $M$ . The dimensional tangential gradients to  $\Gamma(t)$  and  $\Gamma_{\Omega}(\bar{y}, \bar{t})$  are respectively given by:

$$\bar{\nabla}_{\Gamma}\eta := \frac{\partial\eta}{\partial \bar{s}_1}\mu^1 + \frac{\partial\eta}{\partial \bar{s}_2}\mu^2 \quad (3.14)$$

$$\text{and} \quad \bar{\nabla}_{\Gamma_{\Omega}(\bar{y}, \bar{t})}\eta := \frac{\partial\eta}{\partial \bar{s}_1}t^1 + \frac{\partial\eta}{\partial \bar{s}_2}t^2. \quad (3.15)$$

In the same way, we define the nondimensional gradient by

$$\nabla\eta := \frac{\partial\eta}{\partial s_1}t^1 + \frac{\partial\eta}{\partial s_2}t^2 + \frac{\partial\eta}{\partial y}t^3 \quad (3.16)$$

and the nondimensional surface gradients by

$$\nabla_{\Gamma}\eta := \frac{\partial\eta}{\partial s_1}\mu^1 + \frac{\partial\eta}{\partial s_2}\mu^2 \quad (3.17)$$

$$\text{and} \quad \nabla_{\Gamma_{\Omega}(y, \bar{t})}\eta := \frac{\partial\eta}{\partial s_1}t^1 + \frac{\partial\eta}{\partial s_2}t^2. \quad (3.18)$$

(3.12), (3.13) to (3.18) give the following relation to the above defined operator:

$$\begin{aligned} \bar{\nabla}_{\Gamma_{\Omega}(\bar{y}, \bar{t})}\eta &= \frac{1}{\mathcal{L}}\nabla_{\Gamma_{\Omega}(y, \bar{t})}\eta = \frac{1}{\mathcal{L}}R_y\nabla_{\Gamma}\eta \\ \bar{\nabla}\eta &= \frac{1}{\mathcal{L}}R_y\nabla_{\Gamma}\eta + \frac{1}{\epsilon\mathcal{L}}\frac{\partial\eta}{\partial y}\nu \end{aligned}$$

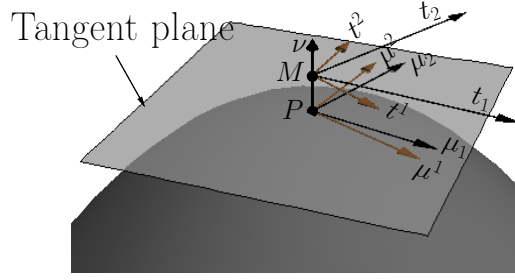


Figure 3.2: Representation of natural basis  $(\mu_1, \mu_2)$ ,  $(t_1, t_2)$ , and the corresponding dual basis  $(\mu^1, \mu^2)$ ,  $(t^1, t^2)$ , at  $P$  and  $M$  at time  $t$ .

We wish to define the gradient of a vector field in the natural coordinate.

**Definition 3.3.3** Let us consider a vector field  $\zeta = \zeta_{tan} + \zeta_\nu \nu$  defined on  $\mathcal{N}(\bar{t})$ , where  $\zeta_\nu = \zeta \cdot \nu$ . The nonscaled gradient of  $\zeta$  is the three dimensional second order tensor

$$\bar{\nabla} \zeta := \sum_{i=1}^2 \frac{\partial \zeta}{\partial \bar{s}_i} \otimes t^i + \frac{\partial \zeta}{\partial \bar{y}} \otimes \nu \quad (3.19)$$

and the nonscaled surface gradient is defined by

$$\bar{\nabla}_r \zeta := \sum_{i=1}^2 \frac{\partial \zeta_{tan}}{\partial \bar{s}_i} \otimes \mu^i - \sum_{i=1}^2 \left( \frac{\partial \zeta_{tan}}{\partial \bar{s}_i} \cdot \nu \right) \nu \otimes \mu^i + \sum_{i=1}^2 \zeta_\nu \frac{\partial \nu}{\partial \bar{s}_i} \otimes \mu^i. \quad (3.20)$$

Their scale counterparts read

$$\nabla \zeta = \sum_{i=1}^2 \frac{\partial \zeta}{\partial s_i} \otimes t^i + \frac{1}{\epsilon} \frac{\partial \zeta}{\partial y} \otimes \nu, \quad (3.21)$$

$$\text{and } \nabla_r \zeta = \sum_{i=1}^2 \frac{\partial \zeta_{tan}}{\partial s_i} \otimes \mu^i - \sum_{i=1}^2 \left( \frac{\partial \zeta_{tan}}{\partial s_i} \cdot \nu \right) \nu \otimes \mu^i + \sum_{i=1}^2 \zeta_\nu \frac{\partial \nu}{\partial s_i} \otimes \mu^i, \quad (3.22)$$

respectively.

**Note 3.3.4** It can be noticed that these definitions give the surface derivative tensor of  $\zeta$ . Some authors [14] explicitly write

$$\bar{\nabla}_r \zeta = (\text{Id} - \nu \otimes \nu) \bar{\nabla} \zeta (\text{Id} - \nu \otimes \nu)$$

for the nonscaled tangential gradient and

$$\nabla_r \zeta = (\text{Id} - \nu \otimes \nu) \nabla \zeta (\text{Id} - \nu \otimes \nu)$$

for the scaled tangential gradient. Since our function is defined not just on the surface  $\Gamma$  (as it is the case in [14]), but in a small domain around the surface, this definition can lead to some confusion while computing the tangential gradient at a point which isn't on the surface. We therefore prefer the full tensorial expression.

**Lemma 3.3.5** For a given vector field  $\zeta = \zeta_{tan} + \zeta_\nu \nu$  defined on  $\mathcal{N}(\bar{t})$  ( $\zeta_\nu = \zeta \cdot \nu$ ); we have

$$a) \quad \bar{\nabla}_r \zeta = \frac{1}{\mathcal{L}} \nabla_r \zeta \quad (3.23)$$

b) The nonscaled gradient can be expressed as

$$\begin{aligned}\bar{\nabla}\zeta &= \bar{\nabla}_{\Gamma\zeta_{tan}}R_{\bar{y}} + \nu \otimes R_{\bar{y}}\bar{\nabla}_{\Gamma}\zeta_{\nu} + \frac{\partial\zeta_{tan}}{\partial\bar{y}} \otimes \nu \\ &+ \frac{\partial\zeta_{\nu}}{\partial\bar{y}}\nu \otimes \nu + \nu \otimes R_{\bar{y}}\bar{K}\zeta_{tan} - \zeta_{\nu}\bar{K}R_{\bar{y}}.\end{aligned}\quad (3.24)$$

c) The nonscaled gradient is expressed in terms of tangential gradient operator as follows

$$\begin{aligned}\bar{\nabla}\zeta &= \frac{1}{\mathcal{L}}\nabla_{\Gamma}\zeta_{tan}R_y + \frac{1}{\mathcal{L}}\nu \otimes R_y\nabla_{\Gamma}\zeta_{\nu} + \frac{1}{\mathcal{L}\epsilon}\frac{\partial\zeta_{tan}}{\partial y} \otimes \nu \\ &+ \frac{1}{\mathcal{L}\epsilon}\frac{\partial\zeta_{\nu}}{\partial y}\nu \otimes \nu + \frac{1}{\mathcal{L}}\nu \otimes R_yK\zeta_{tan} - \frac{1}{\mathcal{L}}\zeta_{\nu}KR_y,\end{aligned}\quad (3.25)$$

where  $R_{\bar{y}} = R(\bar{t}, \bar{s}, \bar{y}) = (\text{Id} - \bar{y}\bar{K}(\bar{t}, \bar{s}))^{-1}$  and  $R_y = R(t, s, y) = (\text{Id} - \epsilon yK(t, s, y))^{-1}$ .

We will now generalize the above results to a general three dimensional second order tensor.

**Definition 3.3.6** Considering a second order tensor

$$T = \sum_{i,j=1}^3 T^{ij}t_i \otimes t_j,$$

the tangential component of  $T$  is the surface tensor given by

$$T_{tan} = \sum_{i,j=1}^2 T^{ij}t_i \otimes t_j.$$

We use the terms nonscaled and scaled tangential gradient of  $T$ , respectively, to denote the third order surface tensors

$$\begin{aligned}\bar{\nabla}_{\Gamma}T &= \sum_{k=1}^2 \sum_{i,j=1}^2 t_i \otimes t_j \otimes t^j \bar{\otimes} t^i \bar{\otimes} \frac{\partial T}{\partial \bar{s}_k} \otimes \mu^k \\ \text{and } \nabla_{\Gamma}T &= \sum_{k=1}^2 \sum_{i,j=1}^2 t_i \otimes t_j \otimes t^j \otimes t^i \otimes \frac{\partial T}{\partial s_k} \otimes \mu^k.\end{aligned}$$

**Remark 3.3.7** The nonscaled and scaled tangential gradient are merely the tangential component of the surface gradient  $\sum_{k=1}^2 \frac{\partial T}{\partial \bar{s}_k} \otimes \mu^k$  and  $\sum_{k=1}^2 \frac{\partial T}{\partial s_k} \otimes \mu^k$ , respectively.

**Lemma 3.3.8** Considering a second order tensor

$$T = \sum_{i,j=1}^3 T^{ij}t_i \otimes t_j,$$

the expressions of the nonscaled and scaled tangential gradient of  $T$  are

$$\begin{aligned}\bar{\nabla}_{\Gamma}T &= \sum_{k=1}^2 \frac{\partial T_{tan}}{\partial \bar{s}_k} \otimes \mu^k - \sum_{i=1}^2 \nu \otimes [T_{tan}^{\top} t^i] \otimes \bar{K}t_i - \sum_{j=1}^2 [T_{tan}t^j] \otimes \nu \otimes \bar{K}t_j - (T\nu)_{tan} \otimes \bar{K} \\ &- \sum_{k=1}^2 \bar{K}\mu_k \otimes (T^{\top}\nu)_{tan} \otimes \mu^k\end{aligned}\quad (3.26)$$

and

$$\begin{aligned}\nabla_r T &= \sum_{k=1}^2 \frac{\partial T_{tan}}{\partial \bar{s}_k} \otimes \mu^k - \sum_{i=1}^2 \nu \otimes [T_{tan}^\top t^i] \otimes K t_i - \sum_{j=1}^2 [T_{tan} t^j] \otimes \nu \otimes K t_j - (T\nu)_{tan} \otimes K \\ &- \sum_{k=1}^2 K \mu_k \otimes (T^\top \nu)_{tan} \otimes \mu^k,\end{aligned}\quad (3.27)$$

respectively. We also have the following relation

$$\bar{\nabla}_r T = \frac{1}{\mathcal{L}} \nabla_r T. \quad (3.28)$$

**Proof** In fact

$$\begin{aligned}\sum_{k=1}^2 \frac{\partial T}{\partial \bar{s}_k} \otimes \mu^k &= \sum_{k=1}^2 \frac{\partial T_{tan}}{\partial \bar{s}_k} \otimes \mu^k + \sum_{k=1}^2 \sum_{i=1}^2 \frac{\partial (T^{i3} t_i \otimes \nu)}{\partial \bar{s}_k} \otimes \mu^k + \sum_{k=1}^2 \sum_{j=1}^2 \frac{\partial (T^{3j} \nu \otimes t_j)}{\partial \bar{s}_k} \otimes \mu^k \\ &+ \sum_{k=1}^2 \frac{\partial (T^{33} \nu \otimes \nu)}{\partial \bar{s}_k} \otimes \mu^k,\end{aligned}$$

$$\begin{aligned}\sum_{k=1}^2 \frac{\partial T_{tan}}{\partial \bar{s}_k} \otimes \mu^k &= \sum_{k=1}^2 \sum_{i,j=1}^2 \frac{\partial (T^{ij} t_i \otimes t_j)}{\partial \bar{s}_k} \otimes \mu^k - \sum_{k=1}^2 \sum_{i,j=1}^2 T^{ij} \left( \frac{\partial t_i}{\partial \bar{s}_k} \cdot \nu \right) \nu \otimes t_j \otimes \mu^k \\ &- \sum_{k=1}^2 \sum_{i,j=1}^2 T^{ij} \left( \frac{\partial t_j}{\partial \bar{s}_k} \cdot \nu \right) t_i \otimes \nu \otimes \mu^k + \sum_{k=1}^2 \sum_{i,j=1}^2 T^{ij} \left( \frac{\partial t_i}{\partial \bar{s}_k} \cdot \nu \right) \nu \otimes t_j \otimes \mu^k \\ &+ \sum_{k=1}^2 \sum_{i,j=1}^2 T^{ij} \left( \frac{\partial t_j}{\partial \bar{s}_k} \cdot \nu \right) t_i \otimes \nu \otimes \mu^k.\end{aligned}$$

Using the fact that  $\frac{\partial t_i}{\partial \bar{s}_i} \cdot \nu = t_i \cdot (\bar{K} \mu_i)$ , we obtain the following:

$$\begin{aligned}\sum_{k=1}^2 \sum_{i,j=1}^2 t_i \otimes t_j \otimes t^j \bar{\otimes} t^i \bar{\otimes} \frac{\partial T_{tan}}{\partial \bar{s}_k} \otimes \mu^k &= \sum_{k=1}^2 \frac{\partial T_{tan}}{\partial \bar{s}_k} \otimes \mu^k - \sum_{i=1}^2 \nu \otimes [T_{tan}^\top t^i] \otimes \bar{K} t_i \\ &- \sum_{j=1}^2 [T_{tan} t^j] \otimes \nu \otimes \bar{K} t_j.\end{aligned}$$

A direct application of derivation formulae gives

$$\begin{aligned}\sum_{l,m=1}^2 \sum_{k=1}^2 \sum_{i=1}^2 t_l \otimes t_m \otimes t^m \bar{\otimes} t^l \bar{\otimes} \frac{\partial (T^{i3} t_i \otimes \nu)}{\partial \bar{s}_k} \otimes \mu^k &= - (T\nu)_{tan} \otimes \bar{K}, \\ \sum_{l,m=1}^2 \sum_{k=1}^2 \sum_{j=1}^2 t_l \otimes t_m \otimes t^m \bar{\otimes} t^l \bar{\otimes} \frac{\partial (T^{3j} \nu \otimes t_j)}{\partial \bar{s}_k} \otimes \mu^k &= - \sum_{k=1}^2 \bar{K} \mu_k \otimes (T^\top \nu)_{tan} \otimes \mu^k,\end{aligned}$$

$$\text{and} \quad \sum_{k=1}^2 t_i \otimes t_j \otimes t^j \bar{\otimes} t^i \bar{\otimes} \frac{\partial (T^{33} \nu \otimes \nu)}{\partial \bar{s}_k} \otimes \mu^k = 0$$

(3.26) is obtained by adding up the equations above. (3.27) is obtained analogously and by replacing the derivative expressions in (3.26) with their equivalents involving derivative expression in (3.27), one easily obtains the relation (3.28).

□

**Theorem 3.3.9** *Considering a second order tensor*

$$T = \sum_{i,j=1}^3 T^{ij} t_i \otimes t_j$$

the expression of the nonscaled gradient of  $T$  is given in terms of the nonscaled and scaled variables as follows

$$\begin{aligned} \bar{\nabla} T &= \bar{\nabla}_\Gamma T_{tan} \bar{\otimes} R_{\bar{y}} + \sum_{i=1}^2 \nu \otimes [T_{tan}^\top t^i] \otimes \mu_i \bar{\otimes} \bar{K} + \sum_{j=1}^2 [T_{tan} t^j] \otimes \nu \otimes \mu_j \bar{\otimes} \bar{K} \\ &+ \sum_{k=1}^2 \frac{\partial (T\nu)_{tan}}{\partial \bar{s}_k} \otimes \nu \otimes t^k - (T\nu)_{tan} \otimes R_{\bar{y}} \bar{K} - \sum_{k=1}^2 \bar{K} \mu_k \otimes (T^\top \nu)_{tan} \otimes t^k \\ &+ \nu \otimes [\bar{\nabla}_\Gamma (T^\top \nu)_{tan}] R_{\bar{y}} + \nu \otimes \nu \otimes R_{\bar{y}} \bar{K} (T^\top \nu) + \nu \otimes \nu \otimes R_{\bar{y}} \bar{\nabla}_\Gamma [(T\nu) \cdot \nu] \\ &- \sum_{k=1}^2 [(T\nu) \cdot \nu] \bar{K} \mu_k \otimes \nu \otimes t^k - [(T\nu) \cdot \nu] \nu \otimes R_{\bar{y}} \bar{K} + \sum_{j=1}^2 \frac{\partial (T(t^j))_{tan}}{\partial \bar{y}} \otimes t_j \otimes \nu \\ &- \sum_{j=1}^2 (T(t^j))_{tan} \otimes \bar{K} \mu_j \otimes \nu + \frac{\partial (T\nu)_{tan}}{\partial \bar{y}} \otimes \nu \otimes \nu + \nu \otimes \frac{\partial (T^\top(\nu))_{tan}}{\partial \bar{y}} \otimes \nu \\ &+ \frac{\partial ((T\nu) \cdot \nu)}{\partial \bar{y}} \nu \otimes \nu \otimes \nu \end{aligned}$$

and

$$\begin{aligned} \bar{\nabla} T &= \frac{1}{\mathcal{L}} \bar{\nabla}_\Gamma T_{tan} \bar{\otimes} R_y + \frac{1}{\mathcal{L}} \sum_{i=1}^2 \nu \otimes [T_{tan}^\top t^i] \otimes \mu_i \bar{\otimes} K + \frac{1}{\mathcal{L}} \sum_{j=1}^2 [T_{tan} t^j] \otimes \nu \otimes \mu_j \bar{\otimes} K \\ &+ \frac{1}{\mathcal{L}} \sum_{k=1}^2 \frac{\partial (T\nu)_{tan}}{\partial s_k} \otimes \nu \otimes t^k - \frac{1}{\mathcal{L}} (T\nu)_{tan} \otimes R_y K - \frac{1}{\mathcal{L}} \sum_{k=1}^2 K \mu_k \otimes (T^\top \nu)_{tan} \otimes t^k \\ &+ \frac{1}{\mathcal{L}} \nu \otimes [\bar{\nabla}_\Gamma (T^\top \nu)_{tan}] R_y + \frac{1}{\mathcal{L}} \nu \otimes \nu \otimes R_y K (T^\top \nu) + \frac{1}{\mathcal{L}} \nu \otimes \nu \otimes R_y \bar{\nabla}_\Gamma [(T\nu) \cdot \nu] \\ &- \frac{1}{\mathcal{L}} \sum_{k=1}^2 [(T\nu) \cdot \nu] K \mu_k \otimes \nu \otimes t^k - \frac{1}{\mathcal{L}} [(T\nu) \cdot \nu] \nu \otimes R_y K \\ &+ \frac{1}{\epsilon \mathcal{L}} \sum_{j=1}^2 \frac{\partial (T(t^j))_{tan}}{\partial y} \otimes t_j \otimes \nu - \frac{1}{\mathcal{L}} \sum_{j=1}^2 (T(t^j))_{tan} \otimes K \mu_j \otimes \nu \\ &+ \frac{1}{\epsilon \mathcal{L}} \frac{\partial (T\nu)_{tan}}{\partial y} \otimes \nu \otimes \nu + \frac{1}{\epsilon \mathcal{L}} \nu \otimes \frac{\partial (T^\top(\nu))_{tan}}{\partial y} \otimes \nu \\ &+ \frac{1}{\epsilon \mathcal{L}} \frac{\partial ((T\nu) \cdot \nu)}{\partial y} \nu \otimes \nu \otimes \nu, \end{aligned}$$

where the index “tan” is meant for the tangential component.

The proof of this theorem is straightforward.

We will now give the definition of divergence in terms of tensor contraction.

**Definition 3.3.10** *The second order identity tensor in  $\mathbb{R}^3$  is defined by*

$$G = \sum_{i,j=1}^3 (t_i \cdot t_j) t^i \otimes t^j = \sum_{i,j=1}^3 (t^i \cdot t^j) t_i \otimes t_j = \sum_{i=1}^3 t_i \otimes t^i = \sum_{i=1}^3 t^i \otimes t_i$$

Considering a first or second order tensor  $T$ , the nonscaled divergence of  $T$  is its trace given by

$$\bar{\nabla} \cdot T = \bar{\nabla} T \bar{\otimes} G.$$

and the tangential divergence by

$$\bar{\nabla}_\Gamma \cdot T = \bar{\nabla}_\Gamma T \bar{\otimes} G.$$

**Theorem 3.3.11** (Divergence of tensors)

Let us consider a vector field  $\zeta$  (first order tensor)

$$\zeta = \sum_{i=1}^3 \zeta^i t_i = \zeta_{tan} + \zeta_\nu \nu \quad (\zeta_\nu = \zeta \cdot \nu).$$

The divergence of  $\zeta$  is given in terms of nonscaled and scaled variables by

$$\begin{aligned} \bar{\nabla} \cdot \zeta &= \bar{\nabla}_\Gamma \zeta_{tan} R_{\bar{y}} \bar{\otimes} G - \zeta_\nu \bar{K} R_{\bar{y}} \bar{\otimes} G + \frac{\partial \zeta_\nu}{\partial \bar{y}}, \\ \bar{\nabla} \cdot \zeta &= \frac{1}{\mathcal{L}} \bar{\nabla}_\Gamma \zeta_{tan} R_{\bar{y}} \bar{\otimes} G - \frac{1}{\mathcal{L}} \zeta_\nu K R_{\bar{y}} \bar{\otimes} G + \frac{1}{\epsilon \mathcal{L}} \frac{\partial \zeta_\nu}{\partial y}. \end{aligned} \quad (3.29)$$

Considering a second order tensor

$$T = \sum_{i,j=1}^3 T^{ij} t_i \otimes t_j,$$

the divergence of  $T$  is given in terms of nonscaled and scaled variables by

$$\begin{aligned} \bar{\nabla} \cdot T &= (\bar{\nabla}_\Gamma T_{tan} \bar{\otimes} R_{\bar{y}}) \bar{\otimes} G + \sum_{i=1}^2 \nu \otimes [T_{tan}^\top t^i] \otimes \bar{K} (\mu_i) \bar{\otimes} G - (T\nu)_{tan} \otimes R_{\bar{y}} \bar{K} \bar{\otimes} G \\ &\quad - \sum_{k=1}^2 \bar{K} \mu_k ((T^\top \nu)_{tan} \cdot t^k) + \nu \otimes [\bar{\nabla}_\Gamma (T^\top \nu)_{tan}] R_{\bar{y}} \bar{\otimes} G \\ &\quad - [(T\nu) \cdot \nu] \nu \otimes R_{\bar{y}} \bar{K} \bar{\otimes} G + \frac{\partial (T\nu)_{tan}}{\partial \bar{y}} + \frac{\partial ((T\nu) \cdot \nu)}{\partial \bar{y}} \nu \end{aligned}$$

and

$$\begin{aligned} \bar{\nabla} \cdot T &= \frac{1}{\mathcal{L}} \left( (\bar{\nabla}_\Gamma T_{tan} \bar{\otimes} R_{\bar{y}}) \bar{\otimes} G + \sum_{i=1}^2 \nu \otimes [T_{tan}^\top t^i] \otimes K (\mu_i) \bar{\otimes} G - (T\nu)_{tan} \otimes R_{\bar{y}} K \bar{\otimes} G \right) \\ &\quad - \frac{1}{\mathcal{L}} \left( \sum_{k=1}^2 K \mu_k ((T^\top \nu)_{tan} \cdot t^k) - \nu \otimes [\bar{\nabla}_\Gamma (T^\top \nu)_{tan}] R_{\bar{y}} \bar{\otimes} G \right) \\ &\quad - \frac{1}{\mathcal{L}} [(T\nu) \cdot \nu] \nu \otimes R_{\bar{y}} K \bar{\otimes} G + \frac{1}{\epsilon \mathcal{L}} \left( \frac{\partial (T\nu)_{tan}}{\partial y} + \frac{\partial ((T\nu) \cdot \nu)}{\partial y} \nu \right) \end{aligned}$$

The Laplacian of a vector field is given in terms of nonscaled and scaled variables by

$$\begin{aligned} \bar{\nabla} \cdot (\bar{\nabla} \zeta) &= (\bar{\nabla}_\Gamma (\bar{\nabla}_\Gamma \zeta_{tan} R_{\bar{y}}) \bar{\otimes} R_{\bar{y}}) \bar{\otimes} G + \nu (\text{tr} [\bar{\nabla}_\Gamma \zeta_{tan} \bar{K} R_{\bar{y}}^2]) - \bar{K} [R_{\bar{y}}^2 (\bar{\nabla}_\Gamma \zeta_\nu)] \\ &\quad + \nu \text{tr} ([\bar{\nabla}_\Gamma (R_{\bar{y}} \bar{\nabla}_\Gamma \zeta_\nu)] R_{\bar{y}}) - \frac{\partial \zeta_{tan}}{\partial \bar{y}} \text{tr} (R_{\bar{y}} \bar{K}) - \text{tr} (R_{\bar{y}} \bar{K}) \left[ \frac{\partial \zeta_\nu}{\partial \bar{y}} \right] \nu \\ &\quad + \frac{\partial^2 \zeta_{tan}}{\partial \bar{y}^2} + \frac{\partial^2 \zeta_\nu}{\partial \bar{y}^2} \nu - (R_{\bar{y}}^2 \bar{K}^2 \zeta_{tan}) + \nu \text{tr} ([\bar{\nabla}_\Gamma (R_{\bar{y}} \bar{K} \zeta_{tan})] R_{\bar{y}}) \\ &\quad - \bar{\nabla}_\Gamma (\zeta_\nu \bar{K} R_{\bar{y}}) \bar{\otimes} R_{\bar{y}} \bar{\otimes} G - \nu \zeta_\nu \text{tr} (\bar{K}^2 R_{\bar{y}}^2) \end{aligned}$$



and

$$\begin{aligned}
 \bar{\nabla} \cdot (\bar{\nabla} \zeta) &= \frac{1}{\mathcal{L}^2} \left( (\nabla_\Gamma (\nabla_\Gamma \zeta_{tan} R_y) \bar{\otimes} R_y) \bar{\otimes} G + \nu \left( \text{tr} [\nabla_\Gamma \zeta_{tan} K R_y^2] \right) - K [R_y^2 (\nabla_\Gamma \zeta_\nu)] \right) \\
 &+ \nu \frac{1}{\mathcal{L}^2} \text{tr} ([\nabla_\Gamma (R_y \nabla_\Gamma \zeta_\nu)] R_y) - \frac{1}{\epsilon \mathcal{L}^2} \frac{\partial \zeta_{tan}}{\partial y} \text{tr} (R_y K) - \frac{1}{\epsilon \mathcal{L}^2} \text{tr} (R_y K) \left[ \frac{\partial \zeta_\nu}{\partial y} \right] \nu \\
 &+ \frac{1}{\epsilon^2 \mathcal{L}^2} \left( \frac{\partial^2 \zeta_{tan}}{\partial y^2} + \frac{\partial^2 \zeta_\nu}{\partial y^2} \nu \right) - \frac{1}{\mathcal{L}^2} (R_y^2 K^2 \zeta_{tan}) + \nu \frac{1}{\mathcal{L}^2} \text{tr} ([\nabla_\Gamma (R_y K \zeta_{tan})] R_y) \\
 &- \frac{1}{\mathcal{L}^2} \nabla_\Gamma (\zeta_\nu K R_y) \bar{\otimes} R_y \bar{\otimes} G - \nu \frac{1}{\mathcal{L}^2} \zeta_\nu \text{tr} (K^2 R_y^2).
 \end{aligned}$$

We finally wish to give some important results which will help us to simplify the thin-film problem presented in ((3.7) – (3.11)).

**Lemma 3.3.12** (*Divergence of a tangential vector under the integral sign*)

Let  $\bar{\zeta} = \sum_{i=1}^2 \bar{\zeta}^i t_i = \sum_{i=1}^2 \bar{\zeta}^i (\text{Id} - \bar{y} \bar{K}) \mu_i$  be a tangential vector field defined in  $\mathcal{N}(t)$  and consider the real functions  $\bar{f}$  and  $\bar{g}$  defined on  $\Gamma(t)$  which are assumed to be sufficiently smooth. Then

$$\bar{\nabla}_\Gamma \cdot \int_{\bar{f}(P)}^{\bar{g}(P)} \bar{\zeta} d\bar{y} = \int_{\bar{f}(P)}^{\bar{g}(P)} \bar{\nabla}_\Gamma \cdot \bar{\zeta} d\bar{y} + \bar{\zeta}(\bar{g}(P)) \cdot \bar{\nabla}_\Gamma \bar{g}(P) - \bar{\zeta}(\bar{f}(P)) \cdot \bar{\nabla}_\Gamma \bar{f}(P) \quad (3.30)$$

**Proof** We have,

$$\int_{\bar{f}(P)}^{\bar{g}(P)} \bar{\zeta} d\bar{y} = \sum_{i=1}^2 \int_{\bar{f}(P)}^{\bar{g}(P)} \bar{\zeta}^i d\bar{y} \mu_i - \sum_{i=1}^2 \int_{\bar{f}(P)}^{\bar{g}(P)} \bar{y} \bar{\zeta}^i d\bar{y} \bar{K} \mu_i$$

and therefore

$$\begin{aligned}
 \bar{\nabla}_\Gamma \cdot \left( \int_{\bar{f}(P)}^{\bar{g}(P)} \bar{\zeta} d\bar{y} \right) &= \sum_{i=1}^2 \left[ \bar{\nabla}_\Gamma \cdot \left( \int_{\bar{f}(P)}^{\bar{g}(P)} \bar{\zeta}^i d\bar{y} \right) \right] \cdot \mu_i + \sum_{i=1}^2 \int_{\bar{f}(P)}^{\bar{g}(P)} \bar{\zeta}^i d\bar{y} [\bar{\nabla}_\Gamma \cdot \mu_i] \\
 &- \sum_{i=1}^2 \left[ \bar{\nabla}_\Gamma \cdot \left( \int_{\bar{f}(P)}^{\bar{g}(P)} \bar{y} \bar{\zeta}^i d\bar{y} \right) \right] \cdot \bar{K} \mu_i - \sum_{i=1}^2 \int_{\bar{f}(P)}^{\bar{g}(P)} \bar{y} \bar{\zeta}^i d\bar{y} [\bar{\nabla}_\Gamma \cdot (\bar{K} \mu_i)].
 \end{aligned}$$

The use of the derivation formula of an integral function in one dimension and a proper identification of terms gives

$$\begin{aligned}
 \bar{\nabla}_\Gamma \cdot \left( \int_{\bar{f}(P)}^{\bar{g}(P)} \bar{\zeta} d\bar{y} \right) &= \sum_{i=1}^2 \int_{\bar{f}(P)}^{\bar{g}(P)} (\bar{\zeta}^i \bar{\nabla}_\Gamma \cdot [(\text{Id} - \bar{y} \bar{K}) \mu^i] + (\bar{\nabla}_\Gamma \bar{\zeta}^i) \cdot [(\text{Id} - \bar{y} \bar{K}) \mu^i]) d\bar{y} \\
 &+ \left( \sum_{i=1}^2 \bar{\zeta}^i [(\text{Id} - \bar{g}(P) \bar{K}) \mu^i] \right) \cdot [\bar{\nabla}_\Gamma \bar{g}(P)] \\
 &- \left( \sum_{i=1}^2 \bar{\zeta}^i [(\text{Id} - \bar{f}(P) \bar{K}) \mu^i] \right) \cdot [\bar{\nabla}_\Gamma \bar{f}(P)],
 \end{aligned}$$

which is what we were looking for.  $\square$

**Lemma 3.3.13** *Let us consider the points  $P = P(t, s) \in \Omega(t) \subset \Gamma(t)$  and  $M$  on the axis  $(P, \nu(t, s))$ . We call  $d\Gamma_\Omega(t, s, y) = \|t_1 \wedge t_2\|$  the surface element at  $M$  of the surface parallel to  $\Omega(t)$ . Then*

$$\nabla \cdot \left( \frac{t_i}{d\Gamma_\Omega(t, s, y)} \right) = \frac{1}{\mathcal{L}} \left( \nabla_\Gamma \left( \frac{t_i}{d\Gamma_\Omega(t, s, y)} \right) R_y \right) \bar{\otimes} G = \nabla_\Gamma \cdot \left( \frac{t_i}{d\Gamma_\Omega(t, s, y)} \right) = 0.$$

**Proof** Let us define the scalar fields  $\eta_i(t, s, y) = s_i$  ( $i = 1, 2$ ), and  $\eta_y(t, s, y) = \epsilon y$  in a bounded subdomain of  $\mathcal{N}(t)$  containing  $\Omega(t)$  and  $[P, M]$ .

$$\nabla \eta_i = t^i, \quad \nabla \eta_y = \nu \quad \text{and therefore} \quad \nabla \cdot (t^i \wedge \nu) = 0,$$

since  $\nabla \cdot (\nabla f \wedge \nabla g) = 0$  for any scalar field  $f$  and  $g$ . We also have  $t^1 \wedge \nu = -\frac{t_2}{d\Gamma_\Omega(t, s, y)}$  and  $t^2 \wedge \nu = \frac{t_1}{d\Gamma_\Omega(t, s, y)}$ . The remaining part is a direct application of (3.29). □

**Remark 3.3.14** We notice using Lemma 3.3.13 that one has for any tangential vector field  $\zeta_{tan}$

$$\begin{aligned} \nabla_\Gamma \zeta_{tan} R_y \overline{\otimes} G &= \nabla \cdot \zeta_{tan} = \sum_{i=1}^2 [\nabla (d\Gamma_\Omega(t, s, y) (\zeta_{tan} \cdot t^i))] \cdot \frac{t_i}{d\Gamma_\Omega(t, s, y)} \\ &= \sum_{i=1}^2 [\nabla_\Gamma (d\Gamma_\Omega(t, s, y) (\zeta_{tan} \cdot t^i))] \cdot \frac{\mu_i}{d\Gamma_\Omega(t, s, y)} \\ &= \left[ \nabla_\Gamma \cdot \left( \frac{d\Gamma_\Omega(t, s, y)}{\|\mu_1 \wedge \mu_2\|} R_y \zeta_{tan} \right) \right] \frac{\|\mu_1 \wedge \mu_2\|}{d\Gamma_\Omega(t, s, y)}. \end{aligned}$$

We will also need some informations on the geometry of the free surface  $\overline{FS}$ . The properties of the problem inspire the natural parameterization

$$\bar{r}_{FS} = \bar{X}(\bar{t}, \bar{s}) + \bar{H}(\bar{t}, \bar{s}) \nu(\bar{t}, \bar{s})$$

of the free surface through the parameterization of the substrate  $\bar{X}(\bar{t}, \bar{s})$  and the height  $\bar{H}(\bar{t}, \bar{s})$  of the film. A tangential basis of the free surface tangent bundle is therefore given by the following vectors:

$$\begin{aligned} t_{1, FS} &:= \frac{\partial \bar{r}_{FS}}{\partial \bar{s}_1} = (\text{Id} - \bar{H} \bar{K}) \mu_1 + \frac{\partial \bar{H}}{\partial \bar{s}_1} \nu = t_1 + \frac{\partial \bar{H}}{\partial \bar{s}_1} \nu \\ t_{2, FS} &:= \frac{\partial \bar{r}_{FS}}{\partial \bar{s}_2} = (\text{Id} - \bar{H} \bar{K}) \mu_2 + \frac{\partial \bar{H}}{\partial \bar{s}_2} \nu = t_2 + \frac{\partial \bar{H}}{\partial \bar{s}_2} \nu. \end{aligned}$$

We also define the unit normal to  $\overline{FS}$  by

$$\nu_{FS} := \frac{t_{1, FS} \wedge t_{2, FS}}{\|t_{1, FS} \wedge t_{2, FS}\|}.$$

A better expression of the free surface normal is given through the computation

$$\begin{aligned} t_{1, FS} \wedge t_{2, FS} &= t_1 \wedge t_2 - \frac{\partial \bar{H}}{\partial \bar{s}_1} t_2 \wedge \nu - \frac{\partial \bar{H}}{\partial \bar{s}_2} \nu \wedge t_1 \\ &= t_1 \wedge t_2 - \frac{\partial \bar{H}}{\partial \bar{s}_1} \|t_2\| \|t_1\| \sin(t_1, t_2) t^1 - \frac{\partial \bar{H}}{\partial \bar{s}_2} \|t_2\| \|t_1\| \sin(t_1, t_2) t^2 \\ &= \|t_1 \wedge t_2\| (\nu - R_{\bar{H}} \bar{\nabla}_\Gamma \bar{H}) \end{aligned}$$

by

$$\nu_{FS} = \frac{\nu - R_{\bar{H}} \bar{\nabla}_\Gamma \bar{H}}{\sqrt{1 + \|R_{\bar{H}} \bar{\nabla}_\Gamma \bar{H}\|^2}}.$$

**Curvature tensor of the free surface:**

Let us now consider  $(t_{FS}^1, t_{FS}^2, \nu_{FS})$ , the dual basis of  $(t_{1,FS}, t_{2,FS}, \nu_{FS})$ . this means

$$\begin{aligned} t_{FS}^1 \cdot t_{1,FS} &= 1, & t_{FS}^1 \cdot t_{2,FS} &= 0, & t_{FS}^1 \cdot \nu_{FS} &= 0, \\ t_{FS}^2 \cdot t_{1,FS} &= 0, & t_{FS}^2 \cdot t_{2,FS} &= 1, & t_{FS}^2 \cdot \nu_{FS} &= 0. \end{aligned}$$

We notice that

$$\begin{aligned} t_{FS}^1 &= t^1 - (t^1 \cdot \nu_{FS}) \nu_{FS} \\ t_{FS}^2 &= t^2 - (t^2 \cdot \nu_{FS}) \nu_{FS}. \end{aligned}$$

The free surface curvature tensor is given by

$$\bar{K}_{FS} = - \sum_{i=1}^2 \frac{\partial \nu_{FS}}{\partial \bar{s}_i} \otimes t_{FS}^i$$

and a good development of this formula leads to the following lemma

**Lemma 3.3.15** (*Free surface mean curvature*)

The free surface mean curvature  $\bar{K}_{FS}$  is given in terms of nonscaled and scaled variables by

$$\begin{aligned} \bar{K}_{FS} = \text{tr} (\bar{K}_{FS}) &= \frac{1}{\sqrt{1 + \|R_{\bar{h}} \bar{\nabla}_\Gamma \bar{H}\|^2}} \text{tr} (\bar{K} R_{\bar{h}}) + \frac{1}{\sqrt{1 + \|R_{\bar{h}} \bar{\nabla}_\Gamma \bar{H}\|^2}} \text{tr} (\bar{\nabla}_\Gamma (R_{\bar{h}} \bar{\nabla}_\Gamma \bar{H})) \\ &- \frac{\|R_{\bar{h}} \bar{\nabla}_\Gamma \bar{H}\| (R_{\bar{h}} \bar{\nabla}_\Gamma \bar{H}) \cdot (R_{\bar{h}} \bar{\nabla}_\Gamma \|R_{\bar{h}} \bar{\nabla}_\Gamma \bar{H}\|)}{\sqrt{1 + \|R_{\bar{h}} \bar{\nabla}_\Gamma \bar{H}\|^2}^3} + \frac{(R_{\bar{h}}^2 \bar{K} \bar{\nabla}_\Gamma \bar{H}) \cdot (R_{\bar{h}} \bar{\nabla}_\Gamma \bar{H})}{\sqrt{1 + \|R_{\bar{h}} \bar{\nabla}_\Gamma \bar{H}\|^2}^3} \\ &- \frac{\|R_{\bar{h}} \bar{\nabla}_\Gamma \bar{H}\| (R_{\bar{h}} \bar{\nabla}_\Gamma \|R_{\bar{h}} \bar{\nabla}_\Gamma \bar{H}\|) \cdot (R_{\bar{h}} \bar{\nabla}_\Gamma \bar{H})}{\sqrt{1 + \|R_{\bar{h}} \bar{\nabla}_\Gamma \bar{H}\|^2}^5} + \frac{(R_{\bar{h}}^2 \bar{K} \bar{\nabla}_\Gamma \bar{H}) \cdot (R_{\bar{h}} \bar{\nabla}_\Gamma \bar{H})}{\sqrt{1 + \|R_{\bar{h}} \bar{\nabla}_\Gamma \bar{H}\|^2}^3} \\ &+ \frac{([\bar{\nabla}_\Gamma (R_{\bar{h}} \bar{\nabla}_\Gamma \bar{H})] R_{\bar{h}} \bar{\nabla}_\Gamma \bar{H}) \cdot (R_{\bar{h}} \bar{\nabla}_\Gamma \bar{H})}{\sqrt{1 + \|R_{\bar{h}} \bar{\nabla}_\Gamma \bar{H}\|^2}^3} \\ &- \frac{\|R_{\bar{h}} \bar{\nabla}_\Gamma \bar{H}\|^3 (R_{\bar{h}} \bar{\nabla}_\Gamma \|R_{\bar{h}} \bar{\nabla}_\Gamma \bar{H}\|) \cdot (R_{\bar{h}} \bar{\nabla}_\Gamma \bar{H})}{\sqrt{1 + \|R_{\bar{h}} \bar{\nabla}_\Gamma \bar{H}\|^2}^5} \end{aligned}$$

and

$$\begin{aligned} \bar{K}_{FS} = \text{tr} (\bar{K}_{FS}) &= \frac{1}{\mathcal{L}} \frac{1}{\sqrt{1 + \epsilon^2 \|R_{\bar{h}} \bar{\nabla}_\Gamma \bar{H}\|^2}} \text{tr} (K R_{\bar{h}}) + \frac{\epsilon}{\mathcal{L}} \frac{1}{\sqrt{1 + \epsilon^2 \|R_{\bar{h}} \bar{\nabla}_\Gamma \bar{H}\|^2}} \text{tr} (\nabla_\Gamma (R_{\bar{h}} \nabla_\Gamma H)) \\ &- \frac{\epsilon^3 \|R_{\bar{h}} \bar{\nabla}_\Gamma \bar{H}\| (R_{\bar{h}} \bar{\nabla}_\Gamma H) \cdot (R_{\bar{h}} \bar{\nabla}_\Gamma \|R_{\bar{h}} \bar{\nabla}_\Gamma \bar{H}\|)}{\sqrt{1 + \epsilon^2 \|R_{\bar{h}} \bar{\nabla}_\Gamma \bar{H}\|^2}^3} + \frac{\epsilon^2 (R_{\bar{h}}^2 K \nabla_\Gamma H) \cdot (R_{\bar{h}} \nabla_\Gamma H)}{\sqrt{1 + \epsilon^2 \|R_{\bar{h}} \bar{\nabla}_\Gamma \bar{H}\|^2}^3} \\ &- \frac{\epsilon^3 \|R_{\bar{h}} \bar{\nabla}_\Gamma \bar{H}\| (R_{\bar{h}} \bar{\nabla}_\Gamma \|R_{\bar{h}} \bar{\nabla}_\Gamma \bar{H}\|) \cdot (R_{\bar{h}} \bar{\nabla}_\Gamma H)}{\sqrt{1 + \epsilon^2 \|R_{\bar{h}} \bar{\nabla}_\Gamma \bar{H}\|^2}^5} + \frac{\epsilon^2 (R_{\bar{h}}^2 K \nabla_\Gamma H) \cdot (R_{\bar{h}} \nabla_\Gamma H)}{\sqrt{1 + \epsilon^2 \|R_{\bar{h}} \bar{\nabla}_\Gamma \bar{H}\|^2}^3} \\ &+ \frac{\epsilon^3 ([\nabla_\Gamma (R_{\bar{h}} \bar{\nabla}_\Gamma H)] R_{\bar{h}} \bar{\nabla}_\Gamma H) \cdot (R_{\bar{h}} \bar{\nabla}_\Gamma H)}{\sqrt{1 + \epsilon^2 \|R_{\bar{h}} \bar{\nabla}_\Gamma \bar{H}\|^2}^3} \\ &- \frac{\epsilon^5 \|R_{\bar{h}} \bar{\nabla}_\Gamma \bar{H}\|^3 (R_{\bar{h}} \bar{\nabla}_\Gamma \|R_{\bar{h}} \bar{\nabla}_\Gamma \bar{H}\|) \cdot (R_{\bar{h}} \bar{\nabla}_\Gamma H)}{\sqrt{1 + \epsilon^2 \|R_{\bar{h}} \bar{\nabla}_\Gamma \bar{H}\|^2}^5}. \end{aligned}$$

With these preliminaries in hand, we wish to rewrite the thin-film problem in a curvilinear coordinate system attached to the substrate.

### 3.4 Derivation of surfactant and thin-film equation

We wish here to derive the dimensionless equations describing the surfactant driven thin-film problem stated in Section 3.2. We will particularly use lubrication approximation to reduce the complexity of the thin-film equations. As already mention in the introduction, this technique (introduced in 1962 by Orchard [97]) aims to replace the problem by a relatively simple problem whose long term behavior is similar to the behavior of the studied model. This is done by neglecting some relatively nonimportant effects in the original problem. In our case, we will take, as usual advantage of the fact that the film is thin and the ratio  $\epsilon = \mathcal{H}/\mathcal{L}$  between the vertical length scale and the horizontal length scale is too small compared to 1 ( $\epsilon \ll 1$ ). Therefore, we will expand the scaled version of (3.9) and (3.10) as power series of  $\epsilon$  and consider the truncated result at lower power of  $\epsilon$  as the simplified equation. Any term of order  $\mathcal{O}(\epsilon^2)$  of such expansion will be neglected. This procedure coincides with the construction of the center manifold for the thin-film equation and, consequently the resulting equation is guaranteed to be stable. The case of stationary surface discussed in [107] using center manifold theory offers a good example in this issue. Now, let us start by defining the velocity and its scaling factors.

#### 3.4.1 Velocity and its derivatives

**Definition and Theorem 3.4.1** *The velocity  $\bar{v}_{\mathcal{F}}$  of a fluid particle  $\bar{r}(\bar{t}, \bar{s}_1(\bar{t}), \bar{s}_2(\bar{t}), \bar{y}(\bar{t}))$  is given by*

$$\bar{v}_{\mathcal{F}} = \frac{d\bar{r}}{d\bar{t}} = \bar{v}_{\Gamma} + \bar{v}_{mF} + \bar{v}_{R,tan} + \bar{v}_{R,\nu} \nu, \quad (3.31)$$

where

$$\bar{v}_{\Gamma} = \frac{\partial \bar{X}}{\partial \bar{t}} \quad (3.32)$$

is the velocity of the substrate,

$$\bar{v}_{R,tan} = (\text{Id} - \bar{y}\bar{K}) \left( \frac{\partial \bar{s}_1}{\partial \bar{t}} \mu_1 + \frac{\partial \bar{s}_2}{\partial \bar{t}} \mu_2 \right) \quad (3.33)$$

is the relative tangential velocity of the fluid in the moving frame attached to the substrate,

$$\bar{v}_{mF} = -\bar{y} (\bar{\nabla}_{\Gamma} (\bar{v}_{\Gamma} \cdot \nu) + \bar{K} \bar{v}_{\Gamma,tan}) \quad (3.34)$$

is the velocity due to the rotation of the moving frame and

$$\bar{v}_{R,\nu} = \frac{d\bar{y}}{d\bar{t}} \quad (3.35)$$

is the scalar normal relative velocity in the direction of the substrate normal  $\nu$ .

**Proof** It is clear that

$$\begin{aligned} \bar{v}_{\mathcal{F}} = \frac{d\bar{r}}{d\bar{t}} &= \frac{\partial \bar{X}}{\partial \bar{t}} + \frac{\partial \bar{X}}{\partial \bar{s}_1} \frac{\partial \bar{s}_1}{\partial \bar{t}} + \frac{\partial \bar{X}}{\partial \bar{s}_2} \frac{\partial \bar{s}_2}{\partial \bar{t}} + \frac{d\bar{y}}{d\bar{t}} \nu + \bar{y} \frac{\partial \nu}{\partial \bar{t}} + \bar{y} \left( \frac{\partial \nu}{\partial \bar{s}_1} \frac{\partial \bar{s}_1}{\partial \bar{t}} + \frac{\partial \nu}{\partial \bar{s}_2} \frac{\partial \bar{s}_2}{\partial \bar{t}} \right) \\ &= \bar{v}_{\Gamma} + (\text{Id} - \bar{y}\bar{K}) \left( \frac{\partial \bar{s}_1}{\partial \bar{t}} \mu_1 + \frac{\partial \bar{s}_2}{\partial \bar{t}} \mu_2 \right) + \bar{y} \frac{\partial \nu}{\partial \bar{t}} + \frac{d\bar{y}}{d\bar{t}} \nu. \end{aligned} \quad (3.36)$$

It remains to differentiate the unit normal with respect to time. In fact,

$$\frac{\partial \bar{\nu}}{\partial \bar{t}} \cdot \nu = 0,$$

which means that  $\frac{\partial \bar{\nu}}{\partial \bar{t}}$  is a tangential vector. Knowing that  $\mu_i = \frac{\partial \bar{X}}{\partial \bar{s}_i}$ , we have

$$\begin{aligned} \frac{\partial \nu}{\partial \bar{t}} &= \sum_{i=1}^2 \left( \frac{\partial \nu}{\partial \bar{t}} \cdot \mu_i \right) \mu^i = - \sum_{i=1}^2 \left( \nu \cdot \frac{\partial}{\partial \bar{s}_i} \left( \frac{\partial \bar{X}}{\partial \bar{t}} \right) \right) \mu^i \\ &= - \sum_{i=1}^2 \left( \frac{\partial \bar{v}_\Gamma \cdot \nu}{\partial \bar{s}_i} \right) \mu^i + \sum_{i=1}^2 \left( \bar{v}_\Gamma \cdot \left( \frac{\partial \nu}{\partial \bar{s}_i} \right) \right) \mu^i. \end{aligned}$$

The use of the symmetry of  $K$  leads to

$$\frac{\partial \nu}{\partial \bar{t}} = -\bar{\nabla} (\bar{v}_\Gamma \cdot \nu) - \bar{K} \bar{v}_{\Gamma, \tan}. \quad (3.37)$$

Plugging (3.37) into (3.36) and identify the terms in (3.32), (3.33), (3.34) and (3.35) proves (3.31).  $\square$

It is easy to see that the expression of these velocity components in terms of scaled variables are

$$\bar{v}_\Gamma = \frac{\mathcal{L}}{\mathcal{T}} \frac{\partial X}{\partial t} \quad (3.38)$$

$$\bar{v}_{R, \tan} = \frac{\mathcal{L}}{\mathcal{T}} (\text{Id} - \epsilon y K) \left( \frac{\partial s_1}{\partial t} \mu_1 + \frac{\partial s_2}{\partial t} \mu_2 \right) \quad (3.39)$$

$$\bar{v}_{mF} = -\epsilon \frac{\mathcal{L}}{\mathcal{T}} y (\nabla_\Gamma (v_\Gamma \cdot \nu) + K v_\Gamma) \quad (3.40)$$

$$\bar{v}_{R, \nu} = \epsilon \frac{\mathcal{L}}{\mathcal{T}} \frac{dy}{dt}, \quad (3.41)$$

which give  $\mathcal{V} = \frac{\mathcal{L}}{\mathcal{T}}$  as the natural scaling of the velocity of the substrate and the relative tangential velocity. Also,  $\epsilon \mathcal{V}$  appears as the natural scaling of the scalar normal relative velocity and the velocity due to the rotation of the moving frame. This naturally leads to the following expression of  $\bar{v}_\mathcal{F}$  in terms of scaled variables

$$\bar{v}_\mathcal{F} = \mathcal{V} (v_\Gamma + v_{R, \tan}) + \epsilon \mathcal{V} (v_{mF} + v_{R, \nu}), \quad (3.42)$$

where  $v_\Gamma, v_{mF}, v_{R, \tan}, v_{R, \nu}$  identified in (3.38), (3.39), (3.40) and (3.41) are the scaled substrate velocity, the scaled velocity due to the rotation of the moving frame, the scaled tangential relative velocity and the scaled scalar normal relative velocity, respectively.

**Lemma 3.4.2** *Let us consider the velocity field  $\bar{v}_\mathcal{F}$  as described above. The time derivative of  $\bar{v}_\mathcal{F}$  in terms of nonscaled and scaled variables is given as*

$$\begin{aligned} \frac{d\bar{v}_\mathcal{F}}{d\bar{t}} &= \left( \frac{\partial (\bar{v}_{\Gamma, \tan} + \bar{v}_{mF} + \bar{v}_{R, \tan})}{\partial \bar{t}} \right)_{\tan} + \bar{\nabla}_\Gamma (\bar{v}_{\Gamma, \tan} + \bar{v}_{mF} + \bar{v}_{R, \tan}) \bar{\otimes} R_{\bar{y}} (\bar{v}_{R, \tan}) \\ &- (\bar{v}_{\Gamma, \nu} + \bar{v}_{R, \nu}) [(\bar{\nabla}_\Gamma \bar{v}_{\Gamma, \nu} + \bar{K} \bar{v}_{\Gamma, \tan}) + \bar{K} R_{\bar{y}} (\bar{v}_{R, \tan})] \\ &+ [(\bar{v}_{\Gamma, \tan} + \bar{v}_{mF} + \bar{v}_{R, \tan}) \cdot (\bar{\nabla}_\Gamma \bar{v}_{\Gamma, \nu} + \bar{K} \bar{v}_{\Gamma, \tan})] \nu \\ &+ [(\bar{\nabla}_\Gamma \bar{v}_{\Gamma, \nu} + \bar{K} (\bar{v}_\Gamma + \bar{v}_{mF} + \bar{v}_{R, \tan})) \cdot R_{\bar{y}} (\bar{v}_{R, \tan})] \nu + \frac{\partial (\bar{v}_{\Gamma, \nu} + \bar{v}_{R, \nu})}{\partial \bar{t}} \nu \end{aligned} \quad (3.43)$$

$$\begin{aligned}
 \frac{d\bar{v}_{\mathcal{F}}}{dt} &= \frac{\mathcal{U}}{\mathcal{T}} \left( \frac{\partial(v_{\Gamma,tan} + \epsilon v_{mF} + v_{R,tan})}{\partial t} \right)_{tan} + \frac{\mathcal{U}^2}{\mathcal{L}} \nabla_{\Gamma} (v_{\Gamma,tan} + \epsilon v_{mF} + v_{R,tan}) \otimes R_y(v_{R,tan}) \\
 &- \frac{\mathcal{U}^2}{\mathcal{L}} (v_{\Gamma,\nu} + \epsilon v_{R,\nu}) [(\nabla_{\Gamma} v_{\Gamma,\nu} + K v_{\Gamma,tan}) + K R_y(v_{R,tan})] \\
 &+ \frac{\mathcal{U}^2}{\mathcal{L}} [(v_{\Gamma,tan} + \epsilon v_{mF} + v_{R,tan}) \cdot (\nabla_{\Gamma} v_{\Gamma,\nu} + K v_{\Gamma,tan})] \nu \\
 &+ \frac{\mathcal{U}^2}{\mathcal{L}} [(\nabla_{\Gamma} v_{\Gamma,\nu} + K (v_{\Gamma} + \epsilon v_{mF} + v_{R,tan})) \cdot R_y(v_{R,tan})] \nu + \frac{\mathcal{U}}{\mathcal{T}} \frac{\partial(v_{\Gamma,\nu} + \epsilon v_{R,\nu})}{\partial t} \nu, \quad (3.44)
 \end{aligned}$$

where  $\bar{v}_{\Gamma,\nu} = \bar{v}_{\Gamma} \cdot \nu$  and the index “tan” refers to the tangential part of a vector.

### 3.4.2 Scaled surfactant equation

We scale the surfactant concentration by the equilibrium concentration  $\Pi_{eq}$  ( $\bar{\Pi} = \Pi_{eq} \Pi$ ), the surface tension by  $\gamma_{eq}$  ( $\bar{\gamma} = \gamma_{eq} \gamma$ ), the surface tension of the equilibrium concentration of surfactant. We also scale the diffusivity tensor by the constant diffusivity coefficient  $D_{surf}$  ( $\bar{D}_{FS} = D_{surf} D_{FS}$ ). Then the scaled version of the surfactant equation (3.7) reads

$$\frac{\partial \bar{\Pi}}{\partial t} + (\nabla_{FS} \cdot (\bar{\Pi} v_{FS})) = \frac{1}{\mathcal{P}_e} \nabla_{FS} \cdot (D_{FS} \nabla_{FS} \bar{\Pi}) \quad \text{on the free surface } \bar{FS}, \quad (3.45)$$

where  $\mathcal{P}_e = \frac{\mathcal{L} \mathcal{U}}{D_{surf}}$  is the Peclet number,  $\nabla_{FS} = \mathcal{L} \bar{\nabla}_{FS}$  is the dimensionless tangential nabla operator of  $\bar{FS}$  and  $v_{FS} = \bar{v}_{FS} / \mathcal{U}$  is the dimensionless velocity of the fluid particle on  $\bar{FS}$ . The scaled version of the boundary condition (3.8) at the contact line (Substrate-Fluid-Air) reads

$$(D_{FS} \nabla_{FS} \bar{\Pi}) \cdot n_{FS}^l = 0; \quad (3.46)$$

$n_{FS}^l$  being the free surface outer unit conormal. Finally, let us denote by  $x = \frac{\Pi_{eq}}{\Pi_{\infty}}$  the surfactant coverage and by  $E = \frac{RT_0 \bar{\Pi}_{\infty}}{\gamma_0}$  the surfactant elasticity. The dimensionless Langmuir equation of state obtained from equation (3.11) is then given by

$$\gamma = \frac{1 + E \ln(1 - x \bar{\Pi})}{1 + E \ln(1 - x)}. \quad (3.47)$$

In cases where  $E$  and  $x$  are small (for example, for a polymer  $0.1 \lesssim E \lesssim 0.5$  and  $x$  is small for dilute surfactant coverage), (3.47) can be approximated by

$$\gamma = 1 + Ex(1 - \bar{\Pi}). \quad (3.48)$$

This equation has been used by early researchers [98, 114]. However, as surfactant accumulates at the tip of a drop for example,  $\bar{\Pi}$  gets large at the tip and this approximation fails. The linear approximation should then be used only in reasonable cases. Although it is very easy to cope with the linear equation and the essential physics of the surfactant is captured in the linear approximation, we will use the nonlinear setup to avoid the mentioned above problem.

### 3.4.3 Model reduction for the thin-film equation using lubrication approximation

Let us first define the nonscaled mean curvature  $\bar{K} = \text{tr } \bar{K}$ , the scaled mean curvature  $\mathcal{K} = \text{tr } K$ , the Reynolds number  $\mathcal{R}_e = \rho \mathcal{U} \mathcal{L} / \mu$  and the Bond number  $\mathcal{B}_0 = \mathcal{G} \mathcal{H}^2 / (\mu \mathcal{U})$ , where  $\mathcal{G}$  is the scale of the gravity  $\bar{g}$  ( $\bar{g} = \mathcal{G} g$ ). We also scale the pressure  $\bar{P}$  by  $\mathcal{P} = \mu \mathcal{U} \mathcal{L} / \mathcal{H}^2$  ( $\bar{P} = \mathcal{P} P$ ) and the sum

of body forces  $\bar{f}$  by  $\mathcal{G}$  ( $\bar{f} = \mathcal{G}f$ ). Body forces include for example gravity. Depending on the body force considered, an appropriate scaling factor should be chosen. If we are to consider van der Waals forces, they scale with  $\mathcal{P}$ . We choose  $\mathcal{G}$  as we would like to concentrate on gravity. So far, we haven't explicitly specified how to choose the scaling factors. This plays an important role in the lubrication approximation process since we need a clear way to quantitatively compare effects that influence the model. In the present model for surfactant driven thin-film modeling on evolving surfaces, for example, we have two independent sources of velocity that act at the same time: the substrate velocity  $\bar{v}_\Gamma$ , and the relative velocity of the fluid  $\bar{v}_R$ . Since the thin-film evolution is known to be a slow process, we might then face the situation where  $\|\bar{v}_R\|/\|\bar{v}_\Gamma\|$  is very small ( $\|\bar{v}_R\|/\|\bar{v}_\Gamma\| \ll 1$ ). We would need here to incorporate only the dominant effects coming from each source; Equation (3.44) for example shows how these velocities appear in the acceleration of a fluid particle. Moreover, taking the velocity scale only based on one of these velocities makes it difficult to choose an appropriate time step for numerical computation, so that the interplay of the substrate deformation and the fluid flow can be well resolved. However, depending on the model studied and the focus, a compromise should be found. In the present case, we assume the velocity scale  $\mathcal{U}$  to be based on the relative evolution of the thin-film while the time and space derivatives of the scaled substrate velocity  $v_\Gamma$  are assumed to be of order  $\mathcal{O}(1)$ . This simply means that the norm of substrate acceleration  $\|\partial v_\Gamma/\partial t\|$  and the rate of change in the substrate deformation are proportional to the rate of change in the tangential fluid movement. Thus this setup forbids high constant rotation velocity while allowing high constant translation velocity. We will then finally assume  $\epsilon^2 \mathcal{R}_e \|\partial v_\Gamma/\partial t\| = \mathcal{O}(\epsilon^2)$  as well as  $\epsilon^2 \mathcal{R}_e \|\partial v_{R,tan}/\partial t\| = \mathcal{O}(\epsilon^2)$ ,  $\epsilon^3 \mathcal{R}_e \|\partial v_{mF}/\partial t\| = \mathcal{O}(\epsilon^3)$ ,  $\epsilon^2 \mathcal{K}^2 = \mathcal{O}(\epsilon^2)$  and  $\epsilon^2 \mathcal{B}_0 = \mathcal{O}(\epsilon^2)$ . Let us now multiply each term of equation (3.10) by  $\mathcal{L}/\mathcal{P}$ .

$$\begin{aligned} \frac{\mathcal{L}}{\mathcal{P}} \rho \frac{d\bar{v}_\mathcal{F}}{dt} &= \epsilon^2 \mathcal{R}_e \left( \frac{\partial(v_{\Gamma,tan} + \epsilon v_{mF} + v_{R,tan})}{\partial t} \right)_{tan} + \epsilon^2 \mathcal{R}_e \nabla_\Gamma (v_{\Gamma,tan} + \epsilon v_{mF} + v_{R,tan}) \otimes R_y(v_{R,tan}) \\ &- \epsilon^2 \mathcal{R}_e (v_{\Gamma,\nu} + \epsilon v_{R,\nu}) [(\nabla_\Gamma v_{\Gamma,\nu} + K v_{\Gamma,tan}) + K R_y(v_{R,tan})] \\ &+ \epsilon^2 \mathcal{R}_e [(v_{\Gamma,tan} + \epsilon v_{mF} + v_{R,tan}) \cdot (\nabla_\Gamma v_{\Gamma,\nu} + K v_{\Gamma,tan})] \nu + \epsilon^2 \mathcal{R}_e \frac{\partial(v_{\Gamma,\nu} + \epsilon v_{R,\nu})}{\partial t} \nu \\ &+ \epsilon^2 \mathcal{R}_e [(\nabla_\Gamma v_{\Gamma,\nu} + K(v_\Gamma + \epsilon v_{mF} + v_{R,tan})) \cdot R_y(v_{R,tan})] \nu, \end{aligned} \quad (3.49)$$

$$\frac{\mathcal{L}}{\mathcal{P}} \bar{\nabla} \bar{P} = R_y \nabla_\Gamma P + \frac{1}{\epsilon} \frac{\partial P}{\partial y} \nu, \quad (3.50)$$

$$-\frac{\mathcal{L}}{\mathcal{P}} \bar{f} = -\mathcal{B}_0 f_{tan} - \mathcal{B}_0 f_\nu \nu \quad (f_\nu = f \cdot \nu, f_{tan} = f - f_\nu \nu), \quad (3.51)$$

$$\begin{aligned} \frac{\mathcal{L}}{\mathcal{P}} \mu \bar{\nabla} \cdot (\bar{\nabla} \bar{v}_\mathcal{F}) &= \epsilon^2 \left( (\nabla_\Gamma (\nabla_\Gamma (v_{\Gamma,tan} + \epsilon v_{mF} + v_{R,tan}) R_y) \otimes R_y) \otimes \bar{G} - K [R_y^2 (\nabla_\Gamma (v_{\Gamma,\nu} + \epsilon v_{R,\nu}))] \right) \\ &+ \epsilon^2 \nu \left( \text{tr} [\nabla_\Gamma (v_{\Gamma,tan} + \epsilon v_{mF} + v_{R,tan}) K R_y^2] + \text{tr} ([\nabla_\Gamma (R_y \nabla_\Gamma (v_{\Gamma,\nu} + \epsilon v_{R,\nu}))] R_y) \right) \\ &- \epsilon \frac{\partial(v_{\Gamma,tan} + \epsilon v_{mF} + v_{R,tan})}{\partial y} \text{tr} (R_y K) - \epsilon \text{tr} (R_y K) \left[ \frac{\partial(v_{\Gamma,\nu} + \epsilon v_{R,\nu})}{\partial y} \right] \nu \\ &- \epsilon^2 (R_y^2 K^2 (v_{\Gamma,tan} + \epsilon v_{mF} + v_{R,tan})) - \epsilon^2 \nabla_\Gamma ((v_{\Gamma,\nu} + \epsilon v_{R,\nu}) K R_y) \otimes R_y \otimes \bar{G} \\ &+ \epsilon^2 \nu \text{tr} ([\nabla_\Gamma (R_y K (v_{\Gamma,tan} + \epsilon v_{mF} + v_{R,tan}))] R_y) - \epsilon^2 \nu (v_{\Gamma,\nu} + \epsilon v_{R,\nu}) \text{tr} (K^2 R_y^2) \\ &+ \left( \frac{\partial^2 (v_{\Gamma,tan} + \epsilon v_{mF} + v_{R,tan})}{\partial y^2} + \frac{\partial^2 (v_{\Gamma,\nu} + \epsilon v_{R,\nu})}{\partial y^2} \right) \nu. \end{aligned} \quad (3.52)$$

Next, we introduce these terms in the result of the multiplication of equation (3.10) by  $\mathcal{L}/\mathcal{P}$ . Noticing that  $R_y = \text{Id} + \epsilon y K + \mathcal{O}(\epsilon^2)$ , the resulting equation reads

$$-\epsilon \mathcal{K} \frac{\partial v_{R,tan}}{\partial y} + \frac{\partial^2 v_{R,tan}}{\partial y^2} + \epsilon \frac{\partial^2 v_{R,\nu}}{\partial y^2} \nu = \nabla_\Gamma P + \epsilon y K \nabla_\Gamma P + \frac{1}{\epsilon} \frac{\partial P}{\partial y} \nu - \mathcal{B}_0 f_{tan} - \mathcal{B}_0 f_\nu \nu + \mathcal{O}(\epsilon^2).$$

The projection of this equation on the normal direction as well as on the tangential plane leads to a system of partial differential equations (PDEs). An approximation of these PDEs at order  $\epsilon^2$  reads

$$\begin{cases} \frac{\partial P}{\partial y} & = \epsilon \mathcal{B}_0 f_\nu \end{cases} \quad (3.53)$$

$$\begin{cases} -\epsilon \mathcal{K} \frac{\partial v_{R,tan}}{\partial y} + \frac{\partial^2 v_{R,tan}}{\partial y^2} & = \nabla_\Gamma P + \epsilon y K \nabla_\Gamma P - \mathcal{B}_0 f_{tan} \end{cases} \quad (3.54)$$

The system of PDEs (3.53) – (3.54) is a reduced system representing the momentum equation. Taking  $\mathcal{U} = \epsilon(\gamma_{eq}/\mu)$  as mentioned above and scaling the slip tensor  $\bar{\beta}$  by  $\mu/\mathcal{H}$  ( $\bar{\beta} = (\mu/\mathcal{H})\beta$ ), we approximate the boundary conditions associated to the Navier-Stokes equations up to  $\mathcal{O}(\epsilon^2)$  by

$$\text{No penetration on } \Gamma : \quad v_{R,\nu} = 0 \quad (3.55)$$

$$\text{Friction slip condition on } \Gamma : \quad \frac{\partial v_{R,tan}}{\partial y} + \epsilon K v_{R,tan} = \beta v_{R,tan} \quad (3.56)$$

$$\text{Share stress condition on } FS : \quad \frac{\partial v_{R,tan}}{\partial y} + \epsilon K v_{R,tan} = (\text{Id} + \epsilon H K) \nabla_\Gamma \gamma \quad (3.57)$$

$$\text{Laplace-Young's law on } FS : \quad P = P_0 - C' \gamma \mathcal{K}_{FS}, \quad (3.58)$$

where  $C' = \epsilon^2(\gamma_{eq}/\mu \mathcal{U})$  is the inverse capillary number which represents the ratio between surface tension and viscous forces. We differentiate  $C'$  to the standard inverse capillary number  $C = \epsilon^3(\gamma_{eq}/\mu \mathcal{U})$ .  $\mathcal{K}_{FS} = \mathcal{L} \bar{\mathcal{K}}_{FS}$  is the scaled free surface mean curvature. Its  $\mathcal{O}(\epsilon^2)$  approximation deduced from Lemma 3.3.15 and which is effectively incorporated in this model reads

$$\mathcal{K}_{FS} = \mathcal{K} + \epsilon(H\mathcal{K}_2 + \Delta_\Gamma H) \quad (\mathcal{K}_2 = \text{tr}(K^2)). \quad (3.59)$$

It can be noticed that for  $\mathcal{K} = \mathcal{O}(\epsilon)$  (almost flat surface), the capillary number  $C$  is recovered in (3.58). Also, for  $\mathcal{K} = \text{constant} + \mathcal{O}(\epsilon)$  (almost cylinder or spherical surface) all the surface tension term in the pressure gradient in (3.54) become  $\mathcal{O}(\epsilon C')$ .

**Remark 3.4.3** *The surface tensor  $\beta$  describes the properties of the substrate. If we set  $\beta = 0 \text{Id}$ , there is no friction at the contact of the substrate and we are in the case of perfect slip. If the eigenvalues of  $\beta$  tend to infinity, then the friction is too high on the substrate interface and therefore prevents any movement of fluid particles at the surface contact; this is the well known “no-slip condition” commonly applied in fluid mechanics. Unfortunately, in the context of thin-film flow, this condition gives rise to nonintegrable singularities at the triple line junction (Substrate-Fluid-Air) [68]. This problem is overcome by assuming either a precursor layer or the slip condition we have already introduced. In this context of lubrication approximation, the no-slip condition will be obtained once the smallest eigenvalue of  $\beta$  is greater than  $1/\epsilon^2$ ; which is equivalent to say that  $\xi \cdot (\beta \xi) \geq (1/\epsilon^2) \|\xi\|^2$  for all tangential vector  $\xi$ . To avoid influences of the boundary conditions which will take us away from the real world application, we must remain near the no-slip condition. A good range is to choose  $\beta$  such that its eigenvalues lie between  $1/\sqrt{\epsilon}$  and  $1/\epsilon^2$  which is equivalent to say that  $(1/\sqrt{\epsilon}) \|\xi\|^2 \leq \xi \cdot (\beta \xi) \leq (1/\epsilon^2) \|\xi\|^2$  for all tangential vector  $\xi$ . The whole model is done by using the minimal assumption  $(1/\sqrt{\epsilon}) \|\xi\|^2 \leq \xi \cdot (\beta \xi)$ .*

Let us now look for the expression of  $v_{R,tan}$  in terms of  $\epsilon$ . First integrating (3.53) from the high position  $y$  to  $H$  and using the boundary condition (3.58) gives

$$P(y) = P_0 - C' \gamma \mathcal{K}_{FS} + \epsilon \mathcal{B}_0 f_\nu (y - H). \quad (3.60)$$

Secondly, we should notice the system of ordinary differential equations (ODE) (3.54) with the boundary condition (3.56) and (3.57) can be solved using power series. We will therefore set

$$v_{R,tan} = v_0 + y v_1 + y^2 v_2 + y^3 v_3 + y^4 v_4 + y^5 v_5 + \dots,$$



where the coefficients  $v_i$  ( $i = 0, 1, \dots$ ) to be determined from the equations are vectors which do not depend on  $y$ . The  $\mathcal{O}(\epsilon^2)$  approximation of  $v_{R,tan}$  reads

$$\begin{aligned}
 v_{R,tan} &= \left[ \left( yH - \frac{1}{2}\epsilon yH^2\mathcal{K} - \frac{1}{2}(y^2 - \epsilon y^2H\mathcal{K}) - \frac{1}{6}\epsilon y^3\mathcal{K} \right) \text{Id} - \frac{1}{6}\epsilon y^3K \right] \nabla_\Gamma (C'\gamma\mathcal{K}_{FS}) \\
 &+ \left[ \left( H - \frac{1}{2}\epsilon H^2\mathcal{K} \right) \text{Id} - \epsilon yHK \right] \beta^{-1} \nabla_\Gamma (C'\gamma\mathcal{K}_{FS}) + \left[ H\beta^{-1} + \left( yH - \frac{1}{2}y^2 \right) \text{Id} \right] \epsilon \mathcal{B}_0 f_\nu \nabla_\Gamma H \\
 &+ \left[ \left( (1 - \epsilon H\mathcal{K}) \text{Id} - \epsilon yK \right) \beta^{-1} + \left( y - \epsilon yH\mathcal{K} + \frac{1}{2}\epsilon y^2\mathcal{K} \right) \text{Id} \right] \nabla_\Gamma \gamma \\
 &+ \left[ \frac{1}{2}H^2\beta^{-1} + \left( \frac{1}{2}yH^2 - \frac{1}{2}y^2H + \frac{1}{6}y^3 \right) \text{Id} \right] \epsilon \mathcal{B}_0 \nabla_\Gamma f_\nu \\
 &+ \left[ \left( yH - \frac{1}{2}\epsilon yH^2\mathcal{K} - \frac{1}{2}(y^2 - \epsilon y^2H\mathcal{K}) - \frac{1}{6}\epsilon y^3\mathcal{K} \right) \text{Id} - \frac{1}{2}\epsilon yH^2K \right] \mathcal{B}_0 f_{tan} \\
 &+ \left( H\beta^{-1} - \frac{1}{2}\epsilon H^2\beta^{-1}K - \frac{1}{2}\epsilon H^2\mathcal{K}\beta^{-1} - \epsilon yHK\beta^{-1} \right) \mathcal{B}_0 f_{tan}. \tag{3.61}
 \end{aligned}$$

Finally, it remains to consider the mass conservation equation (3.9). A direct use of Theorem 3.3.11 gives the following dimensionless counterpart

$$\nabla_\Gamma (v_{\Gamma,tan} + v_{R,tan} + \epsilon v_{mF}) R_y \overline{\otimes} G - (v_{\Gamma,\nu} + \epsilon v_{R,\nu}) K R_y \overline{\otimes} G + \frac{\partial v_{R,\nu}}{\partial y} = 0. \tag{3.62}$$

Let us multiply this equation by the rate of change of the surface element of the parallel surface to  $\Gamma$  along the normal  $dS_{\Gamma,var} = [(t_1 \wedge t_2) \cdot \nu] [(\mu_1 \wedge \mu_2) \cdot \nu]^{-1} = 1 - \epsilon y\mathcal{K} + \frac{1}{2}\epsilon^2 y^2(\mathcal{K}^2 - \mathcal{K}_2)$ . Observing that  $K^2 - \mathcal{K}K + \frac{1}{2}(\mathcal{K}^2 - \mathcal{K}_2)(\text{Id} - \nu \otimes \nu) = 0$  one obtains

$$\begin{aligned}
 &dS_{\Gamma,var} \left( \nabla_\Gamma v_{\Gamma,tan} \overline{\otimes} G - \mathcal{K} v_{\Gamma,\nu} \right) + \epsilon y \left( \nabla_\Gamma v_{\Gamma,tan} K \overline{\otimes} G - \mathcal{K}_2 v_{\Gamma,\nu} \right) + \epsilon^2 y^2 \left( \nabla_\Gamma v_{\Gamma,tan} K^2 \overline{\otimes} G - \mathcal{K}_3 v_{\Gamma,\nu} \right) \\
 &- \epsilon^2 y^2 \mathcal{K} \left( \nabla_\Gamma v_{\Gamma,tan} K^2 \overline{\otimes} G - \mathcal{K}_2 v_{\Gamma,\nu} \right) - [\nabla_\Gamma (\nabla_\Gamma v_{\Gamma,\nu} + K v_{\Gamma,tan})] [\epsilon y \text{Id} - \epsilon^2 y^2 (\mathcal{K} \text{Id} - K)] \overline{\otimes} G \\
 &+ dS_{\Gamma,var} \left( \nabla_\Gamma v_{R,tan} R_y \overline{\otimes} G \right) + (-\epsilon \mathcal{K} + \epsilon^2 y (\mathcal{K}^2 - \mathcal{K}_2)) v_{R,\nu} + dS_{\Gamma,var} \frac{\partial v_{R,\nu}}{\partial y} = 0.
 \end{aligned}$$

where  $\mathcal{K}_3$  is the trace of  $K^3$ . The integration of this equation along the normal  $\nu$  of the substrate using the no-penetration boundary condition (3.55) ( $v_{R,\nu} = 0$ ) on  $\Gamma$  gives

$$\begin{aligned}
 &\eta \left( \nabla_\Gamma v_{\Gamma,tan} \overline{\otimes} G - \mathcal{K} v_{\Gamma,\nu} \right) + \frac{1}{2}\epsilon H^2 \left( \nabla_\Gamma v_{\Gamma,tan} K \overline{\otimes} G - \mathcal{K}_2 v_{\Gamma,\nu} \right) + \frac{1}{3}\epsilon^2 H^3 \left( \nabla_\Gamma v_{\Gamma,tan} K^2 \overline{\otimes} G - \mathcal{K}_3 v_{\Gamma,\nu} \right) \\
 &- \frac{1}{3}\epsilon^2 H^3 \mathcal{K} \left( \nabla_\Gamma v_{\Gamma,tan} K^2 \overline{\otimes} G - \mathcal{K}_2 v_{\Gamma,\nu} \right) - [\nabla_\Gamma (\nabla_\Gamma v_{\Gamma,\nu} + K v_{\Gamma,tan})] \left[ \frac{1}{2}\epsilon H^2 \text{Id} - \frac{1}{3}\epsilon^2 H^3 (\mathcal{K} \text{Id} - K) \right] \overline{\otimes} G \\
 &+ \int_0^H dS_{\Gamma,var} \left( \nabla_\Gamma v_{R,tan} R_y \overline{\otimes} G \right) dy + (dS_{\Gamma,var} v_{R,\nu})|_H = 0, \tag{3.63}
 \end{aligned}$$

where the index  $H$  refers to the point where the given expression is evaluated and  $\eta = \int_0^H dS_{\Gamma,var} dy = H - \frac{1}{2}\epsilon H^2\mathcal{K} + \frac{1}{6}\epsilon^2 H^3 (\mathcal{K}^2 - \mathcal{K}_2)$  is the fluid density above the point  $P(t, s_1(t), s_2(t))$  on  $\Gamma(t)$ . Considering a fluid particle  $M(X(t, s_1(t), s_2(t)), H(t, X(t, s_1(t), s_2(t))))$  in the substrate coordinate system, the kinematic condition reads

$$(v_{R,\nu})|_H = \frac{dH}{dt} = \frac{\partial^\Gamma H}{\partial t} + \sum_{i=1}^2 \frac{\partial H}{\partial s_i} \frac{\partial s_i}{\partial t} = \frac{\partial H}{\partial t} + R_H \nabla_\Gamma H \cdot v_{R,tan}, \tag{3.64}$$

where  $\frac{\partial^\Gamma H}{\partial t} := \frac{\partial H}{\partial t} + \nabla H \cdot v_\Gamma$ . This notation will only be used when the functions explicitly depends on  $X(t, s_1, s_2)$  (i.e.  $H(t, X(t, s_1, s_2))$ ) to differentiate between the usual partial time derivative and

the material derivative taking by fixing the surface parametric coordinates  $(s_1, s_2)$ . Now, combining (3.64) and (3.30) gives

$$\begin{aligned} (dS_{\Gamma, var} v_{R, \nu})|_{\mathbb{H}} &= dS_{\Gamma, var} \frac{\partial^{\Gamma} \mathbb{H}}{\partial t} + \nabla_{\Gamma} \cdot \int_0^{\mathbb{H}} [dS_{\Gamma, var} R_y (v_{R, tan})] dy \\ &\quad - \int_0^{\mathbb{H}} \nabla_{\Gamma} \cdot [dS_{\Gamma, var} R_y (v_{R, tan})] dy. \end{aligned} \quad (3.65)$$

Let us introduce the following useful lemma which gives the partial derivative of the curvature with respect to time. Its proof, which we omit here, follows the same path as the computation of the partial derivative of the normal with respect to time.

**Lemma 3.4.4** *Let  $K = K(t, s)$  be the nondimensional curvature tensor of  $\Gamma(t)$ ,  $\mathcal{K} = \text{tr}(K)$  and  $\mathcal{K}_2 = \text{tr}(K^2) = \text{tr}(K \otimes K)$ ; then*

$$\begin{aligned} \frac{\partial K}{\partial t} &= \nabla_{\Gamma} (\nabla_{\Gamma} v_{\Gamma, \nu} + K v_{\Gamma, tan}) - \sum_{i=1}^2 \left[ K \left( \frac{\partial u_{\Gamma}}{\partial s_i} \right) \right] \otimes \mu^i \\ &\quad + [K (\nabla_{\Gamma} v_{\Gamma, \nu} + K v_{\Gamma, tan})] \otimes \nu - \nu \otimes [K (\nabla_{\Gamma} v_{\Gamma, \nu} + K v_{\Gamma, tan})] \\ \frac{\partial \mathcal{K}}{\partial t} &= \nabla_{\Gamma} \cdot (\nabla_{\Gamma} v_{\Gamma, \nu} + K v_{\Gamma, tan}) - \text{tr}(K \nabla_{\Gamma} v_{\Gamma}) \\ \frac{\partial \mathcal{K}^2}{\partial t} &= 2\mathcal{K} \nabla_{\Gamma} \cdot (\nabla_{\Gamma} v_{\Gamma, \nu} + K v_{\Gamma, tan}) - 2\mathcal{K} \text{tr}(K \nabla_{\Gamma} v_{\Gamma}) \\ \frac{\partial \mathcal{K}_2}{\partial t} &= 2\text{tr}(K [\nabla_{\Gamma} (\nabla_{\Gamma} v_{\Gamma, \nu} + K v_{\Gamma, tan})]) - 2\text{tr}(K^2 (\nabla_{\Gamma} v_{\Gamma})). \end{aligned}$$

This lemma leads eventually to the following formula

$$\begin{aligned} (dS_{\Gamma, var})|_{\mathbb{H}} \frac{\partial^{\Gamma} \mathbb{H}}{\partial t} &= \frac{\partial^{\Gamma} \eta}{\partial t} + \frac{1}{2} \epsilon \mathbb{H}^2 \nabla_{\Gamma} \cdot (\nabla_{\Gamma} v_{\Gamma, \nu} + K v_{\Gamma, tan}) - \frac{1}{2} \epsilon \mathbb{H}^2 \text{tr}(K \nabla_{\Gamma} v_{\Gamma}) \\ &\quad - \frac{1}{3} \epsilon^2 \mathbb{H}^3 [\mathcal{K} \nabla_{\Gamma} \cdot (\nabla_{\Gamma} v_{\Gamma, \nu} + K v_{\Gamma, tan}) - \text{tr}(K [\nabla_{\Gamma} (\nabla_{\Gamma} v_{\Gamma, \nu} + K v_{\Gamma, tan})]) \\ &\quad \quad - \mathcal{K} \text{tr}(K \nabla_{\Gamma} v_{\Gamma}) + \text{tr}(K^2 (\nabla_{\Gamma} v_{\Gamma}))] \end{aligned}$$

and (3.65) becomes now

$$\begin{aligned} (dS_{\Gamma, var} v_{R, \nu})|_{\mathbb{H}} &= \frac{\partial^{\Gamma} \eta}{\partial t} + \nabla_{\Gamma} \cdot \int_0^{\mathbb{H}} [dS_{\Gamma, var} R_y (v_{R, tan})] dy - \int_0^{\mathbb{H}} \nabla_{\Gamma} \cdot [dS_{\Gamma, var} R_y (v_{R, tan})] dy \\ &\quad + \frac{1}{2} \epsilon \mathbb{H}^2 \nabla_{\Gamma} \cdot (\nabla_{\Gamma} v_{\Gamma, \nu} + K v_{\Gamma, tan}) - \frac{1}{2} \epsilon \mathbb{H}^2 \text{tr}(K \nabla_{\Gamma} v_{\Gamma}) \\ &\quad - \frac{1}{3} \epsilon^2 \mathbb{H}^3 [\mathcal{K} \nabla_{\Gamma} \cdot (\nabla_{\Gamma} v_{\Gamma, \nu} + K v_{\Gamma, tan}) - \text{tr}(K [\nabla_{\Gamma} (\nabla_{\Gamma} v_{\Gamma, \nu} + K v_{\Gamma, tan})]) \\ &\quad \quad - \mathcal{K} \text{tr}(K \nabla_{\Gamma} v_{\Gamma}) + \text{tr}(K^2 (\nabla_{\Gamma} v_{\Gamma}))]. \end{aligned}$$

A proper development of this last equation using Remark 3.3.14 gives

$$\begin{aligned} (dS_{\Gamma, var} v_{R, \nu})|_{\mathbb{H}} &= \frac{\partial^{\Gamma} \eta}{\partial t} + \nabla_{\Gamma} \cdot \int_0^{\mathbb{H}} [(\text{Id} - \epsilon y (\mathcal{K} \text{Id} - K)) v_{R, tan}] dy - \int_0^{\mathbb{H}} dS_{\Gamma, var} (R_y \nabla_{\Gamma} v_{R, tan}) \overline{\otimes} G dy \\ &\quad + [\nabla_{\Gamma} (\nabla_{\Gamma} v_{\Gamma, \nu} + K v_{\Gamma, tan})] \left( \frac{1}{2} \epsilon \mathbb{H}^2 \text{Id} - \frac{1}{3} \epsilon^2 \mathbb{H}^3 (\mathcal{K} \text{Id} - K) \right) \overline{\otimes} G \\ &\quad - \frac{1}{2} \epsilon \mathbb{H}^2 \text{tr}(K \nabla_{\Gamma} v_{\Gamma}) + \frac{1}{3} \epsilon^2 \mathbb{H}^3 \mathcal{K} \text{tr}(K \nabla_{\Gamma} v_{\Gamma}) - \frac{1}{3} \epsilon^2 \mathbb{H}^3 \text{tr}(K^2 (\nabla_{\Gamma} v_{\Gamma})) \end{aligned}$$

and, finally, the combination of this equation with (3.63) gives

$$\frac{\partial^\Gamma \eta}{\partial t} + \eta \nabla_\Gamma \cdot v_\Gamma + \nabla_\Gamma \cdot \int_0^{\mathbb{H}} [(\text{Id} - \epsilon y (\mathcal{K} \text{Id} - K)) v_{R,tan}] dy = 0,$$

where we recall that  $\nabla_\Gamma \cdot v_\Gamma = \nabla_\Gamma v_{\Gamma,tan} \overline{\otimes} G - \mathcal{K} v_{\Gamma,\nu}$ . The above equation can be summarized as

$$\frac{\partial^\Gamma \eta}{\partial t} + \eta \nabla_\Gamma \cdot v_\Gamma + \nabla_\Gamma \cdot F = 0, \quad (3.66)$$

where the flux  $F$  is given by

$$\begin{aligned} F &= \int_0^{\mathbb{H}} (v_{R,tan} - \epsilon y \mathcal{K} v_{R,tan} + \epsilon y K v_{R,tan}) dy \\ &= \left[ \frac{1}{3} \mathbb{H}^3 \text{Id} - \frac{1}{3} \epsilon \mathbb{H}^4 \left( \mathcal{K} \text{Id} - \frac{1}{2} K \right) + (\mathbb{H}^2 - \epsilon \mathbb{H}^3 \mathcal{K}) \beta^{-1} \right] \nabla_\Gamma (C' \gamma \mathcal{K}_{FS}) + \left[ \mathbb{H}^2 \beta^{-1} + \frac{1}{3} \mathbb{H}^3 \text{Id} \right] \epsilon \mathcal{B}_0 f_\nu \nabla_\Gamma \mathbb{H} \\ &+ \left[ \left( \mathbb{H} \text{Id} - \frac{3}{2} \epsilon \mathbb{H}^2 \mathcal{K} \text{Id} \right) \beta^{-1} + \left( \frac{1}{2} \mathbb{H}^2 - \frac{2}{3} \epsilon \mathbb{H}^3 \mathcal{K} \right) \text{Id} + \frac{1}{3} \epsilon \mathbb{H}^3 K \right] \nabla_\Gamma \gamma + \left[ \frac{1}{2} \mathbb{H}^3 \beta^{-1} + \frac{1}{8} \mathbb{H}^4 \text{Id} \right] \epsilon \mathcal{B}_0 \nabla_\Gamma f_\nu \\ &+ \left[ \frac{1}{3} \mathbb{H}^3 \text{Id} - \frac{1}{3} \epsilon \mathbb{H}^4 \mathcal{K} \text{Id} - \frac{1}{24} \epsilon \mathbb{H}^4 K \right] \mathcal{B}_0 f_{tan} + \left( (\mathbb{H}^2 - \epsilon \mathbb{H}^3 \mathcal{K}) \beta^{-1} - \frac{1}{2} \epsilon \mathbb{H}^3 \beta^{-1} K \right) \mathcal{B}_0 f_{tan}. \end{aligned} \quad (3.67)$$

In the special case where gravity  $\bar{g} = \mathcal{G}g = \mathcal{G}(g_{tan} + g_\nu \nu)$  ( $g_\nu = g \cdot \nu$ ) is the only body force, we can notice that  $\nabla_\Gamma g_\nu = -K g_{tan}$  and (3.67) becomes

$$\begin{aligned} F &= \left[ \frac{1}{3} \mathbb{H}^3 \text{Id} - \frac{1}{3} \epsilon \mathbb{H}^4 \left( \mathcal{K} \text{Id} - \frac{1}{2} K \right) + (\mathbb{H}^2 - \epsilon \mathbb{H}^3 \mathcal{K}) \beta^{-1} \right] \nabla_\Gamma (C' \gamma \mathcal{K}_{FS}) + \left[ \mathbb{H}^2 \beta^{-1} + \frac{1}{3} \mathbb{H}^3 \text{Id} \right] \epsilon \mathcal{B}_0 g_\nu \nabla_\Gamma \mathbb{H} \\ &+ \left[ \left( \mathbb{H} \text{Id} - \frac{3}{2} \epsilon \mathbb{H}^2 \mathcal{K} \text{Id} \right) \beta^{-1} + \left( \frac{1}{2} \mathbb{H}^2 - \frac{2}{3} \epsilon \mathbb{H}^3 \mathcal{K} \right) \text{Id} + \frac{1}{3} \epsilon \mathbb{H}^3 K \right] \nabla_\Gamma \gamma \\ &+ \frac{1}{3} \left[ \mathbb{H}^3 \text{Id} - \epsilon \mathbb{H}^4 \left( \mathcal{K} \text{Id} + \frac{1}{2} K \right) \right] \mathcal{B}_0 g_{tan} + ((\mathbb{H}^2 - \epsilon \mathbb{H}^3 \mathcal{K}) \beta^{-1} - \epsilon \mathbb{H}^3 \beta^{-1} K) \mathcal{B}_0 g_{tan}. \end{aligned} \quad (3.68)$$

In case of constant surface tension  $\gamma$ , no-slip condition and static surface, the terms in (3.66) and (3.68) involving  $\nabla_\Gamma \gamma$ ,  $\beta^{-1}$ , and  $v_\Gamma$  cancel out and we recover exactly the equation presented by Roy, Roberts and Simpson in [107]. Let us now consider the dual effect of gravity and van der Waals forces. Van der Waals forces are intermolecular forces that come into play when the film's thickness become very small (order of several hundreds of Ångströms (100–1000)). These forces are expressed as potential forces often called disjoining pressure. There are many expressions for this potential in the literature. We refer to [117] for the derivation of a more general formula which reads

$$\bar{\phi} = \sum_{i=1}^4 \bar{A}_i \bar{\mathbb{H}}^{-i},$$

where  $A_i$  are coefficients determined by specific intermolecular forces brought into consideration. In our model, we will consider the potential adopted by Ida and Miksis in [72]

$$\bar{\phi} = \bar{A}_3 \bar{\mathbb{H}}^{-3}, \quad (3.69)$$

where  $\bar{A}_3 = \bar{A}/(6\pi\rho)$ .  $\bar{A}$  is a physical constant called Hamaker constant. When  $\bar{A} > 0$ , the two interfaces (Substrate and Free Surface) attract each other and when  $\bar{A} < 0$  they repel each other. To include this effect in the present context, we can either consider an extra body force  $\bar{f}_\nu = \nabla \bar{\phi}$  which can be taken into account in the sum of body forces  $\bar{f}$ , or replace the pressure  $\bar{P}$  in (3.10) by  $\bar{P} + \bar{\phi}$ . In either case  $\bar{\phi}$  which is originally defined on the substrate is extended as constant along the

normal  $\nu$ . Also, the scaling procedure should be done carefully. Here we have scaled  $\bar{f}$  by  $\mathcal{G}$  while  $\bar{\phi}$  scales like pressure ( $\bar{\phi} = \mathcal{P}\phi$ ), therefore the best way to incorporate the effect is to replace  $\bar{P}$  in (3.10) by  $\bar{P} + \bar{\phi}$ . This results in replacing the term  $C'\gamma\mathcal{K}_{FS}$  in the flux  $F$  in (3.67) by  $(-\phi + C'\gamma\mathcal{K}_{FS})$ , where  $\phi = AH^{-3}$  and  $A = \epsilon\bar{A}/(6\pi\rho\mu\mathcal{V}\mathcal{H}^2)$  is the dimensionless Hamaker constant. The resulting flux is therefore

$$\begin{aligned}
 F &= \left[ \frac{1}{3}\mathcal{H}^3 \text{Id} - \frac{1}{3}\epsilon\mathcal{H}^4 \left( \mathcal{K} \text{Id} - \frac{1}{2}K \right) + (\mathcal{H}^2 - \epsilon\mathcal{H}^3\mathcal{K})\beta^{-1} \right] \nabla_{\Gamma} (-\phi + C'\gamma\mathcal{K}_{FS}) \\
 &+ \left[ \mathcal{H}^2\beta^{-1} + \frac{1}{3}\mathcal{H}^3 \text{Id} \right] \epsilon\mathcal{B}_0g_{\nu}\nabla_{\Gamma}\mathcal{H} + \left[ \left( \mathcal{H}\text{Id} - \frac{3}{2}\epsilon\mathcal{H}^2\mathcal{K}\text{Id} \right)\beta^{-1} + \left( \frac{1}{2}\mathcal{H}^2 - \frac{2}{3}\epsilon\mathcal{H}^3\mathcal{K} \right)\text{Id} + \frac{1}{3}\epsilon\mathcal{H}^3K \right] \nabla_{\Gamma}\gamma \\
 &+ \frac{1}{3} \left[ \mathcal{H}^3 \text{Id} - \epsilon\mathcal{H}^4 \left( \mathcal{K} \text{Id} + \frac{1}{2}K \right) \right] \mathcal{B}_0g_{tan} + ((\mathcal{H}^2 - \epsilon\mathcal{H}^3\mathcal{K})\beta^{-1} - \epsilon\mathcal{H}^3\beta^{-1}K) \mathcal{B}_0g_{tan} \quad (3.70)
 \end{aligned}$$

and, in this case, the relative velocity  $v_{R,tan}$  becomes

$$\begin{aligned}
 v_{R,tan} &= \left[ \left( y\mathcal{H} - \frac{1}{2}\epsilon y\mathcal{H}^2\mathcal{K} - \frac{1}{2}(y^2 - \epsilon y^2\mathcal{H}\mathcal{K}) - \frac{1}{6}\epsilon y^3\mathcal{K} \right)\text{Id} - \frac{1}{6}\epsilon y^3K \right] \nabla_{\Gamma} (-\phi + C'\gamma\mathcal{K}_{FS}) \\
 &+ \left[ \left( \mathcal{H} - \frac{1}{2}\epsilon\mathcal{H}^2\mathcal{K} \right)\text{Id} - \epsilon y\mathcal{H}K \right] \beta^{-1}\nabla_{\Gamma} (-\phi + C'\gamma\mathcal{K}_{FS}) + \left[ \mathcal{H}\beta^{-1} + \left( y\mathcal{H} - \frac{1}{2}y^2 \right)\text{Id} \right] \epsilon\mathcal{B}_0g_{\nu}\nabla_{\Gamma}\mathcal{H} \\
 &+ \left[ ((1 - \epsilon\mathcal{H}\mathcal{K})\text{Id} - \epsilon yK)\beta^{-1} + \left( y - \epsilon y\mathcal{H}\mathcal{K} + \frac{1}{2}\epsilon y^2\mathcal{K} \right)\text{Id} \right] \nabla_{\Gamma}\gamma \\
 &+ \left[ \left( y\mathcal{H} - \frac{1}{2}y^2 - \frac{1}{2}\epsilon y\mathcal{H}^2\mathcal{K} + \frac{1}{2}\epsilon y^2\mathcal{H}\mathcal{K} - \frac{1}{6}\epsilon y^3\mathcal{K} \right)\text{Id} - \left( \epsilon y\mathcal{H}^2 - \frac{1}{2}\epsilon y^2\mathcal{H} + \frac{1}{6}\epsilon y^3 \right)K \right] \mathcal{B}_0g_{tan} \\
 &+ \left( \mathcal{H}\beta^{-1} - \frac{1}{2}\epsilon\mathcal{H}^2\mathcal{K}\beta^{-1} - \epsilon\mathcal{H}^2\beta^{-1}K - \epsilon y\mathcal{H}K\beta^{-1} \right) \mathcal{B}_0g_{tan}. \quad (3.71)
 \end{aligned}$$

# 4 Simulation of surfactant driven thin-film flow on moving surfaces

## 4.1 Introduction

Fourth order partial differential equations (PDEs) appear in numerous fields of mathematics and physics among those are image processing, surface diffusion, computer graphic, chemical coating, cell membrane deformation and fluid dynamics [23, 35, 52, 53, 93, 98, 107]. Unfortunately, compared to second order equations, the literature on the numeric of fourth order PDEs is almost inexistent. One will nevertheless notice a burgeoning interest in the simulation of these equations in the last decade. In [5, 6, 9, 62], the authors analyse numerical methods for both thin film equations and a coupled surfactant driven thin film flow system of equations on planar surfaces. In [39, 57] the level set approach for fourth order PDEs on curved surfaces is discussed. In this class of methods, the original PDE stated on a curved surface modeled by a level set is first extended as a degenerated equation in the whole space, then the new equation is solved in a narrow band near the original surface and the solution projected on the surface. This method will eventually require a new boundary condition on the narrow band boundary. The boundary condition must be well chosen, otherwise the final solution will be severely affected. Most often, the obtained equation is solved using finite element method or finite difference method which of course have very good properties on structured grid [39, 57].

Recently, the finite volume method has been discussed in [34] for the direct simulation of a linear fourth order PDE on curved surfaces. As already mentioned in Chapter II, the finite volume method remains unexplored for direct simulations of PDEs on curved surfaces in general, although it has proven to be advantageous in number of problems such as strong advection dominant problems, simulation on general anisotropic and unstructured meshes and problem requiring conservation of mass. Furthermore, since curved surface meshes are unstructured by nature, the finite volume method appears to be an interesting tool for simulation of PDEs on surfaces. In this chapter, we extend the finite volume methodology developed in Chapter II to the computation of the coupled surfactant driven thin film flow system of equations on a moving surface. In fact, on an evolving substrate, the flow of a thin film on top of which a surfactant concentration spreads, is considered. Different from [5, 6, 9], where the authors project the surfactant equation onto the substrate (planar in their case) using lubrication approximation and discretize the coupled system of equations stated on the same domain, we consider a surfactant equation defined on the free surface. In the context of thin films, the height of the film parameterizes the free surface onto the substrate, thus we transform the diffusion equation of the surfactant concentration into a convection diffusion equation onto a virtual free surface which moves only in the direction of the substrate's normal. In the new setup, the surfactant concentration is advected with the fluid particle velocity tangent to the free surface. We then combine the methodologies proposed in [62] and [57] with our finite volume methodology described in Chapter II to discretize the model thin film problem obtained in Chapter III. Next, we make use of the above mentioned parameterization of the free surface to project the finite volume setup onto the free surface interface for the discretization of the surfactant equation. This process leads to a system of nonlinear equations whose solution gives the height of the thin film as well as the surfactant concentration at the finite volumes cell center.

We should mention that the most used technique for computation of interfacial flows remains the interface tracking methods; we refer to [71, 127] and references therein. The actual method developed

in this chapter can be taken as a variant of this class of methods. Despite the fact that we do not explicitly reconstruct the free surface boundary as it is usually the case in this class of methods, we discretize our surfactant equation on a discrete ghost surface represented by the height of the thin film at finite volumes center point. Let us also mention that the interface tracking method include surface tracking methods [54, 118], volume tracking methods [104, 127] and moving mesh methods [51]. Finally, the chapter is presented as follows: in 4.2 we define the method, in 4.3 we develop the method and in 4.4 we present the numerical results for some test problems.

## 4.2 Problem Setting

As already mentioned in Chapter III, we consider a family of compact, smooth and oriented hyper-surfaces  $\Gamma(t) \subset \mathbb{R}^n$  ( $n = 2, 3$ ) for  $t \in [0, t_{max}]$  generated by a flux function  $\Phi : [0, t_{max}] \times \Gamma^0 \rightarrow \mathbb{R}^n$  defined on a reference surface (substrate)  $\Gamma^0 = \Gamma(0)$  with  $\Gamma(t) = \Phi(t, \Gamma^0)$ . We assume  $\Phi$  to be the restriction of a function also called  $\Phi : [0, t_{max}] \times \mathcal{N}_0 \rightarrow \mathbb{R}^n$ , where  $\mathcal{N}_0 = \mathcal{N}(0)$  is a neighborhood of  $\Gamma^0$  in which the lines normal to  $\Gamma^0$  do not intersect. We also assume that  $\mathcal{N}(t) = \Phi(t, \mathcal{N}_0)$  is a neighborhood of  $\Gamma(t)$  in which the lines normal to  $\Gamma(t)$  do not intersect. We finally assume our initial surface  $\Gamma^0$  to be at least  $C^5$  smooth and  $\Phi \in C^1([0, t_{max}], C^5(\mathcal{N}_0))$ . Considering the restriction of  $\Phi$  onto  $\Gamma^0$ , we denote by  $v_\Gamma = \partial_t \Phi$  the velocity of a substrate material point and assume its decomposition  $v_\Gamma = v_{\Gamma, \nu} \nu + v_{\Gamma, tan}$  into a scalar velocity  $v_{\Gamma, \nu}$  in the direction of the surface normal  $\nu$  and a tangential velocity  $v_{\Gamma, tan}$ . It is clear from the definitions that the latter functions depend on time and space variables. This will be the case for any function considered in this chapter and we will be omitting the arguments unless necessary. Let us consider a thin viscous and incompressible liquid flowing on the above described substrate  $\Gamma^0$  as it undergoes its movement as described in Chapter III. We assume the entire fluid to be included in the domain  $\mathcal{N}(t)$  at any time  $t$ . On top of this film (at the free surface (fluid-air interface)) a surfactant is spreading while the film is evolving. We assume the effect of gravity and Van-der Waals forces on the system. We refer to Chapter III, Figure 3.1, for an illustration of this setup. This phenomenon is governed by a set of PDEs derived in Chapter III. First, the evolution of surfactant on the free surface  $\overline{FS}(t)$  is governed by

$$\frac{\partial \Pi}{\partial t} + (\nabla_{FS} \cdot (\Pi v_{FS})) = \frac{1}{\mathcal{P}_e} \nabla_{FS} \cdot (D_{FS} \nabla_{FS} \Pi), \quad (4.1)$$

where  $\Pi$  is the surfactant concentration on the free surface,  $\mathcal{P}_e$  is the Peclet number,  $\nabla_{FS}$  is the dimensionless free surface tangential gradient operator,  $v_{FS}$  is the dimensionless velocity of the fluid particle on  $\overline{FS}(t)$  and the free surface tangential operator  $D_{FS}$  is the surfactant diffusivity tensor. We assume  $D_{FS}$  to be the restriction on the free surface tangent bundle of a global elliptic operator in  $C^0([0, t_{max}], C^1(\mathcal{N}_0))$ . The free surface velocity is defined by  $v_{FS} = v_\Gamma - \epsilon H (\nabla_\Gamma v_{\Gamma, \nu} + K v_{\Gamma, tan}) + v_{RFS}$ , where  $v_{RFS}$  is the relative velocity of the fluid particle at the free surface. The component  $v_{RFS, tan} = v_{RFS} - (v_{RFS} \cdot \nu) \nu$  of  $v_{RFS}$  tangent to the substrate is explicitly defined by

$$\begin{aligned} v_{RFS, tan} &= \left( \frac{1}{2} H^2 \text{Id} - \frac{1}{6} \epsilon H^3 (\mathcal{K} \text{Id} + K) + \left[ H \text{Id} - \epsilon H^2 \left( \frac{1}{2} \mathcal{K} \text{Id} + K \right) \right] \beta^{-1} \right) \nabla_\Gamma (-\phi + C' \gamma \mathcal{K}_{FS}) \\ &+ \left[ (\text{Id} - \epsilon H (\mathcal{K} \text{Id} + K)) \beta^{-1} + \left( H - \frac{1}{2} \epsilon H^2 \mathcal{K} \right) \text{Id} \right] \nabla_\Gamma \gamma + \left[ H \beta^{-1} + \frac{1}{2} H^2 \text{Id} \right] \epsilon \mathcal{B}_0 g_\nu \nabla_\Gamma H \\ &+ \left( \frac{1}{2} H^2 \text{Id} - \frac{1}{6} \epsilon H^3 (\mathcal{K} \text{Id} + 4K) + H \beta^{-1} - \epsilon H^2 \left[ \frac{1}{2} \mathcal{K} \beta^{-1} + (\beta^{-1} K + K \beta^{-1}) \right] \right) \mathcal{B}_0 g_{tan}, \end{aligned} \quad (4.2)$$

where  $H$  is the height of the film,  $\text{Id}$  is the identity matrix in  $\mathbb{R}^3$ ,  $K$  is the curvature tensor of the substrate,  $\mathcal{K} := \text{tr}(K)$  (trace of  $K$ ) is the mean curvature of the substrate and  $\phi := A H^{-3}$  is the disjoining pressure with  $A$  being the dimensionless Hamaker constant. If  $A$  is negative, the substrate-fluid interface and the fluid-air interface repel each other and the parallel fluid-air interface

to the substrate persists; if  $A$  is positive these interfaces attract each other and instability occurs (cf. [98]). By  $C'$  we denote the inverse capillary number,  $\mathcal{B}_0$  the Bond number,  $g_{tan}$  the component of the unit gravity vector  $g$  tangent to the substrate,  $g_\nu = g \cdot \nu$ ,  $\nabla_\Gamma$  the substrate gradient operator,  $\mathcal{K}_{FS}$  the free surface mean curvature,  $\beta$  the substrate slip tensor,  $\gamma$  the surface tension and  $\epsilon = \mathcal{H}/\mathcal{L}$  the ratio between the vertical length scale  $\mathcal{H}$  and the horizontal length scale  $\mathcal{L}$ . We recall that

$$\mathcal{K}_{FS} := \mathcal{K} + \epsilon(\mathcal{H}\mathcal{K}_2 + \Delta_\Gamma \mathcal{H}), \quad (4.3)$$

where  $\Delta_\Gamma$  is the substrate Laplace-Beltrami operator and  $\mathcal{K}_2 := \text{tr}(K^2)$  the trace of  $K^2$ . The substrate slip tensor  $\beta$  is assumed to be the restriction on the substrate tangent bundle of a uniformly elliptic tensor also called  $\beta$  in  $C^0([0, t_{max}], C^1(\mathcal{N}_0))$ . Only the restriction of the matrix  $\beta^{-1}$  to the substrate tangential bundle  $(\text{Id} - \nu \otimes \nu)\beta^{-1}(\text{Id} - \nu \otimes \nu)$ , that we again miscall  $\beta^{-1}$ , is included in the model. We will assume  $\beta\nu = \nu$ , and as mentioned in Chapter III the eigen values of  $(\text{Id} - \nu \otimes \nu)\beta(\text{Id} - \nu \otimes \nu)$  will be taken between  $1/\sqrt{\epsilon}$  and  $1/(\epsilon^2)$  for the numerical simulation. We finally recall that

$$\gamma = \frac{1 + E \ln(1 - x\Pi)}{1 + E \ln(1 - x)}, \quad (4.4)$$

where  $x = \frac{\Pi_{eq}}{\bar{\Pi}_\infty}$  is the surfactant coverage with  $\Pi_{eq}$  being the equilibrium concentration of surfactant and  $\bar{\Pi}_\infty$  being the surfactant concentration in the maximum packing limit.  $x$  will be taken between 0 and 0.5 in the numerical simulation.  $E = \frac{RT_a \bar{\Pi}_\infty}{\bar{\gamma}_0}$  represents the surfactant elasticity with  $T_a$  being the absolute temperature in Kelvin,  $\bar{\gamma}_0$  the surface tension of the clean surface ( $\Pi = 0$ ) and  $R$  the universal gas constant. The initial surfactant concentration  $\Pi_0 = \Pi(0, \cdot)$  on the free surface is given and we associate to (4.1) the homogeneous Neumann boundary condition

$$(D_{FS} \nabla_{FS} \Pi) \cdot n_{\partial FS}^l = 0 \quad (4.5)$$

at the boundary  $\partial \overline{FS}(t)$  of the free surface;  $n_{\partial \overline{FS}}^l$  being the free surface outer unit conormal. On the other hand, the thin-film evolution is modeled by

$$\frac{\partial^\Gamma \eta}{\partial t} + \eta \nabla_\Gamma \cdot v_\Gamma + \nabla_\Gamma \cdot F = 0, \quad (4.6)$$

where  $\frac{\partial^\Gamma \eta}{\partial t} := \frac{\partial \eta}{\partial t} + v_\Gamma \cdot \nabla_\Gamma \eta$  is the material derivative of the fluid density

$\eta = \mathcal{H} - \frac{1}{2}\epsilon \mathcal{H}^2 \mathcal{K} + \frac{1}{6}\epsilon^2 \mathcal{H}^3 (\mathcal{K}^2 - \mathcal{K}_2)$  above the substrate  $\Gamma(t)$  and the flux function  $F$  is defined by

$$\begin{aligned} F &= \left[ \frac{1}{3} \mathcal{H}^3 \text{Id} - \frac{1}{3} \epsilon \mathcal{H}^4 \left( \mathcal{K} \text{Id} - \frac{1}{2} K \right) + (\mathcal{H}^2 - \epsilon \mathcal{H}^3 \mathcal{K}) \beta^{-1} \right] \nabla_\Gamma (-\phi + C' \gamma \mathcal{K}_{FS}) \\ &+ \left[ \mathcal{H}^2 \beta^{-1} + \frac{1}{3} \mathcal{H}^3 \text{Id} \right] \epsilon \mathcal{B}_0 g_\nu \nabla_\Gamma \mathcal{H} + \left[ \left( \mathcal{H} - \frac{3}{2} \epsilon \mathcal{H}^2 \mathcal{K} \right) \beta^{-1} + \left( \frac{1}{2} \mathcal{H}^2 - \frac{2}{3} \epsilon \mathcal{H}^3 \mathcal{K} \right) \text{Id} + \frac{1}{3} \epsilon \mathcal{H}^3 K \right] \nabla_\Gamma \gamma \\ &+ \frac{1}{3} \left[ \mathcal{H}^3 \text{Id} - \epsilon \mathcal{H}^4 \left( \mathcal{K} \text{Id} + \frac{1}{2} K \right) \right] \mathcal{B}_0 g_{tan} + ((\mathcal{H}^2 - \epsilon \mathcal{H}^3 \mathcal{K}) \beta^{-1} - \epsilon \mathcal{H}^3 \beta^{-1} K) \mathcal{B}_0 g_{tan}. \end{aligned} \quad (4.7)$$

We assume the initial configuration of the interface  $\mathcal{H}_0 = \mathcal{H}(0, \cdot)$  being given, whereby the whole surface is wetted. We finally consider the homogeneous Neumann boundary condition

$((\nabla_\Gamma \mathcal{H}) \cdot n_{\partial \Gamma}^l = 0)$  at the boundary  $\partial \Gamma(t)$ ;  $n_{\partial \Gamma(t)}^l$  being the unit outer conormal to the substrate. The Dirichlet boundary condition can be easily integrated in the model; of course, if the surface has no boundary, there will be no need to specify any. The functions, operators and tensors defined here are either explicitly or implicitly defined on the substrate  $\Gamma(t)$  through the parametric domain; we will be seeing them as functions defined in the domain  $\mathcal{N}(t)$  via an extension as constant in the normal direction  $\nabla d(\cdot, \Gamma(t))$ , where  $d(\cdot, \Gamma(t))$  is a signed distance to the substrate  $\Gamma(t)$ .

The above mentioned problem has not yet acquired a careful analysis of existence and regularity of a solution. Meanwile the existence of the solution of a slightly modified problem has been recently studied by Uwe Fermum in his PhD thesis [48]. We will nevertheless assume the existence of a sufficiently regular solution which confere a reasonable meaning to our equations.

## 4.3 Derivation of the scheme

### 4.3.1 Reformulation of the problem

As usual in the discretization of fourth order operators, we start by splitting our operator into two second order operators (cf. [6, 34, 59, 61]). First we consider the operator  $\mathfrak{P} = -\epsilon\Delta_\Gamma H$  to which we associate the boundary condition  $(\nabla_\Gamma H) \cdot n_{\partial\Gamma}^l = 0$  on the boundary  $\partial\Gamma$  of the substrate  $\Gamma$ . Next  $\mathfrak{P}$  is taken as variable in (4.2) and (4.7); and our problem is transformed into a system of second order equations. This is clearly the reason of the extensive development of finite volumes for second order operators in the first two chapters. Our discretization problem will be divided into three coupled discretization problems:

**The pressure problem:**

$$\begin{cases} -\epsilon\Delta_\Gamma H & = \mathfrak{P} \\ (\nabla_\Gamma H) \cdot n_{\partial\Gamma}^l & = 0 \text{ on } \partial\Gamma \end{cases} \quad (4.8)$$

The mean curvature of the free surface is redefined by  $\mathcal{K}_{FS} = \mathcal{K} + \epsilon H \mathcal{K}_2 - \mathfrak{P}$ .

**The thin-film problem:**

The thin-film problem is defined by (4.6) and the boundary condition  $[-\mathfrak{D}_5 \nabla_\Gamma (\Phi + C' \gamma \mathfrak{P})] \cdot n_{\partial\Gamma}^l = 0$  on  $\partial\Gamma$  with  $\mathfrak{D}_5 = [\mathbb{H}^2 \beta^{-1} + \frac{1}{3} \mathbb{H}^3 (\text{Id} - 3\epsilon \mathcal{K} \beta^{-1}) - \frac{1}{3} \epsilon \mathbb{H}^4 (\mathcal{K} \text{Id} - \frac{1}{2} K)]$ . Here again, one should replace  $\mathcal{K}_{FS}$  with its new expression in the complementary term  $F$  defined in (4.7).

**The Surfactant problem:**

This problem is defined by (4.1), (4.5) and the definition of  $v_{FS}$  in which (4.2) and (4.4) are important.

Let us group some terms appearing in the fluid velocity (4.2) and in the flux function (4.7).

$$\begin{aligned} \mathfrak{D}_1 &:= (\text{Id} - 3\epsilon \mathcal{K} \beta^{-1}), \mathfrak{D}_2 := (\mathcal{K} \text{Id} - \frac{1}{2} K), \\ \mathfrak{D}_3 &:= (\text{Id} - 3\epsilon \mathcal{K} \beta^{-1} - 3\epsilon \beta^{-1} K), \mathfrak{D}_4 := (\mathcal{K} \text{Id} + \frac{1}{2} K), \mathfrak{D}_5 := [\mathbb{H}^2 \beta^{-1} + \frac{1}{3} \mathbb{H}^3 \mathfrak{D}_1 - \frac{1}{3} \epsilon \mathbb{H}^4 \mathfrak{D}_2], \\ \mathfrak{D}_6 &:= ((C' \mathcal{K} + \epsilon C' H \mathcal{K}_2) [\mathbb{H}^2 \beta^{-1} + \frac{1}{3} \mathbb{H}^3 \mathfrak{D}_1 - \frac{1}{3} \epsilon \mathbb{H}^4 \mathfrak{D}_2] + [\mathbb{H} \beta^{-1} + \frac{1}{2} \mathbb{H}^2 \mathfrak{D}_1 - \frac{2}{3} \epsilon \mathbb{H}^3 \mathfrak{D}_2]), \\ \mathfrak{D}_7 &:= (\epsilon C' \gamma \mathcal{K}_2 [\mathbb{H}^2 \beta^{-1} + \frac{1}{3} \mathbb{H}^3 \mathfrak{D}_1 - \frac{1}{3} \epsilon \mathbb{H}^4 \mathfrak{D}_2] + \epsilon \mathcal{B}_0 g_\nu [\mathbb{H}^2 \beta^{-1} + \frac{1}{3} \mathbb{H}^3 \text{Id}]), \\ \mathfrak{D}_8 &:= [\text{Id} - \epsilon (\mathcal{K} \text{Id} + 2K) \beta^{-1}], \mathfrak{D}_9 := (\mathcal{K} \text{Id} + K), \mathfrak{D}_{10} := (\text{Id} - \epsilon [\mathcal{K} \beta^{-1} + 2(\beta^{-1} K + K \beta^{-1})]), \\ \mathfrak{D}_{11} &:= (\mathcal{K} \text{Id} + 4K), \mathfrak{D}_{12} := (\mathbb{H} \beta^{-1} + \frac{1}{2} \mathbb{H}^2 \mathfrak{D}_8 - \frac{1}{6} \epsilon \mathbb{H}^3 \mathfrak{D}_9), \\ \mathfrak{D}_{13} &:= [C' (\mathcal{K} + \epsilon H \mathcal{K}_2) (\mathbb{H} \beta^{-1} + \frac{1}{2} \mathbb{H}^2 \mathfrak{D}_8 - \frac{1}{6} \epsilon \mathbb{H}^3 \mathfrak{D}_9) + [\beta^{-1} + \mathbb{H} (\text{Id} - \epsilon \mathfrak{D}_9 \beta^{-1}) - \frac{1}{2} \epsilon \mathbb{H}^2 \mathcal{K} \text{Id}]] \\ \mathfrak{D}_{14} &:= [\epsilon C' \gamma \mathcal{K}_2 (\mathbb{H} \beta^{-1} + \frac{1}{2} \mathbb{H}^2 \mathfrak{D}_8 - \frac{1}{6} \epsilon \mathbb{H}^3 \mathfrak{D}_9) + \epsilon \mathcal{B}_0 g_\nu (\mathbb{H} \beta^{-1} + \frac{1}{2} \mathbb{H}^2 \text{Id})]. \end{aligned}$$

In the sequel, we will assume  $\epsilon$  being chosen such that  $\mathfrak{D}_1$  and  $\mathfrak{D}_3$  are strictly positive definite;  $\mathfrak{D}_5$  too will be assumed strictly positive definite if  $\mathbb{H}$  is not zero. The flux function  $F$  defined in (4.7) can now be rewritten as

$$\begin{aligned} F &= -\mathfrak{D}_5 \nabla_\Gamma (\phi + C' \gamma \mathfrak{P}) + \mathfrak{D}_6 \nabla_\Gamma \gamma + \mathfrak{D}_7 \nabla_\Gamma H + C' \gamma \left[ \frac{1}{3} \mathbb{H}^3 \mathfrak{D}_1 - \frac{1}{3} \epsilon \mathbb{H}^4 \mathfrak{D}_2 + \mathbb{H}^2 \beta^{-1} \right] \nabla_\Gamma \mathcal{K} \\ &+ \epsilon C' \gamma \mathbb{H} \left[ \frac{1}{3} \mathbb{H}^3 \mathfrak{D}_1 - \frac{1}{3} \epsilon \mathbb{H}^4 \mathfrak{D}_2 + \mathbb{H}^2 \beta^{-1} \right] \nabla_\Gamma \mathcal{K}_2 + \left[ \frac{1}{3} \mathbb{H}^3 \mathfrak{D}_3 - \epsilon \frac{1}{3} \mathbb{H}^4 \mathfrak{D}_4 + \mathbb{H}^2 \beta^{-1} \right] \mathcal{B}_0 g_{tan} \quad (4.10) \end{aligned}$$

and the component of the interface fluid particle relative velocity tangent to the substrate is transformed to

$$\begin{aligned} v_{RFS,tan} &= -\mathfrak{D}_{12} \nabla_\Gamma (\phi + C' \gamma \mathfrak{P}) + \mathfrak{D}_{13} \nabla_\Gamma \gamma + \mathfrak{D}_{14} \nabla_\Gamma H + C' \gamma \left( \mathbb{H} \beta^{-1} + \frac{1}{2} \mathbb{H}^2 \mathfrak{D}_8 - \frac{1}{6} \epsilon \mathbb{H}^3 \mathfrak{D}_9 \right) \nabla_\Gamma \mathcal{K} \\ &+ \epsilon C' \gamma \mathbb{H} \left( \mathbb{H} \beta^{-1} + \frac{1}{2} \mathbb{H}^2 \mathfrak{D}_8 - \frac{1}{6} \epsilon \mathbb{H}^3 \mathfrak{D}_9 \right) \nabla_\Gamma \mathcal{K}_2 + \left( \mathbb{H} \beta^{-1} + \frac{1}{2} \mathbb{H}^2 \mathfrak{D}_{10} - \frac{1}{6} \epsilon \mathbb{H}^3 \mathfrak{D}_{11} \right) \mathcal{B}_0 g_{tan}. \quad (4.11) \end{aligned}$$



Let us notice that (4.1) can be written as

$$\begin{aligned} & \frac{\partial \Pi}{\partial t} + \nabla_{FS} \cdot [\Pi(v_\Gamma - \epsilon H(\nabla_\Gamma v_{\Gamma, \nu} + K v_{\Gamma, tan}) + (v_{RFS} \cdot (\nu - \epsilon R_h \nabla_\Gamma H))\nu)] \\ & + \nabla_{FS} \cdot [\Pi(\text{Id} - \nu \otimes (\nu - \epsilon R_h \nabla_\Gamma H))v_{RFS, tan}] - \frac{1}{\mathcal{P}_e} \nabla_{FS} \cdot (D_{FS} \nabla_{FS} \Pi) = 0. \end{aligned} \quad (4.12)$$

Let us remark that the free surface normal is given by  $\nu_{FS} = (\nu - \epsilon R_h \nabla_\Gamma H) / \|\nu - \epsilon R_h \nabla_\Gamma H\|$  and the operator  $\mathcal{P}_{FS, \nu} := (\text{Id} - \nu \otimes (\nu - \epsilon R_h \nabla_\Gamma H))$  is the projection operator onto the free surface tangent plane in the direction of the surface normal  $\nu$ . Thus  $v_{FS, pt} := (v_\Gamma - \epsilon H(\nabla_\Gamma v_{\Gamma, \nu} + K v_{\Gamma, tan}) + (v_{RFS} \cdot (\nu - \epsilon R_h \nabla_\Gamma H))\nu)$  is the velocity of the free surface material point  $M(t, s_1, s_2)$  parameterized by  $r(t, s_1, s_2) = X(t, s_1, s_2) + \nu(t, s_1, s_2)H(t, s_1, s_2)$ . Now, plugging (4.10) into (4.6) and (4.11) into (4.12) gives together with (4.8) the following system of PDEs

$$\left\{ \begin{aligned} & \mathfrak{P} = -\epsilon \Delta_\Gamma H & (4.13) \\ & \frac{\partial^\Gamma \eta}{\partial t} + \eta \nabla_\Gamma \cdot v_\Gamma + \nabla_\Gamma \cdot \left[ -\mathfrak{D}_5 \nabla_\Gamma (\phi + C' \gamma \mathfrak{P}) + \mathfrak{D}_6 \nabla_\Gamma \gamma + \mathfrak{D}_7 \nabla_\Gamma H \right. \\ & + C' \gamma \left( \frac{1}{3} H^3 \mathfrak{D}_1 - \frac{1}{3} \epsilon H^4 \mathfrak{D}_2 + H^2 \beta^{-1} \right) \nabla_\Gamma \mathcal{K} + \epsilon C' \gamma H \left( \frac{1}{3} H^3 \mathfrak{D}_1 - \frac{1}{3} \epsilon H^4 \mathfrak{D}_2 + H^2 \beta^{-1} \right) \nabla_\Gamma \mathcal{K}_2 \\ & \left. + \left( \frac{1}{3} H^3 \mathfrak{D}_3 - \epsilon \frac{1}{3} H^4 \mathfrak{D}_4 + H^2 \beta^{-1} \right) \mathcal{B}_0 g_{tan} \right] = 0 & (4.14) \\ & \frac{\partial \Pi}{\partial t} + \nabla_{FS} \cdot (\Pi v_{FS, pt}) + \nabla_{FS} \cdot \left[ \Pi \mathcal{P}_{FS, \nu} \right. \\ & \left[ -\mathfrak{D}_{12} \nabla_\Gamma (\phi + C' \gamma \mathfrak{P}) + \mathfrak{D}_{13} \nabla_\Gamma \gamma + \mathfrak{D}_{14} \nabla_\Gamma H + C' \gamma \left( H \beta^{-1} + \frac{1}{2} H^2 \mathfrak{D}_8 - \frac{1}{6} \epsilon H^3 \mathfrak{D}_9 \right) \nabla_\Gamma \mathcal{K} \right. \\ & \left. + \epsilon C' \gamma H \left( H \beta^{-1} + \frac{1}{2} H^2 \mathfrak{D}_8 - \frac{1}{6} \epsilon H^3 \mathfrak{D}_9 \right) \nabla_\Gamma \mathcal{K}_2 + \left( H \beta^{-1} + \frac{1}{2} H^2 \mathfrak{D}_{10} - \frac{1}{6} \epsilon H^3 \mathfrak{D}_{11} \right) \mathcal{B}_0 g_{tan} \right] \\ & \left. - \frac{1}{\mathcal{P}_e} \nabla_{FS} \cdot (D_{FS} \nabla_{FS} \Pi) = 0. \right. & (4.15) \end{aligned} \right.$$

The following boundary condition is associated to this system of PDEs:

$$\begin{cases} (\nabla_\Gamma H) \cdot n_{\partial\Gamma}^l = 0 & \text{on } \partial\Gamma \end{cases} \quad (4.16)$$

$$\begin{cases} [-\mathfrak{D}_5 \nabla_\Gamma (\phi + C' \gamma \mathfrak{P})] \cdot n_{\partial\Gamma}^l = 0 & \text{on } \partial\Gamma \end{cases} \quad (4.17)$$

$$\begin{cases} (D_{FS} \nabla_{FS} \Pi) \cdot n_{\partial\overline{FS}}^l = 0 & \text{on } \partial\overline{FS}. \end{cases} \quad (4.18)$$

Reformulated in this way, the discretization process will be similar to the one of a convection diffusion and reaction problem and therefore we need to properly identify the role of each term in the concerned equations before applying the well known operator splitting commonly used in the finite volume methodology. Thus, the discretization of the above system will depend on how the substrate advection term  $\nabla_\Gamma \cdot (u \mathfrak{D}_\Gamma \nabla_\Gamma \varpi)$ , the free surface advection term  $\nabla_{FS} \cdot (u(\text{Id} - \nu_{FS} \otimes \nu_{FS}) \mathfrak{D}_\Gamma \nabla_\Gamma \varpi)$ , the surface diffusion operator  $\nabla_\Gamma \cdot (\mathfrak{D}_\Gamma \nabla_\Gamma u)$ , the free surface diffusion operator  $\nabla_{FS} \cdot (\mathfrak{D}_{FS} \nabla_{FS} u)$ , the mixed free surface diffusion operator  $\nabla_{FS} \cdot ((\text{Id} - \nu_{FS} \otimes \nu_{FS}) \mathfrak{D}_\Gamma \nabla_\Gamma u)$ , the substrate gradient  $\nabla_\Gamma u$  and the free surface gradient  $\nabla_{FS} u$  are approximated.  $u$  represents a scalar variable,  $\varpi$  represents a geometric scalar variable such as  $\mathcal{K}$ ,  $\mathfrak{D}_\Gamma$  and  $\mathfrak{D}_{FS}$  represent second order tensor on the tangent bundle of  $\Gamma(t)$  and  $\overline{FS}(t)$ , respectively. We recall that any scalar variable or tensor here is viewed as defined in the entire domain  $\mathcal{N}(t)$  via an extension as constant in the normal direction  $\nabla d(\cdot, \Gamma(t))$ , where  $d(\cdot, \Gamma(t))$  is a signed distance to the substrate  $\Gamma(t)$ . Let us now introduce an appropriate geometric setting for the finite volume discretization of the system of PDEs (4.13), (4.14), (4.15).

### 4.3.2 Geometric setting

We will restrict our presentation to a two dimensional surface in  $\mathbb{R}^3$ . The generalization of the numerical method presented here is straight forward. Let us consider the same setup as in Chapter II which consist of a family of uniformly admissible polygonal surfaces  $\{\Gamma_h^k\}_{k=0, \dots, k_{max}}$ , with  $\Gamma_h^k$  approximating  $\Gamma^k := \Gamma(t_k)$  for  $t_k = k\tau$  and  $k_{max}\tau = t_{max}$  (cf. Figure 4.1).  $h$  represents the maximum diameter of cells on the whole family of polygonizations,  $\tau$  the time step size and  $k$  the index of a time step. Successive polygonizations share the same grid topology and given the set of vertices  $p_j^0$  on the initial polygonal surface  $\Gamma_h^0$ , the vertices of  $\Gamma_h^k$  lie on motion trajectories; thus they are evaluated based on the flux function  $\Phi$ , i.e.,  $p_j^k = \Phi(t_k, p_j^0)$ . Upper indices denote the explicit geometric realization at the corresponding time step. Different from Chapter II, we assume

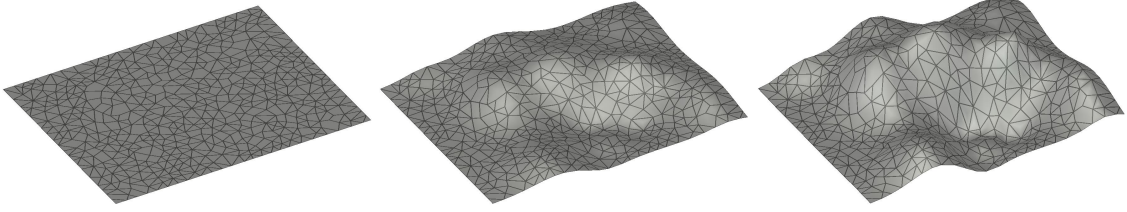


Figure 4.1: Sequence of polygonizations  $\Gamma_h^k$  approximating an evolving surface.

our polygonizations to be uniformly admissible  $(4, h)$ -polygonizations. This globally means that there exists a uniform constant  $\mathcal{C}$  such that the maximum distance between a point  $X$  on a polygonal surface  $\Gamma_h^k$  and the surface  $\Gamma^k$  is less than  $\mathcal{C}h^2$  while the maximum distance between a vertex  $p_j^k$  and  $\Gamma^k$  is less than  $\mathcal{C}h^4$ . We refer to Definition 2.3.5 in Chapter II for the extensive definition of this notion. This main assumption will allow for consistency of the fourth order operators, as well as for the consistency of the geometric operator  $K$ , computed from the meshes using an algorithm which combines polygonal fitting and least square method similar to the algorithm described in [22]. Let us now denote by  $S^{l,k} := \mathcal{P}^k S^k$  the orthogonal projection of the cell  $S^k \subset \Gamma_h^k$  onto  $\Omega^k \supset \Gamma^k$ . With a slight misuse of notation, we also denote by  $\mathcal{P}_{FS, \nu}^k$  the affine projection onto the free surface  $\overline{FS}^k$  in the direction of the substrate normal  $\nu$ . Let us define  $S_{FS}^{l,k} := \mathcal{P}_{FS, \nu}^k S^{l,k} = \mathcal{P}_{FS, \nu}^k S^k$  the projection of  $S^{l,k}$  and  $S^k$  onto  $\overline{FS}^k$ ; here, the free surface is extended continuously after the triple line (Substrate-Fluid-Air interface) to allow for the definition of this cell near the boundary  $\partial \overline{FS}$ . We should notice that  $m\left(\overline{FS}^k \setminus \bigcup_{S^k} (\overline{S}_{FS}^{l,k} \cap \overline{FS}^k)\right) \leq \mathcal{C}h^2$ ;  $m(\cdot)$  denotes the two dimensional Hausdorff measure and  $\overline{S}^{l,k}$  the closure of  $S^{l,k}$ . Our finite volume scheme for the discretization of the above mentioned problem will be based on a suitable approximation of the height  $H$  on the substrate curved cells  $S^{l,k}$  via the discretization of (4.13) and (4.14) on the approximated surfaces  $\Gamma_h^k$  and a suitable discretization of the surfactant concentration  $\Pi$  on the curved free surface cells  $S_{FS}^{l,k}$  via a direct discretization of (4.15) on  $\overline{FS}^k$  using the local parametric description  $r(t, X(t, s_1, s_2))$  of the free surface from the substrate local parameterization  $X(t, s_1, s_2)$ . In the same way as in Chapter II, we subdivide cells  $S^k$  into virtual subcells  $S_{p_i}^k$  attached to vertices  $p_i^k$  (cf. Chapter II, Figure 2.4) in such a way that the edges of cells are subdivided into two subedges and the subcells  $S_{p_i}^k$  form a conformal mesh of  $\Gamma_h^k$  (cf. Chapter II, Figure 2.5). Next, we denote by  $S_{p_i}^{l,k} := \mathcal{P}^k S_{p_i}^k$  the orthogonal projection of the subcell  $S_{p_i}^k$  onto  $\Omega^k \supset \Gamma^k$  and by  $S_{FS, p_i}^{l,k} := \mathcal{P}_{FS, \nu}^k S_{p_i}^k = \mathcal{P}_{FS, \nu}^k S_{p_i}^{l,k}$  the projection of  $S_{p_i}^k$  and  $S_{p_i}^{l,k}$  onto  $\overline{FS}^k$  in the direction of  $\nu$ . Finally, as in Chapter II, our approach will be based on defining a suitable interpolation of scalar functions  $u$  as well as the approximation of the surface gradient operator  $\nabla_{\Gamma} u$  and the free surface gradient operator  $\nabla_{FS} u$  around the vertices  $p_i^k$  from the

value of  $u$  at cell centers. We will then consider the linear interpolation presented in Chapter II for any approximation on the substrate  $\Gamma^k$  and the procedure that leads to this construction will be reproduced on the free surface subcells using the local parameterization  $r(t_k, X(t_k, s_1, s_2))$  of the free surface and a proper use of Proposition 2.4.1, Chapter II.

### 4.3.3 Discrete gradient operators

The procedure of reconstructing the gradient operator is the same as in Chapter II up to slight modifications due to the adaptation of the results to special use (surface flow or interface flow). Let us then consider a vertex  $p_i^k$ . As in Chapter II, we locally order the subcells  $S_{p_i,j}^k$  around  $p_i^k$  counter clockwise around the substrate normal  $\nu$  through  $p_i^k$  and rename the center points  $X_{S_j}^k$  by  $X_{p_i,j}^k$ . The subedges  $\sigma_{p_i,j-1/2}^k$  around  $p_i^k$  inherit the same order and we assume  $\sigma_{p_i,1/2}^k$  and  $\sigma_{p_i,3/2}^k$  being edge segments of  $S_{p_i,1}^k$ . Here too, “ $j+1$ ” will be used in a cyclic way for closed system and therefore  $j+1 \equiv j+1 \pmod{n_{p_i}}$  in that case;  $n_{p_i}$  denotes the number of cells around  $p_i^k$ . We define on each subedge  $\sigma_{p_i,j-1/2}^k$  a virtual point  $X_{p_i,j-1/2}^k$  and on each subcell  $S_{p_i,j}^k$ , we define the covariant vectors  $e_{p_i,j|j-1/2}^k := X_{p_i,j-1/2}^k - X_{p_i,j}^k$  and  $e_{p_i,j|j+1/2}^k := X_{p_i,j+1/2}^k - X_{p_i,j}^k$  which are used to approximate the tangent plane  $T_{p_i,j}^k := \text{Span}\{e_{p_i,j|j-1/2}^k, e_{p_i,j|j+1/2}^k\}$  to points of  $S_{p_i,j}^k$  (cf. Figure 2.6 Chapter II). Next we construct the contravariant (dual) basis  $(\mu_{p_i,j|j-1/2}^k, \mu_{p_i,j|j+1/2}^k)$  on  $T_{p_i,j}^k$  such that  $e_{p_i,j|j-1/2}^k, \mu_{p_i,j|j-1/2}^k = 1$ ,  $e_{p_i,j|j-1/2}^k, \mu_{p_i,j|j+1/2}^k = 0$ ,  $e_{p_i,j|j+1/2}^k, \mu_{p_i,j|j-1/2}^k = 0$  and  $e_{p_i,j|j+1/2}^k, \mu_{p_i,j|j+1/2}^k = 1$ . Let us define the curved segments  $\sigma_{p_i,j-1/2}^{l,k} := \{y \in \Gamma^k | y = \text{argmin } d(x, \Gamma^k), x \in \sigma_{p_i,j-1/2}^{l,k}\}$  and the approximate normal  $\nu_{p_i,j}^k := (e_{p_i,j|j+1/2}^k \wedge e_{p_i,j|j-1/2}^k) / \|e_{p_i,j|j+1/2}^k \wedge e_{p_i,j|j-1/2}^k\|$  to points of  $S_{p_i,j}^k$ ; the approximate unit outer conormals to  $\sigma_{p_i,j-1/2}^{l,k}$  and  $\sigma_{p_i,j+1/2}^{l,k}$  will be taken as the unit vectors  $n_{p_i,j|j-1/2}^k$  and  $n_{p_i,j|j+1/2}^k$  of  $T_{p_i,j}^k$  normal to  $\sigma_{p_i,j-1/2}^k$  and  $\sigma_{p_i,j+1/2}^k$  respectively and pointing outward from  $S_{p_i,j}^k$ . We again refer to Figure 2.6 Chapter II for this setup. Finally, given a substrate tensor  $\mathcal{D}^k$  defined such that  $\mathcal{D}^k \nabla_{\Gamma(t_k)} u$  has a weak surface divergence in  $\mathbb{L}^2 \left( \bigcup_j (S_{p_i,j}^{l,k} \cap \Gamma^k) \right)$ , we define the gradient

$$\nabla_{\mathcal{D},p_i,j}^k u := (U_{\mathcal{D},p_i,j-1/2}^k - U_{p_i,j}^k) \mu_{p_i,j|j-1/2}^k + (U_{\mathcal{D},p_i,j+1/2}^k - U_{p_i,j}^k) \mu_{p_i,j|j+1/2}^k, \quad (4.19)$$

where the virtual values  $U_{\mathcal{D},p_i,j-1/2}^k$  at subedge virtual points  $X_{p_i,j-1/2}^k$  are related to values  $U_{p_i,j}^k$  at cell centers  $X_{p_i,j}^k$  by

$$\tilde{U}_{\mathcal{D},p_i,\sigma}^k = \mathbf{Coef}_{\mathcal{D},p_i}^k \tilde{U}_{p_i}^k. \quad (4.20)$$

The vector  $\tilde{U}_{\mathcal{D},p_i,\sigma}^k := (U_{\mathcal{D},p_i,1/2}^k, U_{\mathcal{D},p_i,3/2}^k, \dots)^\top$  represents the subedge virtual values, the vector  $\tilde{U}_{\mathcal{D},p_i}^k := (U_{\mathcal{D},p_i,1}^k, U_{\mathcal{D},p_i,2}^k, \dots)^\top$  the cell center values and the matrix  $\mathbf{Coef}_{\mathcal{D},p_i}^k$  is defined by

$$\mathbf{Coef}_{\mathcal{D},p_i}^k = \left( \sqrt{\mathbf{B}_{p_i}^k} \right)^{-1} \left( M_{\mathcal{D},p_i}^k \left( \sqrt{\mathbf{B}_{p_i}^k} \right)^{-1} \right)^\dagger \left( N_{\mathcal{D},p_i}^k - M_{\mathcal{D},p_i}^k \left( \mathbf{B}_{p_i}^k \right)^{-1} \mathbf{C}_{p_i}^k \right) + \left( \mathbf{B}_{p_i}^k \right)^{-1} \mathbf{C}_{p_i}^k. \quad (4.21)$$

The matrices involved here are sparse matrices whose nonzeros entries are given by

$$\begin{aligned}
 (\mathbf{B}_{p_i}^k)_{j,j} &= m_{p_i,j-1}^k \|\mu_{p_i,j-1|j-1/2}^k\|^2 + m_{p_i,j}^k \|\mu_{p_i,j|j-1/2}^k\|^2, \\
 (\mathbf{B}_{p_i}^k)_{j+1,j} &= (\mathbf{B}_{p_i}^k)_{j,j+1} = m_{p_i,j}^k \mu_{p_i,j|j-1/2}^k \cdot \mu_{p_i,j|j+1/2}^k, \\
 (\mathbf{C}_{p_i}^k)_{j,j} &= m_{p_i,j}^k \left( \|\mu_{p_i,j|j-1/2}^k\|^2 + \mu_{j|j-1/2}^k \cdot \mu_{p_i,j|j+1/2}^k \right), \\
 (\mathbf{C}_{p_i}^k)_{j+1,j} &= m_{p_i,j}^k \left( \|\mu_{p_i,j|j+1/2}^k\|^2 + \mu_{j|j-1/2}^k \cdot \mu_{p_i,j|j+1/2}^k \right), \\
 (M_{\mathcal{D},p_i}^k)_{j,j-1} &= m_{p_i,j-1/2}^k \lambda_{p_i,j-3/2|j-1|j-1/2}^k, \\
 (M_{\mathcal{D},p_i}^k)_{j,j} &= m_{p_i,j-1/2}^k (\lambda_{p_i,j-1|j-1/2}^k + \lambda_{p_i,j|j-1/2}^k), \\
 (M_{\mathcal{D},p_i}^k)_{j,j+1} &= m_{p_i,j-1/2}^k \lambda_{p_i,j+1/2|j|j-1/2}^k, \\
 (N_{\mathcal{D},p_i}^k)_{j,j-1} &= m_{p_i,j-1/2}^k (\lambda_{p_i,j-1|j-1/2}^k + \lambda_{p_i,j-3/2|j-1|j-1/2}^k), \\
 (N_{\mathcal{D},p_i}^k)_{j,j} &= m_{p_i,j-1/2}^k (\lambda_{p_i,j|j-1/2}^k + \lambda_{p_i,j+1/2|j|j-1/2}^k),
 \end{aligned}$$

where  $m_{p_i,j}^k$  is the two dimensional Hausdorff measure of  $S_{p_i,j}^k$ ,  $m_{p_i,j-1/2}^k$  the one dimensional Hausdorff measure of  $\sigma_{p_i,j-1/2}^k$ ,

$$\begin{aligned}
 \lambda_{p_i,j|j-1/2}^k &= n_{p_i,j|j-1/2}^k \cdot \mathcal{D}_{p_i,j}^k \mu_{p_i,j|j-1/2}^k, & \lambda_{p_i,j+1/2|j|j-1/2}^k &= n_{p_i,j|j-1/2}^k \cdot \mathcal{D}_{p_i,j}^k \mu_{p_i,j|j+1/2}^k, \\
 \lambda_{p_i,j-1/2|j|j+1/2}^k &= n_{p_i,j|j+1/2}^k \cdot \mathcal{D}_{p_i,j}^k \mu_{p_i,j|j-1/2}^k, & \lambda_{p_i,j|j+1/2}^k &= n_{p_i,j|j+1/2}^k \cdot \mathcal{D}_{p_i,j}^k \mu_{p_i,j|j+1/2}^k,
 \end{aligned}$$

with  $\mathcal{D}_{p_i,j}^k = (\text{Id} - \nu_{p_i,j}^k \wedge \nu_{p_i,j}^k) \mathcal{D}^k(X_{p_i,j}^k) (\text{Id} - \nu_{p_i,j}^k \wedge \nu_{p_i,j}^k) \cdot \left( M_{p_i}^k \left( \sqrt{\mathbf{B}_{p_i}^k} \right)^{-1} \right)^\dagger$  is the Moore-

Penrose inverse of  $M_{p_i}^k \left( \sqrt{\mathbf{B}_{p_i}^k} \right)^{-1}$ . We refer to Chapter II for details on the construction of these matrices.

Now let us define  $S_{FS,p_i,j}^{l,k} := \mathcal{P}_{FS,\nu}^k S_{p_i,j}^{l,k}$  and assume being given a free surface tensor  $\mathcal{D}_{FS}^k$  such that  $\mathcal{D}_{FS}^k \nabla_{\Gamma(t_k)} u$  has a weak free surface divergence in  $\mathbb{L}^2 \left( \bigcup_j (S_{FS,p_i,j}^{l,k} \cap \overline{FS}^k) \right)$ ; the approximation of  $\nabla_{\Gamma(t_k)} u$  will then require a slight modification to satisfy the Proposition 2.4.1 in Chapter II on the free surface. For this purpose, we introduce some geometric approximations on the free surface. To begin with, we notice that, given a covariant basis  $(e_1, e_2)$  of the tangent plane at the point  $X(t, s_1, s_2) \in \Gamma(t)$ , the corresponding contravariant basis at the point  $r(t, X(t, s_1, s_2)) := X(t, s_1, s_2) + \nu(X(t, s_1, s_2))H(t, X(t, s_1, s_2)) \in \overline{FS}(t)$  reads

$$((\text{Id} - \epsilon HK)e_1 + \epsilon[(\nabla_{\Gamma} H) \cdot e_1]\nu, (\text{Id} - \epsilon HK)e_2 + \epsilon[(\nabla_{\Gamma} H) \cdot e_2]\nu). \quad (4.22)$$

Thus, if  $(\mu_1, \mu_2)$  is the contravariant basis of  $(e_1, e_2)$ , the contravariant basis of (4.22) reads

$$(R_{\mathbb{H}}\mu_1 - [(R_{\mathbb{H}}\mu_1) \cdot \nu_{FS}]\nu_{FS}, R_{\mathbb{H}}\mu_2 - [(R_{\mathbb{H}}\mu_2) \cdot \nu_{FS}]\nu_{FS}). \quad (4.23)$$

We recall that  $R_{\mathbb{H}} := (\text{Id} - \epsilon HK)^{-1}$  and the free surface normal is given by  $\nu_{FS} := \frac{\nu - \epsilon R_{\mathbb{H}} \nabla_{\Gamma} H}{\sqrt{1 + \epsilon^2 \|R_{\mathbb{H}} \nabla_{\Gamma} H\|^2}}$ .

Next we denote by  $H_{p_i,j}^k = H_{S_j}^k = H(t_k, X_{S_j}^k)$  the height at the center point  $X_{S_j}^k = X_{p_i,j}^k$  and we approximate the curvature tensor at points on the subcells  $S_{p_i,j}^{l,k}$  by  $K(X(t, s_1, s_2)) \approx K_{p_i,j}^k := \mathcal{P}_{FS,\nu}^k K(X_{p_i,j}^k) \mathcal{P}_{FS,\nu}^k$ . The free surface tangent plane at points  $r(t, X(t, s_1, s_2))$  on  $S_{p_i,j}^{l,k}$  can then be approximated by

$$\begin{aligned}
 T_{FS,p_i,S_j}^k &:= \text{Span} \left\{ (\text{Id} - \epsilon H_{p_i,j}^k K_{p_i,j}^k) e_{p_i,j|j-1/2}^k + \epsilon[(\nabla_{\text{Id},p_i,j}^k H) \cdot e_{p_i,j|j-1/2}^k] \nu_{p_i,j}^k, \right. \\
 &\quad \left. (\text{Id} - \epsilon H_{p_i,j}^k K_{p_i,j}^k) e_{p_i,j|j+1/2}^k + \epsilon[(\nabla_{\text{Id},p_i,j}^k H) \cdot e_{p_i,j|j+1/2}^k] \nu_{p_i,j}^k \right\},
 \end{aligned}$$

where  $\nabla_{\text{Id}, p_i, j}^k \mathbf{H}$  is determined by the formulae (4.19), (4.20) and (4.21). We conclude using (4.23) that the contravariant basis of the above mentioned basis of  $T_{FS, p_i, S_j}^k$  is  $(\mu_{FS, p_i, j|j-1/2}^k, \mu_{FS, p_i, j|j+1/2}^k)$  defined by

$$\begin{aligned} \mu_{FS, p_i, j|j-1/2}^k &:= R_{p_i, j}^k \mu_{p_i, j|j-1/2}^k - [(R_{p_i, j}^k \mu_{p_i, j|j-1/2}^k) \cdot \nu_{FS, p_i, j}^k] \nu_{FS, p_i, j}^k, \text{ and} \\ \mu_{FS, p_i, j|j+1/2}^k &:= R_{p_i, j}^k \mu_{p_i, j|j+1/2}^k - [(R_{p_i, j}^k \mu_{p_i, j|j+1/2}^k) \cdot \nu_{FS, p_i, j}^k] \nu_{FS, p_i, j}^k, \end{aligned}$$

where  $R_{p_i, j}^k := (\text{Id} - \epsilon \mathbf{H}_{p_i, j}^k K_{p_i, j}^k)^{-1}$  approximates  $R_{\mathbb{H}}^{-1}$  and  $\nu_{FS, p_i, j}^k := \frac{\nu_{p_i, j}^k - \epsilon R_{p_i, j}^k \nabla_{\text{Id}, p_i, j}^k \mathbf{H}}{\sqrt{1 + \epsilon^2 \|R_{p_i, j}^k \nabla_{\text{Id}, p_i, j}^k \mathbf{H}\|^2}}$

approximates  $\nu_{FS}$ . Let us now denote by  $q_{p_i, j-1/2}^k$  and  $q_{p_i, j+1/2}^k$  the points that satisfy  $\sigma_{p_i, j-1/2}^k = [p_i^k, q_{p_i, j-1/2}^k]$  and  $\sigma_{p_i, j+1/2}^k = [p_i^k, q_{p_i, j+1/2}^k]$  (cf. Figure 2.4, Chapter II). We define the vectors  $\varrho_{p_i, j|j-1/2}^k := q_{p_i, j-1/2}^k - p_i^k$ ,  $\varrho_{p_i, j|j+1/2}^k := q_{p_i, j+1/2}^k - p_i^k$  and approximate the unit conormal to  $\sigma_{FS, p_i, j-1/2}^{l, k}$  and  $\sigma_{FS, p_i, j+1/2}^{l, k}$  outward from  $S_{FS, p_i, j}^{l, k}$  by the respective unit vectors  $n_{FS, p_i, j|j-1/2}^k \in T_{FS, p_i, S_j}^k$  and  $n_{FS, p_i, j|j+1/2}^k \in T_{FS, p_i, S_j}^k$  perpendicular to

$$\begin{aligned} \varrho_{FS, p_i, j|j-1/2}^k &:= (\text{Id} - \epsilon \mathbf{H}_{p_i, j}^k K_{p_i, j}^k) \varrho_{p_i, j-1/2}^k + \epsilon [(\nabla_{p_i, j}^k \mathbf{H}) \cdot \varrho_{p_i, j-1/2}^k] \nu_{p_i, j}^k \text{ and} \\ \varrho_{FS, p_i, j|j+1/2}^k &:= (\text{Id} - \epsilon \mathbf{H}_{p_i, j}^k K_{p_i, j}^k) \varrho_{p_i, j+1/2}^k + \epsilon [(\nabla_{p_i, j}^k \mathbf{H}) \cdot \varrho_{p_i, j+1/2}^k] \nu_{p_i, j}^k, \text{ respectively,} \end{aligned}$$

and which point outward from  $S_{FS, p_i, j}^{l, k}$ . We also denote by

$$m_{FS, p_i, j+1/2}^k := \left( \|\varrho_{FS, p_i, j|j+1/2}^k\| + \|\varrho_{FS, p_i, j+1|j+1/2}^k\| \right) / 2$$

the approximation of the one dimensional Hausdorff measure of  $\sigma_{FS, p_i, j+1/2}^{l, k}$ .

Now, on subedges  $\sigma_{FS, p_i, j-1/2}^{l, k}$ , we apply a discrete version of Proposition 2.4.1 in Chapter II, namely

$$\begin{aligned} m_{FS, p_i, j-1/2}^k \mathcal{D}_{FS, p_i, j-1/2}^k \nabla_{\mathcal{D}_{FS, p_i, j-1/2}^k} u \cdot n_{FS, p_i, j-1/2}^k \\ + m_{FS, p_i, j-1/2}^k \mathcal{D}_{FS, p_i, j}^k \nabla_{\mathcal{D}_{FS, p_i, j}^k} u \cdot n_{FS, p_i, j|j-1/2}^k = 0, \end{aligned} \quad (4.24)$$

where  $\mathcal{D}_{FS, p_i, j-1}^k := (\text{Id} - \nu_{FS}^k \otimes \nu_{FS}^k) \mathcal{D}_{FS}^k (X_{p_i, j}^k) (\text{Id} - \nu_{FS}^k \otimes \nu_{FS}^k)$  and as in formula (4.19),

$$\nabla_{\text{mix}, \mathcal{D}_{FS, p_i, j}^k} u := (U_{\text{mix}, \mathcal{D}_{FS, p_i, j-1/2}^k} - U_{p_i, j}^k) \mu_{p_i, j|j-1/2}^k + (U_{\text{mix}, \mathcal{D}_{FS, p_i, j+1/2}^k} - U_{p_i, j}^k) \mu_{p_i, j|j+1/2}^k. \quad (4.25)$$

The subedge virtual values  $U_{\text{mix}, \mathcal{D}_{FS, p_i, j-1/2}^k}^k$  and  $U_{\text{mix}, \mathcal{D}_{FS, p_i, j+1/2}^k}^k$  approximate  $u(t_k, X_{p_i, j-1/2}^k)$  and  $u(t_k, X_{p_i, j+1/2}^k)$  respectively. The equations defined by (4.24) together with the boundary conditions can be written in a matrix form as

$$M_{\text{mix}, \mathcal{D}_{FS, p_i}^k}^k \tilde{U}_{\text{mix}, \mathcal{D}_{FS, p_i, \sigma}^k}^k = N_{\text{mix}, \mathcal{D}_{FS, p_i}^k}^k \tilde{U}_{p_i}^k, \quad (4.26)$$

where  $\tilde{U}_{\text{mix}, \mathcal{D}_{FS, p_i, \sigma}^k}^k := (U_{\text{mix}, \mathcal{D}_{FS, p_i, 1/2}^k}^k, U_{\text{mix}, \mathcal{D}_{FS, p_i, 3/2}^k}^k, \dots)^\top$  and the matrices involved here are sparse matrices with nonzero entries defined by

$$\begin{aligned} (M_{\text{mix}, \mathcal{D}_{FS, p_i}^k}^k)_{j, j-1} &= m_{FS, p_i, j-1/2}^k \lambda_{\text{mix}, p_i, j-3/2|j-1|j-1/2}^k, \\ (M_{\text{mix}, \mathcal{D}_{FS, p_i}^k}^k)_{j, j} &= m_{FS, p_i, j-1/2}^k (\lambda_{\text{mix}, p_i, j-1|j-1/2}^k + \lambda_{p_i, j|j-1/2}^k), \\ (M_{\text{mix}, \mathcal{D}_{FS, p_i}^k}^k)_{j, j+1} &= m_{FS, p_i, j-1/2}^k \lambda_{\text{mix}, p_i, j+1/2|j-1/2}^k, \\ (N_{\text{mix}, \mathcal{D}_{FS, p_i}^k}^k)_{j, j-1} &= m_{FS, p_i, j-1/2}^k (\lambda_{\text{mix}, p_i, j-1|j-1/2}^k + \lambda_{p_i, j-3/2|j-1|j-1/2}^k), \\ (N_{\text{mix}, \mathcal{D}_{FS, p_i}^k}^k)_{j, j} &= m_{FS, p_i, j-1/2}^k (\lambda_{\text{mix}, p_i, j|j-1/2}^k + \lambda_{p_i, j+1/2|j-1/2}^k) \end{aligned}$$

with

$$\begin{aligned}
 \lambda_{mix,p_i,j|j-1/2}^k &= n_{FS,p_i,j|j-1/2}^k \cdot \mathcal{D}_{FS,p_i,j}^k \mu_{p_i,j|j-1/2}^k, \\
 \lambda_{mix,p_i,j+1/2|j-1/2}^k &= n_{FS,p_i,j|j-1/2}^k \cdot \mathcal{D}_{FS,p_i,j}^k \mu_{p_i,j|j+1/2}^k, \\
 \lambda_{mix,p_i,j-1/2|j+1/2}^k &= n_{FS,p_i,j|j+1/2}^k \cdot \mathcal{D}_{FS,p_i,j}^k \mu_{p_i,j|j-1/2}^k, \\
 \lambda_{mix,p_i,j|j+1/2}^k &= n_{FS,p_i,j|j+1/2}^k \cdot \mathcal{D}_{FS,p_i,j}^k \mu_{p_i,j|j+1/2}^k.
 \end{aligned}$$

We should mention here that the first and the last line will be readjusted for boundary points according to boundary condition. Here, if  $u = H$ , we have an homogeneous Neumann boundary condition and if  $u$  is a substrate intrinsic variable such as mean curvature  $\mathcal{K}$  for example, we have a Dirichlet boundary condition since the values are computed from data as already mentioned. As in Chapter II, we require the solution to guarantee the minimum substrate  $\mathbb{H}^1$  norm to  $\nabla_{\mathcal{D}_{FS,p_i,j-1}}^k u$ ; namely

$$\left\{ \begin{array}{l} \text{Find } \tilde{U}_{mix,\mathcal{D}_{FS,p_i,\sigma}}^k \text{ in } B_{p_i}^k := \left\{ \tilde{V}_{p_i,\sigma}^k := (V_{p_i,1/2}^k, V_{p_i,3/2}^k, \dots)^\top \mid M_{mix,\mathcal{D}_{FS,p_i}}^k \tilde{V}_{p_i,\sigma}^k = N_{mix,\mathcal{D}_{FS,p_i}}^k \tilde{U}_{p_i}^k \right\} \\ \text{such that} \\ \tilde{U}_{mix,\mathcal{D}_{FS,p_i,\sigma}}^k = \underset{\tilde{V}_{p_i,\sigma}^k \in B_{p_i}^k}{\text{arcmi}} \sum_j m_{p_i,j}^k \left\| \left[ V_{p_i,j-1/2}^k - U_{p_i,j}^k \right] \mu_{p_i,j|j-1/2}^k + \left[ V_{p_i,j+1/2}^k - U_{p_i,j}^k \right] \mu_{p_i,j|j+1/2}^k \right\|^2. \end{array} \right.$$

Again, similar arguments as in Chapter II leads to

$$\tilde{U}_{mix,\mathcal{D}_{FS,p_i,\sigma}}^k = \mathbf{Coef}_{mix,\mathcal{D}_{FS,p_i}}^k \tilde{U}_{p_i}^k. \quad (4.27)$$

where the matrix  $\mathbf{Coef}_{mix,\mathcal{D}_{FS,p_i}}^k$  is defined by

$$\begin{aligned}
 \mathbf{Coef}_{mix,\mathcal{D}_{FS,p_i}}^k &= (\mathbf{B}_{p_i}^k)^{-1} \mathbf{C}_{p_i}^k \\
 &+ \left( \sqrt{\mathbf{B}_{p_i}^k} \right)^{-1} \left( M_{mix,\mathcal{D}_{FS,p_i}}^k \left( \sqrt{\mathbf{B}_{p_i}^k} \right)^{-1} \right)^\dagger \left( N_{mix,\mathcal{D}_{FS,p_i}}^k - M_{mix,\mathcal{D}_{FS,p_i}}^k (\mathbf{B}_{p_i}^k)^{-1} \mathbf{C}_{p_i}^k \right). \quad (4.28)
 \end{aligned}$$

The substrate gradient  $\nabla_\Gamma u$  is then fully approximated using (4.25) (4.30) and (4.31) to obtain a discrete gradient whose  $\mathcal{D}_{FS}^k \nabla_\Gamma u$  satisfies Proposition 2.4.1 in Chapter II as requested in this work in the discrete setup.

Let us now have a look at a free surface gradient operator  $\nabla_{FS} u$ , defined such that  $\mathcal{D}_{FS}^k \nabla_{FS} u$  has a weak divergence in  $\mathbb{L}^2 \left( \bigcup_j (S_{FS,p_i,j}^{l,k} \cap \overline{FS}^k) \right)$ . Here the free surface gradient is approximated by

$$\nabla_{FS,\mathcal{D}_{FS,p_i,j}}^k u := (U_{FS,\mathcal{D}_{FS,p_i,j-1/2}}^k - U_{p_i,j}^k) \mu_{FS,p_i,j|j-1/2}^k + (U_{FS,\mathcal{D}_{FS,p_i,j+1/2}}^k - U_{p_i,j}^k) \mu_{FS,p_i,j|j+1/2}^k, \quad (4.29)$$

where the virtual values  $U_{FS,\mathcal{D}_{FS,p_i,j-1/2}}^k$  and  $U_{FS,\mathcal{D}_{FS,p_i,j+1/2}}^k$  approximate the values

$u(t_k, \mathcal{P}_{FS,\nu}^k X_{p_i,j-1/2}^k)$  and  $u(t_k, \mathcal{P}_{FS,\nu}^k X_{p_i,j+1/2}^k)$ , respectively. Following the same reasoning on  $\overline{FS}^k$  as in Chapter II on  $\Gamma^k$  we obtain

$$\tilde{U}_{FS,\mathcal{D}_{FS,p_i,\sigma}}^k = \mathbf{Coef}_{FS,\mathcal{D}_{FS,p_i}}^k \tilde{U}_{p_i}^k, \quad (4.30)$$

where  $\tilde{U}_{FS,\mathcal{D}_{FS,p_i,\sigma}}^k := (U_{FS,\mathcal{D}_{FS,p_i,1/2}}^k, U_{FS,\mathcal{D}_{FS,p_i,3/2}}^k, \dots)^\top$  and

$$\begin{aligned}
 \mathbf{Coef}_{FS,\mathcal{D}_{FS,p_i}}^k &= (\mathbf{B}_{FS,p_i}^k)^{-1} \mathbf{C}_{FS,p_i}^k \\
 &+ \left( \sqrt{\mathbf{B}_{FS,p_i}^k} \right)^{-1} \left( M_{FS,\mathcal{D}_{FS,p_i}}^k \left( \sqrt{\mathbf{B}_{FS,p_i}^k} \right)^{-1} \right)^\dagger \left( N_{FS,\mathcal{D}_{FS,p_i}}^k - M_{FS,\mathcal{D}_{FS,p_i}}^k (\mathbf{B}_{FS,p_i}^k)^{-1} \mathbf{C}_{FS,p_i}^k \right). \quad (4.31)
 \end{aligned}$$

The matrices involved here are also sparse and the nonzero values are given by

$$\begin{aligned}
 (\mathbf{B}_{FS, p_i}^k)_{j,j} &= m_{FS, p_i, j-1}^k \|\mu_{FS, p_i, j-1|j-1/2}^k\|^2 + m_{FS, p_i, j}^k \|\mu_{FS, p_i, j|j-1/2}^k\|^2, \\
 (\mathbf{B}_{FS, p_i}^k)_{j+1,j} &= (\mathbf{B}_{FS, p_i}^k)_{j,j+1} = m_{FS, p_i, j}^k \mu_{FS, p_i, j|j-1/2}^k \cdot \mu_{FS, p_i, j|j+1/2}^k, \\
 (\mathbf{C}_{FS, p_i}^k)_{j,j} &= m_{FS, p_i, j}^k \left( \|\mu_{FS, p_i, j|j-1/2}^k\|^2 + \mu_{j|j-1/2}^k \cdot \mu_{FS, p_i, j|j+1/2}^k \right), \\
 (\mathbf{C}_{FS, p_i}^k)_{j+1,j} &= m_{FS, p_i, j}^k \left( \|\mu_{FS, p_i, j|j+1/2}^k\|^2 + \mu_{j|j-1/2}^k \cdot \mu_{FS, p_i, j|j+1/2}^k \right), \\
 (M_{FS, \mathcal{D}_{FS, p_i}}^k)_{j,j-1} &= m_{FS, p_i, j-1/2}^k \lambda_{FS, p_i, j-3/2|j-1|j-1/2}^k, \\
 (M_{FS, \mathcal{D}_{FS, p_i}}^k)_{j,j} &= m_{FS, p_i, j-1/2}^k (\lambda_{FS, p_i, j-1|j-1/2}^k + \lambda_{FS, p_i, j|j-1/2}^k), \\
 (M_{FS, \mathcal{D}_{FS, p_i}}^k)_{j,j+1} &= m_{FS, p_i, j-1/2}^k \lambda_{FS, p_i, j+1/2|j|j-1/2}^k, \\
 (N_{FS, \mathcal{D}_{FS, p_i}}^k)_{j,j-1} &= m_{FS, p_i, j-1/2}^k (\lambda_{FS, p_i, j-1|j-1/2}^k + \lambda_{FS, p_i, j-3/2|j-1|j-1/2}^k), \\
 (N_{FS, \mathcal{D}_{FS, p_i}}^k)_{j,j} &= m_{FS, p_i, j-1/2}^k (\lambda_{FS, p_i, j|j-1/2}^k + \lambda_{FS, p_i, j+1/2|j|j-1/2}^k),
 \end{aligned}$$

where,

$$\begin{aligned}
 \lambda_{FS, p_i, j|j-1/2}^k &= n_{FS, p_i, j|j-1/2}^k \cdot \mathcal{D}_{p_i, j}^k \mu_{FS, p_i, j|j-1/2}^k, \\
 \lambda_{FS, p_i, j+1/2|j|j-1/2}^k &= n_{FS, p_i, j|j-1/2}^k \cdot \mathcal{D}_{p_i, j}^k \mu_{FS, p_i, j|j+1/2}^k, \\
 \lambda_{FS, p_i, j-1/2|j|j+1/2}^k &= n_{FS, p_i, j|j+1/2}^k \cdot \mathcal{D}_{p_i, j}^k \mu_{FS, p_i, j|j-1/2}^k, \\
 \lambda_{FS, p_i, j|j+1/2}^k &= n_{FS, p_i, j|j+1/2}^k \cdot \mathcal{D}_{p_i, j}^k \mu_{FS, p_i, j|j+1/2}^k
 \end{aligned}$$

and  $m_{FS, p_i, j}^k := \left( 1 - \epsilon H_{p_i, j}^k \mathcal{K}_{p_i, j}^k + \frac{1}{2} \epsilon^2 (H_{p_i, j}^k)^2 [(\mathcal{K}_{p_i, j}^k)^2 - (\mathcal{K}_2)_{p_i, j}^k] \right) \sqrt{1 + \epsilon^2 \|R_{p_i, j}^k \nabla_{\text{Id}, p_i, j}^k \mathbb{H}\|^2} m_{p_i, j}^k$  is the approximation of the two dimensional Hausdorff measure of  $S_{FS, p_i, j}^{l, k}$ . The variables  $\mathcal{K}_{p_i, j}^k$  and  $(\mathcal{K}_2)_{p_i, j}^k$ , respectively, approximate  $\mathcal{K}$  and  $\mathcal{K}_2$  at  $\mathcal{P}^k X_{p_i, j}^k$ . With this preliminaries at hand, we can now introduce the finite volume discretization of the coupled surfactant driven thin-film flow (4.13)-(4.14)-(4.15)-(4.16)-(4.17)-(4.18).

#### 4.3.4 Finite volume discretization

In this section, we derive the finite volume formulation of the above mentioned problem. This is done by giving a discrete integration of equation (4.13) on each cell  $S^{l, k} \cap \Gamma^k$ , a discrete integration of equation (4.14) in the domain  $\{(t, a) | t \in [t_k, t_{k+1}], a \in S^{l, k}(t) \cap \Gamma(t)\}$  and a discrete integration of equation (4.15) in the domain  $\{(t, a) | t \in [t_k, t_{k+1}], a \in S_{FS}^{l, k}(t) \cap \overline{FS}(t)\}$ . We approximate the integration of (4.13) on the cell  $S^{l, k} \cap \Gamma^k$

$$\int_{S^{l, k} \cap \Gamma^k} \mathfrak{P} da = -\epsilon \int_{S^{l, k} \cap \Gamma^k} \Delta_{\Gamma} \mathbb{H} da$$

by

$$m_S^k \mathfrak{P}_S^k = -\epsilon m_S^k \mathbb{D}_{\Gamma, S}^k(\text{Id}, \mathbb{H}), \quad (4.32)$$

where  $m_S^k := m(S^k)$ ,  $\mathfrak{P}_S^k := \mathfrak{P}(t_k, X_S^k)$  and  $m_S^k \mathbb{D}_{\Gamma, S}^k(\text{Id}, \mathbb{H})$  given through equation (4.37) below approximates the integral  $\int_{S^{l, k} \cap \Gamma^k} \Delta_{\Gamma} \mathbb{H} da$ . Let us now split the Van der Waals potential  $\phi$  into an increasing function  $\phi_{inc}$  and a decreasing function  $\phi_{dec}$  as proposed in [5, 62] (i.e.  $\phi = \phi_{inc} + \phi_{dec}$ ). In this simple case,  $\phi = A\mathbb{H}^{-3} = \phi_{inc}$  if  $A$  is negative and  $\phi = A\mathbb{H}^{-3} = \phi_{dec}$  else. We also split the tensor  $-\mathfrak{D}_7$  into a positive semi definite tensor  $\mathfrak{D}_{7,+}$  and a negative semidefinite tensor  $\mathfrak{D}_{7,-}$  (i.e.  $-\mathfrak{D}_7 = \mathfrak{D}_{7,+} + \mathfrak{D}_{7,-}$ ). For this purpose, given a scalar function  $u$  we denote by  $u_+ := (u + |u|)/2$  and by  $u_- := (u - |u|)/2$ . We then define

$$\mathfrak{D}_{7,+} := - \left( \epsilon C' \gamma_- \mathcal{K}_2 \left[ H^2 \beta^{-1} + \frac{1}{3} H^3 \mathfrak{D}_1 - \frac{1}{3} \epsilon H^4 \mathfrak{D}_2 \right] + \epsilon \mathcal{B}_0 g_{\nu,-} \left[ H^2 \beta^{-1} + \frac{1}{3} H^3 \text{Id} \right] \right),$$

$$\mathfrak{D}_{7,-} := - \left( \epsilon C' \gamma_+ \mathcal{K}_2 \left[ H^2 \beta^{-1} + \frac{1}{3} H^3 \mathfrak{D}_1 - \frac{1}{3} \epsilon H^4 \mathfrak{D}_2 \right] + \epsilon \mathcal{B}_0 g_{\nu,+} \left[ H^2 \beta^{-1} + \frac{1}{3} H^3 \text{Id} \right] \right),$$

where  $g_{\nu,+} := (g_\nu + |g_\nu|)/2$  and  $g_{\nu,-} := (g_\nu - |g_\nu|)/2$ . The discretization of operators involving  $\phi_{inc}$  or  $\mathfrak{D}_{7,+}$  ( $\phi_{dec}$  or  $\mathfrak{D}_{7,-}$ ) will be implicit (explicit). A similar operation, usually called convexity splitting has already been used to solve second and fourth order diffusion on surface (see [57, 126] and references therein). In these papers, the authors require the splitting to be such that the matrices  $\mathfrak{D}_{7,+}$  and  $\mathfrak{D}_{7,-}$  are respectively strictly positive definite and strictly negative definite tensors. This would be achieved here by simply adding  $c\text{Id}$  to  $\mathfrak{D}_{7,+}$  and subtracting  $c\text{Id}$  to  $\mathfrak{D}_{7,-}$ ;  $c$  being a small strictly positive constant. Let us mention that the aim in the context of their work was to obtain a stable scheme and to avoid the implicit discretization of the nonlinear operator; thus they would choose to have  $\mathfrak{D}_{7,+} = C\text{Id}$  where  $C$  is a positive constant and  $\mathfrak{D}_{7,-} = -C\text{Id} - \mathfrak{D}_{7,-}$ . Unfortunately, the advantage of doing so is not always certain as reported in [57] in the context of solving a fourth order parabolic problem on a surface having area of very high curvatures. One needs for such a geometry a very small time step and the computation time is even increased compared to the fully explicit discretization of the problem. Also, the numerical viscosity introduced in the system might be very important since, as reported again in [57], big value of  $C$  slow down the process and the positivity is not guaranteed for problems having positive solutions. In the context of a thin film on a moving surface, it is difficult to avoid an implicit nonlinear term. Our main concern here is to separate diffusion from backward diffusion caused by the discretization, without adding too much numerical viscosity in the scheme and preserve at the same time the structure of the problem. If the surface is flat for example, the terms containing the curvatures should dissapear so that we remain with a typical discretization on a flat surface. It is clear that a wrong discretization of diffusion or backward diffusion will lead to instabilities. Let us remark here that the tensors  $\mathfrak{D}_{7,+}$  and  $\mathfrak{D}_{7,-}$  might be degenerated; this will not affect our method since the optimization procedure used to construct the fluxes remains consistent in these cases. The integral of (4.14) on  $\{(t, a) | t \in [t_k, t_{k+1}], a \in S^{l,k}(t) \cap \Gamma(t)\}$

$$\begin{aligned} & \int_{t_k}^{t_{k+1}} \int_{S^{l,k}(t) \cap \Gamma(t)} \left( \frac{\partial^\Gamma \eta}{\partial t} + \eta \nabla_\Gamma \cdot v_\Gamma \right) da dt + \int_{t_k}^{t_{k+1}} \int_{S^{l,k}(t) \cap \Gamma(t)} \nabla_\Gamma \cdot [-\mathfrak{D}_5 \nabla_\Gamma (\phi + C' \gamma \mathfrak{P})] da dt \\ & + \int_{t_k}^{t_{k+1}} \int_{S^{l,k}(t) \cap \Gamma(t)} \nabla_\Gamma \cdot [\mathfrak{D}_6 \nabla_\Gamma \gamma + \mathfrak{D}_7 \nabla_\Gamma H] da dt \\ & + \int_{t_k}^{t_{k+1}} \int_{S^{l,k}(t) \cap \Gamma(t)} \nabla_\Gamma \cdot \left[ C' \gamma \left( \frac{1}{3} H^3 \mathfrak{D}_1 - \frac{1}{3} \epsilon H^4 \mathfrak{D}_2 + H^2 \beta^{-1} \right) \nabla_\Gamma \mathcal{K} \right] da dt \\ & + \int_{t_k}^{t_{k+1}} \int_{S^{l,k}(t) \cap \Gamma(t)} \nabla_\Gamma \cdot \left[ \epsilon C' \gamma H \left( \frac{1}{3} H^3 \mathfrak{D}_1 - \frac{1}{3} \epsilon H^4 \mathfrak{D}_2 + H^2 \beta^{-1} \right) \nabla_\Gamma \mathcal{K}_2 \right] da dt \\ & + \int_{t_k}^{t_{k+1}} \int_{S^{l,k}(t) \cap \Gamma(t)} \nabla_\Gamma \cdot \left[ \left( \frac{1}{3} H^3 \mathfrak{D}_3 - \epsilon \frac{1}{3} H^4 \mathfrak{D}_4 + H^2 \beta^{-1} \right) \mathcal{B}_0 g_{tan} \right] da dt = 0 \end{aligned}$$

is then approximated using a semi-implicit scheme as follows

$$\begin{aligned} & m_S^{k+1} \eta_S^{k+1} - m_S^k \eta_S^k \\ & + \tau \int_{S^{l,k}(t_{k+1}) \cap \Gamma^{k+1}} \left( \nabla_\Gamma \cdot [-\mathfrak{D}_5 \nabla_\Gamma (\phi_{inc} + C' \gamma_+ \mathfrak{P})] - \nabla_\Gamma \cdot [\mathfrak{D}_{7,+} \nabla_\Gamma H] \right) da \\ & + \tau \int_{S^{l,k} \cap \Gamma^k} \nabla_\Gamma \cdot [-\mathfrak{D}_5 \nabla_\Gamma (\phi_{dec} + C' \gamma_- \mathfrak{P})] da + \tau \int_{S^{l,k} \cap \Gamma^k} \nabla_\Gamma \cdot [\mathfrak{D}_6 \nabla_\Gamma \gamma - \mathfrak{D}_{7,-} \nabla_\Gamma H] da \\ & + \tau \int_{S^{l,k} \cap \Gamma^k} \nabla_\Gamma \cdot \left[ C' \gamma \left( \frac{1}{3} H^3 \mathfrak{D}_1 - \frac{1}{3} \epsilon H^4 \mathfrak{D}_2 + H^2 \beta^{-1} \right) \nabla_\Gamma \mathcal{K} \right] da \\ & + \tau \int_{S^{l,k} \cap \Gamma^k} \nabla_\Gamma \cdot \left[ \epsilon C' \gamma H \left( \frac{1}{3} H^3 \mathfrak{D}_1 - \frac{1}{3} \epsilon H^4 \mathfrak{D}_2 + H^2 \beta^{-1} \right) \nabla_\Gamma \mathcal{K}_2 \right] da \end{aligned}$$



$$+ \tau \int_{S^{l,k} \cap \Gamma^k} \nabla_\Gamma \cdot \left[ \left( \frac{1}{3} \mathbb{H}^3 \mathfrak{D}_3 - \epsilon \frac{1}{3} \mathbb{H}^4 \mathfrak{D}_4 + \mathbb{H}^2 \beta^{-1} \right) \mathcal{B}_{0g_{tan}} \right] da = 0. \quad (4.33)$$

The detailed discretization of the space integrals appearing here is presented below in Section 4.3.4 (Discretization of the substrate diffusion operator  $\mathfrak{D}_\Gamma(\mathcal{D}_\Gamma, u) = \nabla_\Gamma \cdot (\mathcal{D}_\Gamma \nabla_\Gamma u)$ ) and Section 4.3.4 (Discretization of the substrate advection operator  $\mathfrak{D}_{\Gamma,1}(\mathcal{D}_\Gamma, \varpi, u) = \nabla_\Gamma \cdot (u \mathcal{D}_\Gamma \nabla_\Gamma \varpi)$ ). Finally, we approximate the integral of (4.15)

$$\begin{aligned} & \int_{t_k}^{t_{k+1}} \int_{S_{FS}^{l,k}(t) \cap \overline{FS}(t)} \left[ \frac{\partial \Pi}{\partial t} + \nabla_{FS} \cdot (\Pi v_{FS,pt}) \right] da dt \\ & + \int_{t_k}^{t_{k+1}} \int_{S_{FS}^{l,k}(t) \cap \overline{FS}(t)} \nabla_{FS} \cdot (\Pi \mathcal{P}_{FS,\nu} [-\mathfrak{D}_{12} \nabla_\Gamma (\phi + C' \gamma \mathfrak{P}) + \mathfrak{D}_{13} \nabla_\Gamma \gamma + \mathfrak{D}_{14} \nabla_\Gamma \mathbb{H}]) da dt \\ & + \int_{t_k}^{t_{k+1}} \int_{S_{FS}^{l,k}(t) \cap \overline{FS}(t)} \nabla_{FS} \cdot \left[ \Pi \mathcal{P}_{FS,\nu} \left[ +C' \gamma \left( \mathbb{H} \beta^{-1} + \frac{1}{2} \mathbb{H}^2 \mathfrak{D}_8 - \frac{1}{6} \epsilon \mathbb{H}^3 \mathfrak{D}_9 \right) \nabla_\Gamma \mathcal{K} \right] \right] da dt \\ & + \epsilon C' \int_{t_k}^{t_{k+1}} \int_{S_{FS}^{l,k}(t) \cap \overline{FS}(t)} \nabla_{FS} \cdot \left[ \Pi \mathcal{P}_{FS,\nu} \left[ \gamma \mathbb{H} \left( \mathbb{H} \beta^{-1} + \frac{1}{2} \mathbb{H}^2 \mathfrak{D}_8 - \frac{1}{6} \epsilon \mathbb{H}^3 \mathfrak{D}_9 \right) \nabla_\Gamma \mathcal{K}_2 \right] \right] da dt \\ & + \int_{t_k}^{t_{k+1}} \int_{S_{FS}^{l,k}(t) \cap \overline{FS}(t)} \nabla_{FS} \cdot \left[ \Pi \mathcal{P}_{FS,\nu} \left( \mathbb{H} \beta^{-1} + \frac{1}{2} \mathbb{H}^2 \mathfrak{D}_{10} - \frac{1}{6} \epsilon \mathbb{H}^3 \mathfrak{D}_{11} \right) \mathcal{B}_{0g_{tan}} \right] da dt \\ & - \frac{1}{\mathcal{P}_e} \int_{t_k}^{t_{k+1}} \int_{S_{FS}^{l,k}(t) \cap \overline{FS}(t)} \nabla_{FS} \cdot (D_{FS} \nabla_{FS} \Pi) da dt = 0 \end{aligned} \quad (4.34)$$

by

$$\begin{aligned} & \sum_{p_i \in \partial S^k} \left( m_{FS,p_i,\mathcal{J}(p_i,S)}^{k+1} \Pi_S^{k+1} - m_{FS,p_i,\mathcal{J}(p_i,S)}^k \Pi_S^k \right) \\ & + \tau \int_{S_{FS}^{l,k} \cap \overline{FS}^k} \nabla_{FS} \cdot (\Pi \mathcal{P}_{FS,\nu} [-\mathfrak{D}_{12} \nabla_\Gamma (\phi + C' \gamma \mathfrak{P}) + \mathfrak{D}_{13} \nabla_\Gamma \gamma + \mathfrak{D}_{14} \nabla_\Gamma \mathbb{H}]) da dt \\ & + \tau \int_{S_{FS}^{l,k} \cap \overline{FS}^k} \nabla_{FS} \cdot \left[ \Pi \mathcal{P}_{FS,\nu} \left[ +C' \gamma \left( \mathbb{H} \beta^{-1} + \frac{1}{2} \mathbb{H}^2 \mathfrak{D}_8 - \frac{1}{6} \epsilon \mathbb{H}^3 \mathfrak{D}_9 \right) \nabla_\Gamma \mathcal{K} \right] \right] da dt \\ & + \epsilon C' \tau \int_{S_{FS}^{l,k} \cap \overline{FS}^k} \nabla_{FS} \cdot \left[ \Pi \mathcal{P}_{FS,\nu} \left[ \gamma \mathbb{H} \left( \mathbb{H} \beta^{-1} + \frac{1}{2} \mathbb{H}^2 \mathfrak{D}_8 - \frac{1}{6} \epsilon \mathbb{H}^3 \mathfrak{D}_9 \right) \nabla_\Gamma \mathcal{K}_2 \right] \right] da dt \\ & + \tau \int_{S_{FS}^{l,k} \cap \overline{FS}^k} \nabla_{FS} \cdot \left[ \Pi \mathcal{P}_{FS,\nu} \left( \mathbb{H} \beta^{-1} + \frac{1}{2} \mathbb{H}^2 \mathfrak{D}_{10} - \frac{1}{6} \epsilon \mathbb{H}^3 \mathfrak{D}_{11} \right) \mathcal{B}_{0g_{tan}} \right] da dt \\ & - \frac{1}{\mathcal{P}_e} \tau \int_{S_{FS}^{l,k}(t_{k+1}) \cap \overline{FS}(t_{k+1})} \nabla_{FS} \cdot (D_{FS} \nabla_{FS} \Pi) da dt = 0. \end{aligned} \quad (4.35)$$

By  $\mathcal{J}(p_i, S)$  we denote the local index of  $S^k$  around  $p_i$  and we recall that the approximation of the free surface virtual cell  $S_{FS,p_i,j}^{l,k} \cap \overline{FS}^k$  is given by

$m_{FS,p_i,j}^k := \left( 1 - \epsilon \mathbb{H}_{p_i,j}^k \mathcal{K}_{p_i,j}^k + \frac{1}{2} \epsilon^2 (\mathbb{H}_{p_i,j}^k)^2 [(\mathcal{K}_{p_i,j}^k)^2 - (\mathcal{K}_2)_{p_i,j}^k] \right) \sqrt{1 + \epsilon^2 \|R_{p_i,j}^k \nabla_{\text{Id},p_i,j}^k \mathbb{H}\|^2} m_{p_i,j}^k$ . The detailed discretization of the space integral involved here is presented in Section 4.3.4 (Discretization of the free surface mix advection operator  $\mathfrak{D}_{FS,2}(\mathfrak{D}_{FS}, u) = \nabla_{FS} \cdot (\Pi \mathfrak{D}_{FS} \nabla_\Gamma u)$ ) and Section 4.3.4 (Discretization of the free surface diffusion operator  $\mathfrak{D}_{FS,1}(\mathcal{D}_{FS}, \Pi) = \nabla_{FS} \cdot (\mathfrak{D}_{FS} \nabla_{FS} \Pi)$ ).

Let us now introduce the discretization of the substrate diffusion operator  $\nabla_\Gamma \cdot (\mathcal{D}_\Gamma \nabla_\Gamma u)$ . This includes  $\Delta_\Gamma \mathbb{H}$ ,  $\nabla_\Gamma \cdot [\mathfrak{D}_{7,+} \nabla_\Gamma \mathbb{H}]$ ,  $\nabla_\Gamma \cdot [\mathfrak{D}_{7,-} \nabla_\Gamma \mathbb{H}]$ ,  $\nabla_\Gamma \cdot [\mathfrak{D}_5 \nabla_\Gamma (\phi_{inc} + C' \gamma_+ \mathfrak{P})]$ ,  $\nabla_\Gamma \cdot [\mathfrak{D}_5 \nabla_\Gamma (\phi_{dec} + C' \gamma_- \mathfrak{P})]$ .

**Discretization of the substrate diffusion operator**  $\mathbf{D}_\Gamma(\mathcal{D}_\Gamma, u) = \nabla_\Gamma \cdot (\mathcal{D}_\Gamma \nabla_\Gamma u)$

We integrate the diffusion operator  $\mathbf{D}_\Gamma$  on the curved domain  $S^{l,k} \cap \Gamma^k$ , thus

$$\begin{aligned} \int_{S^{l,k} \cap \Gamma^k} \mathbf{D}_\Gamma(\mathcal{D}_\Gamma, u) da &= \int_{S^{l,k} \cap \Gamma^k} \nabla_\Gamma \cdot (\mathcal{D}_\Gamma \nabla_\Gamma u) da \\ &= \int_{\partial(S^{l,k} \cap \Gamma^k)} (\mathcal{D}_\Gamma \nabla_\Gamma u) \cdot n_{\partial(S^{l,k} \cap \Gamma^k)} dl, \end{aligned} \quad (4.36)$$

where  $n_{\partial(S^{l,k} \cap \Gamma^k)}$  is the unit outer conormal to the boundary  $\partial(S^{l,k} \cap \Gamma^k)$  of  $S^{l,k} \cap \Gamma^k$ . An approximation of (4.36) is given by

$$\begin{aligned} m_S^k \mathbf{D}_{\Gamma,S}^k(\mathcal{D}_\Gamma, u) &= \sum_{p_i \in \partial S^k} \left[ m_{p_i, \mathcal{J}(p_i, S)-1/2}^k \left( \mathcal{D}_{p_i, \mathcal{J}(p_i, S)}^k \nabla_{\mathcal{D}_\Gamma, p_i, \mathcal{J}(p_i, S)}^k u \right) \cdot n_{p_i, \mathcal{J}(p_i, S)|\mathcal{J}(p_i, S)-1/2}^k \right. \\ &\quad \left. + m_{p_i, \mathcal{J}(p_i, S)+1/2}^k \left( \mathcal{D}_{p_i, \mathcal{J}(p_i, S)}^k \nabla_{\mathcal{D}_\Gamma, p_i, \mathcal{J}(p_i, S)}^k u \right) \cdot n_{p_i, \mathcal{J}(p_i, S)|\mathcal{J}(p_i, S)+1/2}^k \right], \end{aligned} \quad (4.37)$$

where  $\mathbf{D}_{\Gamma,S}^k(\mathcal{D}_\Gamma, u)$  is the value of  $\mathbf{D}_\Gamma(\mathcal{D}_\Gamma, u)$  at the cell center point  $X_S^k$  and time instant  $t_k$ . The discrete gradient operator  $\nabla_{\mathcal{D}_\Gamma, p_i, \mathcal{J}(p_i, S)}^k u$  is determined by the formulae (4.19), (4.20) and (4.21). Let us introduce  $\mathcal{V}_h^k$ , the set of piecewise constant functions on cells,

$$\mathcal{V}_h^k := \{U^k : \Gamma_h^k \rightarrow \mathbb{R} \mid \forall S^k \subset \Gamma_h^k, U^k|_{S^k} = \text{const}\}. \quad (4.38)$$

As already mentioned here, elements of this set too will be seen as defined in the entire domain  $\mathcal{N}(t_k)$  via the extension as constant in the direction of  $\nabla d(\cdot, \Gamma(t_k) \cap \mathcal{P}^k \Gamma_h^k)$ , where  $d(\cdot, \Gamma(t_k) \cap \mathcal{P}^k \Gamma_h^k)$  is a sign distance function to the surface  $\Gamma(t_k) \cap \mathcal{P}^k \Gamma_h^k$ . Our solution at the time step  $t_k$  will then be seen as an element of this set. We wish to build a seminorm on  $\mathcal{V}_h^k$ . For this purpose, we first multiply each equation of (4.37) by the corresponding cell center value  $-U_S^k$  and then sum the resulting equations over all cells and use (4.20) to obtain

$$-\sum_{S^k} m_S^k \mathbf{D}_{\Gamma,S}^k(\mathcal{D}_\Gamma, u) U_S^k = \sum_{p_i \in \partial S^k} \left( \tilde{U}_{p_i}^k \right)^\top A_{\mathcal{D}_\Gamma, p_i}^k \tilde{U}_{p_i}^k, \quad (4.39)$$

where  $A_{\mathcal{D}_\Gamma, p_i}^k := A_{\mathcal{D}_\Gamma, p_i, c}^k - A_{\mathcal{D}_\Gamma, p_i, \sigma}^k \mathbf{Coef}_{\mathcal{D}_\Gamma, p_i}^k$  with  $A_{\mathcal{D}_\Gamma, p_i, c}^k$  being a diagonal matrix and  $A_{\mathcal{D}_\Gamma, p_i, \sigma}^k$  a sparse rectangular matrix whose nonzero elements are given by

$$\begin{aligned} (A_{\mathcal{D}_\Gamma, p_i, c}^k)_{j,j} &:= m_{p_i, j-1/2}^k (\lambda_{p_i, j|j-1/2}^k + \lambda_{p_i, j+1/2|j-1/2}^k) \\ &\quad + m_{p_i, j+1/2}^k (\lambda_{p_i, j|j+1/2}^k + \lambda_{p_i, j-1/2|j+1/2}^k), \\ (A_{\mathcal{D}_\Gamma, p_i, \sigma}^k)_{j,j} &:= m_{p_i, j-1/2}^k \lambda_{p_i, j|j-1/2}^k + m_{p_i, j+1/2}^k \lambda_{p_i, j-1/2|j+1/2}^k, \\ (A_{\mathcal{D}_\Gamma, p_i, \sigma}^k)_{j,j+1} &:= m_{p_i, j-1/2}^k \lambda_{p_i, j+1/2|j-1/2}^k + m_{p_i, j+1/2}^k \lambda_{p_i, j|j+1/2}^k. \end{aligned}$$

For boundary points, the first and the last lines of these matrices will be readjusted according to the boundary condition. The submatrices  $A_{\mathcal{D}_\Gamma, p_i}^k$  satisfy  $A_{\mathcal{D}_\Gamma, p_i}^k \mathbf{1}_{p_i} = \mathbf{0}_{p_i}$ , where  $\mathbf{1}_{p_i} := (1, 1, \dots)^\top$  and  $\mathbf{0}_{p_i} := (0, 0, \dots)^\top$ . This is due to the minimization procedure introduced in the interpolation of the virtual values on subedges. The procedure forces the system to pick the solution of minimum gradient. This is particularly important at the flow front since the spatial variation in cells diffusion tensor is important and the local system solved for the interpolation of virtual values around front vertices can become noninvertible. Furthermore it may happen that some of the discrete diffusion tensors in cells around a vertex are identically null ( $\mathcal{D}_{p_i, j}^k \equiv 0 \text{Id}$ ); for example in the transition region “from curved to flat region” when the diffusion tensor depends only on the curvature tensor. In this case too, as already said, the minimization procedure allows to obtain a good interpolation of

virtual unknown and therefore a consistent approximation of fluxes. Let us also remark that if the submatrices  $A_{\mathcal{D}_\Gamma, p_i}^k + (\mathbf{1}_{p_i} \otimes \mathbf{1}_{p_i})/n_{p_i}$  are positive semi-definite respectively strictly positive definite for all vertices, then the right hand side of (4.39) defines a seminorm respectively a norm when the homogeneous Dirichlet boundary condition is considered at the boundary. We recall that  $n_{p_i}$  denotes the number of cells around the vertex point  $p_i$ . Since the submatrices  $A_{\mathcal{D}_\Gamma, p_i}^k$  basically depend on the choice of the subedges virtual points and the discrete cell tensor  $\mathcal{D}_\Gamma^k$  around  $p_i^k$ , we assume the virtual points being chosen such that the submatrices  $A_{\mathcal{D}_\Gamma, p_i}^k + (\mathbf{1}_{p_i} \otimes \mathbf{1}_{p_i})/n_{p_i}$  are positive semi-definite if these diffusion tensors around  $p_i^k$  are positive semi-definite and strictly positive definite if the diffusion tensors are strictly positive definite.

We will now introduce the discretization of substrate advection operators involving the substrate gradient operator. These operators are of the form  $\mathfrak{D}_{\Gamma,1}(\mathcal{D}_\Gamma, \varpi, u) = \nabla_\Gamma \cdot (u \mathcal{D}_\Gamma \nabla_\Gamma \varpi)$ , where  $u$  is a power of  $H$ ,  $\mathcal{D}_\Gamma$  is a matrix which does not depend on  $H$  and  $\varpi$  is either the surfactant concentration  $\Pi$  or a geometric quantity ( $\mathcal{K}$ ,  $\mathcal{K}_2$  or the third Cartesian coordinate  $z$  of points). Noticing that  $g_{tan} := -\nabla_\Gamma z$  and  $\nabla_\Gamma \gamma = \frac{1}{1 + E \ln(1-x)} \frac{-x}{1-x\Pi} \nabla_\Gamma \Pi$ , the relevant terms here are  $\nabla_\Gamma \cdot (\mathfrak{D}_6 \nabla_\Gamma \gamma)$ ,  $\nabla_\Gamma \cdot [C' \gamma (\frac{1}{3} H^3 \mathfrak{D}_1 - \frac{1}{3} \epsilon H^4 \mathfrak{D}_2 + H^2 \beta^{-1}) \nabla_\Gamma \mathcal{K}]$ ,  $\nabla_\Gamma \cdot [\epsilon C' \gamma H (\frac{1}{3} H^3 \mathfrak{D}_1 - \frac{1}{3} \epsilon H^4 \mathfrak{D}_2 + H^2 \beta^{-1}) \nabla_\Gamma \mathcal{K}_2]$ ,  $\nabla_\Gamma \cdot [(\frac{1}{3} H^3 \mathfrak{D}_3 - \epsilon \frac{1}{3} H^4 \mathfrak{D}_4 + H^2 \beta^{-1}) \mathcal{B}_0 g_{tan}]$ .

#### Discretization of the substrate advection operator $\mathfrak{D}_{\Gamma,1}(\mathcal{D}_\Gamma, \varpi, u) = \nabla_\Gamma \cdot (u \mathcal{D}_\Gamma \nabla_\Gamma \varpi)$

Here, the discretization is based on a second order upwind method similar to the one described in Chapter II, Section 2.7. First, we define a unique slope limited gradient operator on each cell, next we define an upwind value of  $u$  at each edge midpoint and finally we integrate  $\mathfrak{D}_{\Gamma,1}(\mathcal{D}_\Gamma, \varpi, u)$  using appropriate approximation of variables. Let us start with the definition of the slope limited gradient. Considering a cell  $S$ , we define a local  $\mathbb{R}^3$  basis made of the pseudo unit normal  $e_{3,S}^k := \nu_S^k = \sum_{p_i^k \in S^k} ((p_i^k - p_1^k) \wedge (p_{i+1}^k - p_1^k)) / \|\sum_{p_i^k \in S^k} ((p_i^k - p_1^k) \wedge (p_{i+1}^k - p_1^k))\|$  of  $S$ , the vector  $e_{1,S}^k := ((p_1^k - X_S^k) - ((p_1^k - X_S^k) \cdot e_{3,S}^k) e_{3,S}^k) / \|(p_1^k - X_S^k) - ((p_1^k - X_S^k) \cdot e_{3,S}^k) e_{3,S}^k\|$  and  $e_{2,S}^k := e_{3,S}^k \wedge e_{1,S}^k$ ; then, we define  $\nabla_S^k u := ((\nabla_S^k u) \cdot e_{1,S}^k) e_{1,S}^k + ((\nabla_S^k u) \cdot e_{2,S}^k) e_{2,S}^k + ((\nabla_S^k u) \cdot e_{3,S}^k) e_{3,S}^k$  the slope limited gradient as follows:

$$\left\{ \begin{array}{l} (\nabla_S^k u) \cdot e_{j,S}^k := \text{sign} \left( (\nabla_{\text{Id}, p_1, \mathcal{J}(p_1, S)}^k u) \cdot e_{j,S}^k \right) \min_{p_i^k \in S^k} \left| (\nabla_{\text{Id}, p_i, \mathcal{J}(p_i, S)}^k u) \cdot e_{j,S}^k \right| \\ \quad \text{if } \text{sign} \left( (\nabla_{\text{Id}, p_i, \mathcal{J}(p_i, S)}^k u) \cdot e_{j,S}^k \right) = \text{const } \forall p_i \in \partial S^k, \\ (\nabla_S^k u) \cdot e_{j,S}^k := 0 \quad \text{else,} \end{array} \right.$$

for all  $j = 1, 2, 3$ . Here,  $\nabla_{\text{Id}, p_1, \mathcal{J}(p_1, S)}^k u$  is determined by the formulae (4.19), (4.20) and (4.21) using  $\mathcal{D}_\Gamma$  as the substrate identity tensor that we denote with a slight misuse of notation  $\text{Id}$ . Also the induced matrices  $A_{\text{Id}, p_i}^k$  should be such that  $A_{\text{Id}, p_i}^k + (\mathbf{1}_{p_i} \otimes \mathbf{1}_{p_i})/n_{p_i}$  is strictly positive definite for interior points and boundary points around which a Neumann boundary condition is defined. For boundary points around which a Dirichlet boundary condition is defined, we assume  $A_{\text{Id}, p_i}^k$  to be strictly positive definite. Next, we define an upwind value  $U_{\sigma,+}^k(\mathcal{D}_\Gamma, \varpi)$  at edge midpoints. In fact, considering an edge  $\sigma^k := S^k | L^k = [p_i^k, p_{i+1}^k]$  shared by two cells  $S^k$  and  $L^k$ , we first assume  $j, j+1$  being respectively the local index of  $S^k$  and  $L^k$  around  $p_i^k$  and  $m, m-1$  being respectively the local index of  $S^k$  and  $L^k$  around  $p_{i+1}^k$ ; i.e.  $S_{p_i, j}^k = S_{p_i}^k$ ,  $S_{p_i, j+1}^k = L_{p_i}^k$ ,  $S_{p_{i+1}, m}^k = S_{p_{i+1}}^k$ ,  $S_{p_{i+1}, m-1}^k = L_{p_{i+1}}^k$  (cf. Figure 4.2). Also we denote by

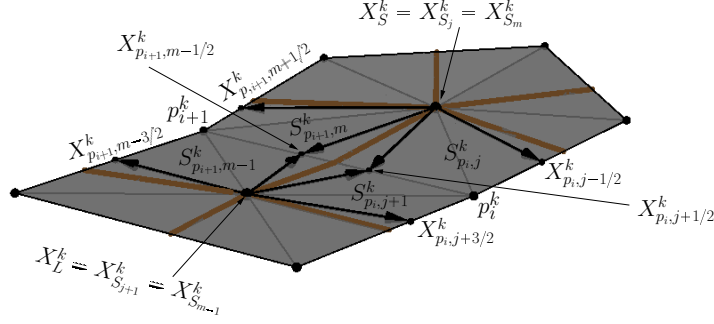


Figure 4.2: Subcells across the edge  $\sigma^k = [p_i^k, p_{i+1}^k]$  and virtual points around  $p_i^k$  and  $p_{i+1}^k$ .

$$F_{S,\sigma}^k(\mathcal{D}_\Gamma^k, \varpi) := m_{j+1/2}^k (\mathcal{D}_{\Gamma,p_{i,j}}^k \nabla_{\mathcal{D}_{\Gamma,p_{i,j}}}^k \varpi) \cdot n_{p_{i,j}|j+1/2}^k + m_{m-1/2}^k (\mathcal{D}_{\Gamma,p_{i+1,m}}^k \nabla_{\mathcal{D}_{\Gamma,p_{i+1,m}}}^k \varpi) \cdot n_{p_{i+1,m}|m-1/2}^k$$

the discrete flux from  $S^k$  through  $\sigma$ . Let us recall that for  $\varpi$  being the geometric quantities  $\mathcal{K}$ ,  $\mathcal{K}_2$ , or  $z$ , one can compute the value at edge virtual points; thus the interpolation for the computation of above mentioned fluxes can be done only on interior edges using the Dirichlet boundary condition. In case the Neumann boundary condition is known for these variable such as in the first and second examples of Section 4.4, it is preferable to consider the last to preserve the numerical conservation of fluid. We now define the upwind value  $U_{\sigma,+}^k(\mathcal{D}_\Gamma, \varpi)$  at the edge midpoint  $p_\sigma^k := \frac{p_i^k + p_{i+1}^k}{2}$  by

$$\begin{cases} U_{\sigma,+}^k(\mathcal{D}_\Gamma, \varpi) := U_S^k + (\nabla_S^k u) \cdot (p_\sigma^k - X_S^k) & \text{if } F_{S,\sigma}^k(\mathcal{D}_\Gamma^k, \varpi) > 0, \\ U_{\sigma,+}^k(\mathcal{D}_\Gamma, \varpi) := U_L^k + (\nabla_L^k u) \cdot (p_\sigma^k - X_L^k) & \text{else,} \end{cases}$$

for interior edges. For boundary edges with Dirichlet boundary condition, we define

$$\begin{cases} U_{\sigma,+}^k(\mathcal{D}_\Gamma, \varpi) := U_S^k + (\nabla_S^k u) \cdot (p_\sigma^k - X_S^k) & \text{if } F_{S,\sigma}^k(\mathcal{D}_\Gamma^k, \varpi) > 0, \\ U_{\sigma,+}^k(\mathcal{D}_\Gamma, \varpi) := U_\sigma^k & \text{else} \end{cases}$$

and for boundary edges with Neumann boundary condition, we define

$$U_{\sigma,+}^k(\mathcal{D}_\Gamma, \varpi) := U_S^k + (\nabla_S^k u) \cdot (p_\sigma^k - X_S^k).$$

By  $U_\sigma^k$  we denote the value of  $u^k$  at  $p_\sigma^k$ . Finally, we integrate  $\mathfrak{D}_{\Gamma,1}(\mathcal{D}_\Gamma, \varpi, u) = \nabla_\Gamma \cdot (u \mathcal{D}_\Gamma \nabla_\Gamma \varpi)$  on the curved domain  $S^{l,k} \cap \Gamma^k$  as follows:

$$\begin{aligned} \int_{S^{l,k} \cap \Gamma^k} \mathfrak{D}_{\Gamma,1}(\mathcal{D}_\Gamma, \varpi, u) da &= \int_{S^{l,k} \cap \Gamma^k} \nabla_\Gamma \cdot (u \mathcal{D}_\Gamma \nabla_\Gamma \varpi) da \\ &= \int_{\partial(S^{l,k} \cap \Gamma^k)} u (\mathcal{D}_\Gamma \nabla_\Gamma \varpi) \cdot n_{\partial(S^{l,k} \cap \Gamma^k)} dl \\ &\approx \sum_{\sigma^k := S^k|L^k} U_{\sigma,+}^k F_{S,\sigma}^k(\mathcal{D}_\Gamma^k, \varpi). \end{aligned} \quad (4.40)$$

Let us now introduce the discretization of a free surface diffusion tensor

$$\mathfrak{D}_{FS,1}(\mathcal{D}_{FS}, \Pi) = \nabla_{FS} \cdot (\mathcal{D}_{FS} \nabla_{FS} \Pi).$$

**Discretization of the free surface diffusion operator**  $\mathbf{\Omega}_{FS,1}(\mathcal{D}_{FS}, \Pi) = \nabla_{FS} \cdot (\mathfrak{D}_{FS} \nabla_{FS} \Pi)$

We approximate the integral of  $\mathbf{\Omega}_{FS,1}(\mathcal{D}_{FS}, \Pi)$  on the curved free surface cell  $S_{FS}^{l,k} \cap \overline{FS}^k$  as follows

$$\begin{aligned}
 & \int_{S_{FS}^{l,k} \cap \overline{FS}^k} \mathbf{\Omega}_{FS,1}(\mathcal{D}_{FS}, \Pi) da = \int_{S_{FS}^{l,k} \cap \overline{FS}^k} \nabla_{FS} \cdot (\mathfrak{D}_{FS} \nabla_{FS} \Pi) da \\
 &= \int_{\partial(S_{FS}^{l,k} \cap \overline{FS}^k)} (\mathfrak{D}_{FS} \nabla_{FS} \Pi) \cdot n_{\partial(S_{FS}^{l,k} \cap \overline{FS}^k)} dl \\
 &\approx \sum_{p_i \in \partial S^k} m_{FS,p_i,\mathcal{J}(p_i,S)+1/2}^k (\nabla_{FS,\mathcal{D}_{FS,p_i,\mathcal{J}(p_i,S)}}^k \Pi) \cdot n_{FS,p_i,\mathcal{J}(p_i,S)+1/2}^k \\
 &+ m_{FS,p_i,\mathcal{J}(p_i,S)-1/2}^k (\nabla_{FS,\mathcal{D}_{FS,p_i,\mathcal{J}(p_i,S)}}^k \Pi) \cdot n_{FS,p_i,\mathcal{J}(p_i,S)-1/2}^k, \tag{4.41}
 \end{aligned}$$

where  $\nabla_{FS,\mathcal{D}_{FS,p_i,\mathcal{J}(p_i,S)}}^k u$  is given by (4.29), (4.30), (4.31). Since  $\mathcal{V}_h^k$  is viewed as a set of functions defined in the entire domain  $\mathcal{N}(t_k)$ , a piecewise constant function on free surface curved cells  $S_{FS}^{l,k}$  can be viewed as the trace of a function from  $\mathcal{N}(t_k)$  on  $\overline{FS}$ ; therefore the surfactant concentration  $\Pi^k$ , solution of the surfactant equation (4.15) which originally stays on the free surface will be considered as element of  $\mathcal{V}_h^k$ . We now wish to define an  $\mathbb{H}^1$  seminorm in  $\mathcal{V}_h^k$  which will be used to measure the trace of elements on the free surface. For this purpose, we multiply the equations (4.41) by the corresponding free surface cell value  $-\Pi_S^k$ , sum over all the cells and use (4.30) to obtain

$$- \sum_S \Pi_S^k \int_{S_{FS}^{l,k} \cap \overline{FS}^k} \mathbf{\Omega}_{FS,1} da \approx \sum_S \left( \tilde{\Pi}_{p_i}^k \right)^\top A_{FS,\mathcal{D}_{FS,p_i}}^k \tilde{\Pi}_{p_i}^k, \tag{4.42}$$

where  $A_{FS,\mathcal{D}_{FS,p_i}}^k$  is defined as in the Section 4.3.4 (Discretization of the substrate diffusion operator  $\mathbf{\Omega}_\Gamma(\mathcal{D}_\Gamma, u) = \nabla_\Gamma \cdot (\mathcal{D}_\Gamma \nabla_\Gamma u)$ );  $A_{FS,\mathcal{D}_{FS,p_i}}^k := A_{FS,\mathcal{D}_{FS,p_i,c}}^k - A_{FS,\mathcal{D}_{FS,p_i,\sigma}}^k \mathbf{Coef}_{FS,\mathcal{D}_{FS,p_i}}^k$  with  $A_{FS,\mathcal{D}_{FS,p_i,c}}^k$  being a diagonal matrix and  $A_{FS,\mathcal{D}_{FS,p_i,\sigma}}^k$  a sparse rectangular matrix whose nonzero elements are given by

$$\begin{aligned}
 (A_{FS,\mathcal{D}_{FS,p_i,c}}^k)_{j,j} &:= m_{FS,p_i,j-1/2}^k (\lambda_{FS,p_i,j|j-1/2}^k + \lambda_{FS,p_i,j+1/2|j-1/2}^k) \\
 &\quad + m_{FS,p_i,j+1/2}^k (\lambda_{FS,p_i,j|j+1/2}^k + \lambda_{FS,p_i,j-1/2|j+1/2}^k), \\
 (A_{FS,\mathcal{D}_{FS,p_i,\sigma}}^k)_{j,j} &:= m_{FS,p_i,j-1/2}^k \lambda_{FS,p_i,j|j-1/2}^k + m_{FS,p_i,j+1/2}^k \lambda_{FS,p_i,j-1/2|j+1/2}^k, \\
 (A_{FS,\mathcal{D}_{FS,p_i,\sigma}}^k)_{j,j+1} &:= m_{FS,p_i,j-1/2}^k \lambda_{FS,p_i,j+1/2|j-1/2}^k + m_{FS,p_i,j+1/2}^k \lambda_{FS,p_i,j|j+1/2}^k.
 \end{aligned}$$

Here again, the first and the last lines of these matrices at boundary points will be adjusted according to boundary condition. The matrix  $A_{FS,\mathcal{D}_{FS,p_i}}^k$  too, satisfies  $A_{FS,\mathcal{D}_{FS,p_i}}^k \mathbf{1}_{p_i}^k = \mathbf{0}_{p_i}$ . Similar as in the above mentioned section, we assume the virtual points on subedges being chosen such that  $A_{FS,\mathcal{D}_{FS,p_i}}^k + (\mathbf{1}_{p_i} \otimes \mathbf{1}_{p_i})/n_{p_i}$  is positive definite for all interior vertices and all boundary vertices around which a Neumann boundary condition is stated. For boundary vertices around which a Dirichlet boundary condition is stated, we assume  $A_{FS,\mathcal{D}_{FS,p_i}}^k$  to be strictly positive definite.

Let us finally introduce the discretization of free surface mix advection operators. These operators are of the form  $\mathbf{\Omega}_{FS,2}(\mathfrak{D}_{FS}, u) = \nabla_{FS} \cdot (\Pi \mathfrak{D}_{FS} \nabla_\Gamma u)$ . With the knowledge that  $g_{tan} := -\nabla_\Gamma z$ ,  $\gamma = \frac{1 + E \ln(1 - x \Pi)}{1 + E \ln(1 - x)}$  and  $\nabla_\Gamma \gamma = \frac{1}{1 + E \ln(1 - x)} \frac{-x}{1 - x \Pi} \nabla_\Gamma \Pi$ , we conclude that  $\mathfrak{D}_{FS}$  is a free surface tangential operator which might depend on the height  $H$ , the surfactant concentration  $\Pi$ , the geometric variables  $K, \mathcal{K}, \mathcal{K}_2$  and  $z$ . The variable  $u$  represents  $\Pi, H, \mathcal{K}, \mathcal{K}_2$ , or  $z$ .

**Discretization of the free surface mix advection operator**  $\mathbf{\Pi}_{FS,2}(\mathcal{D}_{FS}, u) = \nabla_{FS} \cdot (\Pi \mathcal{D}_{FS} \nabla_{\Gamma} u)$

Let us first notice that the relative velocity of the free surface particle tangent to the free surface is given by

$$\begin{aligned} & \mathcal{P}_{FS,\nu} v_{RFS,tan} \\ = & \mathcal{P}_{FS,\nu} \left[ -\mathcal{D}_{12} \nabla_{\Gamma} (\phi + C' \gamma \mathfrak{P}) + \mathcal{D}_{13} \nabla_{\Gamma} \gamma + \mathcal{D}_{14} \nabla_{\Gamma} H + C' \gamma \left( H \beta^{-1} + \frac{1}{2} H^2 \mathcal{D}_8 - \frac{1}{6} \epsilon H^3 \mathcal{D}_9 \right) \nabla_{\Gamma} \mathcal{K} \right. \\ & \left. + \epsilon C' \gamma H \left( H \beta^{-1} + \frac{1}{2} H^2 \mathcal{D}_8 - \frac{1}{6} \epsilon H^3 \mathcal{D}_9 \right) \nabla_{\Gamma} \mathcal{K}_2 + \left( H \beta^{-1} + \frac{1}{2} H^2 \mathcal{D}_{10} - \frac{1}{6} \epsilon H^3 \mathcal{D}_{11} \right) \mathcal{B}_0 g_{tan} \right]. \end{aligned} \quad (4.43)$$

Thus we compute the fluxes induced on edges of cells by the terms of this expression ( $\mathcal{D}_{FS} \nabla_{\Gamma} u$ ) in the continuous manner using the appropriate gradient reconstruction and only the surfactant concentration  $\Pi$  is advected using a second order upwind on the free surface similar to the one described above. Let us consider a cell  $S$  and the same setup as above in the Section 4.3.4 (Discretization of the substrate advection operator  $\mathbf{\Pi}_{\Gamma,1}(\mathcal{D}_{\Gamma}, \varpi, u) = \nabla_{\Gamma} \cdot (u \mathcal{D}_{\Gamma} \nabla_{\Gamma} \varpi)$ ). In the same way as before, we define with  $\nabla_{FS,S}^k \Pi := ((\nabla_{FS,S}^k \Pi) \cdot e_{1,S}^k) e_{1,S}^k + ((\nabla_{FS,S}^k \Pi) \cdot e_{2,S}^k) e_{2,S}^k + ((\nabla_{FS,S}^k \Pi) \cdot e_{3,S}^k) e_{3,S}^k$ , the slope limited gradient on the free surface as follows:

$$\left\{ \begin{array}{l} (\nabla_{FS,S}^k \Pi) \cdot e_{j,S}^k := \text{sign} \left( (\nabla_{\text{Id}_{FS}, p_i, \mathcal{J}(p_i, S)}^k \Pi) \cdot e_{j,S}^k \right) \min_{p_i^k \in S^k} \left| (\nabla_{\text{Id}_{FS}, p_i, \mathcal{J}(p_i, S)}^k \Pi) \cdot e_{j,S}^k \right| \\ \quad \text{if } \text{sign} \left( (\nabla_{\text{Id}_{FS}, p_i, \mathcal{J}(p_i, S)}^k \Pi) \cdot e_{j,S}^k \right) = \text{const } \forall p_i \in \partial S^k, \\ (\nabla_{FS,S}^k \Pi) \cdot e_{j,S}^k := 0 \quad \text{else,} \end{array} \right.$$

for all  $j = 1, 2, 3$ . By  $\nabla_{\text{Id}_{FS}, p_i, \mathcal{J}(p_i, S)}^k \Pi$  we denote the free surface gradient of  $\Pi$  determined using the formulae (4.29), (4.30), (4.31) and the free surface identity tensor  $\text{Id}_{FS}$  (i.e.  $\mathcal{D}_{FS} = \text{Id}_{FS}$ ). Here too, the induced matrix  $A_{\text{Id}_{FS}, p_i}^k$  are supposed to be such that  $A_{\text{Id}_{FS}, p_i}^k + \mathbf{1}_{p_i} \otimes \mathbf{1}_{p_i} / n_{p_i}$  is strictly positive for interior points and boundary points around which the Neumann boundary condition is stated. For boundary points around which the Dirichlet boundary condition is stated, we assume  $A_{\text{Id}_{FS}, p_i}^k$  to be strictly positive. Next, we define an upwind value  $\Pi_{\sigma,+}^k(\mathcal{D}_{FS}, \varpi)$  at edge midpoints. For this purpose, let us consider as in the above mentioned section an edge  $\sigma^k := S^k | L^k = [p_i^k, p_{i+1}^k]$  shared by two cells  $S^k$  and  $L^k$ . We adopt the same setup by assuming that  $j, j+1$  respectively are the indices of  $S^k$  and  $L^k$  around  $p_i^k$  and  $m, m-1$  respectively are the indices of  $S^k$  and  $L^k$  around  $p_{i+1}^k$ ; i.e.,  $S_{p_i, j}^k = S_{p_i}^k$ ,  $S_{p_i, j+1}^k = L_{p_i}^k$ ,  $S_{p_{i+1}, m}^k = S_{p_{i+1}}^k$ ,  $S_{p_{i+1}, m-1}^k = L_{p_{i+1}}^k$ . Let us denote by

$$\begin{aligned} F_{FS,S,\sigma}^k(\mathcal{D}_{FS}, u) & := m_{FS, p_i, j+1/2}^k (\mathcal{D}_{FS, p_i, j} (\nabla_{FS, p_i, j}^k u)) \cdot n_{FS, p_i, j|j+1/2}^k \\ & + m_{FS, p_{i+1}, m-1/2}^k (\mathcal{D}_{FS, p_{i+1}, m} (\nabla_{FS, p_{i+1}, m}^k u)) \cdot n_{FS, p_{i+1}, m|m-1/2}^k \end{aligned}$$

the flux from  $S_{FS}^{l,k}$  through  $\sigma_{FS}^{l,k}$  and define the upwind value  $\Pi_{\sigma,+}^k(\mathcal{D}_{FS}, \varpi)$  at the edge midpoint  $p_{FS,\sigma}^k := \mathcal{P}_{FS,\nu} p_{\sigma}^k = \mathcal{P}_{FS,\nu} \left( \frac{p_i^k + p_{i+1}^k}{2} \right)$  by

$$\left\{ \begin{array}{l} \Pi_{\sigma,+}^k(\mathcal{D}_{FS}, \varpi) := \Pi_S^k + (\nabla_{FS,S}^k \Pi) \cdot \left[ (\text{Id} - \epsilon H_S^k K_S^k) (p_{\sigma}^k - X_S^k) + \epsilon ((\nabla_S^k H) \cdot (p_{\sigma}^k - X_S^k)) \nu_S^k \right] \\ \quad \text{if } F_{FS,S,\sigma}^k(\mathcal{D}_{FS}, u) > 0 \\ \Pi_{\sigma,+}^k(\mathcal{D}_{FS}, \varpi) := \Pi_L^k + (\nabla_{FS,L}^k \Pi) \cdot \left[ (\text{Id} - \epsilon H_L^k K_L^k) (p_{\sigma}^k - X_L^k) + \epsilon ((\nabla_L^k H) \cdot (p_{\sigma}^k - X_L^k)) \nu_L^k \right] \quad \text{else,} \end{array} \right.$$

for interior edges. For boundary edges on which a Dirichlet boundary condition is stated, we define

$$\begin{cases} \Pi_{\sigma,+}^k(\mathcal{D}_{FS}, \varpi) := \Pi_S^k + (\nabla_{FS,S}^k \Pi) \cdot \left[ (\text{Id} - \epsilon \mathbf{H}_S^k K_S^k)(p_\sigma^k - X_S^k) + \epsilon ((\nabla_S^k \mathbf{H}) \cdot (p_\sigma^k - X_S^k)) \nu_S^k \right] \\ \quad \text{if } F_{FS,S,\sigma}^k(\mathcal{D}_{FS}, u) > 0 \\ \Pi_{\sigma,+}^k(\mathcal{D}_{FS}, \varpi) := \Pi_\sigma^k \quad \text{else} \end{cases}$$

and for boundary edges on which a Neumann boundary condition is stated, we define

$$\Pi_{\sigma,+}^k(\mathcal{D}_{FS}, \varpi) := \Pi_S^k + (\nabla_{FS,S}^k \Pi) \cdot \left[ (\text{Id} - \epsilon \mathbf{H}_S^k K_S^k)(p_\sigma^k - X_S^k) + \epsilon ((\nabla_S^k \mathbf{H}) \cdot (p_\sigma^k - X_S^k)) \nu_S^k \right].$$

By  $\Pi_\sigma^k$ , we denote the value of  $\Pi^k$  at  $\mathcal{P}_{FS,\nu}^k p_\sigma^k$ . The approximation of the integral of

$\mathfrak{D}_{FS,2}(\mathfrak{D}_{FS}, u) = \nabla_{FS} \cdot (\Pi \mathfrak{D}_{FS} \nabla_\Gamma u)$  on the curved cell  $S_{FS}^{l,k} \cap \overline{FS}^k$  is then given by

$$\begin{aligned} \int_{S_{FS}^{l,k} \cap \overline{FS}^k} \mathfrak{D}_{FS,2}(\mathfrak{D}_{FS}, u) da &= \int_{S_{FS}^{l,k} \cap \overline{FS}^k} \nabla_{FS} \cdot (\Pi \mathfrak{D}_{FS} \nabla_\Gamma u) da \\ &= \int_{\partial(S_{FS}^{l,k} \cap \overline{FS}^k)} (\Pi \mathfrak{D}_{FS} \nabla_\Gamma u) \cdot n_{\partial(S_{FS}^{l,k} \cap \overline{FS}^k)} dl \\ &\approx \sum_{\sigma^k \in \partial S^k} \Pi_{\sigma,+}^k(\mathcal{D}_{FS}, \varpi) F_{FS,S,\sigma}^k(\mathcal{D}_{FS}, u). \end{aligned} \quad (4.44)$$

Let us define the following entities of  $\mathcal{V}^k$ :  $\mathbf{1}_{\mathcal{V}}^k := (1, 1, \dots)^\top$ ,  $m_\Gamma^k := (m_{S_1}^k, m_{S_2}^k, \dots)^\top$ ,  $\mathbf{H}^k := (\mathbf{H}_{S_1}^k, \mathbf{H}_{S_2}^k, \dots)^\top$ ,  $\Pi^k := (\Pi_{S_1}^k, \Pi_{S_2}^k, \dots)^\top$ ,  $\mathcal{K}^k := (\mathcal{K}_{S_1}^k, \mathcal{K}_{S_2}^k, \dots)^\top$ ,  $\mathcal{K}_2^k := ((\mathcal{K}_2)_{S_1}^k, (\mathcal{K}_2)_{S_2}^k, \dots)^\top$ ,  $\eta^k := (\eta_{S_1}^k, \eta_{S_2}^k, \dots)^\top$ ,  $\gamma_+^k := (\gamma_{S_1,+}^k, \gamma_{S_2,+}^k, \dots)^\top$ ,  $\gamma_-^k := (\gamma_{S_1,-}^k, \gamma_{S_2,-}^k, \dots)^\top$  and  $\mathfrak{P}^k := (\mathfrak{P}_{S_1}^k, \mathfrak{P}_{S_2}^k, \dots)^\top$ .

For a generic element  $U^k := (U_{S_1}^k, U_{S_2}^k, \dots)^\top \in \mathcal{V}^k$  we denote by  $\mathcal{I}_h^k(U^k)$  the square diagonal matrix with diagonal  $U^k$ . We also denote by  $\mathbf{L}_h^k(\mathcal{D}_\Gamma)$  the matrix obtained from the discretization of the substrate diffusion operator  $\mathfrak{D}_\Gamma(\mathcal{D}_\Gamma, u) = \nabla_\Gamma \cdot (\mathcal{D}_\Gamma \nabla_\Gamma u)$  in Section 4.3.4 (Discretization of the substrate diffusion operator  $\mathfrak{D}_\Gamma(\mathcal{D}_\Gamma, u) = \nabla_\Gamma \cdot (\mathcal{D}_\Gamma \nabla_\Gamma u)$ ) by writing (4.37) for all cells in the matrix form (i.e.  $(m_{S_1}^k \mathfrak{D}_{\Gamma,S_1}^k(\mathcal{D}_\Gamma, u), m_{S_2}^k \mathfrak{D}_{\Gamma,S_2}^k(\mathcal{D}_\Gamma, u), \dots)^\top = \mathbf{L}_h^k(\mathcal{D}_\Gamma) U^k$ ). Similarly, we denote by  $\mathbf{L}_{FS,h}(\mathcal{D}_{FS})$  the matrix of diffusion on the free surface obtained from the discretization of  $\mathfrak{D}_{FS,1}(\mathcal{D}_{FS}, \Pi) = \nabla_{FS} \cdot (\mathfrak{D}_{FS} \nabla_{FS} \Pi)$  in Section 4.3.4 (Discretization of the free surface diffusion operator  $\mathfrak{D}_{FS,1}(\mathcal{D}_{FS}, \Pi) = \nabla_{FS} \cdot (\mathfrak{D}_{FS} \nabla_{FS} \Pi)$ ) by writing (4.41) for all cell in the matrix form. Finally, we denote by  $f_\Gamma(\mathbf{H}^k, \Pi^k)$  and  $f_{FS}(\mathbf{H}^k, \Pi^k)$  the vectors which correspond to the explicit discretization of the substrate advection operators and the free surface advection operators respectively.

From these notation, it follows that

$$\mathfrak{P}^k = -\epsilon \mathcal{I}^k (1/m_\Gamma^k) \mathbf{L}_h^k(\text{Id}) \mathbf{H}^k, \quad (4.45)$$

where  $1/m_\Gamma^k := (1/m_{S_1}^k, 1/m_{S_2}^k, \dots)$  and we conclude that our problem is reduced to

$$\left\{ \begin{array}{l} \text{Find } \mathbf{H}^{k+1} \in \mathcal{V}^{k+1} \text{ and } \Pi^{k+1} \in \mathcal{V}^{k+1} \text{ such that} \\ \mathcal{I}_h(m_\Gamma^{k+1}) \eta^{k+1} \\ - \tau \left[ \mathbf{L}_h^{k+1}(\mathfrak{D}_5) \left[ \mathcal{I}_h \left( \phi_{inc}^{k+1} / \mathbf{H}^{k+1} \right) - \epsilon C' \mathcal{I}_h(\gamma_+^{k+1}) \mathcal{I}_h(1/m_\Gamma^{k+1}) \mathbf{L}_h^{k+1}(\text{Id}) \right] + \mathbf{L}_h^{k+1}(\mathfrak{D}_{7,+}) \right] \mathbf{H}^{k+1} \\ = \tau \left[ \mathbf{L}_h^k(\mathfrak{D}_5) \left[ \mathcal{I}_h \left( \phi_{dec}^k / \mathbf{H}^k \right) - \epsilon C' \mathcal{I}_h(\gamma_-^k) \mathcal{I}_h(1/m_\Gamma^k) \mathbf{L}_h^k(\text{Id}) \right] \mathbf{H}^k - \mathbf{L}_h^k(-\mathfrak{D}_{7,-}) \right] \mathbf{H}^k \\ + \mathcal{I}_h(m_\Gamma^k) \eta^k - \tau f_\Gamma(\mathbf{H}^k, \Pi^k) \end{array} \right. \quad (4.46)$$

$$\mathcal{I}_h(m_{FS}^{k+1}) \Pi^{k+1} - \tau \frac{1}{\mathcal{P}_e} \mathbf{L}_{FS,h}^{k+1}(\mathcal{D}_{FS}) \Pi^{k+1} = \mathcal{I}_h(m_{FS}^k) \Pi^k - \tau f_{FS}(\mathbf{H}^k, \Pi^k), \quad (4.47)$$

where  $(\phi_{dec}^k/H^k) := (\phi_{dec,S_1}^k/H_{S_1}^k, \phi_{dec,S_2}^k/H_{S_2}^k, \dots)^\top$  and  $(\phi_{inc}^{k+1}/H^{k+1})$  are defined similarly. The system (4.46)-(4.47) can be rewritten as

$$\left\{ \begin{array}{l} \text{Find } H^{k+1} \in \mathcal{V}^{k+1} \text{ and } \Pi^{k+1} \in \mathcal{V}^{k+1}, \text{ such that} \\ \left( \mathcal{I}_h(m_\Gamma^{k+1}) \mathcal{I}_h(\mathbf{1}_V^{k+1} - \frac{1}{2}\epsilon(H^{k+1})\mathcal{K}^{k+1} + \frac{1}{6}\epsilon^2(H^{k+1})^2 [(\mathcal{K}^{k+1})^2 - (\mathcal{K}_2)^{k+1}]) \right. \\ \left. - \tau \left[ \mathbf{L}_h^{k+1}(\mathfrak{D}_5) \left[ \mathcal{I}_h(\phi_{inc}^{k+1}/H^{k+1}) - \epsilon C' \mathcal{I}_h(\gamma_+^{k+1}) \mathcal{I}_h(1/m_\Gamma^{k+1}) \mathbf{L}_h^{k+1}(\text{Id}) \right] + \mathbf{L}_h^{k+1}(\mathfrak{D}_{7,+}) \right] \right) H^{k+1} \\ = \tau \left[ \mathbf{L}_h^k(\mathfrak{D}_5) \left[ \mathcal{I}_h(\phi_{dec}^k/H^k) - \epsilon C' \mathcal{I}_h(\gamma_-^k) \mathcal{I}_h(1/m_\Gamma^k) \mathbf{L}_h^k(\text{Id}) \right] H^k - \mathbf{L}_h^k(-\mathfrak{D}_{7,-}) \right] H^k \\ + \mathcal{I}_h(m_\Gamma^k) \eta^k - \tau f_\Gamma(H^k, \Pi^k) \\ \left( \mathcal{I}_h(m_{FS}^{k+1}) - \tau \frac{1}{\mathcal{P}_e} \mathbf{L}_{FS,h}^{k+1}(D_{FS}) \right) \Pi^{k+1} = \mathcal{I}_h(m_{FS}^k) \Pi^k - \tau f_{FS}(H^k, \Pi^k). \end{array} \right.$$

Let us denote by  $\mathcal{M}_\Gamma^{k+1}(H^m, \Pi^m)$  and  $\mathcal{M}_{FS}^{k+1}(H^m, \Pi^m)$  the matrices

$$\begin{aligned} \mathcal{M}_\Gamma^{k+1}(H^m, \Pi^m) &:= \left( \mathcal{I}_h(m_\Gamma^{k+1}) \mathcal{I}_h \left( \mathbf{1}_V^{k+1} - \frac{1}{2}\epsilon(H^m)\mathcal{K}^{k+1} + \frac{1}{6}\epsilon^2(H^m)^2 [(\mathcal{K}^{k+1})^2 - (\mathcal{K}_2)^{k+1}] \right) \right. \\ &\quad \left. - \tau \left[ \mathbf{L}_h^{k+1}(\mathfrak{D}_5(H^m)) \left[ \mathcal{I}_h(\phi_{inc}(H^m)/H^m) - \epsilon C' \mathcal{I}_h(\gamma_+(\Pi^m)) \mathcal{I}_h(1/m_\Gamma^{k+1}) \mathbf{L}_h^{k+1}(\text{Id}) \right] \right. \right. \\ &\quad \left. \left. + \mathbf{L}_h^{k+1}(\mathfrak{D}_{7,+}(H^m)) \right] \right) \\ \mathcal{M}_{FS}(H^k, \Pi^k) &:= \left( \mathcal{I}_h(m_{FS}^{k+1}(H^m)) - \tau \frac{1}{\mathcal{P}_e} \mathbf{L}_{FS,h}^{k+1}(D_{FS}) \right), \end{aligned}$$

where  $H^m, \Pi^m$  are elements of  $\mathcal{V}^{k+1}$ , the variables  $\mathfrak{D}_5(H^m), \mathfrak{D}_{7,+}(H^m), \phi_{inc}(H^m), m_{FS}^{k+1}(H^m)$  are functions of  $H^m$  and  $\gamma_+(\Pi^m)$  is a function of  $\Pi^m$ . We also denote by  $\mathcal{F}_\Gamma(H^k, \Pi^k)$  and  $\mathcal{F}_{FS}(H^k, \Pi^k)$  the vectors

$$\begin{aligned} \mathcal{F}_\Gamma(H^k, \Pi^k) &:= \tau \left[ \mathbf{L}_h^k(\mathfrak{D}_5) \left[ \mathcal{I}_h(\phi_{dec}^k/H^k) - \epsilon C' \mathcal{I}_h(\gamma_-^k) \mathcal{I}_h(1/m_\Gamma^k) \mathbf{L}_h^k(\text{Id}) \right] H^k - \mathbf{L}_h^{k+1}(-\mathfrak{D}_{7,-}) \right] H^k \\ &\quad + \mathcal{I}_h(m_\Gamma^k) \eta^k - \tau f_\Gamma(H^k, \Pi^k) \\ \mathcal{F}_{FS}(H^k, \Pi^k) &:= \mathcal{I}_h(m_{FS}^k) \Pi^k - \tau f_{FS}(H^k, \Pi^k). \end{aligned}$$

The system (4.46)-(4.47) is finally written as

$$\left\{ \begin{array}{l} \text{Find } \mathcal{F}_\Gamma(H^k, \Pi^k) \in \mathcal{V}^{k+1} \text{ and } \Pi^{k+1} \in \mathcal{V}^{k+1} \text{ which satisfies} \\ H^{k+1} = \left( \mathcal{M}_\Gamma^{k+1}(H^{k+1}, \Pi^{k+1}) \right)^{-1} \mathcal{F}_\Gamma(H^k, \Pi^k) \\ \Pi^{k+1} = \left( \mathcal{M}_{FS}(H^{k+1}, \Pi^{k+1}) \right)^{-1} \mathcal{F}_{FS}(H^k, \Pi^k). \end{array} \right. \quad (4.48)$$



We solve the above mentioned system using the fixed point iteration

$$\begin{cases} \mathbb{H}^{k+1,j} = \left( \mathcal{M}_{\Gamma}^{k+1}(\mathbb{H}^{k+1,j-1}, \Pi^{k+1,j-1}) \right)^{-1} \mathcal{F}_{\Gamma}(\mathbb{H}^k, \Pi^k) \\ \Pi^{k+1,j} = \left( \mathcal{M}_{FS}^{k+1}(\mathbb{H}^{k+1,j-1}, \Pi^{k+1,j-1}) \right)^{-1} \mathcal{F}_{FS}(\mathbb{H}^k, \Pi^k), \\ \mathbb{H}^{k+1,0} = \mathbb{H}^k, \quad \Pi^{k+1,0} = \Pi^k \end{cases} \quad (4.49)$$

$$(4.50)$$

which converges for small  $\tau$ . Practically we have found that the iterations converge for  $\tau \leq Ch^2$  and the stop criterion for our numerical examples was  $\|\mathbb{H}^{k+1,j} - \mathbb{H}^{k+1,j-1}\| + \|\Pi^{k+1,j} - \Pi^{k+1,j-1}\| \leq 10^{-10}$ .

Let us remind that the  $\|\mathbb{H}^k\| = \sqrt{\sum_S (\mathbb{H}_S^k)^2}$ .

## 4.4 Numerical results

In this section, we present the numerical results of some simulation on triangular domain. Here, we adopt the configuration described in Chapter II, Remark 2.4.2, Item *a*, Part *i*. In fact, the center points are chosen to be the center of gravity of triangles. For a given triangle  $S^k$  and a vertex  $p_i^k$  of  $S^k$ , the subcell  $S_{p_i}^k$  is delimited on the triangle edges incident at  $p_i^k$  by the midpoints  $q_{p_i,j-1/2}^k$  and  $q_{p_i,j+1/2}^k$  of the respective edges;  $j$  being the local index of  $S^k$  around  $p_i^k$ . Finally the edge virtual points  $X_{p_i,j-1/2}^k$  and  $X_{p_i,j+1/2}^k$  on the subedges incident at  $p_i^k$  are placed such that  $\overrightarrow{p_i^k X_{p_i,j-1/2}^k} = (2/3)\overrightarrow{p_i^k q_{p_i,j-1/2}^k}$  and  $\overrightarrow{p_i^k X_{p_i,j+1/2}^k} = (2/3)\overrightarrow{p_i^k q_{p_i,j+1/2}^k}$ . We refer to Figure 4.3 for the illustration of this setup. The present setup ensures that the discretization of a substrate diffusion operator,

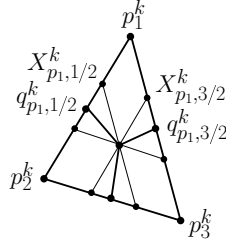


Figure 4.3: Subdivision of triangle cell using isobarycenter and the middle of edges.

respectively of a free surface diffusion operator, involving a strictly elliptic substrate diffusion tensor, respectively a strictly elliptic free surface diffusion tensor, leads to local elliptic submatrices around vertices as required for the above described algorithm in the Sections 4.3.4 (Discretization of the substrate diffusion operator  $\mathbb{D}_{\Gamma}(\mathcal{D}_{\Gamma}, u) = \nabla_{\Gamma} \cdot (\mathcal{D}_{\Gamma} \nabla_{\Gamma} u)$ ) and 4.3.4 (Discretization of the free surface diffusion operator  $\mathbb{D}_{FS,1}(\mathcal{D}_{FS}, \Pi) = \nabla_{FS} \cdot (\mathcal{D}_{FS} \nabla_{FS} \Pi)$ ). Also, if the diffusion tensors involved here are elliptic and degenerated, the local matrices around the vertices become automatically elliptic and degenerated, again as prescribed in the above mentioned sections. Furthermore, the matrix  $\mathbf{L}_h^k(\mathcal{D}_{\Gamma})$  obtained from the discretization of the surface diffusion operator  $\nabla_{\Gamma} \cdot (\mathcal{D}_{\Gamma} \nabla_{\Gamma} u)$  is symmetric if  $\mathcal{D}_{\Gamma}$  is symmetric and if  $\mathcal{D}_{\Gamma}$  is not strongly anisotropic and the mesh not too stretched,  $\nabla_{\Gamma} \cdot (\mathcal{D}_{\Gamma} \nabla_{\Gamma} u)$  is also an M-matrix. On the free surface, we obtain the same properties for the matrix  $\mathbf{L}_{FS,h}^k(\mathcal{D}_{FS})$  obtained from the discretization of the free surface diffusion operator  $\nabla_{FS} \cdot (\mathcal{D}_{FS} \nabla_{FS} u)$  if we replace the flux continuity condition (4.24) on free surface subedges  $\sigma_{FS,p_i,j-1/2}^{l,k}$  around  $p_i^k$  by

$$\begin{aligned} & \|\mathcal{D}_{FS,p_i,j-1|j-1/2}^k\| \mathcal{D}_{FS,p_i,j-1}^k \nabla_{\mathcal{D}_{FS,p_i,j-1}}^k u \cdot n_{FS,p_i,j-1|j-1/2}^k \\ + & \|\mathcal{D}_{FS,p_i,j|j-1/2}^k\| \mathcal{D}_{FS,p_i,j}^k \nabla_{\mathcal{D}_{FS,p_i,j}}^k u \cdot n_{FS,p_i,j|j-1/2}^k = 0, \end{aligned} \quad (4.51)$$

where  $\|\varrho_{FS,p_i,j-1|j-1/2}^k\|$  and  $\|\varrho_{FS,p_i,j|j-1/2}^k\|$  defined in Section 4.3.3 represent the approximate measure of  $\sigma_{FS,p_i,j-1/2}^{l,k}$  from the subcells  $S_{p_i,j-1}^k$  and  $S_{p_i,j}^k$  respectively. We should mention here that the choice of center points as center of gravity improves the consistency of the quadrature rule used for the integration of functions. This was an aim of the algorithm proposed in Chapter II Section 2.4.5. Let us now introduce our simulation results. On the first example depicted on Figure 4.4 we study the flow of a thin-film with an initial constant height  $H^0 = 0.5$  in the inner part of an alveolus that we stretch and slightly change the form. At the pole of the alveolus, we place on top of the film, a concentration of nonsoluble surfactant whose the configuration is a hat function with the maximum value 1 at the pole. The support can be seen on Figure 4.4, second line, first picture. The surfactant concentration is assumed to diffuse isotropically with the free surface diffusion tensor  $D_{FS} = \text{Id}$  and the Peclet number  $\mathcal{P}_e = 10^4$ . At the substrate-fluid interface, we assume the presence of repulsive Van der Waals forces of potential  $\phi = -10^{-14}H^{-3}$  and we consider a slip boundary condition with the slip tensor  $\beta^{-1} = \epsilon \text{Id}$ , where  $\epsilon = 0.00125$  is effectively the ratio between the height length scale and the horizontal length scale. We also consider the inverse capillary number  $C' = 1000\epsilon^2$ , the Bond number  $\mathcal{B}_0 = 40$ , the surfactant elasticity constant  $E = 0.9354$ , the surfactant coverage  $x = 0.6$  and the time interval  $[0, 2]$ . We do not take the effect of gravity into account.

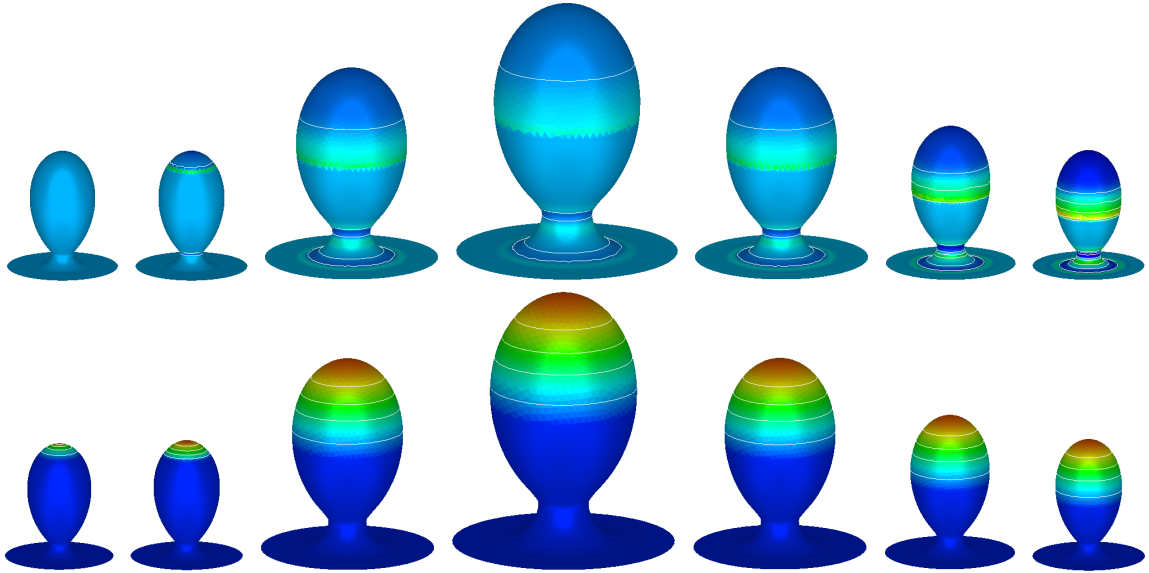


Figure 4.4: Thin film and surfactant distribution on an expanding and then contracting alveolus. The first line shows the evolution of the thin film height and the second line the evolution of the surfactant concentration. The alveolus surface is made up of 8052 triangles and contains 4072 points. The initial minimum and maximum diameter of triangles are 0.0043 and 0.0588, respectively and at  $t = 1$  (fourth picture of the first and second lines), the minimum and maximum diameter of triangles are 0.0056 and 0.0933, respectively. The small triangles are located in the region of higher curvature to resolve the geometric features. The time step is  $\tau = 1/4000$ .

In the first line of Figure 4.4, we depict the evolution of the thin film height and on the second line, the evolution of the surfactant concentration. The color shading ranges from blue to red representing minimum to maximum values. This will be the same for all numerical results in this part. We observe that the fluid is pushed from places, where the surfactant concentration is high to places having low surfactant concentration (see figure 4.4 first line). In fact, the substrate gradient of

the surface tension gives rise to Marangoni forces which dominate the advection due to the gradient in the substrate curvature and then initiate the motion of the fluid which at its turn transports the fluid particles along its way. Similar observations have already been made for simulation of surfactant driven thin film flow on a line segment in [9]. On the tail of the alveolus, we observe that the fluid moves to regions of higher curvature. At the neck of the alveolus in the first line for example, the fluid quits the region of very height negative curvature; the flow is then driven by the curvature. This is in adequation with the result on flow around corners presented in [107] (Example 5). Let us mention the green band near the pole on the second picture of the first line of Figure 4.4 which has a maximum diameter of two triangles and represents the bubble at the fluid front due pressure difference between the front and the tail of the fluid. We also notice the sharp transition from maximum values to smaller values at the fluid front which represent the sharp front interface of the fluid. This proves that the method is less dissipative and very sharp feature, of the flow can be resolved even on relatively coarse triangulation. This observation will be confirmed in the next simulation results.

In a second experiment, we simulate the flow of the above described thin film in the same alveolus which also expands and then contracts during the process. Different from Figure 4.4, where the scaling is pronounced, we adopt a movement where the upper part of the alveolus tends to become spherical (compare picture 1 to picture 4 of Figure 4.5 for the evolution in the expansion phase). The surfactant concentration is removed ( $\Pi^0 = 0$ ) and the surface tension is therefore constant  $\gamma = 6.9978$ . Figure 4.5 shows the evolution of the film height. Here the main observation is that

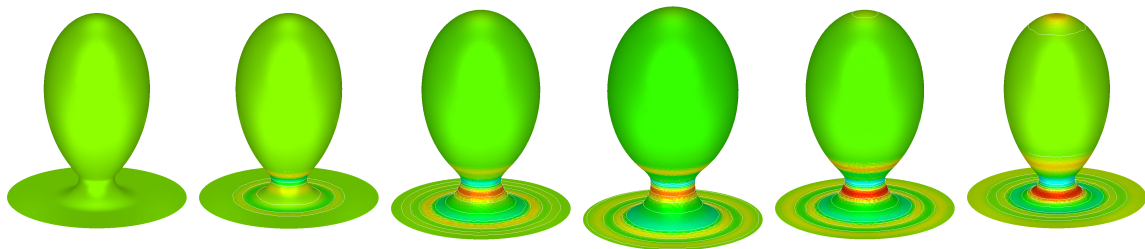


Figure 4.5: Thin film driven by surface tension on an expanding and then contracting alveolus. The setup is similar to the one in first experiment (see Figure 4.4), but the alveolus expands in a way that the upper part becomes almost spherical (picture 4).

the fluid flows toward region of higher curvature. We can clearly notice (picture 7, Figure 4.5) an inflow at the pole which creates a region of maximum height in accordance with the flow of thin film inside an ellipsoid presented in [107]. In comparison with the simulation above, the absence of surfactant leaves room to the substrate gradient of the substrate's curvature to control the flow. Again, important features such as the local extrema at the tail of the alveolus are resolved though the substrate discretization is not fine.

Now, in the third example (Figure 4.7), we study the flow of a gravity driven thin film through a surfactant obstacle on an expanding and then, contracting sphere. As above, we consider the parameters  $\epsilon = 0.00125$ ,  $C' = 1000\epsilon^2$ ,  $\mathcal{B}_0 = 40$  and  $\beta^{-1} = \epsilon \text{Id}$ . We assume the presence of repulsive Van der Waals forces of potential  $\phi = -10^{-18}\text{H}^{-3}$ . As initial film height we consider a perturbed Gaussian function with the maximum height being 0.995 at the pole to which we add 0.005 which represents the thickness of the initial precursor layer. The support of the Gaussian function can be seen from above on the first picture of the first line of Figure 4.5. At the equator, we place six localized spots of surfactant, of which three are at the front side of the sphere as can be seen on the first picture of the second line of Figure 4.7. The rests are placed at the back side of the sphere symmetrically to the ones in the front. We should also mention that the middle surfactant concentration at the front and the back of the sphere are on the trajectory of the front main flow

and the back main flow, respectively. The shape of each surfactant concentration is Gaussian, its maximum is 1.995 and its support is elliptic. Let us now consider the three band depicted on the rescaled initial sphere on Figure 4.6, the initial surfactant concentration are respectively centered in each band; thus their support do not intersect. The bands in fact represent the support

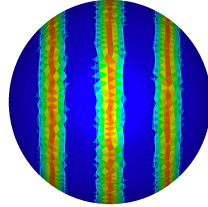


Figure 4.6:  $SCF$  (surfactant coefficient function).

of a piecewise linear pseudo hat function “ $SCF$ ” (surfactant coefficient function) which takes the value 3 on the ring center of each band and the value 0 outside of the bands. Let us consider a point  $p = (\cos(\theta_1)\cos(\theta_2), \cos(\theta_1)\sin(\theta_2), \cos(\theta_1))$  on the initial unit sphere;  $\theta_1$  and  $\theta_2$  being respectively the elevation and the azimuth at  $p$ . We denote by  $\nu$  the normal at  $p$  and by  $e_1 := (-\sin(\theta_2), \cos(\theta_2), 0)$  a unit tangent vector at  $p$  parallel to the  $(X, Y)$  plane. We define the tensor  $D_{FS} = (3 + 10^{-6})(\text{Id} - \nu \otimes \nu - e_1 \otimes e_1) + (SCF(p) + 10^{-6})e_1 \otimes e_1$  if  $p$  is not a pole and  $D_{FS} = (3 + 10^{-6})(\text{Id} - \nu \otimes \nu)$  else. The free surface tangential part of  $D_{FS}$  that we still call  $D_{FS}$  is incorporated in the model. With this setup, the surfactant concentrations diffuse in such a way that the path of the blocs do not intersect far from the poles. We should notice that the diffusion is almost one dimensional out of the bands of Figure 4.6. We assume the surfactant parameters  $\mathcal{P}_e = 500$ ,  $E = 0.9354$ ,  $x = 0.48$ . The first line of Figure 4.7 shows the evolution of the thin film while the second line presents the evolution of the surfactant concentration. We should mention that the first two pictures on the first line of Figure 4.7 are seen from above and the two last pictures on both lines are seen from a perspective of  $50^\circ$  below. Here we observe that the surfactant

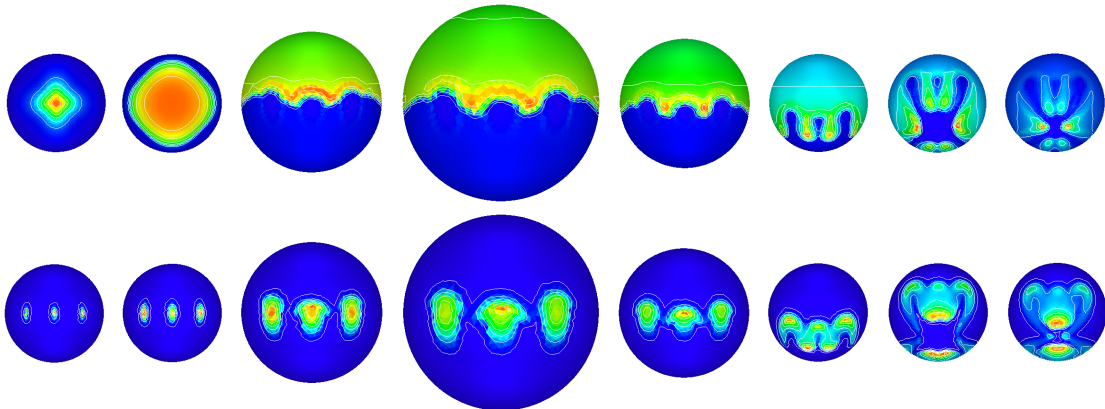


Figure 4.7: Gravity driven thin film flowing around surfactant obstacles on an expanding and then contracting sphere.

The sphere is made of 6426 triangles and 3215 points. The initial minimum and maximum diameter of triangles are 0.0249 and 0.1061, respectively and at  $t = 1$  (fourth picture of the first and second lines) they are 0.0498 and 0.2122, respectively. The time step is  $\tau = 1/3000$  and the time interval  $[0, 3]$ .

deviates the fluid flow which goes around the concentration (see picture 3, first line, Figure 4.7). This creates more fingering as can be seen on pictures 3-8 of the first line of Figure 4.7. While going around the surfactant, the fluid transports surfactant particles along (see pictures 3-6, second line, Figure 4.7) which quickly occupies the front of the film flow (see pictures 6-8, second line, Figure 4.7). The combined effort of gravity and Marangoni forces created by the surface gradient of the surfactant concentration accelerates the flow of the fluid front toward the south pole. When an important amount of surfactant is gathered in the front of the film and the Marangoni forces balancing the gravity pressure, the fluid gets accumulated just behind the surfactant as can be seen through the comparison of pictures 7-8, first line of Figure 4.7. Following computations only confirm this through an increase of height at the fluid front which is equivalent to the formation of drops. Since the lubrication approximation that we used to model the flow does not take into account the formation of drops, we had to stop the simulation.

The fourth example is devoted to the above mentioned fluid in the absence of surfactant. On Figure 4.8 we report some sequences of this simulation. The first two pictures are seen from above and the last pictures are seen from a perspective of  $50^\circ$  below. Here we observed the fingering conform to

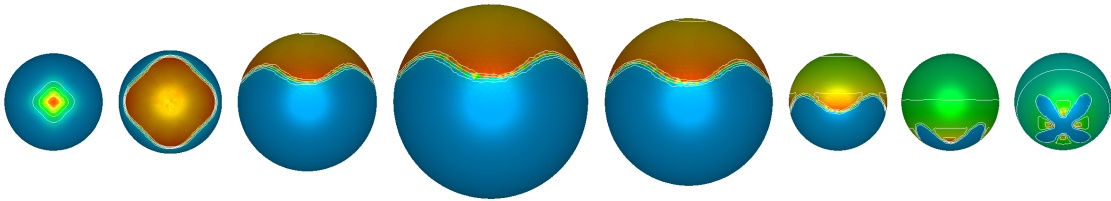


Figure 4.8: Flow of gravity driven thin film on an expanding and then contracting sphere. The setup is the same as the one of Figure 4.7.

the simulation done in [57] example 9.2. As for other examples, one will notice the steepness of the front which is resolved. This again confirms that the method is less dissipative.

Let us now introduce a fifth example in which we study the flow on a static bumpy sphere (Figure 4.9) of a gravity driven thin film. We consider as initial value, a localized Gaussian function which

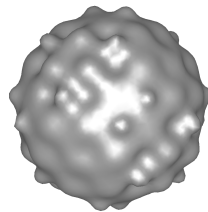


Figure 4.9: Rescaled bumpy sphere.

has a maximum value of 1 at the north pole and whose support can be seen from above on picture 1, Figure 4.10. To this Gaussian function, we add 0.005 which represents the height of the precursor layer. On Figure 4.10, we present some sequences of this simulation. The two first pictures are seen from above and the last picture is seen in the perspective of  $50^\circ$  from below. Here the irregularity of the surface creates a competition between advection by gravity and advection by gradient of curvatures. This leads to the creation of fingering as can be seen on pictures 3-8.

We introduce a sixth example which deals with the gravity driven thin film on a moving plane in the presence of surfactant. In fact, we consider the planar domain  $[0, 1] \times [0, 1]$  which moves perpendicularly (in the Z-direction) to fit an area of an ellipsoid. At the end of the process, the

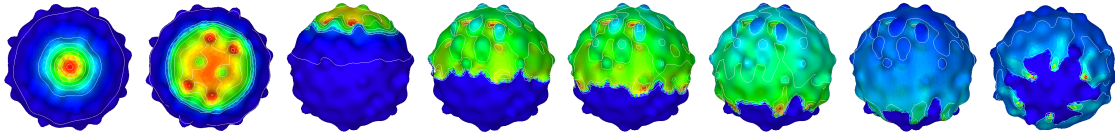


Figure 4.10: Flow of gravity driven thin film on a bumpy sphere.

The bumpy sphere is made up of 9794 triangles and 4899 points. The minimum and maximum diameter of triangles are 0.0267 and 0.1650, respectively, the time step is  $\tau = 1/2500$  and the time interval is  $[0, 2]$ .

segment  $[0, 1] \times \{0\}$  maps onto the circular equator of the ellipsoid. On this substrate, we consider the evolution of a thin film and a surfactant concentration which have the property of the first example. Different from other examples, we assume a nonexistence of Van der Waals interfacial forces (i.e.  $\phi = 0$ ) and we consider a partially wetted substrate. Thus we assume at the initial instant, a liquid film of local support above which a surfactant concentration of local support too is placed. The third picture of the first line of Figure 4.11 clearly presents the support of the film height and the diameter of the support of the thin film is taken to be the double of the diameter of the support of the surfactant concentration. The initial film height and the surfactant concentration are functions of Gaussian shape with respective maximum 1.5 and 0.75 at the center of the surface. The free surface diffusion tensor considered is  $D_{FS} = \text{Id}$  if  $H \neq 0$  and  $D_{FS} = 0\text{Id}$  else. The first two lines of Figure 4.11 show a sequence of the evolution of the fluid while the two last lines give the corresponding sequence of evolution of the surfactant concentration. Similar as in the first example, the gradient in the surfactant concentration gives rise to Marangoni forces which initiate the movement of the fluid from regions of height surfactant concentration to regions of lower surfactant concentration. This can be seen by looking at the crater that appears in the middle of picture 4 in the first line of Figure 4.11. Also a competition is installed between Marangoni forces, gravity and advection due to the gradient of curvatures. Similar to the third example above (Gravity driven thin film around surfactant obstacle), when the gravity becomes dominant, the fluid which has been pushed in the northern part tries to find a way around the surfactant (see picture 2-3 on the second line of Figure 4.11). On its way down, the fluid transports surfactant particles along as already reported in the third example. Once the surfactant reaches the front, it causes the fluid to spread. This observation was already done in [9] for simulation of a surfactant driven thin film on a planar line segment.

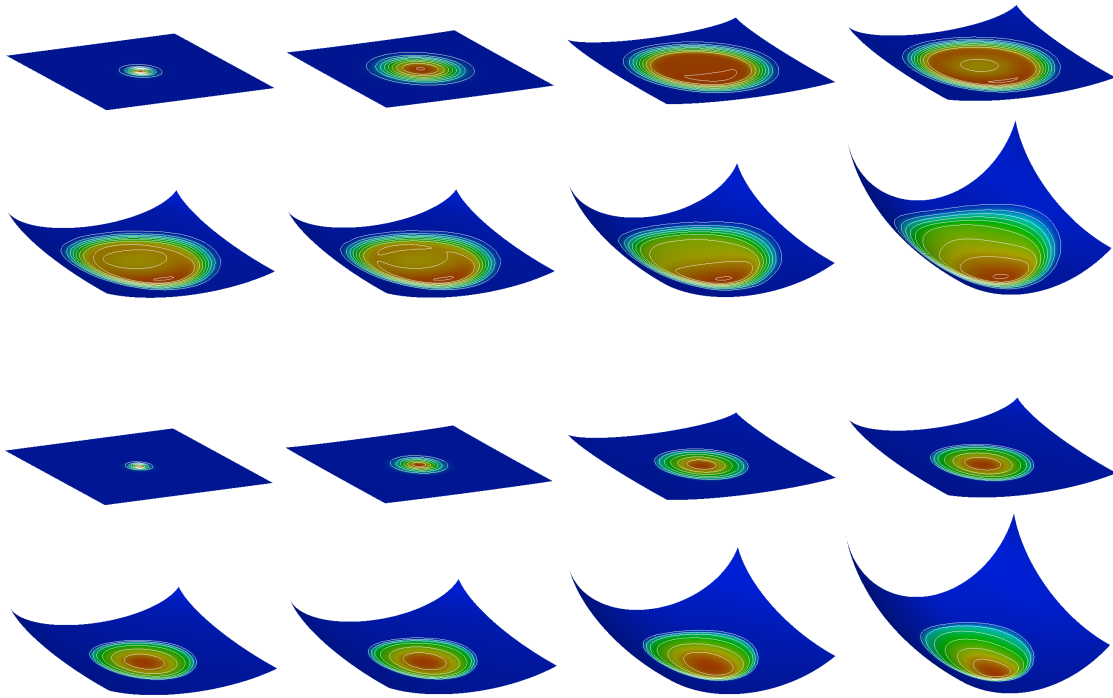


Figure 4.11: Flow of gravity driven thin film in the presence of surfactant on a deforming plane. The surface is made up of 9728 triangles 5009 and points. The minimum and the maximum diameter of triangles at the initial time is 0.0088 and 0.0316, respectively, the time step is  $\tau = 1/8000$  and the time frame is  $[0, 0.75]$ .





## Conclusion and perspectives

In this work, we have developed finite volume schemes for direct simulation of second and fourth order equations on evolving curved surfaces and interfacial surfaces. We have, in particular, described a method for computations on a very broad range of polygonal surfaces, which takes into account the major advances in the finite volume community nowadays: computation on unstructured meshes, computation on non conformal meshes, high order upwinding amongst others. The stability of the methods have been proven for the second order problems and we have provided several simulation results to support the theory. As usual in moving mesh methods, it can happen that cells degenerate during the evolution. One can nevertheless handle this issue by combining our method with an appropriate mesh optimization strategy which will reposition the vertices at each time step. As a byproduct, the gradient reconstruction method developed here can be used as an approximation tool on the curved surface to reallocate values to cells, in case of remeshing for example. We should also mention that the method can be extended to higher order finite volumes. In this case, quadrature rules used for integration would be different, the surface approximation would be done through polygonal fitting and the gradient reconstruction would be improved too. We plan to deal with these issues in future work.

We have also presented a model reduction method for thin film equations using lubrication approximation. Our model allows the easy incorporation of additional effects, like inertia. This model allows also the easy coupling of interfacial flow, since the height of the film parameterizes already the free surface on the beneath substrate. This parameterization can be used together with lubrication approximation to pull back the free surface flow equation on the substrate as it has been the case for surfactant driven thin film flow on flat surfaces, or one can take advantage of it for a direct computation on the free surface as we have presented in this thesis. This second alternative is suitable for computation of more complicated flows on the free surface.



# Bibliography

- [1] IVAR AAVATSMARK, *Multipoint flux approximation methods for quadrilateral grids*, 9th International Forum on Reservoir Simulation, Abu Dhabi, 9–13 December, (2007), pp. 1–44.
- [2] MOHAMMED AFIF AND BRAHIM AMAZIANE, *Numerical simulation for the anisotropic benchmark by a vertex-centred finite volume method*, in *Finite Volume for Complex Application V: Problems & Perspectives*, eds. R. Eymard and J. M. Hérard, 2008, pp. 693–704.
- [3] D. AHRENS, *Industrial thin-film deodorization of seed oils with SoftColumn<sup>TM</sup> technology*, Wiley, Lipid / Fett, 101 (1999), pp. 230–234.
- [4] H. W. ALT, *The entropy principle for fluid interfaces*, Preprint, (2007).
- [5] J. W. BARRETT, H. GARCKE, AND R. NUERNBERG, *Finite element approximation of surfactant spreading on a thin film*, SIAM J. Numer. Anal., 41 (2003), pp. 1427–1464.
- [6] J. W. BARRETT AND R. NÜRNBERG, *Convergence of a finite-element approximation of surfactant spreading on a thin film in the presence of van der Waals forces*, IMA J. of Numer. Anal., 24 (2004), pp. 323–363.
- [7] R. A. BARRIO, C. REA, J. L. ARAGÓN, AND P. K. MAINI, *A two-dimensional numerical study of spatial pattern formation in interacting turing systems*, Bull. Math. Biol., 61 (1999), pp. 483–505.
- [8] TIMOTHY BARTH AND MARIO OHLBERGER, *Finite volume methods: Foundation and analysis*, In E. Stein, R. de Borst, and T.J.R. Hughes, ed., Enc. Comput. Mech. John Wiley & Sons, 2004.
- [9] J. BECKER, G. GRÜN, M. LENZ, AND M. RUMPF, *Numerical methods for fourth order nonlinear degenerate diffusion problems*, Applications of Mathematics, 47 (2002), pp. 517–543.
- [10] M. BERTALMIÓ, F. MÉMILI, L. T. CHENG, G. SAPIRO, AND S. OSHER, *Variational problems and partial differential equations on implicit surfaces: Bye bye triangulated surfaces?*, in *Geometric level Set Methods in Imaging, Vision, and Graphics*, Springer, New York, (2003), pp. 381–397.
- [11] A. L. BERTOZZI AND M. BOWEN, *Thin film dynamics: theory and applications*, (2002).
- [12] A. L. BERTOZZI AND M. P. BRENNER, *Linear stability and transient growth in driven contact lines*, Phys. Fluids, 9 (1997), pp. 530–539.
- [13] J. J. BIKERMAN, *Foam*, Springer-Verlag, New York, 1973.
- [14] M. G. BLYTH AND C. POZRIKIDIS, *Evolution equations for the surface concentration of an insoluble surfactant; applications to the stability of an elongating thread and a stretched interface*, J. Theor. Comput. Fluid Dyn., 17 (2004), pp. 147–164.
- [15] J. L. BULL AND J. B. GROTBORG, *Surfactant spreading on thin viscous film: film thickness evolution and periodic wall stretch*, Exp. Fluids, 34 (2003), pp. 1–15.

- [16] M. BURGER, *Finite element approximation of elliptic partial differential equations on implicit surfaces*, *Comput. Vis. Sci.*, 12 (2009), pp. 87–100.
- [17] J. W. CAHN, P. FIFE, AND O. PENROSE, *A phase-field model for diffusion-induced grain-boundary motion*, *Acta Materialia*, 45 (1997), pp. 4397–4413.
- [18] D. A. CALHOUN AND C. HELZEL, *A finite volume methods for solving parabolic equations on logically cartesian curved surface meshes*, *SIAM J. Sci. Comput.*, 31 (2009), pp. 4066–4099.
- [19] D. A. CALHOUN, C. HELZEL, AND R. J. LEVEQUE, *Logically rectangular grids and finite volume methods for PDEs in circular and spherical domains*, *SIAM Rev.*, 50 (2008), pp. 723–752.
- [20] S. L. CAMPBELL, *On continuity of the Moore-Penrose and Drazin generalized inverses*, *Linear Algebra and its Applications*, (1977), pp. 53–57.
- [21] J. CARR, *Applications of Centre Manifold Theory*, Springer, 1981.
- [22] F. CAZALS AND M. POUGET, *Estimating differential quantities using polynomial fitting of osculating jets*, *Computer Aided Geometric Design*, 22 (2005), pp. 121–146.
- [23] U. CLARENZ, U. DIEWALD, AND M. RUMPF, *Processing textured surfaces via anisotropic geometric diffusion*, *IEEE Trans Image Process.*, 2 (2004), pp. 248–261.
- [24] G. CORACH AND A. MAESTRIPIERI, *Weighted generalized inverses, oblique projections and least squares problems*, *Numerical Functional Analysis and Optimization*, 26 (2005), pp. 659–673.
- [25] P. H. COULLET AND E. A. SPIEGEL, *Amplitude equations for systems with competing instabilities*, *SIAM J. Appl. Math.*, 43 (1983), pp. 776–821.
- [26] EGGLETON C. D., TSE-MIN TSAI, AND K. J. STEBE, *Tip streaming from a drop in the presence of surfactants*, *Phys. Rev. Lett.*, 87 (2001), pp. (048302–1)–(048302–4).
- [27] T DAMM AND H. K. WIMMER, *A cancellation property of the Moore-Penrose inverse of triple products*, *J. Aust. Math. Soc.*, 86 (2009), pp. 33–44.
- [28] B. R. DE ARAÚJO AND J. A. P. JORGE, *Curvature dependent polygonization of implicit surfaces*, in *Proceedings of the 17th Brazilian Symposium on Computer Graphics and Image Processing/II Ibero- American Symposium on Computer Graphics*, IEEE, (2004).
- [29] ———, *Adaptive polygonization of implicit surfaces*, *Comput. Graphics*, 29 (2005), pp. 686–696.
- [30] K. DECKELNICK, G. DZIUK, C. M. ELLIOTT, AND C. J. HEINE, *An  $h$ -narrow band finite-element method for elliptic equations on implicit surfaces*, *IMA J. Numer. Anal.*, 30 (2010), pp. 351–376.
- [31] J. A. DIEZ, L. KONDIC, AND A. BERTOZZI, *Global models for moving contact lines*, *Phys Rev E*, 63 (2001), pp. (011208–1)–(011208–13).
- [32] K. DOMELEVO AND P. OMNES, *A finite volume method for the Laplace equation on almost arbitrary two-dimensional grids*, *ESAIM, Math. Model. Numer. Anal.*, 39 (2005), pp. 1203–1249.
- [33] Q. DU AND L. JU, *Finite volume methods on spheres and spherical centroidal Voronoi meshes*, *SIAM J. Numer. Anal.*, 43 (2005), pp. 1673–1692.

- 
- [34] Q. DU, L. JU, AND L. TIAN, *Analysis of a mixed finite-volume discretization of fourth-order equations on general surfaces*, IMA J. Numer. Anal., 29 (2009), pp. 376–403.
- [35] ———, *Finite element approximation of the Cahn-Hilliard equation on surfaces*, Comput. Meth. Appl. Mech. Eng., 200 (2011), pp. 2458–2470.
- [36] Q. DU AND D. WANG, *Anisotropic centroidal Voronoi tessellations and their applications*, SIAM J. Sci. Comput., 26 (2005), pp. 737–761.
- [37] G. DZIUK AND C. M. ELLIOTT, *Finite elements on evolving surfaces*, IMA J. Numer. Anal., 27 (2007), pp. 262–292.
- [38] G. DZIUK AND C. M. ELLIOTT, *Surface finite elements for parabolic equations.*, J. Comput. Math., 25 (2007), pp. 385–407.
- [39] G. DZIUK AND C. M. ELLIOTT, *Eulerian finite element method for parabolic PDEs on implicit surfaces*, Interf. Free Bound., 10 (2008), pp. 119–138.
- [40] LARS ELDÉN, *Perturbation theory for the least squares problem with linear equality constraints*, SIAM J. Numer. Anal., 17 (1980), pp. 338–350.
- [41] ———, *A weighted pseudoinverse, generalized singular values, and constrained least squares problems*, Numer. Math., 22 (1982), pp. 487–502.
- [42] B. ELIZABETH, V. DUSSAN, AND S. H. DAVIS, *On the motion of a fluid-fluid interface along a solid surface*, J. Fluid Mech., 65 (1974), pp. 71–95.
- [43] B. ENGQUIST AND S. OSHER, *One-sided difference approximations for nonlinear conservation laws*, Math. Comp., 31 (1981), pp. 321–351.
- [44] D. EXEROWA AND P. M. KRUGLYAKOV, *Foam and Foam Films: Theory, Experiment, Application*, Elsevier Science & Technology, 1997.
- [45] R. EYMARD, T. GALLOUËT, AND R. HERBIN, *Finite volume methods*, in Special Volume Foundation of Computational Mathematics, Handb. of numer. anal. VII, P. G. Ciarlet, ed., North-Holland, Amsterdam, 2000, pp. 713–1020.
- [46] ———, *Discretisation of heterogeneous and anisotropic diffusion problems on general non-conforming meshes. SUSHI: a scheme using stabilisation and hybrid interfaces*, IMA J. Numer. Anal., 30 (2010), pp. 1009–1043.
- [47] R. EYMARD AND J. M. HÉRARD, *Finite Volume for Complex Application V: Problems & Perspectives*, Wiley, 2008.
- [48] UWE WOLFRAM FERMUM, *Modellierung und Existenztheorie dünner Filme auf evolvierenden Flächen*, Rheinischen Friedrich-Wilhelms-Universität Bonn, Dissertation, 2010.
- [49] JAROSLAV FOŘT, JIŘÍ FÜRST, JAN HALAMA, RAPHAËLE HERBIN, AND FLORENCE HUBERT, *Finite Volumes for Complex Applications VI: Problems & Perspectives*, Springer Proceedings in Mathematics, 2011.
- [50] G. L. GAINES, *Insoluble Monolayers at Liquid-gas Interfaces*, John Wiley & Sons Inc, 1966.
- [51] SASHIKUMAAR GANESAN AND LUTZ TOBISKA, *A coupled arbitrary Lagrangian-Eulerian and Lagrangian method for computation of free surface flows with insoluble surfactants*, J. Comput. Phys., 228 (2009), pp. 2859–2873.

- [52] H. GARCKE, M. RUMPF, AND U. WEIKARD, *The Cahn-Hilliard equation with elasticity - finite element approximation and qualitative studies*, Interf. Free Bound., 3 (2001), pp. 101–118.
- [53] D. P. GAVER III AND J. B. GROTBORG, *The dynamics of a localized surfactant on a thin film*, J. Fluid Mech., 213 (1990), pp. 127–148.
- [54] J. GLIMM, D. MARCHESIN, AND O. MCBRYAN, *A numerical method for two phase flow with an unstable interface*, J. Comp. Phys. 39, 39 (1981), pp. 179–200.
- [55] ERIC GONCALVÈS, *Resolution numérique des équations d'Euler monodimensionnelles*, Lecture notes, Institut National Polytechnique de Grenoble, 2004.
- [56] J. B. GREER, *An improvement of a recent Eulerian method for solving PDEs on general geometries*, J. Sci. Comput., 29 (2006), pp. 321–352.
- [57] JOHN B. GREER, ANDREA L. BERTOZZI, AND GUILLERMO SAPIRO, *Fourth order partial differential equations on general geometries*, Journal of Computational Physics, 216 (2006), pp. 216–246.
- [58] J. B. GROTBORG, *Pulmonary flow and transport phenomena*, Annu. Rev. Fluid Mech., 26 (1994), pp. 43–58.
- [59] GÜNTHER GRÜN, *On the convergence of entropy consistent schemes for lubrication type equations in multiple space dimensions*, Math. Comp., 72 (2003), pp. 1251–1279.
- [60] G. GRÜN, M. LENZ, AND M. RUMPF, *A finite volume scheme for surfactant driven thin film flow*, in Finite Volumes for Complex Applications III, R. Herbin and D. Kröner, eds. Hermes Scientific, Paris, 2002, pp. 553–560.
- [61] G. GRÜN AND M. RUMPF, *Nonnegativity preserving convergent schemes for the thin film equation*, Numer. Math., 87 (2000), pp. 113–152.
- [62] ———, *Simulation of singularities and instabilities arising in thin film flow*, Eur. J. Appl. Math., 12 (2001), pp. 293–320.
- [63] H. HAMM, FABEL H., AND BARTSCH W., *The surfactant system of the adult lung: physiology and clinical perspectives*, J. Molec. Med., 70 (2004), pp. 637–657.
- [64] F. HERMELINE, *A finite volume method for the approximation of diffusion operators on distorted meshes*, J. Comput. Phys., 160 (2000), pp. 481–499.
- [65] I. HERRERA, R. E. EWING, M. A. CELIA, AND T. F. RUSSELL, *Eulerian-Lagrangian localized adjoint method for the advection-diffusion equation*, Adv. Water Res., 13 (1990), pp. 187–206.
- [66] B. A. HILLS, *The role of lung surfactant*, Br. J. Anaesth., 65 (1990), pp. 13–29.
- [67] P. D. HOWELL, *Surface-tension-driven flow on a moving curved surface*, J. Eng. Math., 45 (2009), pp. 283–308.
- [68] CHUN HUH AND L. E. SCRIVEN, *Hydrodynamic model of steady movement of a solid/liquid/fluid contact line*, J. Coll. Interf. Sci., 35 (1971), pp. 85–101.
- [69] H. E. HUPPERT, *The propagation of two dimensional and axisymmetric viscous gravity currents over a rigid horizontal surface*, J. Fluid Mech., 121 (1982), pp. 43–58.
- [70] H. E. HUPPERT AND J. E. SIMPSON, *The slumping of gravity currents*, J. Fluid Mech. 99, 99 (1980), pp. 785–799.

- 
- [71] JAMES M. HYMAN, *Numerical methods for tracking interfaces*, *Physica D: Nonl. Phen.*, 12 (1984), pp. 396–407.
- [72] M. P. IDA AND M. J. MIKSI, *The dynamics of thin films I: General theory*, *SIAM J. Appl. Math.*, 58 (1998), pp. 456–473.
- [73] A. J. JAMES AND J. LOWENGRUB, *A surfactant-conserving volume-of-fluid method for interfacial flows with insoluble surfactant*, *J. Comput. Phys.*, 201 (2004), pp. 685–722.
- [74] O. E. JENSEN AND J. B. GROTHBERG, *Insoluble surfactant spreading on a thin viscous film: shock evolution and rupture*, *J. Fluid Mech.*, 240 (1992), pp. 259–288.
- [75] M. B. JONES, C. P. PLEASE, AND M. J. COLLINS, *Dynamics of tear film deposition and draining*, *Math. Med. Biol.*, 22 (2005), pp. 265–288.
- [76] L. JU AND Q. DU, *A finite volume method on general surfaces and its error estimates*, *J. Math. Anal. Appl.*, 352 (2009), pp. 645–668.
- [77] A. J. KINFACK AND A. NJIFENJOU, *Convergence analysis of an MPFA method for flow problems in anisotropic heterogeneous porous media*, *IJFV*, 5 (2008).
- [78] J. RICHARD KING, *Pulmonary surfactant*, *J. Appl. Physiol.*, 53 (1982), pp. 1–8.
- [79] J. J. KOLIHA, *Continuity and differentiability of the Moore–Penrose inverse in  $c^*$ -algebras*, *Math. Scand.*, 88 (2001), pp. 154–160.
- [80] L. KONDIC, *Instabilities in gravity driven flow of thin fluid films*, *SIAM Rev.*, 45 (2003), pp. 95–115.
- [81] L. KONDIC AND J. DIEZ, *Instabilities in the flow of thin films on heterogeneous surfaces*, *Phys. Fluids*, 16 (2004), pp. 3341–3360.
- [82] L. KONDIC AND DIEZ J., *Instabilities in the flow of thin films on heterogeneous surfaces*, *Phys. Fluids*, (2004), pp. 3341–3360.
- [83] Y. W. KRUIJT-STEGEMAN, F. N. VAN DE VOSSE, AND H. E. H. MEIJER, *Droplet behavior in the presence of insoluble surfactants*, *Phys. of Fluids*, 16 (2004), pp. 2785–2796.
- [84] BOZENA KURASZKIEWICZ AND M. PRZYTULSKA, *A new mathematical approach modeling surfactant transport in pulmonary airways*, in *IFMBE Proceedings*, 14, Part 2, (2007), pp. 92–94.
- [85] C. LE POTIER, *Schéma volumes finis pour des opérateurs de diffusion fortement anisotropes sur des maillages non structurés*, *C.R. Acad. Sci. Paris Ser. I* 340, (2005), pp. 921–926.
- [86] M. LENZ, S. F. NEMADJIEU, AND M. RUMPF, *A convergent finite volume scheme for diffusion on evolving surfaces*, *SIAM J. Numer. Anal.*, 49 (2011), pp. 15–37.
- [87] K. LIPNIKOV, M. SHASHKOV, AND I. YOTOV, *Local flux mimetic finite difference methods*, *Numer. Math.*, 112 (2009), pp. 115–152.
- [88] R. T. LIU, S. S. LIAW, AND MAINI P. K., *Two-stage turing model for generating pigment patterns on the leopard and the jaguar*, *Phys. Rev. E* 74, 011914, (2006), pp. 011914(1)–011914(8).
- [89] J. A. MACKENZIE AND W. R. MEKWI, *On the use of moving mesh methods to solve PDEs*, in *Adaptive Computations: Theory and Algorithms*, T. Tang and J. Xu, ed., Science Press, Beijing, 2007, pp. 243–278.

- [90] K. L. MAKI, R. J. BRAUN, W. D. HENSHAW, AND P. E. KING-SMITH, *Tear film dynamics on an eye-shaped domain I: pressure boundary conditions*, *Math. Med. Biol.*, 27 (2010), pp. 227–254.
- [91] K. L. MAKI, R. J. BRAUN, P. UCCIFERRO, W. D. HENSHAW, AND P. E. KING-SMITH, *Tear film dynamics on an eye-shaped domain II: flux boundary conditions*, *J. Fluid Mech.*, (2010), pp. 361–390.
- [92] O. K. MATAR AND S. M. TROIAN, *Linear stability analysis of an insoluble surfactant monolayer spreading on a thin liquid film*, *Phys. Fluids*, 9 (1997), pp. 3645–3657.
- [93] T. G. MYERS, J. P. F. CHARPIN, AND S. J. CHAPMAN, *The flow and solidification of a thin fluid film on an arbitrary three-dimensional surface*, *Phys. of Fluids*, 14 (2002), pp. 2788–2803.
- [94] I. M. NGUENA AND A. NJIFENJOU, *A finite volume approximation for second order elliptic problems with a full matrix on quadrilateral grids: derivation of the scheme and theoretical analysis*, *IJFV*, 3 (2006).
- [95] S. B. G. O'BRIEN AND L. W. SCHWARTZ, *Theory and modeling of thin film flows*, *Encyclopedia of Surf. and Coll. Sci.*, (2002), pp. 5283–5297.
- [96] CARL OLLIVIER-GOOCH AND MICHAEL VAN ALTENA, *A high-order-accurate unstructured mesh finite-volume scheme for the advection-diffusion equation*, *J. Comput. Phys.*, 181 (2002), pp. 729–752.
- [97] S. E. ORCHARD, *Surface leveling in viscous liquids and gels*, *Appl. Sci. Res. A* 11, (1962), pp. 451–464.
- [98] A. ORON, S. H. DAVIS, AND S. G. BANKOFF, *Long-scale evolution of thin liquid films*, *Rev. of Mod. Phys.*, 69 (1997), pp. 931–980.
- [99] P.-O. PERSSON, *Mesh Generation for Implicit Geometries*, PhD thesis, Massachusetts Institute of Technology, Cambridge, MA, (2005).
- [100] BENOÎT PERTHAME, *Equations de transport non linéaires et systèmes hyperboliques: Théorie et méthodes numériques*, *Lecture notes*, 2003-2004.
- [101] C. POZRIKIDIS, *A finite-element method for interfacial surfactant transport, with application to the flow-induced deformation of a viscous drop*, *J. Eng. Math.*, 49 (2004), pp. 163–180.
- [102] VLADIMIR RAKOCEVIC, *On continuity of the Moore-Penrose and Drazin inverses*, *MATEMATIČKI VESNIK*, 49 (1997), pp. 163–172.
- [103] MURALI RAO AND JAN SOKOLOWSKIT, *Differential stability of solutions to parametric optimization problems*, *Math. Meth. Appl. Sci.*, 14 (1991), pp. 281–294.
- [104] YURIKO Y. RENARDY, MICHAEL RENARDY, AND VITTORIO CRISTINI, *A new volume-of-fluid formulation for surfactants and simulations of drop deformation under shear at a low viscosity ratio*, *Eur. J. Mech. - B/Fluids*, 21 (2002), pp. 49–59.
- [105] A. J. ROBERTS, *Low-dimensional models of thin film fluid dynamics*, *Phys. Letters A*, 212 (1996), pp. 63–71.
- [106] ———, *Low-dimensional modelling of dynamics via computer algebra*, *Comput. Phys. Commun.*, 100 (1997), pp. 215–230.
- [107] R. V. ROY, A. J. ROBERTS, AND M. E. SIMPSON, *A lubrication model of coating flows over a curved substrate in space*, *J. Fluid Mech.*, 454 (2002), pp. 235–261.



- 
- [108] SHWETA SAXENA, *Lung surfactant: The indispensable component of respiratory mechanics*, Resonance, 10 (2008), pp. 91–96.
- [109] L. W. SCHWARTZ AND D. E. WEIDNER, *Modeling of coating flows on curved surfaces*, J. Eng. Math., 29 (1994), pp. 91–101.
- [110] A. SHARMA AND E. RUCKENSTEIN, *An analytical nonlinear theory of thin film rupture and its application to wetting films*, J. Coll. Interf. Sci., 113 (1986), pp. 456–476.
- [111] J. C. SLATTERY, L. SAGIS, AND EUN-SUOK OH, *Interfacial Transport Phenomena*, Springer, Berlin, 2007.
- [112] GEORG STILL, *Lectures on parametric optimization: An introduction*, University of Twente, (2006), pp. 1–19.
- [113] H. A. STONE, *A simple derivation of the time-dependent convective-diffusion equation for surfactant transport along a deforming interface*, Phys. Fluids A 2, 111 (1990), pp. 111–112.
- [114] H. A. STONE AND L. G. LEAL, *The effects of surfactants on drop deformation*, J. Fluid Mech., 220 (1990), pp. 161–186.
- [115] D. TAKAGI AND H. E. HUPPERT, *Flow and instability of thin films on a cylinder and sphere*, Journal of Fluid Mechanics, 647 (2010), pp. 221–238.
- [116] YOSHIO TAKANE, YONGGE TIAN, AND HARUO YANAI, *On constrained generalized inverses of matrices and their properties*, Ann. Inst. Stat. Math., 59 (2007), pp. 807–820.
- [117] G. F. TELETZKE, H. T. DAVIS, AND L. E. SCRIVEN, *Wetting hydrodynamics*, Rev. Phys. Appl., 23 (1988), pp. 989–1007.
- [118] G. TRYGGVASON, B. BUNNER, A. ESMAEELI, D. JURIC, N. AL-RAWAHI, W. TAUBER, J. HAN, S. NAS, AND Y.-J. JAN, *A front-tracking method for the computations of multiphase flow*, J. Computat. Phys., 169 (2001), pp. 708–759.
- [119] ALAN M. TURING, *The chemical basis of morphogenesis*, Philosophical Transactions of the Royal Society of London. B 327, (1952), pp. 37–72.
- [120] G. TURK, *Generating textures on arbitrary surfaces using reaction-diffusion*, ACM SIGGRAPH Comput. Graphics, 25 (1991), pp. 289–298.
- [121] B. W. VAN DE FLIERT, P. D. HOWELL, AND J. R. OCKENDON, *Pressure-driven flow of a thin viscous sheet*, J. Fluid Mech., 292 (1995), pp. 359–376.
- [122] D. T. WASAN, K. KOCZO, AND A. D. NIKOLOV, *Mechanism of aqueous foam stability and antifoaming action with and without oil: a thin film approach*, Foams: Fundamentals and applications in the petroleum Industry, Ed. Schramm, L. L. (American Chemical Society, Washington), (1994), pp. 47–114.
- [123] ANDREW WITKIN AND MICHAEL KASS, *Reaction-diffusion textures*, in Computer Graphics, 1991, pp. 299–308.
- [124] H. WONG, I. FATT, AND C. J. RADKE, *Deposition and thinning of the human tear film*, J. Coll. Interf. Sci., 184 (1996), pp. 44–51.
- [125] H. WONG, C. J. RADKE, AND S. MORRIS, *The motion of long bubbles in polygonal capillaries. part 1. thin films*, J. Fluid Mech., 292 (1995), pp. 71–94.

- [126] JIAN-JUN XU AND HONG-KAI ZHAO, *An Eulerian formulation for solving partial differential equations along a moving interface*, J. Sci. Comput., 19 (2003), pp. 573–594.
- [127] XIAOFENG YANG AND A. J. JAMES, *An arbitrary Lagrangian-Eulerian (ALE) method for interfacial flows with insoluble surfactants*, Fluid Dyn. Mater. Process., 3 (2007), pp. 65–96.